Thesis for the Master's degree in chemistry

Erlend Grenager Sørmo

Mercury in a remote glacier-fed alpine catchment in China

60 study points

DEPARTMENT OF CHEMISTRY
Faculty of mathematics and natural sciences
UNIVERSITY OF OSLO 05/2014

Acknowledgements

The present work was carried out at the Norwegian Institute for Water research (NIVA) and the Department of Chemistry at the University of Oslo (UIO), in the period between September 2012 and May 2014. The work was supervised by: Thorjørn Larssen, professor II at UIO and research director at NIVA; Yan Lin, research scientist at NIVA; and Hans Fredrik Veiteberg Braaten, PhD candidate at UIO and NIVA.

During the course of this work a number of highly appreciated individuals have contributed in aiding, counseling and inspiring me in the process of completing this master's thesis as it is presented here today. I would like to express my deepest gratitude to:

Thorjørn Larssen for giving me the opportunity to work on this fascinating project, for always being efficient and reliable in giving precise and solid feedback and guidance. Also for taking me in and giving me the opportunity to work in the highly professional working environment at NIVA; it has been a valuable experience! Yan Lin for the invaluable help in planning and carrying out the field work, for good academic advice and for stimulating conversation during the long hours of travelling and working in China. Hans Fredrik Braaten for the invaluable help in planning and carrying out the analytical work, for always being available for questions and giving ever reliable advice.

Rolf D. Vogt for always keeping his door open and offering advice to lost souls. Hua Zhang for all the assistance during field work and for infecting us with an unrelenting good mood and determination when faced with tough challenges. Lan Xiaoquan at the Mt. Gongga Research Station for shelter and aid. Everyone in the Environmental Analysis Group for supporting each other and making the last two years at UIO a memorable time.

I would also like to thank NIVA providing the funding for this project and allowing me to use their great facilities for the analytical work.

Finally I want to express my love and thankfulness to Lisa, for all those little things which matter so much.

Abstract

Mercury (Hg) is a toxic trace metal whose environmental concentrations have been increasing throughout modern human history due to anthropogenic releases. Awareness of the toxicity and bioaccumulative properties of organic Hg and the impact of anthropogenic emissions on global and regional cycling of Hg have made the international community acknowledge Hg as major pollution challenge. Recent studies (2000s) have shown that Hg is being transported to and deposited in Tibetan Plateau Glaciers by long range atmospheric transport and cold trapping effects. The Tibetan Plateau glaciers have had an overall negative mass balance throughout the last century. The main hypothesis initiating the work of this thesis was that melting glaciers are re-mobilizing historically deposited Hg and releasing it to glacier-fed (GF) streams. Furthermore, we focused on studying the dynamics and fractionation of Hg in a GF, remote, alpine catchment, for inorganic as well as for organic monomethyl Hg (MMHg).

Two sampling campaigns, in two adjacent valleys at Mt. Gongga, China, on the eastern edge of the Tibetan Plateau, were done during fall 2012 and spring 2013. The sampling times were selected to document late season melting and spring melting. The valleys sampled, Yanzigou (YZG) and Hailuogou (HLG), each have a GF main river in addition to several non-glacier-fed (NGF) tributary mountain streams. The stream waters were sampled for determination of total Hg (THg), MMHg, total suspended solids (TSS), total organic carbon (TOC) and various trace metals. Additionally, a peat bog core was collected, as well as stream sediments.

In fall 2012 THg concentrations were found at 1.3 ± 0.8 ng/L (mean ± one standard deviation) in GF streams and 0.5 ± 0.3 ng/L in NGF streams, whereas in spring 2013 THg concentrations were 2.5 ± 4.8 ng/L and 0.7 ± 0.5 ng/L in GF streams and NGF streams respectively. A significant difference ($p<0.01$) between GF and NGF streams in fall 2012 suggests the release of Hg by glacier related mechanisms. Contrary to the expectations of Hg release from the seasonal snowpack during spring melting, most of the GF sampling points had lower THg concentrations in spring 2013 than in fall 2012. However, there were indications that the timing of the spring field campaign was unfortunate, because the spring melting had not yet started at the time of the sampling. Two GF side rivers in the YZG valley, stemming from a glacier which probably was further ahead in the melting process, had THg concentrations of 13.2 ng/L and 19.3 ng/L. Statistical analysis suggests that these side rivers were releasing atmospherically deposited Hg (Hg_{atm}).

Hg in the GF streams was dominated by particle bound Hg (PHg); dissolved Hg (DHg) was found mostly below the limit of detection (LOD, 0.1 ng/L). In these streams THg was furthermore strongly correlated (R^2>0.9, p<0.001) to TSS, which suggests that the Hg in the GF streams might be primarily of geogenic origin. Statistical analysis gave the same impression for most of the GF sampling points, but the presence of Hg_{atm} from the glacier snow and ice could not be ruled out. MMHg samples from Mt. Gongga were found at very low concentrations in both GF and NGF streams; either below LOD (0.02 ng/L) or values up to 0.04 ng/L and thus do not constitute systems with a high potential for methylation. It is possible, however, that Hg from the streams of Mt. Gongga could end up in a system with higher potential for methylation, like areas represented by the peat bog in this study, where the MMHg fraction was found at 19% of the THg.

Sediments from the different stream systems at Mt. Gongga had low THg concentrations compared to estimates of the average crustal Hg content and unpolluted sediments found in other parts of the world. The sampled peat bog provided an estimated historic record of atmospheric deposition to the Mt. Gongga area, indicating a trend of atmospheric deposition following accordance with historical global atmospheric emission patterns.

Overall, this study served to provide data on the Hg dynamics of a GF, remote, alpine catchment and insights in how glaciers contribute Hg through meltwater to the stream systems below, both in the form of geogenic Hg from the bedrock beneath the glacier and from Hg_{atm} from the glacier snow and ice.

List of abbreviations

General abbreviations

ACAP	Arctic Council Action Plan to Eliminate Pollution of the Arctic
AMDE	Atmospheric mercury depletion events
BLK	Blank sample
BSE	Back scattered electron
CAS	Chinese Academy of Sciences
CCB	Continuing calibration blank
CCV	Continuing calibration verification
CHZ	CHZ bog
CRM	Certified reference material
CVAFS	Cold vapor atomic fluorescence spectrometry
DDH	Dadhing River
DI	De-ionized
DMA	Direct mercury analyzer
DOC	Dissolved organic carbon
EDS	Electron dispersive spectrometry
EF	Enrichment factor
GC	Gas chromatography
GF	Glacier-fed
HLG	Hailouguo valley
ICP-MS	Inductively coupled mass spectrometry
ICV	Initial calibration verification
ISO	International standardization organization
LOD	Limit of detection
LOQ	Limit of quantification
LRAT	Long range atmospheric transport
m.a.s.l.	Meters at sea level
MXH	Streams in the area around Moxizhen
NGF	Non-glacier-fed
NIVA	Norwegian institute for water research
NS	Norwegian standard
PC	Principal component
PCA	Principle component analysis
PMT	Photo multiplier tube
PTWI	Provisional tolerable weekly intake
QA	Quality control
QC	Quality assurance
RPD	Relative percent difference
RSD	Relative standard deviation
SE	Secondary electron
SEM	Scanning electron microscope
SRB	Sulfate-reducing bacteria
STD	Standard deviation
TOC	Total organic carbon
TSS	Total suspended solids
UIO	University of Oslo
UNEP	United Nations Environmental Program
USEPA	United States Environmental Protection Agency
WHO	World Health Organization
YZG	Yanziguo valley

Chemical compounds and fractions

Al	Aluminium
APDC	Pyrrolidine-1-dithiocarboxylic acid ammonium salt
Ar	Argon
Be	Berylium
BrCl	Bromine monoclhoride
$C_8H_{20}BNa$	Sodium tetraethylborate
Cd	Cadmium
Cl^-	Chloride
Co	Cobalt
DHg	Dissolved mercury
DMMHg	Dissolved monomethylmercury
DNOM	Dissolved natural organic matter
HCl	Hydrochloric acid
Hg	Mercury
Hg(I)	Inorganic mercury, oxidation state +1
Hg(0)	Elemental mercury, oxidation state 0
Hg(II)	Inorganic mercury, oxidation state +2
Hg_{atm}	Atmospherically deposited mercury
$HgCl_4^{2-}$	Mercuric chloride
Hg_{geo}	Mercury of a geogenic origin
HgS	Mercuric sulfide, Cinnabar
KI	Potassium iodide
KOH	Potassium hydroxide
MeHg	Methyl mercury
MMHg	Monomethylmercury
MMHgCl	Monomethylmercuric chloride
MMHgOH	Monomethylmercuric hydroxide
Mn	Manganese
Mo	Molybdenum
N_2	Nitrogen gas
NH_2OH-HCl	Hydroxylamine – hydrochloric acid
NOM	Natural organic matter
Ni	Nickel
NO_3^-	Nitrate
O_2	Oxygen gas
Pb	Lead
PHg	Particle bound mercury
S	Sulfur
$SnCl_2$	Stannous chloride
SO_4^{2-}	Sulfate
THg	Total mercury
Ti	Titanium
V	Vanadium
Zn	Zink

Table of Contents

List of figures

List of tables

1. Introduction

Mercury (Hg) is a toxic trace metal which is found naturally in the environment at low concentrations, but these concentrations have been increasing in all environmental compartments (water, soil, atmosphere) throughout modern human history due to anthropogenic emissions (UNEP, 2002). Wide areas of application have been found for the metal since ancient times (1500 B.C) in addition to Hg being a by-product of the combustion of fossil fuels and many industrial processes in modern times (Olmez & Ames, 1997). Recent awareness of the toxicity of Hg and the scale of the pollution has made the international community acknowledge Hg as major global, regional and local pollution challenge (UNEP, 2002).

Large amounts of research on the effects of Hg pollution, they cycling of Hg in soil, water and atmosphere, sources of the pollution and the chronic low dose toxicity of Hg have been done since awareness begun in the late 1950s (UNEP, 2002). Abatement actions and restrictions on use and emissions have led to lower emissions in Europe and North America, but industrial growth has led to increased emissions in Asia. Therefore, the total world emissions are still increasing (Pirrone et al., 2010). Furthermore the physiochemical properties of Hg make it available for long range atmospheric transport (LRAT) and thus global cycling (Schroeder & Munthe, 1998). Due to these facts, Hg is still an increasing global pollution issue.

As a result of LRAT and physiochemical mechanisms such as cold condensation, high wet deposition and enhanced springtime oxidation of atmospheric elemental Hg (Hg(0)), Hg has been found to deposit in Arctic and Antarctic snow and ice (Ariya et al., 2004; Ebinghaus et al., 2002; Lu et al., 2001; UNEP, 2002). In the Arctic, increasing concentrations of Hg has been found in aquatic sediments and the bioaccumulation of Hg in aquatic food webs has been documented (UNEP, 2002). During the last decade several studies have also documented deposition of atmospheric Hg to alpine glaciers as the result of mechanisms similar to those which occur in polar regions (Ferrari, Dommergue, Veysseyre, Planchon, & Boutron, 2002; J. Huang, Kang, Guo, et al., 2012; J. Huang, Kang, Zhang, et al., 2012; Q. Zhang et al., 2012). Alpine glaciers receive atmospheric Hg through LRAT, but also particle bound Hg (PHg) from regional sources such as large dust storms (J. Huang, Kang, Guo, et al., 2012). Alpine glaciers are sensitive to climatic warming and have the potential to release atmospherically deposited Hg (Hg_{atm}) upon glacier melting (Stern et al., 2012).

The purpose of this thesis was to study the dynamics of Hg in a remote, glacier-fed (GF) alpine catchment and to show that Hg_{atm} from glacier snow and ice is being released to the streams below due to glacier melting. This was done by sampling water from GF and non-glacier-fed (NGF) streams for the determination of total Hg (THg), monomethyl Hg (MMHg) and supporting parameters, i.e. total suspended solids (TSS), total organic carbon (TOC) and various trace metals. THg in GF and NGF streams were compared in order to identify the glacier contribution. Additionally, a peat bog core was collected as well as sediments from the various stream systems, in order to describe the historical atmospherical deposition of Hg and the background concentrations in the local environment.

Few studies have focused on the release of Hg to the meltwater of retreating glaciers and particularly so in alpine environments. Among these are two studies from the Antarctic (Lyons, Welch, & Bonzongo, 1999; Vandal, Mason, McKnight, & Fitzgerald, 1998) and two studies from alpine areas (Fu et al., 2010; Nagorski et al., 2014), where glacial Hg has been considered to some degree in the Hg dynamics of the studied areas. Furthermore, China is a large scale emitter of anthropogenic Hg and severe cases of Hg pollution have been documented in many regions of the country (UNEP, 2006). However, most studies in China have been focused on polluted sites which are affected by point sources and much less attention has been given to the effects of atmospheric Hg deposition in remote areas (Lin, Vogt, & Larssen, 2012). Therefore, this study will serve to document further the mechanisms of Hg release from melting alpine glaciers as well as providing information about the Hg dynamics of a remote, GF, alpine catchment in China.

The study area was chosen for this project because it features one of the highest mountains in China, Mt. Gongga (7556 m.a.s.l.); it holds large glaciers which are accessible at relatively low altitudes (around 3000 m.a.s.l.), and these glaciers have had a sustained mass loss throughout the last half of the previous century (Li et al., 2010). There is no point source pollution affecting the area, but the vegetation, soil and water of Mt. Gongga is a net sink for atmospheric Hg (Fu et al., 2010), so there is reason to believe that the glaciers at the Gongga range are accumulating atmospheric Hg in the same way as glaciers across the Tibetan Plateau (Q. Zhang et al., 2012). Additionally Mt. Gongga is reached by an eight hour bus ride from the province capital, Chengdu, which made travelling there feasible.

2. Theory

2.1 Mercury

Mercury (Hg) is a toxic heavy metal which due to its chemical and physical properties and wide use throughout human history has become a large environmental challenge for modern society, both locally and globally. Despite the metal's long history of use and known toxicity, awareness of its environmental impact started as late as the last half of the previous century. Since then, large amounts of research has been done to better understand the mechanisms of environmental cycling and the toxicity of Hg.

2.1.1 General properties

In an environmental context, Hg belongs to the trace metal category, which means that it is commonly found below concentrations of µg/g in a given environmental compartment (Manahan, 2005). The many species of Hg found naturally in the environment have diverse physiochemical properties, which lead to a highly varied behavior. Hg exists in three oxidation states: 0, +1 and +2. Elemental mercury (Hg(0)) is a liquid at standard temperature and pressure (1 atm, 273.15 K) and forms alloys called amalgams with noble metals (Ag, Au, Pd and Pt). Divalent mercury (Hg(II)), is the most common oxidation state for ionic Hg species, which are readily dissolved and will bind strongly with many inorganic and organic ligands. Monovalent mercury (Hg(I)) is highly unstable and not found to any great extent in the environment (Schroeder & Munthe, 1998). Organic Hg is the most toxic Hg specie and will be discussed more in section 2.3.4 and 2.4. Hg is considered a type B metal, due to its high polarizibility. Metals are categorized as type A or B depending on how stable complexes they form with different type of ligands. Type B typically have high ionization potentials and form the most stable complexes with ligands with low electronegativity. This means that Hg will form the strongest complexes with sulfur-ligands (Stumm & Morgan, 1996).

2.1.2 History

Hg has been known to humans and used for various purposes for several millennia. The metal has been found in Egyptian tombs from as early as 1500 B.C and was known to ancient Greeks, Chinese and Hindus. Historically, Hg has been used medicinally, for artisanal crafts and in industry, but the most widespread use has been in relation to mining. Hg's ability to

form amalgams with precious metals, such as gold and silver, has been exploited as an effective way of separating the valuable metals from their ores since 500 B.C and is still in use today (Olmez & Ames, 1997).

The toxicity of Hg was recognized as early as by the Romans, who would use slaves and prisoners to work the Hg mines of Almadén, Spain. Medicinally the metal was used as an antiseptic and in the treatment of syphilis and was not thought to affect humans in the small amounts used for this purpose. With increased use the symptoms of Hg's toxicity became more common. "Mad hatter's disease" stemmed from the use of mercuric nitrate in the making of felt hats and is one well known, historical example of occupational Hg poisoning. The Minamata disaster (1953-56) marks the beginning of modern awareness. Wastewater from a chemical plant, using Hg salts as catalysts, contaminated the fish in the shallow Minamata Bay. The fish, which was the cornerstone of the local communities' diet, ended up killing 52 people while poisoning over 700 only the first year of the tragedy and many more in the following years (Olmez & Ames, 1997). Since then much scientific effort has been put into documenting and understanding Hg-pollution and its impact on humans and the environment, and increased political awareness has led to abatement actions and restrictions on emission and the use of Hg (UNEP, 2002). As recent as last year, a new international convention on Hg was agreed, "The Minamata Convention on Mercury," which includes: a ban on new Hg mines and a phasing out of old ones; control measures on air emissions and international regulations for the informal sector for artisanal, and small-scale gold mining (UNEP, 2013).

2.2 Sources of mercury in the environment

2.2.1 Mercury in the environment

Hg is present in all environmental compartments; soil, water and the atmosphere (Olmez & Ames, 1997). The average Hg content of the upper continental crust has been estimated to 56 µg/kg (Wedepohl, 1995). Significant deposits of Hg-containing minerals are mainly found in a few Hg belts around the world, including: Almadén, Spain; Idrija, Slovenia; Amiata, Italy; Huancavelica, Peru and New Almadén and New Idrija, California, USA. Smaller mineral deposits are also located elsewhere in the world, e.g. in Guizhou, China (Rytuba, 2003). Concentrations of Hg in ocean waters vary between 0.1–3 ng/L for open ocean water and 2–

15 ng/L for costal sea water (Lindqvist, 1985; Outridge, Macdonald, Wang, & Stern, 2008). Hg in freshwater is generally found in the range 1-3 ng/L (Lindqvist, 1985). The global atmospheric background has been found to differ between the two hemispheres: 1.5–1.7 ng/m^3 in the northern hemisphere and 1.1–1.3 ng/m^3 in the southern hemisphere (Ebinghaus et al., 2002; Slemr et al., 2003; Temme, Ebinghaus, Einax, Steffen, & Schroeder, 2004).

2.2.3 Natural sources

Natural processes contribute largely to the total emission of Hg to the atmosphere, primarily in the forms of evaporation from soils/minerals, vegetation and water and from vapors and particles released from volcanic activity and wildfires. Evaporation from oceans is the largest source (36%), followed by biomass burning (9%) and evaporation from deserts and non-vegetated zones (7%), tundra and grasslands (6%) and forests (5%). Volcanic eruptions are sporadic and therefore do not provide a high average contribution (2%) (Pirrone et al., 2010). Estimating the contribution from natural emissions is, however, very complicated, the reason being the challenge of distinguishing primary emission and secondary re-emission (Olmez & Ames, 1997). Therefore estimates of natural emissions include re-emissions. A recent study based on emission numbers from 2008 estimated the yearly contribution from natural sources to be 5207 tonne/yr (Pirrone et al., 2010).

Natural emissions also come in point source format, from areas which are naturally rich in Hg minerals, such as the Hg belts described in section 2.2.1. Here mechanisms of evaporation, erosion and dissolution release Hg to the surrounding atmosphere, soil and water (Rytuba, 2003).

2.2.2 Anthropogenic sources

Anthropogenic Hg emissions are largely produced by the combustion of coal and other fossil fuels, but mining activities, ore processing, the production of cement, waste incinerators and chemical production plants (e.g. Chlor-Alkali Plants) also contribute large shares. Hg is not highly concentrated in coal or other fossil fuels, but the sheer scale of fossil fuel consumption makes this the most influential source. Artisanal small scale gold mining is the second largest source. Miners mix the ore with elemental Hg to amalgamate noble metals and the amalgam is subsequently heated, releasing all the Hg as vapor. Emissions from cement production are due to the release of Hg trapped in limestone, which is consumed in large amounts during the

production process. Mining for Hg-minerals and the subsequent processing of the ores have gone on for millennia, causing both local point source emissions and contributions to the global atmospheric emission. The processing of various other metal ores also releases mercury, concentrated in the mineral along with the metal of interest, as a by-product. Hg in different types of waste is released to the atmosphere when the waste is burned in incinerators without Hg removal technology (Pirrone et al., 2010).

Since industrialization, the global deposition of Hg to the environment has increased by a factor of 3 ± 1 (mean ± one standard deviation). Despite the fact that natural emissions contribute about 70% of the total emissions of Hg to the atmosphere today; the anthropogenic contribution of about 30% is causing an increase of Hg in the environment (Lindberg et al., 2007). Table 2.2.2-1 shows the anthropogenic emission contribution from the different processes discussed in tonne/yr.

Table 2.2.2-1: Global Hg-emission from anthropogenic sources, adapted from Pirrone et al. (2010)

Source category	**Hg-emission (tonne/yr)**
Coal and oil combustion	810
Non-ferrous metal prod.	310
Pig iron and steel prod.	43
Cement production	236
Chlor-Alkali plants	163
Artisanal gold mining	400
Waste disposal	187
Coal bed fires	32
VCM production	24
Other	65
Total	**2320**

Anthropogenic emissions in Europe and North America were declining between 1985 and 2005 due to abatement actions taken and restrictions enforced by national and regional authorities. During the same period of time an opposite trend was seen in Asia due to heavy industrial expansion (ACAP, 2005). Among the Asiatic countries, China is the largest emitter of anthropogenic Hg, contributing as much as 609 tonne/yr (26%) of the world total. The largest fraction of the Chinese emissions (44%) is contributed to the burning of coal (Pirrone et al., 2010). These heavy anthropogenic emissions have led to Hg being an environmental pollutant of primary concern in China today.

2.3 Speciation and cycling of mercury

2.3.1 Mercury speciation in water

Hg is present in water in all three oxidation states (0, +I and +II). Hg(I), however, is only stable as a dimer, and is readily converted to Hg(0) and Hg(II), the most stable forms in water (Ullrich, Tanton, & Abdrashitova, 2001). Dissolved Hg(0) constitutes about 10-30% of Hg in water and is supersaturated compared to atmospheric concentrations, mainly due to microbial conversion of Hg(II) to Hg(0) (Vandal, Mason, & Fitzgerald, 1991). Hg(II) complexed with a variety of organic- and inorganic ligands, are the dominant species in water, in addition a smaller amount of the organic methylmercury (MeHg), which is mainly composed of MMHg and dimethylmercury (DMHg) (Ullrich et al., 2001). MeHg usually accounts for less than 10% of the THg (Lin et al., 2012). Both Hg(II) and the methylmercuric cation (CH_3Hg^+) have a tendency to form complexes with soft ligands such as sulfur, but also with hydroxides and chlorides (Ullrich et al., 2001). In seawater Hg exists primarily as mercuric chloride ($HgCl_4^{2-}$) (Olmez & Ames, 1997).

Positive correlations documented between dissolved natural organic matter (DNOM) and Hg in many types of natural waters along with an increasing amount of other evidence, indicate that there are strong interactions between Hg and DNOM. Hence, DNOM affects Hg speciation, transport and mobility in water. Strong ionic bonds are believed to be formed between Hg and reduced sulfur groups in the DNOM-molecules. Such strong complexation has the potential to facilitate mobilization and transport of Hg from natural sources in soil or sediments or from polluted sites into bodies of water (Ravichandran, 2004).

2.3.2 Mercury speciation in the atmosphere

Mercury exists in the atmosphere as gaseous Hg(0), gaseous or dissolved Hg(II) and suspended PHg. The relatively inert and nearly non-soluble Hg(0) constitutes 90% of the Hg in the atmosphere. Gaseous Hg(II) is a reactive specie which readily undergo chemical reactions or dissolution in water in the atmosphere. PHg can be either Hg(0) or Hg(II) adsorbed to an aerosol, but a distinction is rarely made when discussing PHg. The aerosol can be anything from suspended dust and sand to fly ash, salts or organic carbon. It is the dominance of the gaseous Hg(0) which gives Hg such a unique behavior in the atmosphere

compared to other metals, which are mainly associated with aerosols and thus have a much shorter residence time (Schroeder & Munthe, 1998).

2.3.3 Mercury speciation in sediments and soils

In soils and sediments, Hg is mainly present as divalent Hg(II) in inorganic salts and minerals, but also as the alkylated organic compounds – MeHg (UNEP, 2002). MeHg usually constitutes less than 1% of THg in soils, but MeHg in boreal forest peat has been found to exceed 10% in some cases (Lin et al., 2012). There are more than 25 known Hg-containing minerals in the earth's crust, but Cinnabar (mercuric sulfide, HgS) is by far the most abundant (Schroeder & Munthe, 1998).

In soils and sediments Hg is also found to be positively correlated with natural organic matter (NOM). In the same way as described for an aqueous environment in section 2.3.1, Hg is bound strongly by reduced sulfur groups in NOM molecules in soils or sediments. Soils or sediments which are rich in NOM thus have a naturally high retention for trace metals such as Hg. However, during flooding events or high precipitation, NOM with complexed Hg can dissolve in water and facilitate the transport of Hg into rivers or lakes (Ravichandran, 2004).

2.3.4 Organic mercury – methylation and de-methylation

Organic Hg is formed when methyl groups are added to inorganic- or elemental Hg (Ullrich et al., 2001). Often, a distinction between MMHg and DMHg is not made; MeHg, which constitutes both MMHg and DMHg, is the most widely used term. MMHg, however, is the specific specie detected in the analytical standard for MeHg determination (USEPA, 1998). Here, the term "MeHg" will be used to discuss the total organic Hg fraction and "MMHg" only when specified that it is the actual monomethyl specie being discussed.

Wetlands and fresh water lake sediments with reducing conditions have long been thought to be hot spots for methylation and thereby net sources (Benoit, Gilmour, Heyes, Mason, & Miller, 2003; Hall, Aiken, Krabbenhoft, Marvin-Dipasquale, & Swarzenski, 2008; Ullrich et al., 2001; Warner, Roden, & Bonzongo, 2003), but newer studies show that MeHg is also found in precipitation and rivers in well drained forest areas, suggesting more complex dynamics at play (Larssen, de Wit, Wiker, & Halse, 2008).

A large and growing body of data suggests that there are many factors that influence the methylation process: the presence of microbes, DNOM, redox conditions, pH, nutrients, complexing ligands, demethylation rates and the availability of inorganic Hg. In general methylation seems to be favored under reducing conditions with good access to inorganic Hg and various nutrients. Therefore, methylation takes place predominantly in the top layers of sediments or the sediment-water interface, but methylation in the water column should not be underestimated, as the total volume of water is usually large compared to the volume of surficial sediments (Ullrich et al., 2001).

The methylation process requires a suitable methyl-group donor, which is not readily found outside aquatic biota. Abiotic methylation is possible, but only happens in a minor scale compared to biotic methylation, as bacteria synthesize a large variety of methyl-group donors (Ullrich et al., 2001). Sulfate-reducing bacteria (SRB) have been shown to be the main methylators in anaerobic sediments, soils and bottom waters, along with a possible contribution from iron-reducing bacteria (Benoit et al., 2003; Compeau & Bartha, 1985). In SRB the methylation process is believed to be enzyme catalyzed and therefore oxygen sensitive as well as pH and temperature dependent (Ullrich et al., 2001). A recent study has now also shown that several other microorganisms, such as methanogens and syntrophic, acetogenic, and fermentative Firmicutes, have the capability of Hg methylation (Gilmour et al., 2013).

Methylation and de-methylation occur continuously in the environment, thus the total concentration of MeHg is controlled by net-methylation rates (Ullrich et al., 2001). Abiotic and biotic de-methylation both occur, but the photo-degradation of MeHg has been singled out as the most important process governing demethylation in aquatic environments (Black, Poulin, & Flegal, 2012; Lehnherr & St. Louis, 2009; Seller, Kelly, Rudd, & MacHutchon, 1996). The actual process of MeHg photo-degradation is not fully understood, but several factors influence the process, such as radiation, DNOM, salinity, photo active trace metals and more. Ultra violet (UV) and visible light both drive the process, while DNOM is believed to have a double role; absorbing radiation, which otherwise could have partaken in the de-methylation, and facilitating/catalyzing the demethylation process, through a yet unknown mechanism (Black et al., 2012). Aerobic bacteria, methanogens in particular, appear to be the most important biotic contributors to the MeHg degradation in the water column and sediments. As methylation and partly de-methylation are mediated by microbes, the

availability of nutrients is yet another important factor governing net-methylation (Ullrich et al., 2001). Furthermore, the presence of organic carbon has been shown to have a general positive effect on communities of methylating and de-methylating bacteria (Macalady, Mack, Nelson, & Scow, 2000).

Different landscapes will therefore have unique potentials for net-methylation depending on the complex mixture of all the parameters mentioned above. This concept is exemplified when looking at Hg concentrations in fish in the Yangtze River (MMHg is usually accounts for 72 – 100% of THg in fish), which has a history of point source pollution of Hg. As counterintuitive as it may seem, the fish in the Yangtze has quite low THg concentrations compared to fish from remote rivers in Tibet (Lin et al., 2012).

2.3.5 Global mercury cycles

Hg is involved in complex cycling between all environmental compartments; soils and minerals, water and atmosphere. Globally, Hg is cycled mainly through the atmosphere and ocean currents (UNEP, 2008), and here the focus will be on atmospheric emission-to-deposition since this study is concerned with a high altitude, alpine environment. Figure 2.3.5-1 shows a conceptual framework of the emission to deposition cycle of Hg in the atmosphere.

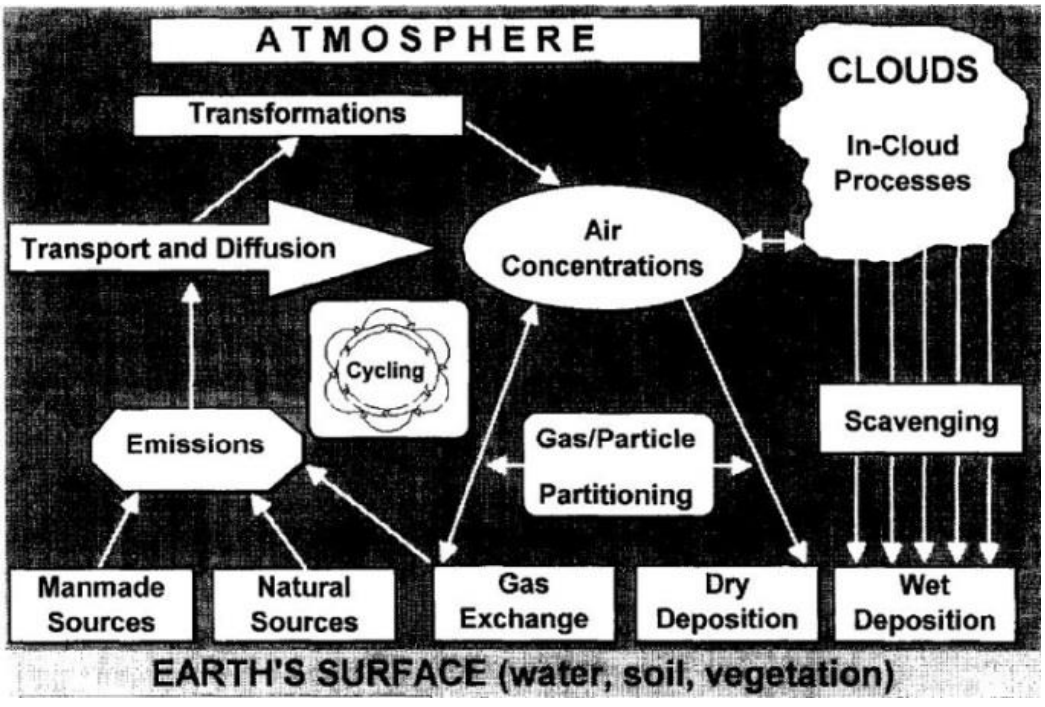

Figure 2.3.5-1: Emission to deposition cycle for mercury, conceptual framework (Schroeder & Munthe, 1998).

Hg has a long residence time in the atmosphere, 0.5-2 yrs, and is thus prone to long range atmospheric transport (LRAT) and global cycling. The long residence time is much owing to the dominating atmospheric Hg specie being gaseous Hg(0). Hg(0) does not readily undergo deposition in temperate and warm regions due to its vapor pressure. Cold regions, however, such as the Arctic and Antarctic, can act as sinks for Hg(0) through the cooling and subsequent settling of the gas – a cold trapping effect. Furthermore, Hg(0) can be oxidized to Hg(II) (e.g. by ozone, hydroxyl radicals and bromine radicals) in the atmosphere or be adsorbed to aerosols. In either of these two forms, (Hg(II) and PHg), Hg is highly available for both wet- and dry deposition (UNEP, 2008). Cold regions can exhibit large amounts of precipitation leading to elevated wet deposition; efficiently scavenging aerosols from the atmosphere (Sakata & Asakura, 2007). Another mechanism of transport of Hg to polar regions, a global distillation effect of alternating deposition to re-emission, has been suggested for Hg due to its volatile properties (Mackay, Wania, & Schroeder, 1995). Such a behavior has been shown for semi-volatile organic compounds, but for Hg, deposition and re-emission is dependent on redox transformations that make modelling and monitoring more complicated (O'Driscoll, Rencz, & Lean, 2005).

The accumulation of Hg in the Arctic and Antarctic has in the recent past been confirmed by a large amount of studies (UNEP, 2008). Berg et al. (2001), Lahoutifard, Sparling, and Lean (2005) and Lu et al. (2001), amongst some, have all reported higher concentrations of Hg in the Arctic than what is expected from natural background contributions. A much studied phenomenon in recent years, which also lead to high deposition of atmospheric Hg in Polar Regions, is atmospheric mercury depletion events (AMDE). Documented both in the Arctic and Antarctic, events of Hg concentrations in the atmosphere being strongly depleted with a concurrent increase of Hg in snow, have been recorded during the three first months after the polar sunrise (Ebinghaus et al., 2002). It is believed that these events are associated with a photochemical oxidation of Hg(0) to Hg(II), by bromine radicals involved in complex radical chain reactions, making Hg more available for deposition (Steffen et al., 2008).

2.4 Toxicity

The toxicity of Hg varies greatly with its chemical form along with the mode of exposure. Hg(0) is most harmful to humans when inhaled in the gas form and the dangers of exposure

are mainly linked to industrial- or mining processes involving Hg fumes. However, dental amalgam has recently been dubbed as a relevant source of human exposure to Hg fumes. Hg(0) is a well-known neurotoxicant as it is readily absorbed by lung tissue and easily penetrates the blood-brain barrier. The major source of inorganic Hg is through food and water. It is not accumulated in the body, but can cause damage to the gastro-intestinal tract as it passes through (UNEP, 2002).

MeHg is the most toxic form of Hg to humans and the main mode of exposure is through diet; fish and seafood in particular. MeHg is also a well-documented neurotoxicant, as it passes the blood-brain barrier and is especially known have harmful effects on the developing brain. In addition, MeHg passes the placental barrier, making exposure to pregnant women and the developing fetus a major concern. Humans and other predators high up in the food chain are particularly prone to high level MeHg exposure as it bioaccumulates (Zahir, Rizwi, Haq, & Khan, 2005). MMHg is believed to be the primary bioaccumulative specie, especially in freshwater organisms, as DMHg is a volatile specie which is often lost from water through evaporation or is readily decomposed (Ullrich et al., 2001). Relatively small concentrations of MeHg in water or soil can be bioconcentrated for every trophic transfer and thus lead to dangerously high biotic concentrations at the top of the food chain (Zahir et al., 2005).

The World Health Organization has set provisional tolerable weekly intake (PTWI) of THg to 5.5 µg/kg body weight of which MMHg should not be more than 3.3 µg/kg body weight. The drinking water limit for THg is set at 1 µg/L (WHO, 2004).

2.5 Mercury in alpine glaciers

2.5.1 Deposition of mercury to alpine glaciers

As explained in section 2.3.4, Hg tends to accumulate in cold regions, like the Arctic and Antarctic, due to cold condensation mechanisms and scavenging by snow and rain. Recent studies have shown that cold mountain regions of high altitudes and their respective glaciers also act as a cold traps for atmospheric Hg. The THg concentrations in the snowpacks of a number of glaciers across the Tibetan Plateau were found to range between <1 and 43.6 ng/L (J. Huang, Kang, Zhang, et al., 2012; Loewen et al., 2007; X. P. Wang, Yao, Wang, Wei, & Tian, 2008; Q. Zhang et al., 2012). Snow samples collected from the French Alps show

further evidence of altitudinal accumulation, as THg was found to range between 13-130 ng/L (Ferrari et al., 2002). The THg concentrations found in the glacier snow are approximately in the same range as THg concentrations found in the European- and Canadian Arctic (Berg et al., 2001; Lu et al., 2001). Table 2.5.1-1 shows a comparison of THg concentrations found in the studies cited above.

Table 2.5.1-1: The range of THg concentrations found in snowpack samples from alpine glaciers and remote arctic regions.

Region	**THg (ng/L)**	**Source**
Tibetan Plateau	<1 - 9	(Loewen et al., 2007)
Tibetan Plateau	2 - 35	(X. P. Wang et al., 2008)
Tibetan Plateau	<1 - 43.6	(Q. Zhang et al., 2012)
Tibetan Plateau	<1 - 15	(J. Huang, Kang, Zhang, et al., 2012)
French Alps	13-130	(Ferrari et al., 2002)
European Arctic	3-30	(Berg et al., 2001)
East Canadian Arctic	25-160	(Lu et al., 2001)
West Canadian Arctic	2.2	(Lu et al., 2001)

The concentrations of Hg in high mountain glaciers also show an altitude gradient, with the highest concentrations at the highest altitudes (J. Huang, Kang, Zhang, et al., 2012), further suggesting an altitudinal cold-trapping effect of Hg. An altitude gradient for Hg has also been found in montane soils as a result of several mechanisms, with weather related phenomena such as cloud cover, wind conditions and precipitation being some of these (H. Zhang et al., 2013).

2.5.2 Release of mercury to runoff from alpine glaciers

Stern et al. (2012) note, that Hg accumulated in glaciers can be stored for decades or millennia, largely depending on the size and turnover time of the glacier in question. However, if the climate warms, premature release of stored contaminants due to rapidly melting glaciers can happen. Furthermore, alpine glaciers have a faster response time to climatic change than polar glaciers, making them high impact areas. A number of studies have already shown how legacy persistent organic pollutants are released from melting alpine glaciers in the Canadian Rocky Mountains, the Swiss Alps and the Italian Alps (Blais et al., 2001; Bogdal et al., 2009; Schmid et al., 2010; Villa, Negrelli, Finizio, Flora, & Vighi, 2006).

Figure 2.5.1-1 shows how more Hg stored in glacier ice can be released upon an increase of temperature. The ablation area is usually the lower elevation part of a glacier which has a net mass loss per year. The ablation area increases proportionally with the temperature causing ice melt from older layers and runoff from the melting of the firn zone and upper layers (Stern et al., 2012).

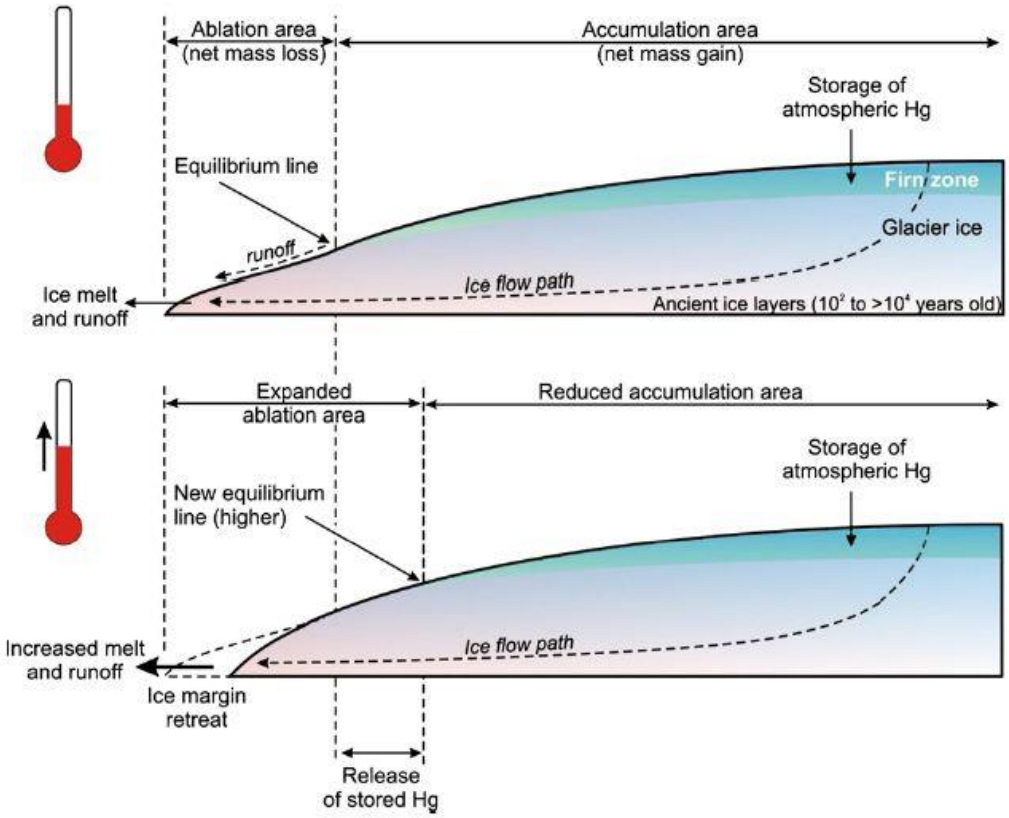

Figure 2.5.1-1: Schematic figure of Hg release from a glacier, illustrating the effect of temperature change on ablation area, accumulation area and melt and runoff (Stern et al., 2012).

Hg_{atm} can only be stored over time if a glacier has a net accumulation area; an area which has a net addition of mass per year (the opposite of the ablation area). Hg stored in the ablation area will be released by melt and runoff during the same year. As the ablation area increase with temperature, more of the legacy Hg from older ice layers will be released along with the annual deposited Hg in the snow pack (Stern et al., 2012).

During the first few days of snowmelt, a large amount of the total ions in the seasonal snowpack are released in an "ionic pulse." Hg has been found to be a part of this pulse; depletion of more than 90% of Hg present in surface snow during a day of snowmelt has

been observed in a sub-arctic site along Hudson Bay, Canada (Dommergue et al., 2003). Consequently, Hg is bound to be depleted from the seasonal glacial snow cover and released to meltwater. The release of legacy Hg from older ice layers will vary according to which layers being subject to melting. Stern et al. (2012) hypothesize, that legacy Hg release will peak in the near future and then decline as the melting of prehistoric ice layers commence.

The last 40 years have seen an estimated loss of 500 km^3 glacier mass on the Tibetan Plateau (TP), which approximates to 450 km^3 of water (Yao et al., 2004). Q. Zhang et al. (2012) used this estimate along with a THg concentration of 5.6 ngL^{-1} (the average concentration of nine sampled glaciers) to make an approximation of the amount of Hg released from TP glaciers to meltwater-fed catchments below; a total of 2.5 tonne in 40 years.

Thus far evidence suggests that alpine glaciers could serve as highly relevant sources of Hg to their respective catchments. However, very few studies have actually documented the amount of Hg in meltwater from alpine glaciers. As a part of a Hg-budget of a remote upland forest, Fu et al. (2010) measured the contribution of Hg from glacial melt water to the total flux of Hg in the area. Nagorski et al. (2014) looked at contributions of Hg to Alaskan streams from different landscape types, with glacierized landscape being one of these. Both studies confirm glacier release of Hg to melt water, but the data gathered is not extensive enough to get a detailed picture of the processes involved. More studies are needed to fully understand the dynamics of Hg release from alpine glaciers to meltwater-fed rivers.

2.6 Analytical principles

2.6.1 The MERX Total-Hg Purge and Trap with CVAFS

All water samples to be analyzed for THg are added bromine monochloride (BrCl) as a preservation/pre-oxidation step which oxidizes Hg(0), strongly organo-complexed Hg(II), several covalent organo-Hg species and Hg adsorbed to particles to free Hg(II) in solution. Analysis pre-treatment includes the reduction of free halogens, which are known interfering species, with hydroxylamine-hydrochloric acid (NH_2OH-HCl) and then reduction of all aqueous Hg species to gas phase Hg(0) by stannous chloride ($SnCl_2$) (USEPA, 2002).

Vapor phase Hg(0) is purged and carried from sample vial to sorb on an amalgamation trap by nitrogen carrier gas (N_2). Subsequent heating of the amalgamation trap desorbs Hg(0) which is then carried by an inter argon gas (Ar) to a cold vapor atomic fluorescence spectrometer (CVAFS). A dual set of traps is included to increase throughput as sample-2 can sorb on trap-Y while sample-1 is desorbing on trap-X. The CVAFS unit has a UV-light source (253.7 nm) irradiating the Hg vapor which absorbs and fluoresces at 253.7 nm. The atomic fluorescence is detected by a photo multiplier tube (PMT) placed perpendicular to the UV-light path. The PMT converts incident photons to a current which is recorded and converted to units of concentration through a calibration curve by the system software (Brooks-Rand-Labs, 2012b).

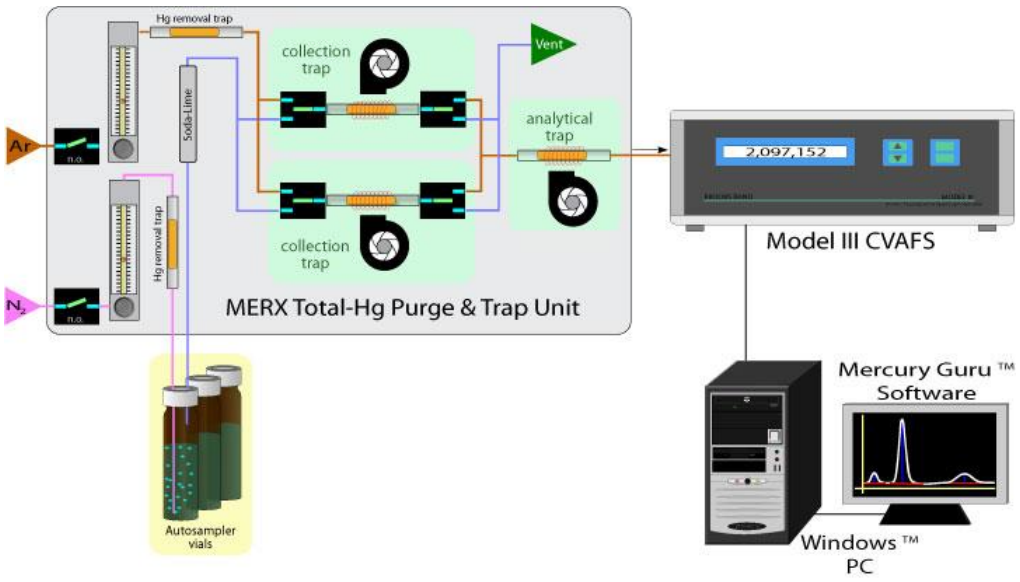

Figure 2.6.1-1: Instrument schematic of the MERX Total-Hg Purge and Trap with CVAFS (Brooks-Rand-Labs, 2012b).

2.6.2 The MERX Methyl-Hg Purge and Trap, GC and pyrolysis with CVAFS

Sample pre-treatment before the MMHg analysis in water samples includes distillation and ethylation (USEPA, 1998). If aqueous samples are ethylated directly, only "reactive" MMHg is released, accounting for only 5-60% of the total MMHg (Horvat, Liang, & Bloom, 1993). This is because species such as chloride interfere with the ethylation while organic matter, inorganic particles and sulphides inhibit the ethylation through complexation and binding of MMHg (Bloom, 1989; Horvat et al., 1993). Pyrrolidine-1-dithiocarboxylic acid ammonium salt (APDC), a complexing agent, is therefore added to competitively complex all the MMHg in the water sample. Distillation at 125 °C under a N_2 flow purges semi-volatile APDC-

complexed MMHg and water vapor from the sample distillation vial to a new vial, leaving the interfering species behind. MMHg in the distillates is ethylated with sodium tetraethyl borate (NaBEt4) in a closed, oxygen free vessel at pH 4.9 (USEPA, 1998).

Volatile ethyl-MMHg is purged from solution with N_2 and sorbed onto a polymer resin trap (Tenax®). Ethyl-MMHg is thermally desorbed from the Tenax® trap and carried by an inert gas (Ar) to a GC-column where the Hg-species are separated at 36 °C. The instrument has a triple Tenax® trap setup which allows for simultaneous sorption, trap drying and trap desorption for three separate samples, to increase sample throughput. After separation, ethyl-MMHg is decomposed to Hg(0) in a pyrolytic column at 700 °C. The Hg(0) vapor is then passed into a CVAFS for detection (Brooks-Rand-Labs, 2012a).

2.6.3 Direct Mercury Analyzer (DMA-80)

The Direct Mercury Analyzer (DMA-80) is an instrument based on sequential steps of high temperature combustion of a liquid or solid sample, to release all Hg as vapor, accumulation of the vapor on an amalgamation trap, re-release of the vapor and detection by CVAFS (figure 2.6.3-1) (Milestone, 2002).

No sample pretreatment is required as a sample is added directly into thermally stable and non-amalgamating Ni sample boats, which are introduced directly into a decomposition furnace. O_2 flow, fuels the thermal decomposition (750°C) of the sample and carries the released Hg to an amalgamator where it is accumulated. Other gasses from the combustion are further decomposed in a catalyst furnace between the decomposition and amalgamator chambers. In the next step, the amalgamator is heated and the accumulated Hg re-released as Hg(0) and passed through two quartz absorption cells, which are situated in the light path of a Hg-vapor lamp (253.7 nm). The two cells have different lengths; strong signals are recorded first in the cell with the longest pathway, but if the signal is too weak another measurement is made in the next cell with a shorter pathway. This allows for a longer linear range of detection, as the DMA-80 can be calibrated in two different concentration ranges, represented by the two cells. The detector is a Si-photodiode sensor which converts the incident photons to a current which is registered by the machine's software and converted to a unit of concentration through the calibration curve by the system software (USEPA, 2007b).

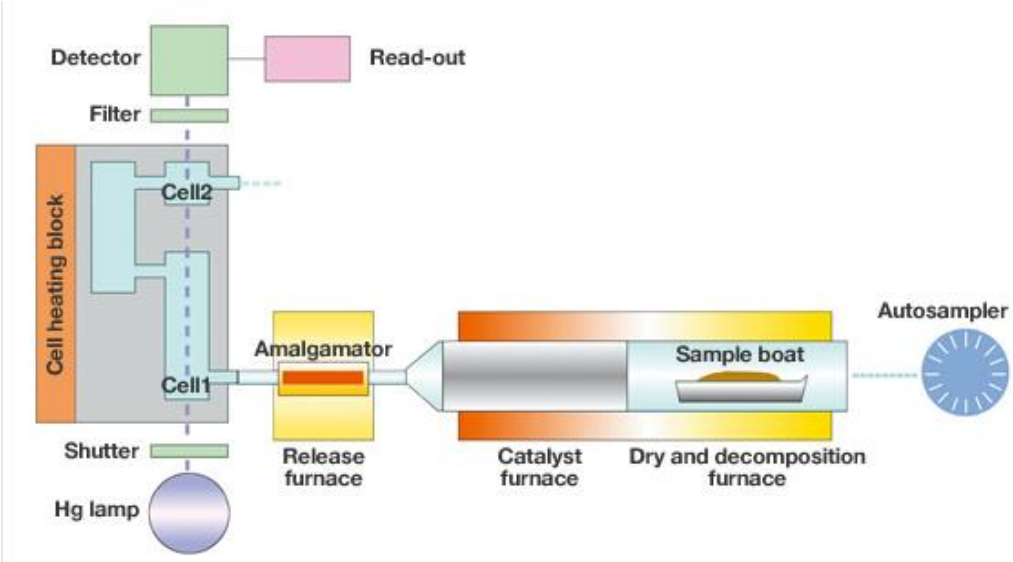

Figure 2.6.3-1: Instrument schematic of the DMA-80 (Jens-Molecular-and-Nanoscale-Analysis-Laboratory)

2.6.4 Scanning electron microscope with energy dispersive spectroscopy

A scanning electron microscope (SEM) image is compiled, pixel by pixel, as an electron beam scans a specimen, frame by frame. As the electron beam hits a discrete area of the specimen surface several processes takes place (figure 2.6.4-1), giving rise to the different types of signals which are compiled to produce the SEM image (Leng, 2008).

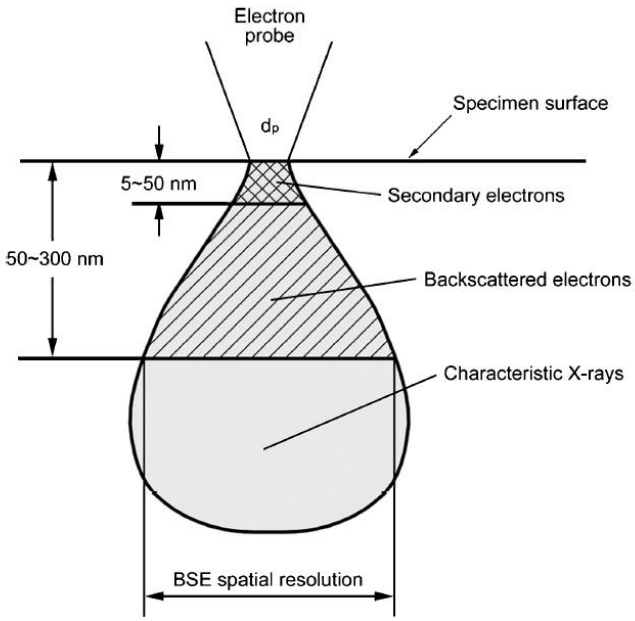

Figure 2.6.4-1: Near surface cross section of a SEM sample specimen, showing interactions of incident electrons with the atoms at- and below the specimen surface (Leng, 2008).

Back scattered electrons (BSEs) are the incident electrons which are elastically scattered by the atoms in the surface layers of the specimen. Heavy elements produce heavy scattering and thus strong signals, which again result in lighter pixels. Lighter elements on the other hand, scatter incident electrons more lightly and give darker pixels due to the weaker signals. Due to these specific characteristics, BSEs are used to produce images with elemental composition contrast (Leng, 2008). Secondary electrons (SEs) from of inelastic scattering processes can also be used to produce images with topographic contrast, but such images were not needed for this study.

The SEM instrument can also set up with energy dispersive spectroscopy (EDS) to detect x-ray photons emitted from the specimen. X-ray photons are produced when SEs are ejected from their orbitals and electrons in higher orbitals relax to fill the empty gaps left by the SEs. The relaxation transition produces excess energy in terms of x-ray photons which are highly element specific. Detecting the x-rays and relating them to the element specific orbital transition gives information about the chemical composition of the specimen (Leng, 2008).

3. Materials and methods

3.1 Study area and sampling procedures

3.1.1 Mt. Gongga

Mt. Gongga (English), Gongga Shan (Chinese) or Minya Konkar (Tibetan) is located in the central part of the Sichuan province, China, at 30^0 N, 102^0 E (figure 3.1.1-1). Mt. Gongga is the highest peak in the Daxue Shan range at 7556 m.a.s.l, which constitutes the first major mountain range between the low South Chinese plains and the Tibetan Plateau (Thomas, 1999).

Figure 3.1.1-1: Mt. Gongga range, China. Showing the YZG and HLG valleys (images adopted from Google Earth).

The eastern side of the Gongga range has a drop in altitude of more than 6300 m across a mere 11 km; from the peak of Mt. Gongga to the Dadu River at the foot of the mountain. This large elevation change creates a drastic gradient between the subtropical lowland climate eastwards and the cool plateau climate west of the range. The mountain is clad by dense forest that start out as evergreen and broad leaved forests, and change gradually to coniferous forests and eventually shrubs, meadows and grasses above the tree line around 3200 m.a.s.l. (Thomas, 1999).

The peaks in the Gongga range are covered with glaciers which contribute significant amounts of water, through runoff, to the catchments on the eastern side of the range. The Hailuogou glacier, southeast of the Mt. Gongga peak, is estimated to have undergone a retreat of 24 m/yr since the 1930s (Li et al., 2010) and similar changes are expected to occur at the other glaciers in the range as most glaciers in Northwestern China have seen negative mass balances over the course of the last century (Yao et al., 2004).

3.1.2 Study area and sampling points

The two main valleys on the eastern face of the mountain, Hailuogou (HLG) and Yanzigou (YZG) (figure 3.1.2-1), have roads making the ascent from Moxizhen, a small village at the foot of the mountain (1675 m.a.s.l.), up through each valley to about 3000 m.a.s.l. possible by car. Each valley has a central glacier-fed (GF) river running down the length of the valley, joined by several non-glacier-fed (NGF) tributary mountain streams coming down along the valley ridges. The YZG valley has a more or less constant elevation gradient; rising slowly from the foot of the mountain up to the glacier fronts. The road runs close to the river most of the way, making sampling conditions ideal. HLG has a steeper elevation gradient however, but the main GF river is accessible from the road through hikes of various lengths at several points throughout the valley. The lower glacier front in HLG is reached by an hour-long hike along a forest trail from where the road ends. A gondola takes one up above the lower glacier to 3600 m.a.s.l., where it is possible to follow another GF stream up towards the upper glaciers, but the high altitude, the steep slope and the ravine-like landscape makes the climb hazardous.

Due to the size of the main rivers, the lack of bridges, steep slopes and dense forest the sampling was limited to accessible sampling points on the same side of the valley as the road. The amount of sampling points was not only limited by accessible locations, but also by the amount of samples possible to take back to Norway. Therefore, a selection of sampling points was chosen as a compromise of accessibility and an even spatial distribution, as shown in figure 3.1.2-1. The distribution of the sampling points within the different systems, GF, NGF, HLG, YZG etc., is summarized in appendix A, table A-3.

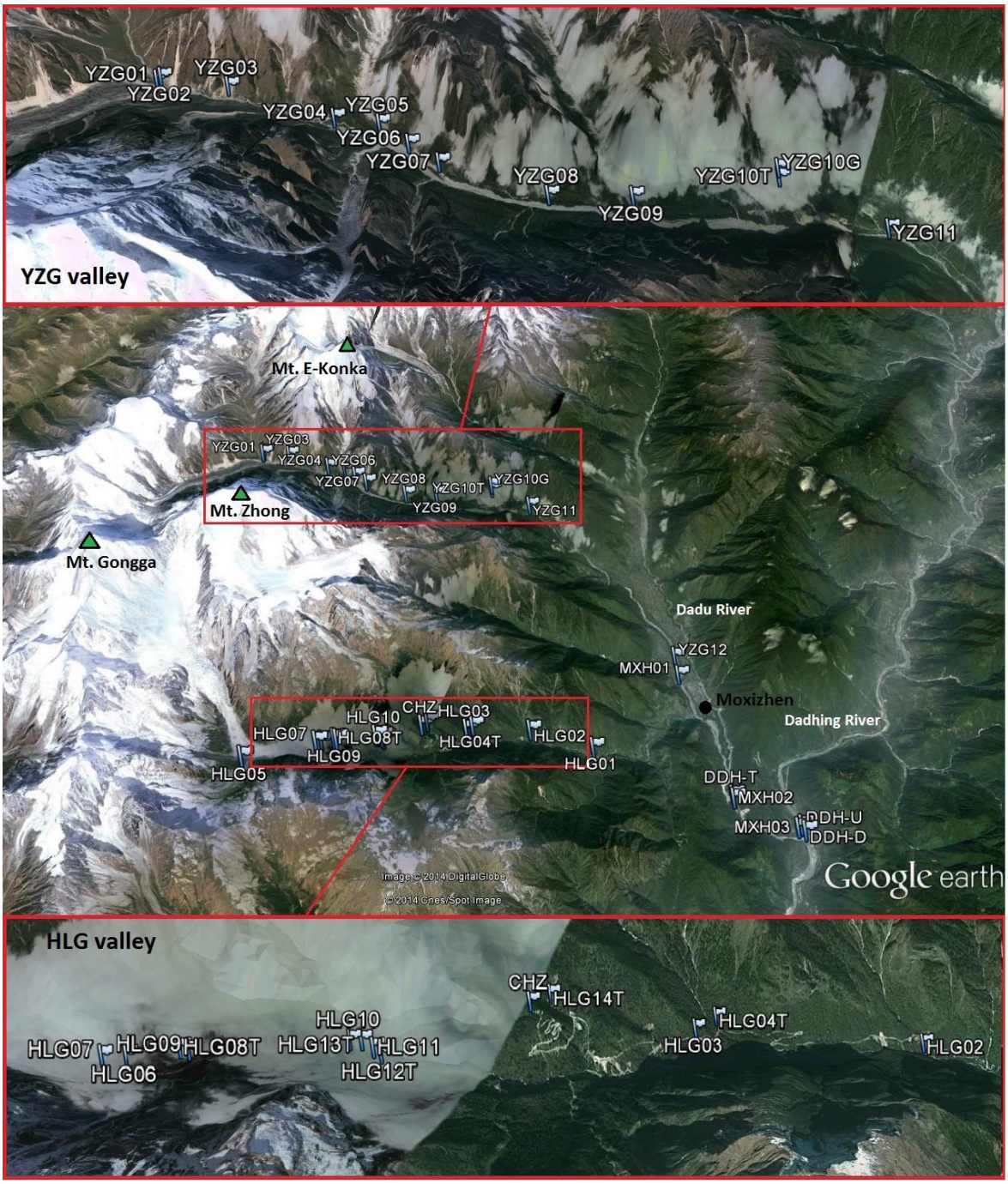

Figure 3.1.2-1: Sampling points (flags – blue/white) with designated names and geography of the study area; including name of major peaks, major rivers, the valleys of interest (HLG – Hailouguo and YZG – Yanziguo) and the town of Moxizhen (images adopted from Google Earth).

The fall 2012 sampling campaign was undertaken in late September, between the 20th and the 27th. Water samples for THg and MMHg were collected for all sampling points. The acid conserved MMHg samples were also used to determine trace elements. For a small selection of sampling points, water samples for TSS, TOC, major ions and pH in addition to sediments

for THg and TOC were taken. A complete sample log for the fall 2012 campaign is shown in appendix A, table A-1.

The spring 2013 sampling campaign was carried out between the 5th and 11th of April. Water samples were taken for THg, MMHg, TSS, TOC, major ions and pH for every sampling point, along with sediment samples for THg and TOC for the sampling points not included in the first campaign, and a peat core from the CHZ bog. Part of the TSS analysis was done in-field at the Chinese Academy of Sciences (CAS) research station at Mt. Gongga. The MMHg samples were also used to determine trace metals. A complete sample log is shown in appendix A, table A-2.

3.1.3 Sampling procedures

Seasonality

The two data sets collected, fall 2012 and spring 2013, were chosen to show reproducibility, but also to capture two different glacial melting profiles: When spring sets in the seasonal snow cover will be the first to melt and will gradually disappear as the temperature rises. The GF streams will therefore possibly contain Hg_{atm} accumulated in the seasonal snow cover. In a glacier with negative mass balance, parts of the firn and older ice-layers in the ablation area will also melt throughout spring, summer and early fall (Stern et al., 2012). Thus streams of glacial origins will constitute mostly firn and ice-melt when sampled in fall.

General sampling strategies

Water samples were collected from well mixed water at a distance from the river bank if possible, or mid-stream for the smaller streams. Clean, unused nitrile gloves were used and the bottles were rinsed three times with the stream water before being filled, with the exception of the MMHg bottles (containing hydrochloric acid (HCl)) which were filled using the THg bottles. Sample replicates were collected submerging two bottles in the water at the same time and as close to each other as possible.

Sediment samples were collected from submerged parts of the river bank or mid-stream for smaller streams. Sediment profiles were collected from dry parts of the stream banks. All solid samples were collected using clean, unused nitrile gloves.

In general, efforts were taken to follow ultraclean sampling procedures to avoid contamination (USEPA, 1996).

THg and MMHg

THg and MMHg samples were collected in fluoropolymer – FLPE bottles (250 mL) in accordance with the USEPA standard for trace metal sampling in ambient water (USEPA, 1996). The bottles were unused and clean, as tested and assured by Brooks Rand Labs (mean THg = 0.02 ng/L) and kept in double plastic bags. Furthermore, separate bottles were used for THg and MMHg to avoid problems related to the loss of Hg, due to sorption of Hg to the inside of the bottle, when splitting a single sample (Braaten, de Wit, Harman, Hageström, & Larssen, 2013; Parker & Bloom, 2005).

Preservation of MMHg and THg samples was done following the United States Environmental Protection Agency (USEPA) Method 1630 (USEPA, 1998) and Method 1631 (USEPA, 2002) respectively. The samples were stored cold, with the exception of parts of the time in transit between Mt. Gongga and Oslo. The MMHg bottles (250 mL) were added HCl (1 mL, conc.) before sampling, to produce a 0.4% solution when full. The THg samples (250 mL) were added BrCl (conc.), to produce a 0.4% solution, within 10 days of the sampling. The THg samples were split into two separate bottles (125 mL in each); for THg and DHg determination. The THg sample (125 mL) was then added BrCl (0.5 mL, conc.) while the DHg sample was not preserved until after filtration. To control if sufficient BrCl had been added three tests were done: 1) seeing the color change to a light yellow in the sample, 2) smelling chlorine fumes coming from the bottle after 24 hrs, as a sign of excess BrCl, and 3) testing with KI/starch-paper, which will be colored a deep purple by the oxidation of iodide if there is excess BrCl (NIVA, 2012).

Unfortunately, a mistake was made in the THg preservation procedure for the fall 2012 samples, as all samples were added BrCl before removing a part for filtration. BrCl will oxidize all Hg species in the sample, dissolved or particle bound, to Hg(II) (USEPA, 2002), thus destroying the means for separating between the dissolved- and particle fractions. Hence there is no DHg data for the fall 2012 data set.

TSS and TOC + major ions + pH

Samples for TSS, and TOC, major ions, and pH were collected using clean and unused high density polyethylene bottles – PD-HD (500-1000 mL) from Emballator Sweden. TSS samples were collected in separate bottles while a joint sample was taken for TOC, major ions and pH. The bottles were stored cold after sampling, with the exception of parts of the time in transit.

Sediments and peat core

The sediment- and peat core samples were collected in clean, unused polypropylene – PP containers (~70 mL) from Nolato Cerbo Sweden. The samples were stored frozen upon arriving at the Norwegian Institute of Water Research (NIVA) (4-9 days after sampling) until used for analysis. The peat core was sampled using a JKH-0204 Piston Sediment Core Sampler. The core was 20 cm deep and separated into layers of 1 cm.

3.2 Analytical Procedures

Complete lists of chemicals, reagents, gases, water type, and standards and CRMs used in the analytic procedures can be found in appendix B.

3.2.1 THg in water samples

The analysis of THg in water was done according to USEPA Method 1631 (USEPA, 2002) using a MERX® Automated Total Mercury System from Brooks Rand with CVAFS detection (figure 3.2.1-1). The sample preparation procedure is summarized below while instrumental operation specifications and experimental parameters are shown in appendix C, tables C-1 and C-2 respectively.

Figure 3.2.1-1: MERX® Automated Total Mercury System from Brooks Rand (image from Brooks Rand Labs).

The instrument is calibrated using seven calibration standards: 5 pg, 10 pg, 25 pg, 100 pg, 500 pg, 2500 pg and 10000 pg, made from three working solutions – 0.1 ng/mL, 1.0 ng/mL and 10.0 ng/mL, prepared from a THg stock solution (1 µg/mL, appendix B, table B.2-1). The standard curve is controlled using a second standard solution (20 µg/mL, appendix B, table B.2-1); an initial calibration verification (ICV). DI H_2O (25 mL) is added to a Cronus® VOA clear borosilicate glass vial (40 mL) with polypropylene cap and PTFE/silicone septum for autosampler use. Then NH_2OH-HCl (0.100 mL) and $SnCl_2$ (0.100 mL) is added before the vial is capped, shaken vigorously and placed in the autosampler. The $SnCl_2$ reagent will reduce all Hg species to elemental Hg(0) (USEPA, 2002), so the vial must be capped immediately after adding the reagent to avoid loss of Hg vapor. Detailed calibration information can be found in appendix D, section D.1.

Sample (25 mL) is measured into to the clear Cronus® VOA autosampler vial (40 mL), using a Sartorius Basic Plus 1200 balance. The sample is then prepared in the same way as the calibration solutions: added NH_2OH-HCl (0.100 mL) and $SnCl_2$ (0.100 mL) before being sealed, shaken vigorously and placed in the autosampler.

Sample (25 mL) for DHg analysis is filtrated into clear Cronos® VOA autosampler vials (40 mL) using a Luer Syringe (30 mL) from BD Plastipack with a double set of filters attached to the tip: the first filter, a Whatman GF/F 25 mm Syringe Filter (pore size 2.7 µm), the second, a VWR 25 mm Polyether Sulfone Membrane Syringe Filter (pore size 0.45 µm). The reason for using a double set of filters with different pore sizes is to collect the larger particles in the largest pores such that the lower pore size filter does not get clogged so fast. DI H_20 was flushed through syringe and filter three times before use. The vials were added BrCl (0.100 mL, conc.), shaken vigorously and left for 30 minutes before being added NH_2OH-HCl (0.100 mL) and $SnCl_2$ (0.100 mL). Contamination from the filters and syringe was tested and corrected for by analyzing syringe-filter-blanks.

3.2.2 MMHg in water samples

The analysis of MMHg in water was done according to USEPA Method 1630 (USEPA, 1998) using a MERX® Automated Methylmercury System from Brooks Rand with CVAFS detection (figure 3.2.2-1). The sample preparation procedure is summarized below while

instrumental operation specifications and experimental parameters are shown in appendix C, tables C-3 and C-4 respectively.

Figure 3.2.2-1: MERX® Automated Methylmercury System from Brooks Rand (image from Brooks Rand Labs)

Before water samples are analyzed for MMHg, a distillation preparation step is necessary in order to isolate MMHg from interfering species (Horvat et al., 1993). Sample (50 mL) is measured into a prewashed Teflon vial, using a Sartorius Basic Plus 1200 scale, and added the complexing agent APDC (0.200 mL, 1%) before being inserted into a the heating block (125 °C) of the Brooks Rand Distillation System with N_2 carrier/purging gas (figure 3.2.2-1). The receiving tubes are added DI H_2O (15 mL) and after completed distillation (2.5-3 hrs) the tubes are topped off with DI H_2O (3 mL) to give a final volume of 58 mL. Distilled samples are stored dark and cold for a maximum of two days before being analyzed.

Figure 3.2.2-2: Distillation step setup in the Brooks Rand distillation system (image from Brooks Rand Labs ®)

The instrument is calibrated using seven calibration standards: 0.5 pg, 1 pg, 2 pg, 10 pg, 50 pg, 250 pg and 1000 pg, made from two working solutions of monomethyl mercuric hydroxide (MMHgOH) – 0.01 ng/mL and 1.0 ng/mL respectively, prepared from a MMHgOH stock solution (1 µg/mL, appendix B, table B.2-1). The calibration curve is controlled by using an ICV made from a monomethyl mercuric chloride (MMHgCl) stock solution (1 µg/mL, appendix B, table B.2-1). Cronus® VOA dark borosilicate glass vials (40 mL) with polypropylene cap and PTFE/silicone septum for autosampler use are added DI H_2O (~40 mL). Appropriate amounts of the working solutions are then added to the seven calibration standards (appendix D, table D.2-1) The pH is adjusted to 4.9 using an acetate buffer (0.600 mL) and controlled by testing with pH-paper, before adding the ethylation reagent, $C_8H_{20}BNa$ (0.050 mL). The ethylation reagent must be stored frozen and handled quickly when in use, to reduce exposure to O_2, which can degrade the potential of the reagent. The vial is then filled to the brim with DI H_2O, capped and shaken vigorously before being placed in the autosampler. Detailed calibration information can be found in appendix D, section D.2.

Pre-distilled sample (40 mL) is measured into a Cronus® VOA dark autosampler vial (40 mL), using a Sartorius Basic Plus 1200 balance. Then the samples are prepared in the same way as described for the calibration solutions above: added acetate buffer (0.600 mL), added $C_8H_{20}BNa$ (0.050 mL) and topped off with DI H_2O to the brim before being capped and placed in the autosampler. MMHg was determined in all the spring 2013 samples, but technical instrument issues led to some of the fall 2012 samples being used up before MMHg could be properly determined.

Samples (50 mL) for dissolve MMHg (DMMHg) analysis were prepared for the distillation vials according to the same procedure as sated for the DHg analysis (section 3.2.1). MMHg and DMMHg were determined in the samples from fall 2012, and were mostly below LOD (0.02 ng/L). Seeing the MMHg concentrations in the spring 2013 set also being mostly below LOD (0.02 ng/L), it was decided not to determine DMMHg in the spring 2013 sample set.

A rigorous washing procedure for the distillation equipment is necessary to maintain low blank values. Teflon vials, caps and tubing are first washed on a regular program on a Miele Professional G7836 CD before being placed in a Deconex® bath for 24 hours. The equipment is then sent through a rinsing program in the washing machine with DI H_2O, before being

placed in a HCl (4 mol/L) bath for 24 hours. Finally everything is rinsed three times in DI H_2O and stored in a closed plastic container.

3.2.3 THg in sediment- and soil samples

The Direct Mercury Analyzer (DMA-80) from Milestone was used to determine THg content in sediment- and soil samples in accordance with the USEPA Method 7473 (USEPA, 2007b). The procedure is summarized below, while instrumental operation specifications and experimental parameters are shown in appendix C, tables C-5 and C-6 respectively.

Empty sample boats of nickel were run through a complete cycle in the DMA-80 as a cleaning procedure, as the heating and combustion cycles will evaporate and thus remove traces of Hg (Milestone, 2002).

A calibration curve was made using six calibration standards composed of sample boats holding different weights of the CRM MESS-3 and an empty sample boat as the 0-standard (appendix B, table B.2-1). The CRM has a known concentration and varying amounts of the material thus represent different concentrations. A range of 0.5 ng to 18 ng was used. Detailed calibration information is found in appendix D, section D.3.

Samples were then weighed into clean sample boats at masses 0.1000-0.5000 g, using an Ohaus Discovery Balance DV215CD, before being placed in the autosampler.

3.2.4 TSS in water samples

Total suspended solids (TSS) in water samples were determined according to ISO 11923 (ISO, 1997), for the samples in the fall 2012 set (appendix A, table A-1). Some modifications to this method were made to accommodate in-field analysis of the spring 2013 sample set (appendix A, table A-2). This was done to avoid having to bring the relatively large volumes of the TSS samples back to Norway. The general method is summarized below along with the changes to the procedure.

Pall Metrigard GF/F filters (47 mm, 0.5 µm) were soaked in DI H_2O for 3 hours before being dried at 105 °C for 2 hours and set to cool down in a desiccator. Once at room temperature, the filters were weighed to 0.1 mg accuracy using an Ohaus Discovery Balance DV215CD.

A sample is shaken vigorously before transferring an appropriate amount (100-1500 mL) to a measuring cylinder. A prepared filter is placed in a Buchner funnel attached to a flask with vacuum suction. The sample aliquot is transferred to the funnel for filtration and the cylinder and funnel are rinsed with 20 mL portions of DI H_2O. The filter is collected, dried at 105 °C for 2 hours, placed to cool down in a desiccator before being weighed again using the same balance.

Before the spring 2013 sampling campaign, GF/F filters were prepared as described above, wrapped in aluminum foil and numbered, to keep track of each filter's recorded weight. The filtration was then performed in-field, at the CAS research station at Mt. Gongga. After the filtration, the filters were placed in their respective aluminum wrappings and brought back to the lab at UIO, Norway to be dried and weighed again.

3.2.5 SEM/EDS study of particle filtrates

Particle filtrates (GF/F filters used for determination of TSS) from four sample locations (HLG01, HLG09, HLG04T and HLG08T) were studied using a FEI Quanta 200 FEG-ESEM with EDAX EDS. Small circular patches (~1.5 cm diameter) were cut from the respective sample filters and mounted on the viewing platform. The instrument was run at low vacuum (60 Pa) with a large field detector, a solid state detector and EDS detecting SEs, BSEs and x-rays respectively. Spot size 4.0 was selected, along with a scanning voltage of 20.0 kV and the working distance at 10-12 mm.

Overview images at 200x magnification were collected for all samples at points assumed representative for the general content of each filter. Further magnification of 500x, was selected for individual points of interest. Focus, contrast and brightness were adjusted manually for each individual image. The BSE images were used in this study as they show elemental contrast.

Points of interest in the BSE images from each sample were selected for EDS analysis. Four criteria for points of interest were used: 1) spots with grey tones (representative for general content), 2) bright spots (elements of higher atomic number) and 3) dark spots (elements of lower atomic number). After selecting a specific point it was made sure that the signal had the required specifications: counts per second >1000 and down time – 33 ± 5. Then, spectra were collected and peaks identified using the peak ID tool. The "compare" option enabled the comparing of spectra from two points of interest by superimposing the one over the other.

3.2.6 Other analysis

Analysis of total organic carbon (TOC), dissolved organic carbon (DOC), major ions (NO_3^-, SO_4^{2-}, Cl^-), pH and trace metals were done by the NIVA laboratory in Oslo in addition to freeze-drying of the sediment samples. Each method is briefly summarized below. Analysis reports from the NIVA laboratory can be found in appendix P.

TOC and DOC

TOC and DOC were analyzed using a Phoenix 8000 TOC Analyzer according to Norwegian Standard NS-EN 1484 (NS, 1997). A sample (100 mL) is acidified with phosphoric acid (H_3PO_4, 4 mol/L, 1 mL) and bubbled with N_2 to remove inorganic carbon. Then it is added sodium persulfate ($Na_2S_2O_8$) and exposed to UV radiation upon which organic material is oxidized to CO_2, which can be measured by the Phoenix 8000. DOC samples are filtered through a Whatman GF/F (47 mm, 0.5 µm) before being run through the procedure above.

Trace metals by ICP-MS

Trace metals were analyzed using a Perkin Elmer ELAN 6000 according to USEPA Method 6020A (USEPA, 2007a). According to preservation procedures for trace metal samples for ICP-MS, nitric acid (HNO_3) is preferred over HCl due to possible molecular ion interferences from chlorine compounds (USEPA, 1996, 2007a). The HCl preserved MMHg samples were used for trace metal determination, something which made for non-ideal conditions, but the NIVA laboratory reported to have carried out the analysis without problems. 30 elements were selected for detection, but only about half of these parameters were used in this project as supporting parameters for statistical analysis.

NO_3^-

Determination of nitrate (NO_3^-) is done according to Norwegian Standard NS 4745 (NS, 1991). Nitrate is reduced by Cu-Co to nitrite, followed by a reaction of the nitrite with sulfanilamide to a diazocompound, which is bound with N-(1-naftyl)-ethylendiamine to form an azo-colored compound. The absorbance of this compound is measured by spectrophotometry at 540 nm on a Skalar AutoAnalyzer.

SO_4^{2-} and Cl^-

SO_4^{2-} and Cl^- were determined using a Dionex Ion Chromatograph DX 320, according to Norwegian Standard NS-EN ISO 10304-1 (NS, 2007). Sample is injected into an eluent stream of potassium hydroxide (KOH), carried to an ion-exchange column where the ions are separated. The eluent is removed by an anion suppressor and the analyte ions are detected and quantified by a conductivity detector.

pH

pH in water samples was determined using a Radiometer PHM 210 with a glass/calomel-electrode GK 2401 according to Norwegian Standard NS 4720 (NS, 1979).The electrode is calibrated using two buffers of pH 7.0 and pH 4.1. pH is measured by placing the electrode in the sample after it has equilibrated with CO_2 in the surrounding atmosphere. pH was determined in water from the TOC sample bottles.

3.3 Quality control and quality assurance

In addition to the quality measures for sampling, sample handling and calibration, strict measures for quality control (QC) and quality assurance (QA) were followed during the analytical procedures. These were: 1) analysis of blank samples, 2) measurement of reproducibility, 3) analysis of replicate samples, 4) the use of internal standards, 5) calibration verification 6) spike-and-recovery assessment, 7) analysis of reference material, and 8) interlaboratory testing. These QC and QA measures are summarized for the analytical methods used by the author in the following sections. As the main analytical focus was on THg and MMHg in water samples, and because concentrations at low levels (ng/L) were determined, the QC and QA are most extensive for these techniques.

3.3.1 Blank samples

Calibration blank

For all the quantitative instrumental analysis procedures (THg and MMHg), calibration blanks were always run before the calibration solutions. This was done in order to correct for the background noise of the instruments and to make sure that there were no carryover issues from the last batch of samples analyzed. For THg and MMHg in water, the calibration blanks were DI H_2O. These were used for automatic correction of calibration standard signals by the system software. For the THg in sediments/soils method, calibration blanks were run first to make sure the system was clean and then a single calibration blank was included as the 0-standard in the calibration curve. In addition to the calibration blanks, continuing calibration blanks (CCBs) were run for every 10 sample analyzed, to control that there were no carryover issues between samples.

Method blank

For the quantitative analytical procedures performed by the author: THg, MMHg and TSS, 10 % blank samples (e.g. n=3 of a total of 29 samples) were included in the analysis, to correct for contamination during sample preparation. Blank samples were composed of: DI H_2O for THg and MMHg in water samples, empty sample boats for THg in sediments and GF/F filters flushed with DI H_2O for TSS. The blanks were treated in the exact same way as a regular sample, and for the THg- and MMHg analysis, the blanks were matrix matched in terms of the preservation agent; BrCl (0.4%) for THg and HCl (0.4%) for MMHg. Blank correction of the analytical results were done for all methods. Specific results from the blank analysis are shown for the respective methods in appendix E, section E.1.

The blank samples for both THg (0.15 ± 0.01 ng/L, mean ± one standard deviation) and MMHg (0.008 ± 0.005 ng/L) in water were low and showed no large deviations (appendix E, tables E.1-4 – E.1-5 and E.1-10). The blanks for DHg (0.16 ± 0.03 ng/L) were slightly higher than the THg blank (appendix E, tables E.1-3 and E.1-6, and E.1-4 – E.1-5); likely due to contamination from the syringe and filter. The MMHg blank is generally more than one magnitude lower than the THg blank, due to there generally being less MMHg than THg in DI H_2O. The distillation step seems to be the dominating factor in contamination from sample preparation, since the DMMHg blanks (0.0034 ± 0.0008 ng/L) do not have higher concentrations than the MMHg blanks (0.005 ± 0.004 ng/L) (appendix E, tables E.1-7 and

E.1-8). The negative blank values (-0.4 ± 0.3 mg/L) seen for the TSS technique (appendix E, table E.1-11 and E.1-12) are due to mass loss from the GF/F filters.

Limit of detection (LOD) and limit of quantification (LOQ)

LOD (equation 3.3.1-1) and LOQ (equation 3.3.1-2) were determined using the blank method, which is an estimation of the level at which the analytical signal can be significantly discriminated from the noise (Skoog, West, Holler, & Crouch, 2004). LOD and LOQ for the methods used by the author are summarized in table 3.3.1-1. Specific details on the blank values used for the calculation of LOD an LOQ for the respective methods are shown in appendix E, section E.1.

$$LOD = 3 \cdot SD_{blank} \quad (3.3.1\text{-}1)$$

$$LOQ = 10 \cdot SD_{blank} \quad (3.3.1\text{-}2)$$

Table 3.3.1-1: LOD and LOQ for the analytical techniques used by the author, as determined by the blank method.

Method (n)	**LOD**	**LOQ**
THg water (ng/L) (n=16)	0.1	0.3
MMHg water (ng/L) (n=30)	0.01	0.05
THg sediment/soil (ng) (n=10)	0.1	0.3
TSS (mg/L) (n=7)	1	3

3.3.2 Reproducibility

To show reproducibility in the analytical results, a random selection of 10% of the samples were analyzed in parallels. If the relative percent difference (RPD) (appendix F, equation F-4) was less than 15% in all parallels, the procedure was concluded to show acceptable levels of reproducibility. For sample parallels with concentrations below LOQ this criteria was not strictly enforced, as the calculated RPDs would not have been reliable. For all samples analyzed in parallels, their respective mean concentrations were reported in the results. For the analysis of THg in sediments, a higher percentage of parallel samples were used due to there being fewer QC/QA measures for this method. The first 10 samples were run in parallels and if they had acceptable RPDs (<15%), the analysis would continue with a random 10% of the remaining samples in parallels. Detailed information about analytical reproducibility in each of the analytical methods is shown in appendix E, section E.2.

All sample parallels in the THg analysis, for both data sets (appendix E, tables E.2-1 and E.2-2), met the RPD<15% reproducibility requirements. The samples analyzed for DHg did not meet the same requirements (appendix E, table E.2-3), as the RPD (%) were large (>45%) for 3 of the 4 parallels. This, however, is owing to the samples having concentrations below LOQ, something which is also the case for the MMHg sample parallels (appendix E, tables E.2-4 and E.2-5). For the TSS analysis only one sample did not meet the requirements – YZG05 (appendix E, table E.2-7). This is probably related to the high TSS concentration (4833.9 mg/L), which gives a filtered mass much higher than the optimum mass range (5-50 mg). A smaller volume of water should have been filtered for the determination of this sample, but unfortunately, as part of the analysis was done in-field, the process could not be repeated. The analysis parallels for THg in sediments were also all below the RDP<15% requirements, as can be seen in appendix E, tables E.2-8 and E.2-9. The mean and standard deviation (STD) of the RPD of the analysis parallels for THg in water, THg in sediments/soil and TSS are summarized in table 3.3.2-1. The DHg and MMHg parallels are excluded here as the resulting concentrations were below LOQ.

Table 3.3.2-1: Summary of mean and STD of the analysis parallels for the THg in water, THg in sediment/soil and TSS methods.

Method (parallels)	**RPD (%)**	
	Mean	**STD**
THg in water (n=8)	7	4
THg in sediments/soil (n=30)	8	6
TSS (n=6)	6	5

3.3.3 Replicate samples

Replicate samples (n=2) were taken at select locations to measure the reproducibility of the sampling process. Unfortunately, limitations on total sample volume lead to a compromise on the amount of replicate samples: n=2 instead of n=3 and a small number of sampling points with replicates. Replicate samples were collected for THg and MMHg determination and are marked in the sample logs (appendix A, table A-1 and A-2) with a "(P)." RPD (equation 3.3.2-1) was calculated for all replicate samples; the results are summarized in table 3.3.3-1. Detailed results from the replicate sample analysis are found in appendix E, section E.3.

Table 3.3.3-1: Summary of mean and STD of the sample replicates for the THg and MMHg methods.

Method (replicates)	RPD (%)	
	Mean	STD
THg (n=5)	12	11
MMHg (n=3)	90	44

The THg sample replicates show decent reproducibility, but two of the single replicate pairs have RPD>20% which contribute to a high standard deviation (appendix E, table E.3-1). The reason for this deviation might be because the replicate samples could have contained different amounts of suspended solids, which is a parameter well correlated with THg (section 4.4.2). The MMHg replicate samples have very poor reproducibility, but that is a direct result of the MMHg concentrations being below LOQ.

3.3.4 Internal standard

For the determination of THg and MMHg in water, internal standards were employed as initial calibration verifications (ICVs), to assure the quality of the calibration. The internal standard for THg analysis has the same chemical make up as the calibration standard, but stem from a different supplier; calibration standard from Brooks Rand and internal standard from Ultra Scientific (appendix B, table B.1-1). Different chemical species are used for calibration- and internal standards in MMHg analysis, MMHgOH and MMHgCl respectively (appendix B, table B.1-1). The quality criteria for ICVs are shown in table 3.3.4-1. Detailed ICV results are found in appendix E, section E.4.

Table 3.3.4-1: ICV recovery criteria for THg in water and MMHg in water. Based on specifications from USEPA Methods 1631 and 1630 (USEPA, 1998, 2002).

Method	ICV (pg)	Recovery Criteria (%)
THg	2000	75-125
MMHg	25	75-125

The recoveries of the THg ICVs were all within the pre-set criteria range (appendix E, table E.4-1.

The recoveries of the MMHg ICVs were all within the pre-set criteria range (75-125%), except one which had a recovery of 128% (appendix E, table E.4-2). The other ICVs, with

acceptable recoveries, were in the upper part of the criteria range (106-125%). The trend of high ICV recoveries (>100%) could be owing to the ICV solution being made by pipetting a minute amount of a standard (MMHgCl, 25 µL, 1.0 ng/mL) into an autosampler vial. The autopipette (20-200 µL) used for this purpose is calibrated regularly, but the precision suffers at the lower range of volume (NIVA, 2013b).

3.3.5 Calibration verification

To control for instrumental drift in THg (water and sediment) and MMHg analysis, continuing calibration verifications (CCV) were included for every 10 samples analyzed. For MMHg analysis (in water) the CCV was a 25 pg solution, made from the same standard as the calibration solutions. For THg (in water) a 500 pg calibration standard was used, while a CRM was used as CCV for THg in sediments (more on this in section 3.3.7). The quality criteria for the CCVs are shown in table 3.3.5-1. Detailed CCV results are shown in appendix E, section E.5.

Table 3.3.5-1: CCV recovery criteria for THg in water and MMHg in water. Based on specifications from USEPA Methods 1631 and 1630 (USEPA, 1998, 2002)

Method	CCV (pg)	Recovery Criteria (%)
THg	500	80-120
MMHg	25	80-120

CCVs for all THg and MMHg analysis runs had satisfactory recoveries (appendix E, tables E.5-1 – E.5-5).

3.3.6 Spike-and-recovery assessment

For THg and MMHg analysis spike-and-recovery assessments were also included. The goal of this QC step is to assess if detection of the analyte is different in the calibration standards compared to the sample matrix. However, one cannot be certain that the spike will behave in the exact same way as the analyte in a natural sample (Keith et al., 1983). Additionally the spike works as a quality parameter for assuring proper recovery of MMHg from the water samples through the distillation step.

The spike is a known concentration of the analyte added to both blanks and samples in similar concentration ranges as the analyte in the natural samples being analyzed. 10% spiked blanks and 10% spiked samples were included in the analysis. Percentage recovery was calculated and accepted according to the criteria in table 3.3.6-1.

Table 3.3.6-1: Recovery criteria for the spike-and-recovery assessment of blanks and samples. Based on specifications from USEPA Methods 1631 and 1630 (USEPA, 1998, 2002).

Method	**Spike type**	**Spike conc. (ng/L)**	**Recovery criteria (%)**
THg	Blank spike	2 or 4	80-120
	Sample spike	2	75-125
MMHg	Blank spike	0.05	70-130
	Sample spike	0.05	65-135

For the THg in water method, all spike recoveries were well within the quality requirements, both the blank spikes (101 ± 4 %) and the sample spikes (100 ± 6 %) (appendix E, tables E.6-1 – E.6-4). In the DHg analysis runs, the blank spikes (111 ± 10 %) and the samples spikes (101 ± 16 %) also had acceptable recoveries (appendix E, tables E.6-5 and E.6-6). For the MMHg in water method, there is more variation in the spike recovery, probably owing to propagation of uncertainty by adding the extra distillation step to the sample preparation (Harris, 2007). The blank spikes all fall within the recovery criteria (89 ± 11 %) (appendix E, tables E.6-8 and E.6-10). The recoveries of the sample spikes, however, show more variation (100 ± 42 %), with several of them being outside the recovery criteria (appendix E, table E.6-7 and E.6-9).

Low spike recovery is a common result of over-distillation. Leaving samples or blanks to distillate for too long can result in co-distillation of chlorine fumes, which interfere destructively with the ethylation reagent. Too high recoveries of the sample spikes on the other hand, can be caused by methylation of inorganic Hg to MMHg by ambient organic matter during the distillation. This can be a problem with samples containing high amounts of inorganic Hg, as approximately 0.01-0.05% of this Hg might be turned in to MMHg (USEPA, 1998).

3.3.7 Reference material

The DMA-80 (for THg sediment/soil analysis) was calibrated using a certified reference material (CRM) – MESS-3 (appendix B, table B.2-1). The CRM was also used as a CCV between every 10 samples analyzed. As a CCV the criterion for the CRM was that the determined concentration would have to be within the standard deviation of the certified concentration: 91 ± 9 µg/kg. Detailed results of this quality control parameter is shown in appendix E, section E.7.

In the analysis of samples from the spring 2013 sample set, the CRM-CCV values were almost all exclusively below 91 µg/kg, but within the criteria range (87 ± 5 µg/kg) (appendix E, table E.7-2). The CRM had been exposed to air during the course of the analytical work and a measurement of water content revealed that the CRM had absorbed some moisture (appendix E, table E.7-3). Correcting for the water content gave slightly improved values for the CRM-CCVs (88 ± 5 µg/kg) (appendix E, table E.7-4).

Advantages of using a CRM are: they have certified concentrations which are traceable to international standards, they have a known uncertainty and they can thus be used to control a method for bias as long as there is no matrix mismatch (Thompson, Ellison, & Wood, 2002). A perfect matrix match, however, is not easily obtained, as reference materials stem from a specific source (e.g. sediment from a specific location with a unique composition) and even though one is using a similar matrix, small differences are likely to exist (Braaten, Harman, Øverjordet, & Larssen, 2014). For the analysis of the sediment and soil samples in this project, a marine sediment CRM was used since this was the best match available at the time of the analysis.

3.3.8. Interlaboratory testing

The author partook in an interlaboratory test of the THg and MMHg in water methods in April 2013, arranged by the instrument provider – Brooks Rand Instruments. THg and MMHg were determined in 3 samples with 3 parallels each (a total of 9 samples), and the three resulting average concentrations were graded (0-5) by how close they were to the true values. Here 0 is "unacceptable" and 5 "very good."

For the THg method the resulting scores were: 5, 5 and 5 for the three average concentrations; giving an average grade of 5 for the method. The scores from the MMHg method were: 4, 5

and 4; giving an average grade of 4.33. Of the total 66 laboratories included in the testing, only 11 got an average grade of 4.33 or higher on both methods (Creswell, Engel, Carter, & Davies, 2013).

3.4 Statistical Analysis

Calculations of means and standard deviations were done in Excel (Microsoft Office 2010), t-tests (Student's t-test), paired t-tests, Wilcoxon-tests (Mann-Whitney-Wilcoxon test), empirical correlations and linear regression plots were done in R 2.15.2, while principal component analysis (PCA) was done using Minitab 16. The theoretical bases for these statistical methods are explained in appendix F.

For statistical analysis, all values below LOD were treated as LOD/2, such that all samples could be included in the statistical assessment of the results. For plots containing such values, notifications of the related data points are included in the figure texts. For statistical tests a result was considered significant if $p<0.05$, which means that the result is significant on a 95% confidence interval.

Significant numbers in data produced by the author were determined by assessing the total uncertainty of the method and identifying the uncertain number. Data produced by the NIVA laboratory is reported here as it was reported in their analysis reports. Data from the NIVA laboratory is produced through accredited methods which follows strict restrictions on QC/QA and reporting of results.

3.5 Uncertainty

3.5.1 Analytical uncertainty

When considering analytical sources of error, one makes a division between systematic and random errors. Random errors are unpredictable and always present, while systematic errors stem from instrumental errors, errors in the method or personal errors. The main difference between the two types of errors is that random errors will only affect single, random samples while systematic errors will affect the whole sample set. Furthermore, it is not possible to correct for random errors while systematic errors can be identified and corrected through

quality control measures (Skoog et al., 2004). Uncertainties related to the different methods will be summarized and discussed for the methods used by the author (THg in water, MMHg in water, THg in sediments/soil, TSS and SEM/EDS). A note on uncertainty in data produced by the NIIVA laboratory is also included.

THg in water

Possible sources of errors related to preservation and storage of samples are: 1) loss of analyte to the bottle, which has been shown to be negligible when a separate bottle is used for THg (Braaten et al., 2013; Parker & Bloom, 2005), 2) contamination of the sample, which is unlikely since the BrCl added is controlled regularly through method blanks and because the sample bottle is just opened for less than a minute inside the fume hood, and 3) pipetting of BrCl. The added BrCl (1 mL to 250 mL sample) only constitutes 0.4% of the total volume and the pipettes are calibrated on a regular basis (further information below), so the small variations in pipetted volume due to uncertainty will only have a minute, if not negligible effect on the potential error in dilution.

Three pipettes are used for the different parts of the method: 1) 20-200 µL, 2) 100-1000 µL and 3) 1-5 mL. The last calibration showed random (R) and systematic (S) errors of 1) R= 0.5% and S= -1.5%, 2) R= 0.3% and S= -0.3% and 3) R= 0.4% and S= 0.4% (NIVA, 2013b). For the two smaller pipettes (1 and 2) the random and systematic errors have opposite signs which means that the total error is partly balanced out by the opposing sources of error in volume. The largest pipette (3) has a total error of 0.8% which would mean an error of 0.008 mL (for 1 mL) when pipetting the BrCl for preservation. It is evident that such a volume has a negligible effect on the total dilution and final concentration values.

The sample preparation step adds to the analytical uncertainty due to the weighing out of the samples (25.00 g) on a balance which has uncertainty related to random errors and calibration errors. A control chart for the Sartorius Basic Plus 1200 shows a standard deviation of 0.01 g over a long time span for a 50 g control weight, and a calibration certificate from 18.02.2013 shows a total uncertainty of ± 0.01 g (NIVA, 2013a). This error will, however, only constitute a 0.04% error in dilution and thus in total concentration. The samples are weighed in at room temperature, but are taken directly from cold storage (4.2 °C) and not allowed to equilibrate with room temperature due to preservation considerations. Therefore, some error related to temperature difference could be present, but it is considered minor as the water is kept at

room temperature for maximum 30 min during sample preparation, so the difference in water density should be insignificant compared to the uncertainty of the balance. Pipetting errors in the addition of NH_2OH-HCl and stannous $SnCl_2$ negligible since both reagents are added in excess.

The analysis of DHg adds extra steps to the procedure and thus more sources of error (Harris, 2007). By splitting the THg sample bottle into two bottles before preservation; one for THg and one for DHg, a bias is created as the original bottle will have a small part of the total Hg content in the sample sorbed to the inside walls (Braaten et al., 2013; Parker & Bloom, 2005). Extra risk of contaminating the DHg samples is also possible during the filtration step, but this is controlled and corrected for with method blanks.

Preparation of calibration solutions will be subject to errors from the use of pipettes and the quality of the stock and working solutions. The calibration solutions are made as dilutions of commercial stock solutions without documented uncertainty (appendix B, table B.2-1). The stock solutions and working solutions both have expiration dates, after which their qualities degrade and they can be contaminated by continued use. The total error from this step, however, is expected to be within acceptable limits as the analyst controls that the size of the analytical peaks of each standard does not change significantly over time.

The total uncertainty related to the actual determination of THg by the instrument was estimated for an accreditation report of the THg in water method at NIVA, Oslo in 2012 and is shown in table 3.5.1-1. From this, it is apparent that the largest source of error is the measurement error, especially at low concentrations: 4.4% at 1 ng/L.

Table 3.5.1-1: Excerpt from the NIVA validation report of the THg in water method where samples at different concentrations were analyzed in multiple parallels (n=5) and the STD calculated as an estimate for the measurement uncertainty (NIVA, 2012).

Expected conc.	Matrix	Measured conc.	STD	RSD
1.0 ng/L	Freshwater	1.01 ng/L	0.04 ng/L	4.4 %
2.0 ng/L	Freshwater	1.92 ng/L	0.02 ng/L	1.2 %
4.0 ng/L	Freshwater	3.88 ng/L	0.04 ng/L	0.9 %

An additional estimate for the measurement uncertainty was determined from the RPD of the analytical parallels (appendix E, tables E.2-1 and E.2-2). The mean of the RPD of the

analytical parallels (n=8), 7 ± 3 %, is higher than the other estimated uncertainties and will therefore be used as an estimate of the total analytical uncertainty.

MMHg in water

For preservation and storage of MMHg samples the sources of errors accounted for in the THg in water method are mostly the same. HCl (1 mL, conc., to 250 mL sample) is used for preservation here and is subject to pipetting errors, but they are assumed negligible due to the same reasons as discussed above. The HCl is also subject to controls through the use of method blanks, so contamination is unlikely.

Sample preparation includes the necessary distillation step to get good results for MMHg (USEPA, 1998). However, an extra step in sample preparation might include extra sources of errors (Harris, 2007). The sample is weighed in twice; once before distillation (50 mL) and again before analysis (40 mL) which doubles the instrumental uncertainty described for the Sartorius Basic Plus 1200 balance. Errors related to temperature difference should also be present here as both the MMHg samples and their respective distillates are kept in cold storage (4 °C) before being weighed out in room temperature, but are considered insignificant for the same reasons as discussed for the THg in water method. Addition of reagents; APDC (0.200 mL) before distillation, and acetate buffer (0.600 mL) and ethylation reagent (0.050 mL) before analysis, has possible errors from pipetting, but all reagents are added in excess so they should be negligible.

The sources of errors related to the calibration are the same for MMHg as described for the THg in water method above.

When it comes to uncertainty measurements for the MMHg method, analytical parallels from data sets in this project cannot be used to make an estimate for this uncertainty either, since the concentrations were below LOQ, and thus the deviations between parallels were high. There is, however, ample data on spiked blank samples (n=29, appendix E, section E.6), which give an indication of how much of the spiked MMH is extracted through the distillation and detected by the instrument. The mean recovery of the blank spikes for all analysis runs were 89 ± 11 %, which means that the amount of MMHg detected can be up to 22% lower than the actual concentration. One must note, however, that the blank spikes and the samples are only matrix matched in terms of the preservation agent, HCl, so there is no guarantee

MMHg in the samples will behave in the same way as the spiked MMHg in the blanks (Keith et al., 1983).

THg in sediments/soil

Sample preservation and storage criteria were not fully complied as the samples were kept cool, but not frozen until 4-9 days after sampling. This could possibly affect the concentration of organic carbon through decomposition, but the effect on THg concentration is probably negligible. Contamination is considered unlikely for the sediment and soil samples as they were kept within the clean sample containers and only opened for less than a minute when extracting sample for analysis.

This method includes limited amounts of sample preparation, but there are some sources of errors related to the steps included. Homogeneity of the sample could be a relevant source of error, as there is no assurance that the small mass selected for analysis is representative for the rest of the sample. Grinding of the sample for homogenization was avoided, however, due to fear of contaminating the sample. Homogeneity was controlled for by adding sample parallels and ensuring relatively low differences (RPD<15%). The Ohaus Discovery Balance DV215CD is used to weigh samples to 0.1 mg precision but unfortunately there is no record of random errors over time or even calibration errors, since the Environmental Chemistry lab at UIO, where the balance is placed, has no responsible technician.

Matrix mismatch between sample and CRM is also a potential source of error. The sediments were matched well with the MESS-3 CRM so little error is expected here, but the soil from the peat bog was analyzed using the same CRM. With the obvious mismatch between the sediment CRM and the soil samples one cannot be completely sure that the Hg in the sediment will behave in the same way as the Hg in the soil when being analyzed (Braaten et al., 2014). Soil CRMs are not easily obtained due to the complex properties of soils, so the sediment CRM was the best available option at the time of the analysis. However, the method is based on high temperature combustion, so one should expect all Hg to be completely released from the sample, whether it is sediment or soil. Furthermore, in literature surveyed by the author, sediment CRMs have been used to study Hg in soil.

The measurement uncertainty was also estimated for this method using the analytical parallels (appendix E, tables E.2-8 and E.2-9). Mean RPD of all the samples analyzed in parallels

(n=29) is 7 ± 5 %. This uncertainty exceeds all the other considered sources of errors and will therefore be used as a total estimate of the analytical uncertainty.

TSS

Samples taken for determination of TSS should preferably be analyzed within 4 hours of sampling. If this is not possible, the samples should be stored cold (8 °C) until analysis and the results should be interpreted with caution (ISO, 1997). The samples from fall 2012 were all brought back to Norway before being analyzed, which means they were stored for several days before being analyzed. Possible sources of error related to storage time are the flocculation and coagulation, or decomposition of suspended solids, such that the net amount of suspended solid increases or decreases relative to the amount at the time of sampling (ISO, 1997). The possibility of suspended solid materials adhering to the sample container could also affect the results. Therefore, the TSS results from fall 2012 are marked and not used for any extensive data analysis. The samples from spring 2013 were all filtrated within 4 hours of sampling, but, as described already, the filters were dried and weighed after being transported back to Norway. Storage could lead to filtrated material being lost from the filter. However, the filters were folded in on themselves and packaged individually in tight aluminum foil wrappings, so mass loss should be negligible.

The filters were weighed to 0.1 mg precision with an Ohaus Discovery Balance DV215CD which errors has been discussed already (THg in sediments). However, the analytical uncertainty of the balance is small compared to the uncertainty of the graduated cylinder used to measure out sample volume, which has an uncertainty of ± 5 mL, that will result in 5 – 0.5% uncertainty in measured volumes of 100 – 1000 mL respectively.

Another source of error to consider is the homogeneity of the sample aliquot. If the sample is not shaken properly before being transferred to the funnel, it might not have a homogenous composition of suspended solids. This was controlled for by adding analysis parallels and ensuring their relative differences were small (RPD<15%).

Using the same analysis parallels to estimate the measurement uncertainty by taking the mean RPD gives an uncertainty of 6 ± 5% (n=6), omitting the YZG05 analysis parallel with an unacceptable high RPD (31.9%).

SEM/EDS

The SEM study was mainly a qualitative study, but there are some sources of error to consider still. For each sample analyzed an image representative of the general content of the filter was created. This was done by studying the entire sample and selecting a location thought representative by the analyst. The location selected, might of course not be properly representative. In a similar way, particles which were considered representative for the bulk and selected for EDS scans, might also not be properly representative despite the indications.

The specific analytical uncertainties related to the elemental composition EDS scan would be important if quantification was included in the method. In this study, however, the particles scanned contained relatively large amounts of O or C, and such light elements are notoriously difficult to quantify using x-rays (Skoog, Holler, & Crouch, 2007). Quantification would include an elemental composition distribution which would be greatly affected by the large uncertainties in the O and C content. Therefore, the qualitative option was chosen as to avoid the large uncertainties.

Uncertainties in data produced by the NIVA laboratory

The NIVA laboratory has a general standard for reporting the total uncertainty in the data they produce (table 3.5.1-2). The total uncertainty estimate is crude, but it ensures that an analytical result is within the estimated range (value ± total uncertainty) on a 95% confidence level.

Table 3.5.1-2: Total uncertainty estimates for a result, X, within a specific concentration range, produced by the NIVA laboratory. LOD = limit of detection.

Concentration range	**Total uncertainty estimate**
LOD < X < 5 × LOD	± LOD
X > 5 × LOD	± 20 %

3.5.2 Representativeness

Experimental setup in analytical chemistry, classically involves controlled conditions and parameters. The uncertainty is limited to random and systematic errors which can be tracked and discussed for each technique as done in section 3.5.1. Natural samples, however, do not only contain the few variables you chose to measure or observe, but rather a whole complex microsystem of chemical species, equilibriums and reactions, which make preservation of the

integrity of the sample and subsequent analysis challenging. Additionally, describing complex, dynamic systems with temporal and spatial variation through single event samplings, which are limited by accessibility of sampling points and equipment- and transport logistics, is all but ideal. When trying to describe the behavior and abundance of a contaminant in a part of the natural environment through sampling and chemical analysis one must therefore discuss representativeness, which can be defined at three different levels (Popek, 2003):

1) Ultimate representativeness: a measure of how well the sampling design and analysis plan ultimately represent the environmental conditions at the study site. The making of a solid plan with good ultimate representativeness requires knowledge of the physical and chemical properties of the contaminant, the nature of its distribution and its fate and transport within the environment (Popek, 2003).
2) Sampling point representativeness: a measure of how well the data of a sample taken represents the characteristic of a parameter or parameter variation at the sampling point. To assure best possible sampling point representativeness one must follow approved sampling procedures and standards specific for the contaminant in question (Popek, 2003).
3) Sample representativeness: a measure of how well the data of a sample represent the sample in question after it has been collected. Sample representativeness can be achieved by following approved procedures and standards for sample handling in the field, sample preservation and analysis procedures (Popek, 2003).

Measures were taken to achieve good representativeness, but the conditions for sampling design and the implementation of this design were not ideal due to challenges and limitations discussed in section 3.6. The implications of not achieving proper representativeness on the total uncertainty of the analytical results are not estimated, but it can be assumed that sources of errors stemming from the analytical process are rather minor in comparison.

3.6 Challenges related to doing field work in remote China

Studying a remote area in China added an extra layer of complexity to the field work process and the experimental design. First of all economic constraints limited the amount of times possible to visit the study area, due to the cost of travelling and the time taken for each

sampling campaign. The scope of this project featured two sampling campaigns, one during fall and one during spring. The limitations of only two visits to the study site meant for careful planning in advance. However, with limited information about the remote study area being available and all field work participants being unfamiliar with this region of China, many decisions, related to logistics and specific sampling locations, had to be decided upon the first arrival. A great deal was learnt about the study are during the first sampling campaign, which made the preparations for the second campaign more ideal. While working in the high altitudes of Mt. Gongga, the weather conditions also posed great challenges in completing the sampling plan. Ideal sampling points were sometimes found inaccessible due to snow, too high risk involved (rock and mud slides, steep slopes) or the physical duress of getting there. Bureaucratic difficulties were also experienced when planning the field work in China. Visa applications, research permits and permits for import of equipment and export of samples are not easily acquired.

The sampling points chosen and the amount of samples to be collected (sample types, variety of parameters to be determined and number of replicates) were therefore, not decided by analytical and statistical parameters alone. It was rather a compromise of the desired amounts and locations versus bureaucratic-, logistical- and economic constraints and health and safety concerns. Furthermore, the logistical challenges of sample transport (storage conditions and time in transport) placed limitations on the sampling, storage and preservation procedures.

4. Results

In section 4.1 follows an overview of the THg concentrations in the streams of Mt. Gongga. THg data from water samples from GF streams, in the two separate valleys (HLG and YZG), will be compared to data from NGF streams, and differences between these systems are presented in section 4.2. Seasonal differences, i.e. differences between THg concentrations in the two sampling campaigns, are shown in section 4.3. Hg fractionation results and correlations with supporting parameters are documented in section 4.4, along with data on MMHg in the stream systems. River sediment analysis (section 4.5) and a peat bog core record (section 4.6) will serve to give background information about Hg in the study area. As a supporting study to the fractionation section, an SEM analysis of stream particle filtrates is shown in section 4.7.

4.1 Total mercury in Mt. Gongga streams – an overview

In this section an overview of the THg concentrations in the streams of Mt. Gongga for both sampling campaigns, fall 2012 and spring 2013, are shown in maps of the study area (figures 4.1-1 and 4.1-2 respectively). Rivers are categorized into glacier-fed (GF) and non-glacier-fed (NGF), and furthermore a distinction is made between sampling points in the Yanzigou (YZG) and Hailuogou (HLG) valleys, sampling points close to the town of Moxizhen (MXH) and sampling points in the Dadhing River (DDH). The maps facilitate spatial comparisons and the relations of subsystems and select locations to the total perspective.

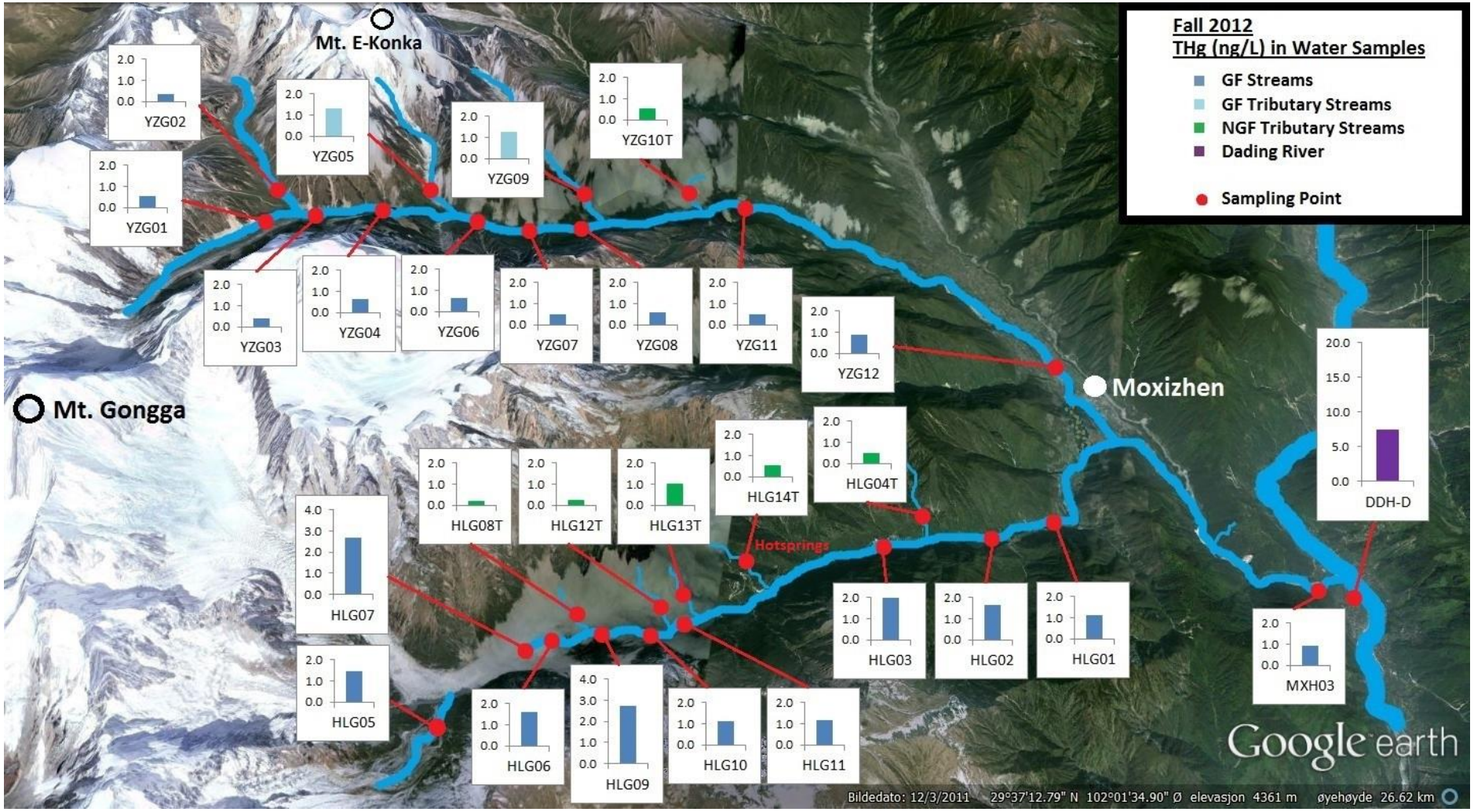

Figure 4.1-1: Map of THg (ng/L) in water for all sampling points in the Mt. Gongga area for the fall 2012 data set. Stream systems are color coded as: GF streams = blue, GF tributary streams = light blue, NGF tributary streams = green and Dadhing River = purple. Sampling points are marked as red dots. Rivers and sampling points are not drawn perfectly to scale (background image adopted from Google Earth).

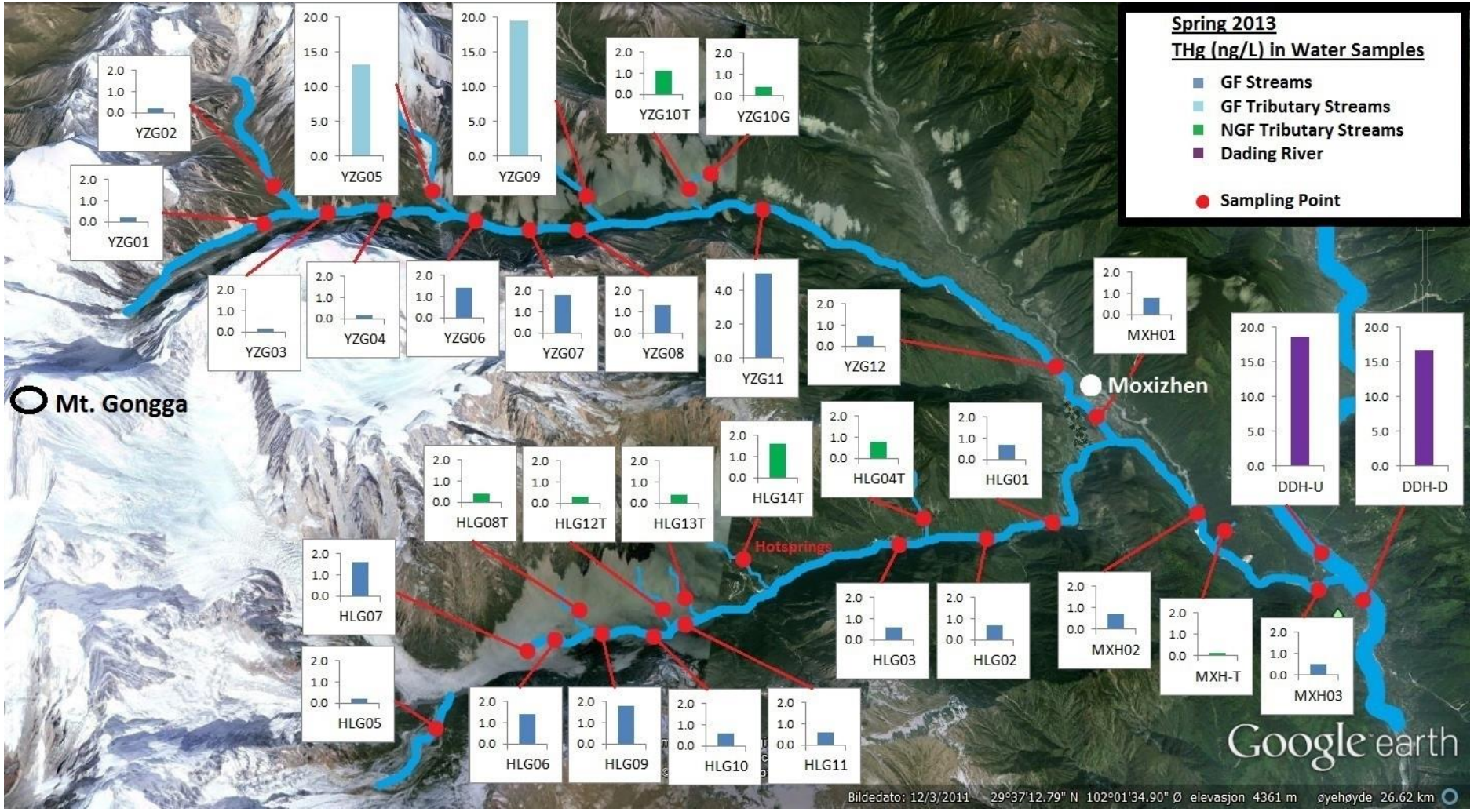

Figure 4.1-2: Map of THg (ng/L) in water for all sampling points in the Mt. Gongga area for the spring 2013 data set. Stream systems are color coded as: GF streams = blue, GF tributary streams = light blue, NGF tributary streams = green and Dadhing River = purple. Sampling points are marked as red dots. Rivers and sampling points are not drawn perfectly to scale (background image adopted from Google Earth).

4.2 Mercury in glacier-fed and non-glacier-fed streams

THg concentrations in water samples from GF streams, from the two separate valleys (HLG and YZG), next to data from NGF streams are shown for both seasons, fall 2012 and spring 2013, in figures 4.2-1 and 4.2-2 respectively. The full table of THg concentrations in water for all the sampling points in the study area is shown in appendix G, table G-1. Specific details of the statistical tests performed are found in appendix L.

No large variations in GF and NGF THg concentrations can be seen in the fall 2012 data set (figure 4.2-1), which ranges from 0.2 to 2.8 ng/L, with mean 1.3 ± 0.8 ng/L (mean ± one standard deviation) in GF streams and mean 0.5 ± 0.3 ng/L in NGF streams. There is a significant difference between HLG GF and NGF streams ($p<0.001$) and between all GF streams and NGF streams ($p<0.01$), but no significant difference between YZG GF and NGF streams ($p=0.11$). Furthermore, the HLG GF streams have significantly higher THg than the YZG GF ($p<0.001$).

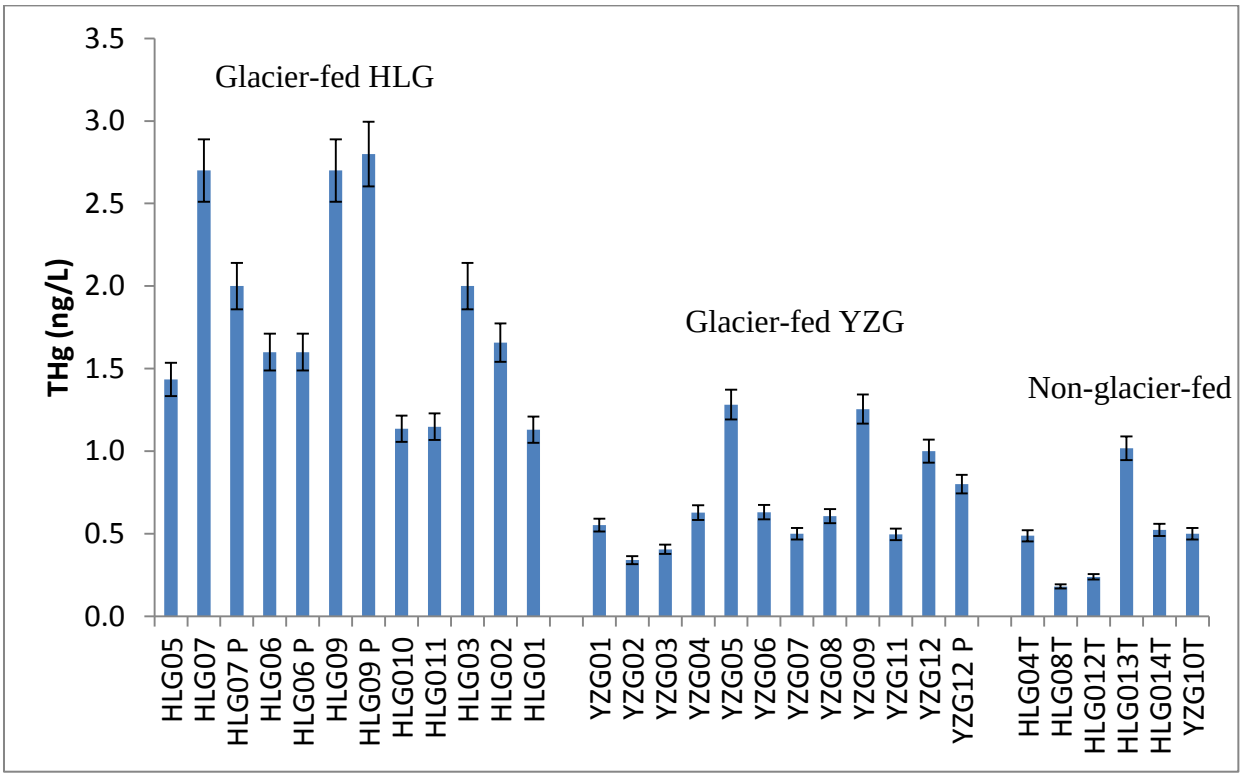

Figure 4.2-1: THg (ng/L) concentrations for the GF streams in HLG (left), YZG (middle), sorted from upstream to downstream (left to right) and the NGF tributary streams (right), fall 2012. Error bars show analytical uncertainty for THg (see section 3.5.1).

In the spring 2013 data set there is much more variation in the THg concentrations (figure 4.2-2), as the range stretches from 0.1 to 19.6 ng/L. Mean THg concentrations were 2.5 ± 4.8 ng/L and 0.7 ± 0.5 ng/L for GF and NGF streams respectively. The high standard deviation of the GF streams (±5 ng/L) is the result of large variations within the YZG valley; min 0.2 ng/L and max 19.6 ng/L. There is no longer a significant difference between the HLG GF and the NGF streams (p=0.26), or between all GF and NGF streams (p=0.26) as were seen in the fall 2012 data set. Additionally, there is no significant difference between YZG GF and NGF streams (p=0.41). What should be noticed, however, are high THg concentrations (5.0, 13.2 and 19.3 ng/L) for several of the YZG GF stream sampling points (figure 4.2-2).

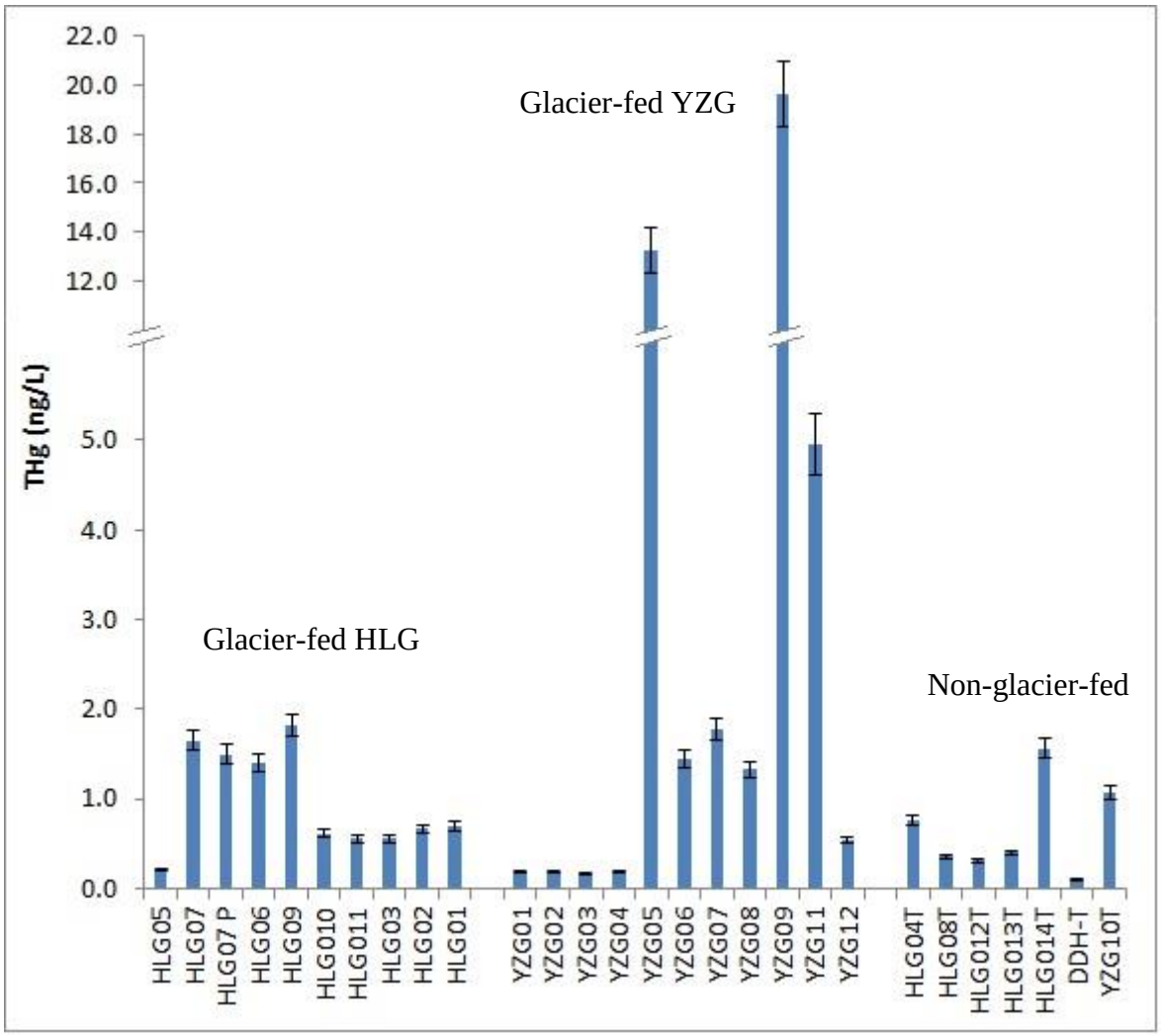

Figure 4.2-2: THg (ng/L) concentrations for the GF streams in HLG (left), YZG (left), sorted from upstream to downstream (left to right) and the NGF tributary streams (right), spring 2013. Error bars show analytical uncertainty for THg (see section 3.5.1).

The two sampling points, YZG05 and YZG09, have THg concentrations two orders of magnitude larger than the lowest measured concentrations; 13.2 ng/L (YZG05) and 19.3 ng/L (YZG09) compared to 0.1 ng/L (DDH-T). In figure 4.1-2, it can be seen that these two sampling points are two side rivers in the YZG valley that drain the glacier of the E-Konka peak, a separate glacier to those of the Gongga peak, which is the origin of the main rivers in both the YZG and HLG valleys. There is a significant rise of THg concentrations ($p<0.05$) in the sampling points downstream (YZG06, YZG07, YZG08 and YZ11) of where the YZG05 and YZG09 side river joins the main river compared to the sampling points upstream (YZG01, YZG02 and YZG03); from 0.2 ng/L upstream to >1.0 ng/L downstream.

The NGF streams all show varying concentrations of THg in both sample sets; the ranges being 0.2-1.0 ng/L in fall 2012 and 0.1-1.6 ng/L in spring 2013.

Other sampling points

THg concentrations in sampling points around the village of Moxizhen (MXH) were similar to that of the two valleys, as can be seen in table 4.2-1. The Dadhing river (DDH), which the streams of Mt. Gongga and the Dadu River drain into, had THg concentrations in the same range as the YZG side rivers, 13 – 19 ng/L (table 4.2-1).

Table 4.2-1: THg concentrations (ng/L) in other sampling points in the study area for the two sampling campaigns.

	THg (ng/L)	
Sample	**Fall 2012**	**Spring 2013**
MXH01	n/a	0.8
MXH02	n/a	0.7
MXH03	0.9	0.5
DDH-U	7.4	18.7
DDH-D	n/a	16.7

4.3 Seasonal differences

Two opposing trends are seen when comparing the sampling points of the GF streams from the two seasons (figure 4.3-2). Higher THg concentrations in fall than spring are seen for the sampling points HLG01-HLG11, and YZG01-YZG04 and YZG12. The exact opposite trend can be observed for the YZG05-YZG11 sampling points, for which the THg concentrations

are higher in spring than in fall. Overall there is no significant difference between the two seasons ($p=0.21$), but if YZG05-YZG11 are removed the difference between the seasons become significant ($p<0.001$). The largest differences are found in YZG05, YZG09 and YZG11 where the THg concentrations are 10, 15 and 5 times higher in spring than in fall respectively. Additionally, a large difference is seen in HLG05 where the THg concentration is 6.6 times higher in fall than in spring. The rest of the sampling points all vary between a 50% to 250% increase or decrease in concentrations between the seasons.

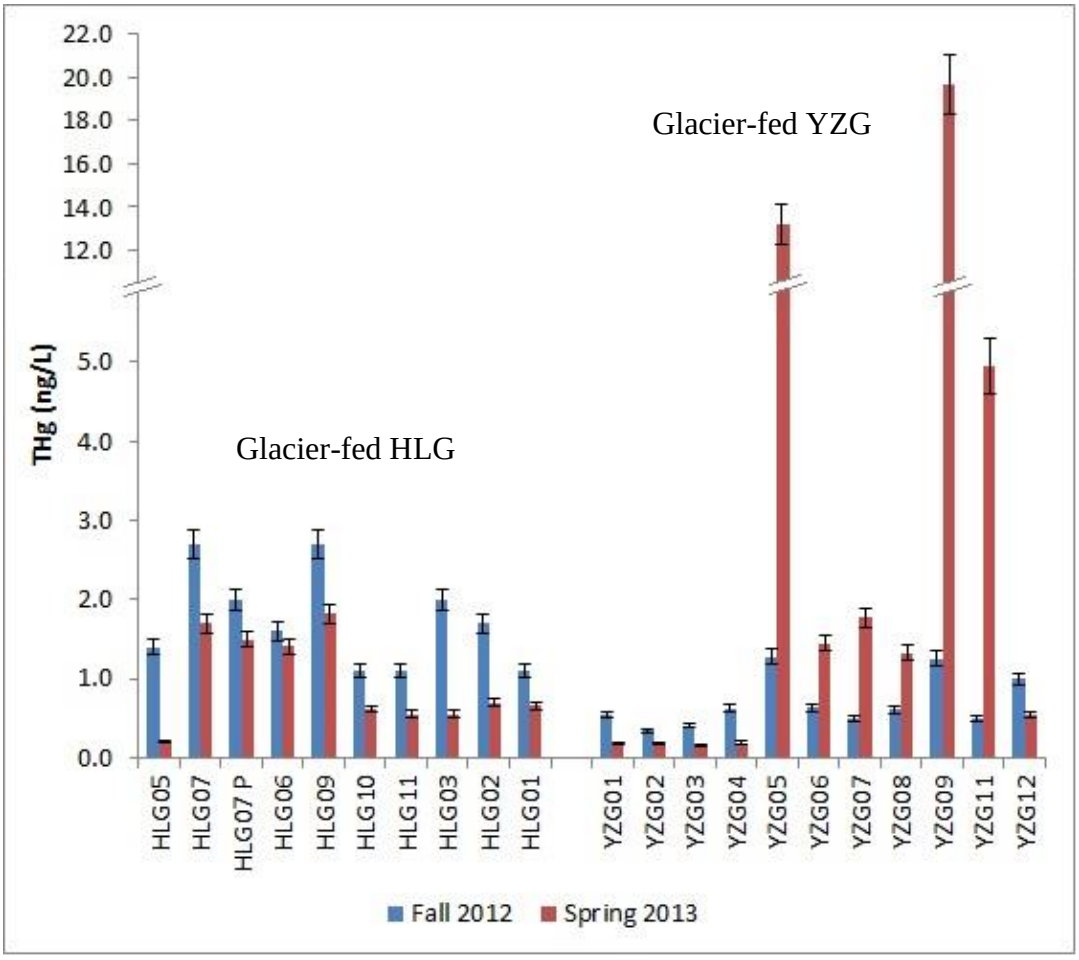

Figure 4.3-2: Seasonal differences (fall and spring) in THg (ng/L) for the GF-streams in the HLG (left) and YZG (right) valleys. Error bars show analytical uncertainty for THg (see section 3.5.1).

4.4 Mercury fractions in the streams of Mt. Gongga

Here the relation between PHg and DHg in the water samples will be shown (section 4.4.1), along with the relation of Hg to TSS and TOC (sections 4.4.2 and 4.4.3 respectively). Results on MMHg, are reported in section 4.4.4. Linear regression analysis of THg and TSS and THg and TOC was only done for the spring 2013 data set due to the lack of data points analyzed for TSS and TOC in the fall 2012 data set. DHg data is only available for the spring data set while DMMHg data is only available for the fall 2012 data set.

4.4.1 Dissolved and particle bound mercury

The DHg concentrations were below LOD (0.1 ng/L) in all but 10 samples in the spring 2013 sample set, as can be seen in appendix G, table G-1. Seven samples from the GF and NGF streams, HLG01, HLG02, YZG05, YZG09, HLG04T, HLG14T and YZG10T, in addition to samples from the DDH River and the CHZ bog, had detectable concentrations (table 4.4.1-1). Figure 4.4.1-2 shows the relative percentages of PHg and DHg for these sampling points.

Table 4.4.1-1: Fractionation results – THg (ng/L), DHg (ng/L) and PHg (ng/L) for the samples in the spring 2013 sample set which had detectable concentrations of DHg.

Sample	THg (ng/L)	DHg (ng/L)	PHg (ng/L)
HLG01	0.7	0.3	0.4
HLG02	0.7	0.1	0.6
YZG05	13.2	0.1	13.1
YZG09	19.3	0.1	19.2
HLG04T	0.8	0.2	0.6
HLG14T	1.6	0.1	1.5
YZG10T	1.1	0.2	0.9
DDH-U	18.7	1.1	17.6
DDH-D	16.7	0.9	15.8
CHZ	3.0	1.2	1.8

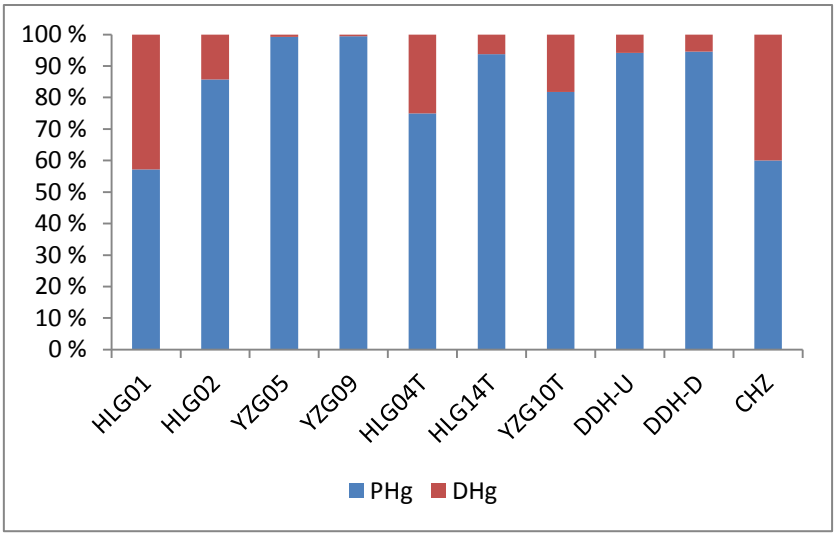

Figure 4.4.1-2: Relative fractions of PHg and DHg of THg for the sampling points from the spring 2013 sample set which had detectable concentrations of DHg, spring 2013.

4.4.2 Mercury correlation with total suspended solids

Tables of THg and TSS concentrations for all sampling points are shown in appendix A, table A-1 and appendix B, table B-1 respectively. All linear regression plots of THg vs. TSS for the different systems in the spring 2013 data set are shown in appendix I, figures I.1-1 – I.1-6. Specific details of the t-tests performed are shown in appendix L.

TSS concentrations were found to be significantly higher ($p<0.001$) in GF streams, 545 ± 1199 mg/L, than in NGF streams, 5 ± 7 mg/L. Three influential data points with particularly high TSS concentrations (YZG05 – 4833.87 mg/L, YZG09 – 2922.97 mg/L and YZG11 – 779.44 mg/L) cause large deviations in the data set. In the fall 2012 data set, the TSS concentrations in GF streams (317 ± 103 mg/L) is not significantly higher ($p<0.20$) than in NGF streams (7 ± 5 mg/L), but this is based on a small number of sampling points; n=3 for GF and n=2 for NGF.

Strong positive correlations between THg and TSS are seen for the GF streams in both HLG (figure 4.4.2-2) and YZG (figure 4.4.2-1). For NGF streams there is no such correlation (figure 4.4.2-3). It must be pointed out that the THg-TSS correlation is stronger for the YZG GF (appendix I, figures I.1-3 vs. I.1-4) and for all the GF sampling points (appendix I, figures I.1-1 vs. I.1-2) when the three influential sampling points, YZG05, YZG09 and YZG11, are removed.

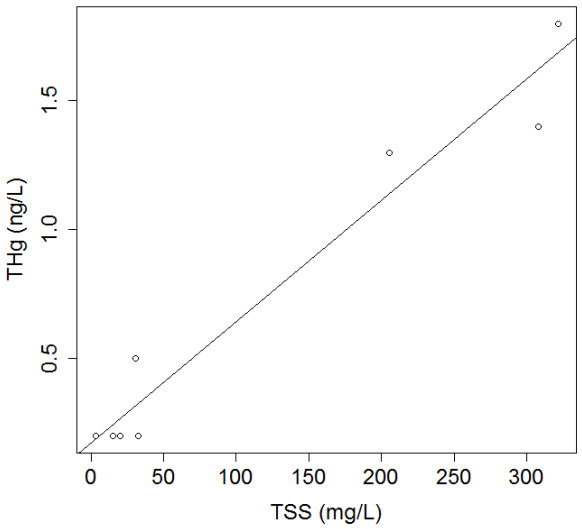

Figure 4.4.2-1: THg vs. TSS for the GF streams in the YZG valley (2013). Influential points removed.
R^2 = 0.9533, p <0.001

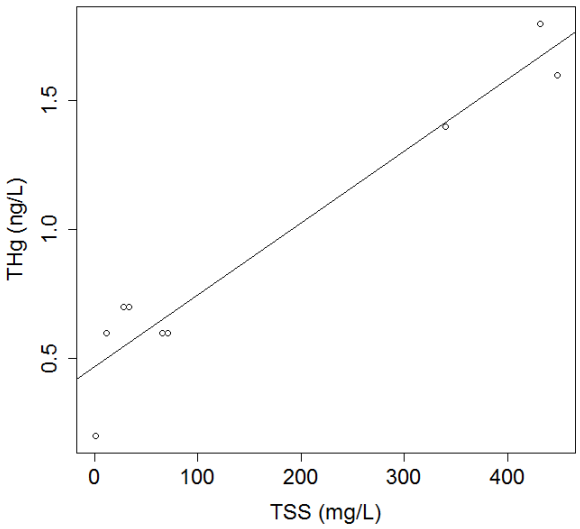

Figure 4.4.2-2: THg vs. TSS for the GF streams in the HLG valley (2013).
R^2 = 0.9316, p <0.001

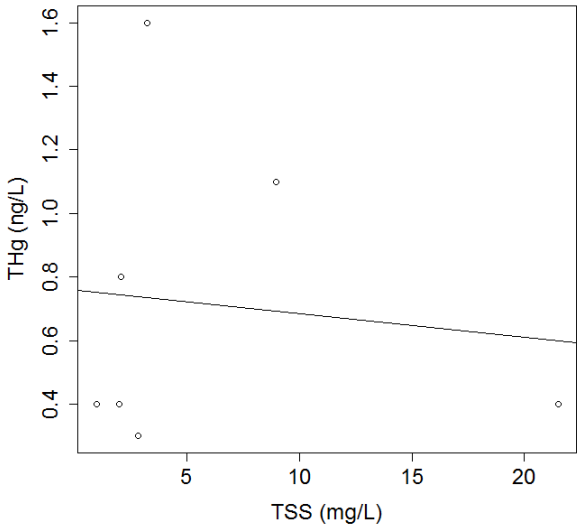

Figure 4.4.2-3: THg vs. TSS for NGF tributary streams (2013).
R^2 = 0.0124, p = 0.81.

4.4.3 Mercury correlation with total organic carbon

THg and TOC concentrations for all samples can be seen in appendix A, table A-1 and appendix B, table B.1 respectively. Linear regression plots of THg vs. TOC for the different systems in the spring 2013 data set are shown in appendix I, figures I.-1 – I.2-6.

TOC concentrations were relatively low for all the studied streams in the Mt. Gongga area; 1 ± 2 mg/L in fall 2012 and 1 ± 1 mg/L in spring 2013. The correlation between TOC and THg, however, is strong both for the GF streams (R^2=0.99, p<0.001) and the NGF streams (R^2=0.93, p<0.001). The correlation is weakest in the GF streams of HLG (R^2=0.49, p<0.05) and stronger for the YZG GF streams (R^2=0.99, p<0.001).

The TOC concentrations are also above the mean in the three influential sampling points mentioned in section 4.4.2: YZG05 – 2.60 mg/L, YZG09 – 3.90 and YZG11 – 1.50 mg/L. The THg-TOC correlation does not change much for YZG GF streams when removing these data points (appendix I, figures I.2-3 vs. I.2-4), although the correlation of all the GF streams decrease about 25% after the same operation (appendix I, figures I.2-1 vs. I.2-2).

4.4.4 Mono methyl mercury

MMHg was found at concentrations below detection limit (LOD = 0.02 ng/L) at most of the sampled sites in the study area for both sampling campaigns (appendix G, table G-3). 13 samples had concentrations above LOD in either one or both data sets as can be seen in table 4.4.4-1, but all concentrations were below LOQ (0.05 ng/L) with the exception of the CHZ-bog. MMHg was determined above LOD in 25% of the NGF stream samples compared to 17% of the GF samples. No systematic seasonal patterns could be rendered from the data, as there was no significant difference between the three stream samples with concentrations above LOD for both seasons (p=0.42). The CHZ bog, however, had a 73% decrease in MMHg from fall 2012 to spring 2013.

Table 4.4.4-1: MMHg concentrations (ng/L) and their relative fractions, MMHg (%) of THg, for the sampling points which had concentrations above LOD in one or both data sets (fall 2012 and spring 2013). Values below LOD are shown as <0.02.

	MMHg (ng/L)		%MMHg	
Sample	**Fall 2012**	**Spring 2013**	**Fall 2012**	**Spring 2013**
HLG03	n/a	0.03	n/a	5.0
HLG07 P	0.03	<0.02	1.5	n/a
HLG11	0.03	<0.02	2.7	n/a
YZG05	<0.02	0.02	n/a	0.2
YZG09	0.02	0.02	1.5	0.1
YZG12	0.02	<0.02	2.0	n/a
HLG04T	0.03	<0.02	6.0	n/a
HLG14T	<0.02	0.02	n/a	1.3
YZG10T	<0.02	0.04	n/a	3.6
MXH03	0.02	0.02	2.2	4.0
DDH-U	n/a	0.04	n/a	0.2
DDH-D	0.03	0.04	n/a	0.2
CHZ	0.56	0.15	19.3	5.0

Determining the fractionation of MMHg, DMMHg and particle bound MMHg (PMMHg) was not successful except for two single samples; DDH-D and CHZ (table 4.4.4-2). As can be seen in appendix A, table A-2 most of the samples had DMMHg concentrations below LOD (0.02 ng/L) and for three of the five samples (HLG10, YZG04 and HLG12T), which had detectable concentrations, the concentrations were higher than the total MMHg concentrations and thus not valid. Both DDH-D and CHZ samples were found to contain almost exclusively DMMHg in fall 2012; 100% and 96% respectively. In spring 2013 however, the amount of DMMHg had dropped to 57% of the total MMHg in the CHZ bog.

Table 4.4.4-2: Fractionation results; MMHg (ng/L), DMMHg (ng/L) and PMMHg (ng/L) for sampling points which had detectable concentrations of MMHg and DMMHg.

Sample	**MMHg (ng/L)**	**DMMHg (ng/L)**	**PMMHg (ng/L)**
DDH-D (2012)	0.03	0.03	0.00
CHZ (2012)	0.56	0.54	0.02
CHZ (2013)	0.14	0.08	0.06

4.5 Mercury in stream sediments

Tables of THg (µg/kg) and TOC (µgC/kg) in sediments and sediment profiles are shown in appendix J, tables J-1 – J-4. THg vs. TOC linear regression plots for sediments and sediment profiles can be found in appendix E. Details about statistical tests are shown in appendix L.

4.5.1 Mercury in surface sediments

With all samples included, the range of THg in surface sediments in the study area is 0.5 – 13.3 µg/kg with mean 1.7 ± 2.3 µg/kg. DDH-D has the maximum THg concentration – 13.3 µg/kg. If this data point is removed the total range becomes 0.5 – 3.7 µg/kg with mean 1.3 ± 0.7 µg/kg. The THg concentrations are low in both GF streams, 1.4 ± 0.7 µg/kg, and NGF streams, 1.0 ± 0.5 µg/kg, and there is no significant difference between the two systems ($p=0.19$). There was no significant difference between sediments from the two valleys, HLG and YZG, either ($p=0.91$). Figure 3.5.1-1 shows THg (µg/kg) and TOC (µgC/mg) in surface sediments for the GF streams in HLG and YZG valleys along with the NGF tributary streams.

TOC was found at low concentrations in the surface sediments from Mt. Gongga; mean 1.2 ± 1.2 µgC/mg for all samples and 60% of these samples had concentrations below LOD (1 µgC/mg) (appendix D, table D-1). Despite low concentrations, a positive correlation between THg and TOC is seen in both the GF streams ($R^2= 0.45$, $p<0.01$) and the NGF streams ($R^2=0.96$, $p<0.01$). Too large an emphasis should not be given to this result as samples which had TOC concentrations below LOD were given a discrete value (LOD/2) and could therefore contribute to inferring a non-existing trend.

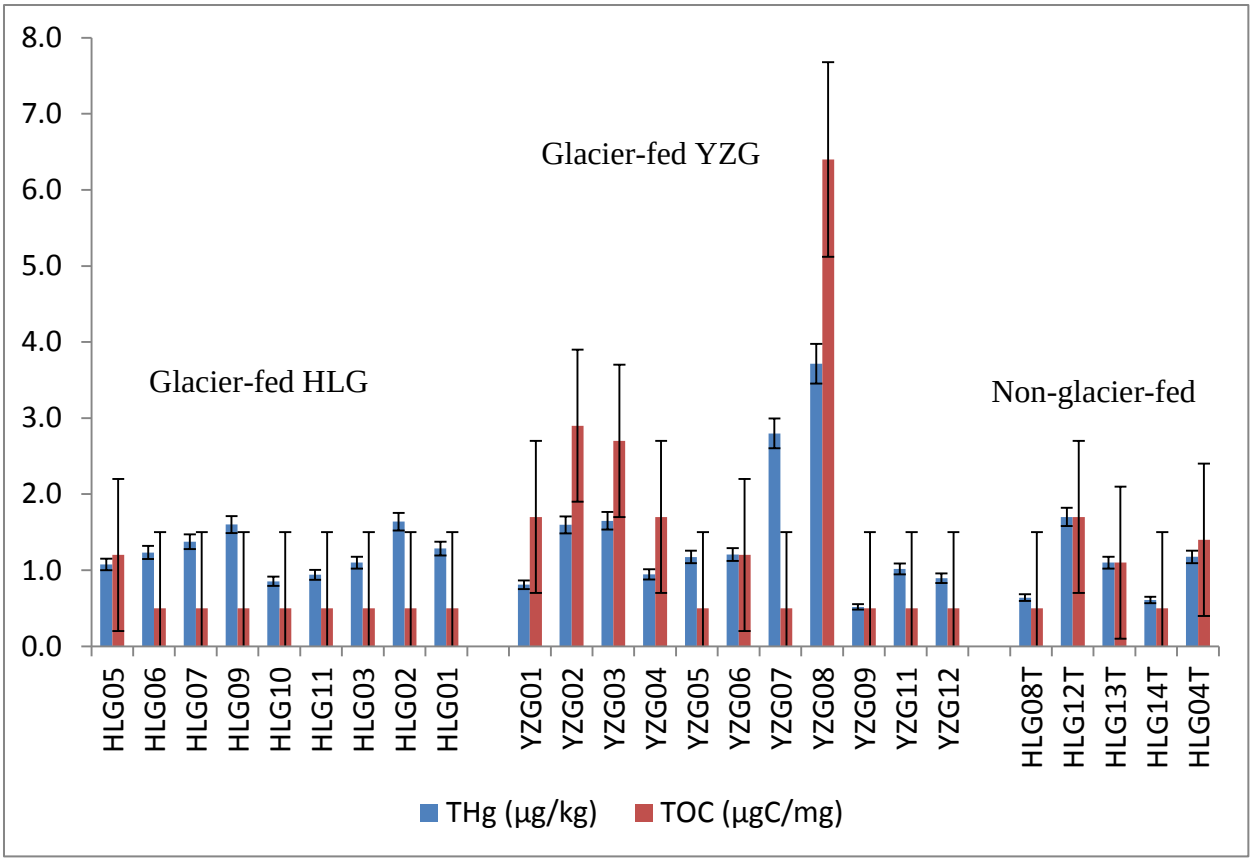

Figure 4.5.1-1: THg (µg/kg) and TOC (µgC/mg) in surface sediments from GF streams in HLG (right), YZG (middle), sorted from upstream to downstream (left to right), and from NGF tributary streams (right). TOC at HLG01, HLG02, HLG03, HLG06, HLG07, HLG09, HLG10, HLG11, YZG05, YZG07, YZG09, YZG11, YZG12, HLG08T and HLG14T shown as LOD/2. Error bars show analytical uncertainty for THg and TOC (see section 3.5.1).

4.5.2 Mercury in sediment profiles

THg sediment profiles for one GF and one NGF sampling site are shown in figure 4.5.2-1 and 4.5.2-2 respectively. An increase in THg with depth, from 1.1 to 3.7 µg/kg, is seen in the NGF HLG13T profile (figure 4.5.2-2). In the GF HLG09 profile however (figure 4.5.2-1), there are very small differences in concentrations between the layers; range 1.0-1.6 µg/kg. TOC is in the same low concentration range in the sediment profiles as in the surface sediments; varying from <1.0 to 1.8 µgC/mg. Neither THg, nor TOC concentrations are significantly higher in the HLG13T profile than in the HLG09 profile ($p=0.12$ and $p=0.20$ respectively). Furthermore, the HLG13T profile shows no significant THg-TOC-correlation ($R^2=0.62$, $p=0.12$).

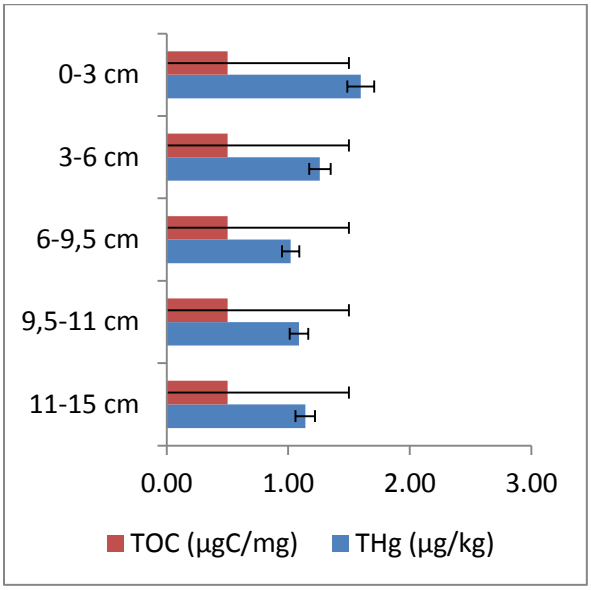

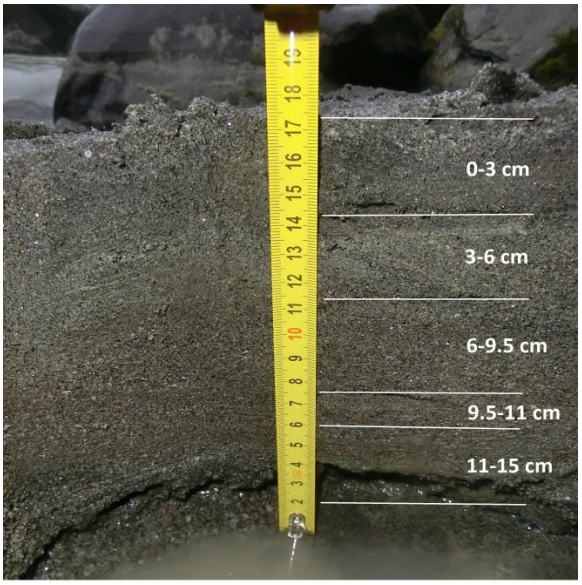

Figure 4.5.2-1: THg (µg/kg) and TOC (µgC/mg) in a sediment profile at HLG09. TOC concentrations for all five layers shown as LOD/2. Error bars show analytical uncertainty for THg and TOC (see section 3.5.1).

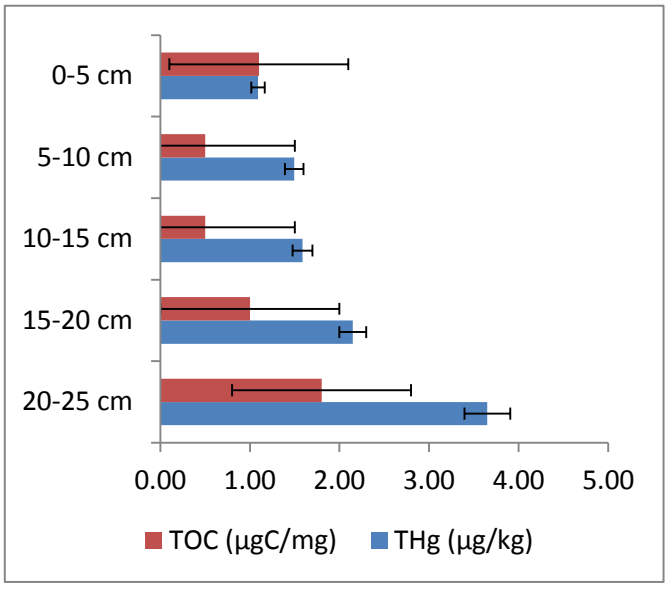

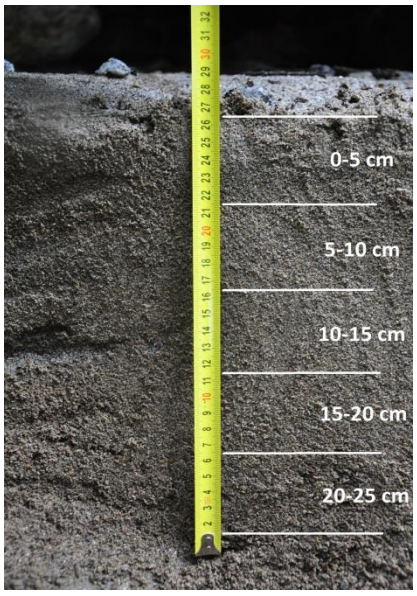

Figure 4.5.2-2: THg (µg/kg) and TOC (µgC/mg) in a sediment profile at HLG013T. TOC concentrations at depths 5-10 cm and 10-15 cm shown as LOD/2. Error bars show analytical uncertainty for THg and TOC (see section 3.5.1).

4.6 Mercury in a peat bog

THg (µg/kg) and TOC (µgC/kg) in the peat core from the CHZ-bog, upslope from the main river in the HLG valley, as marked in section 3.1.2, figure 3.1.2-1, is shown in a downwards depth profile of 20x 1 cm layers in figure 3.6-1. THg ranges between 124 and 232 µg/kg with a mean of 179 ± 32 µg/kg, while TOC ranges from 189 to 382 µgC/kg with a mean of 318 ± 59 µgC/kg. A full table of THg (µg/kg) and TOC (µgC/mg) concentrations is found in appendix J, table J-5. A positive correlation is seen between THg and TOC (R^2=0.75, P<0.001). Linear regression plot is shown in appendix K, table K.2-1.

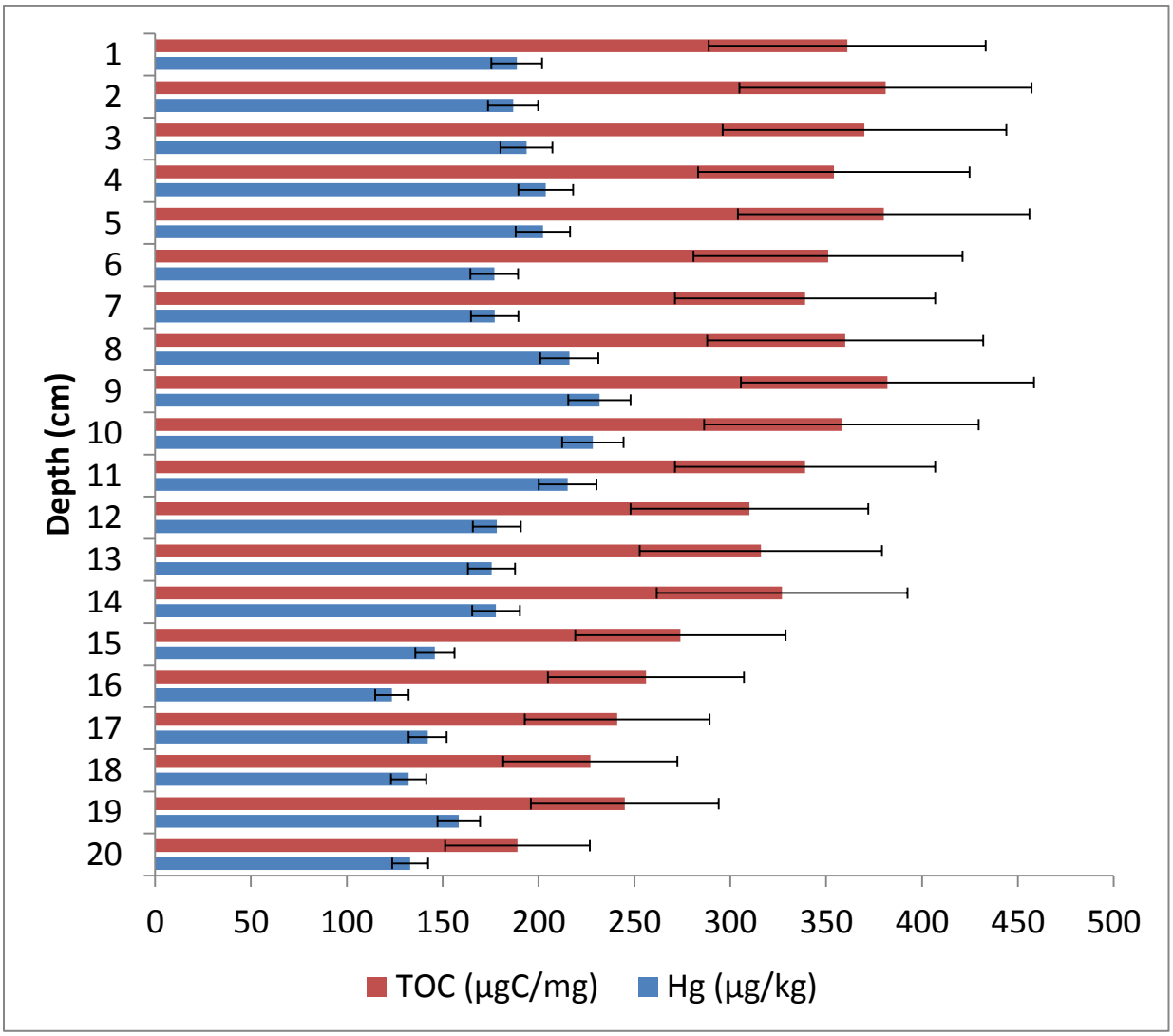

Figure 4.6-1: THg (µg/kg) and TOC (µgC/mg) for the peat core from the CHZ bog with 20x 1 cm layers, shown from top to bottom. Error bars show analytical uncertainty for THg and TOC (see section 3.5.1).

The concentrations of THg, DHg, MMHg, DMMHg, TSS and TOC for the CHZ-bog water are summarized in table 4.6-1. There is little difference in THg between the two seasons (0.1 ng/L), but MMHg is reduced by 75% from fall to spring. DHg constitutes 40% of THg in spring 2013.

Table 4.6-1: Summary of the CHZ-bog water concentrations of the parameters: THg (ng/L), DHg (ng/L), MMHg (ng/L), DMMHg (ng/L), TSS (mg/L) and TOC (mgC/L).

Parameter/ Season	**THg (ng/L)**	**DHg (ng/L)**	**MMHg (ng/L)**	**DMMHg (ng/L)**	**TSS (mg/L)**	**TOC (mgC/L)**
Fall 2012	2.9	n/a	0.56	0.54	n/a	7.60
Spring 2013	3.0	1.2	0.14	0.08	6.3	4.30

4.7 Characterization of suspended particles

BSE-SEM images at 200x magnification, of filtrates from four sampling points (HLG01, HLG09, HLG04T and HLG08T), are shown in figure 4.9-1 below. What can be observed from these images is that there is a larger amount of particles in the GF streams than the NGF streams; in HLG01 and HLG09 the surfaces are completely covered by particles while in HLG04T and HLG08T clusters of particles are seen between the fibers of the GF/F filter. The visual observations are supported by the TSS results: the GF HLG01 – 198.3 mg/L and HLG09 – 378.9 mg/L compared to the NGF HLG04T – 5.5 mg/L and HLG08T – 8.3 mg/L.

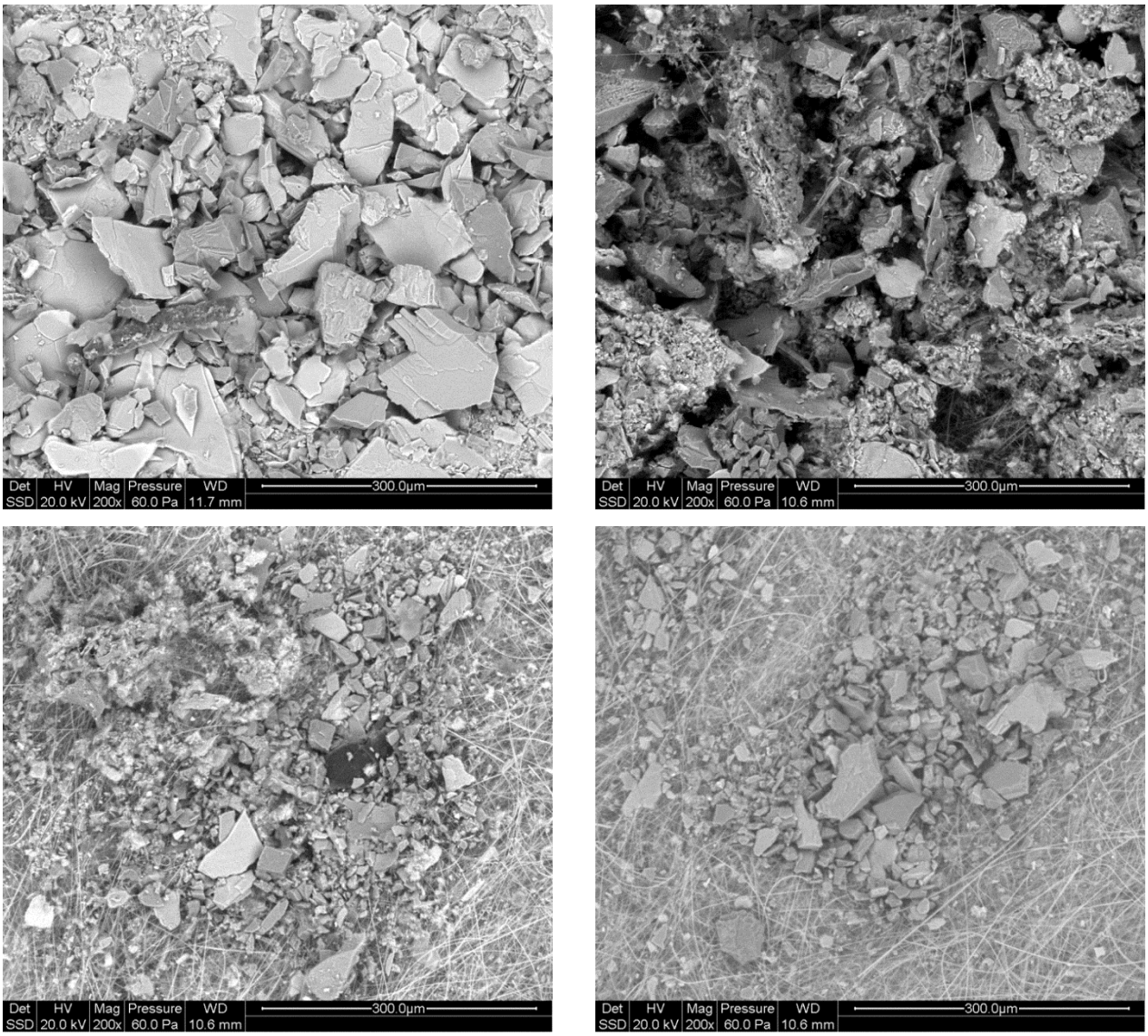

Figure 4.7-1: BSE-SEM images at 200x magnification of filtrated particles from HLG01 (upper left), HLG09 (upper right), HLG04T (lower left) and HLG08T (lower right).

From the elemental contrast within each one of the BSE-SEM images, it can be observed that the elemental composition of the particles in both stream systems is relatively uniform. This is because there are no large variations in brightness within each image, which is the indicator of elemental contrast, except in the case of a small number of singular particles. It must be noted that the focus, contrast and brightness settings are not the same for all the images, so an intercomparison between images should not be made, only intracomparisons of particles within each image.

EDS scans of 11 single particles from the different samples show similar elemental compositions (figures 4.7-2 – 4.7-12). There were only small differences between the average

looking particles (n=7) as they all contained oxygen, silicon, aluminum as the dominating elements, with varying amounts of iron and alkaline- and alkaline earth metals such as calcium, magnesium, potassium and sodium (figures 4.7-2, 4.7-5, 4.7-6, 4.7-7, 4.7-9, 4.7-10 and 4.7-11). Both the darker (n=2) and lighter (n=2) particles had similar compositions to the average particles, in addition to the darker particles containing carbon (figures 4.7-3 and 4.7-8) while the brighter particles contained Ti (figure 4.7-12) or Mo/Pb and elevated amounts of Fe (figure 4.7-4).

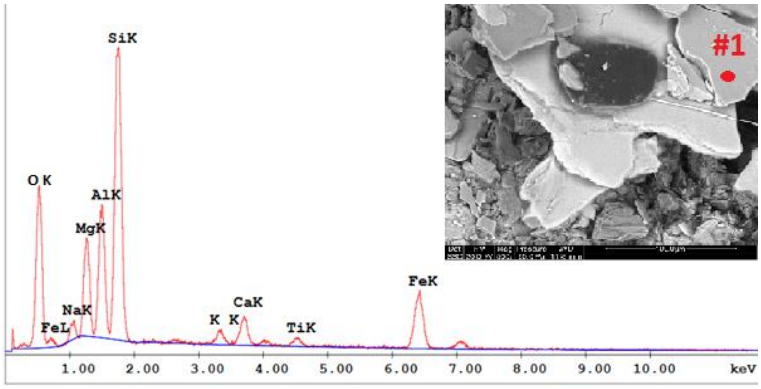

Figure 4.5-2: EDS spectrum of point #1 from HLG01-1. Peaks identified according to keV signal of related elemental orbital transition.

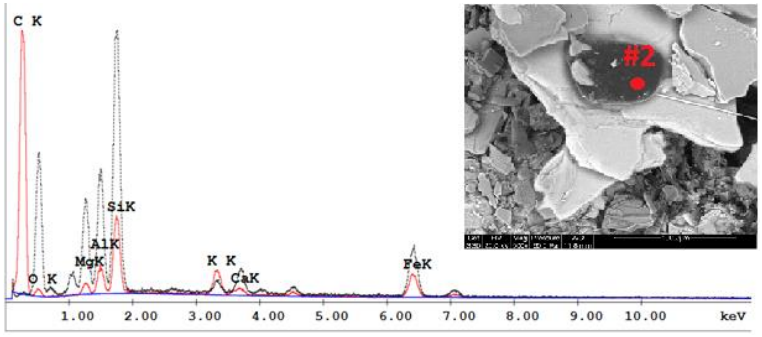

Figure 4.5-3: EDS spectrum of point #2 from HLG01-1, superimposed over point #1. Peaks identified according to keV signal of related elemental orbital transition.

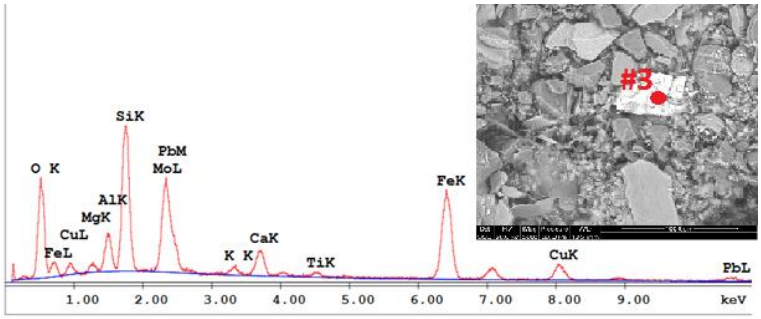

Figure 4.5-4: EDS spectrum of point #3 from HLG01-2. Peaks identified according to keV signal of related elemental orbital transition.

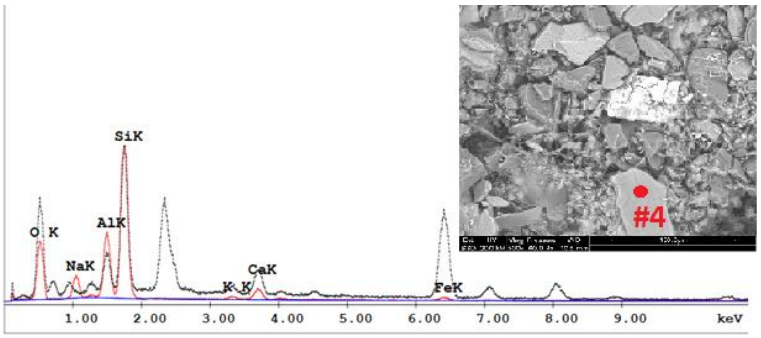

Figure 4.5-5: EDS spectrum of point #4 from HLG01-2, superimposed over point #3. Peaks identified according to keV signal of related elemental orbital transition.

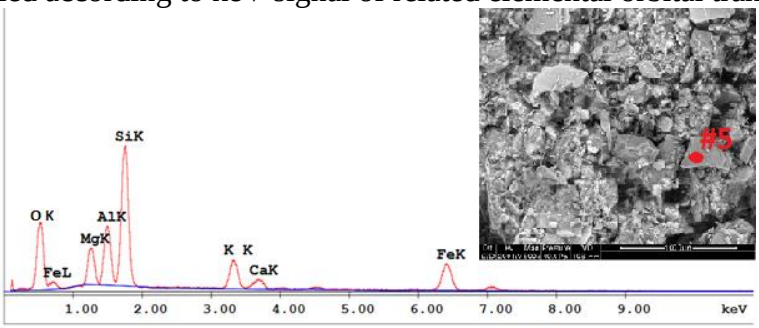

Figure 4.5-6: EDS spectrum of point #5 from HLG09-1. Peaks identified according to keV signal of related elemental orbital transition.

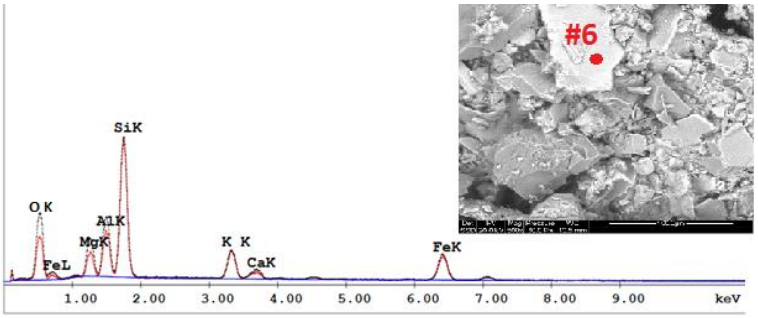

Figure 4.5-7: EDS spectrum of point #6 from HLG09-2, superimposed over point #5. Peaks identified according to keV signal of related elemental orbital transition.

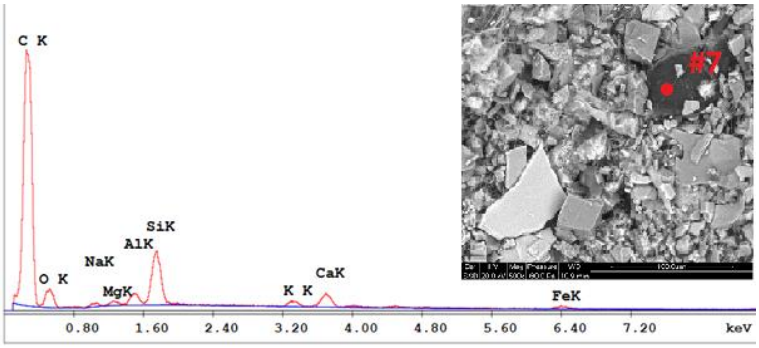

Figure 4.5-8: EDS spectrum of point #7 from HLG04T-1. Peaks identified according to keV signal of related elemental orbital transition.

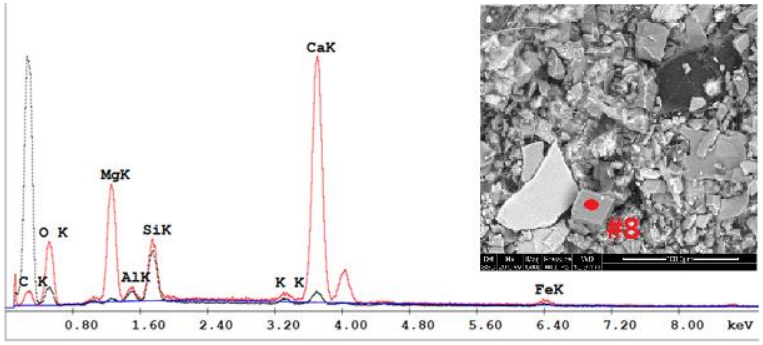

Figure 4.5-9: EDS spectrum of point #8 from HLG04T-1, superimposed over point #7. Peaks identified according to keV signal of related elemental orbital transition.

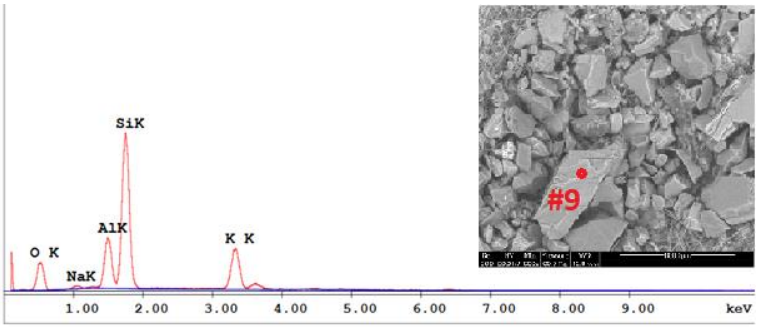

Figure 4.5-10: EDS spectrum of point #9 from HLG08T-1. Peaks identified according to keV signal of related elemental orbital transition.

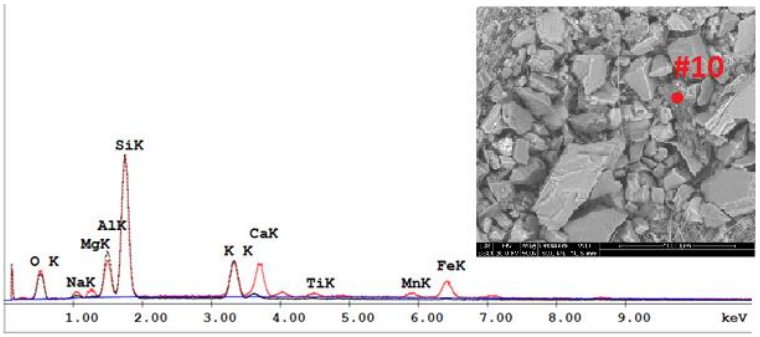

Figure 4.5-11: EDS spectrum of point #10 from HLG08T-1, superimposed over point #9. Peaks identified according to keV signal of related elemental orbital transition.

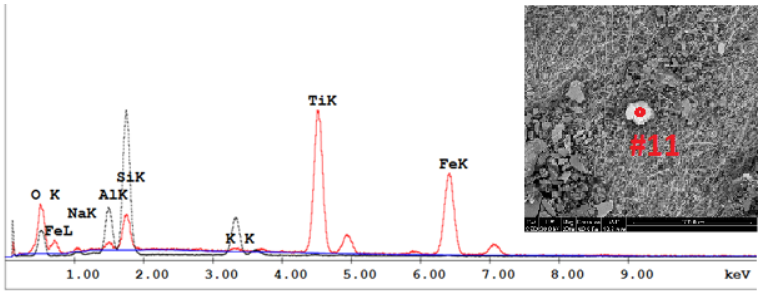

Figure 4.5-12: EDS spectrum of point #11 from HLG08T-2, superimposed over point #9.

Peaks identified according to keV signal of related elemental orbital transition.

5. Discussion

5.1 Mercury in the Mt. Gongga streams compared to other studies

The mean concentrations in the GF streams and NGF tributary streams were lower for both sampling campaigns; fall 2012 GF 1.3 ± 0.8 ng/L and NGF 0.5 ± 0.3 ng/L and spring 2013 GF 2.5 ± 4.8 ng/L and 0.7 ± 0.5 ng/L (appendix A, table A-2), than what was reported in the Hg budget study of the same area, which showed mean GF THg at 3.19 ng/L and NGF THg at 3.60 ng/L (Fu et al., 2010). The relatively small difference between GF and NGF THg and the fact that NGF THg was higher than GF THg is somewhat contradictory to what has been found in this study, but Fu et al. (2010) collected their samples in July, thus capturing a different melting profile. They attributed the higher THg in the NGF streams to soil erosion and runoff due to high precipitation. In general, the THg concentrations in the Mt. Gongga streams found both in this project and by Fu (2010) are in the same range as THg found in Southeastern Alaskan streams by Nagorski et al. (2014). A water quality study of four major rivers originating on the Tibetan Plateau; Salween, Mekong, Yangtze and Yarlung Tsangpo, reported DHg concentrations below 1 ng/L (X. Huang, Sillanpää, Duo, & Gjessing, 2008), which is similar to the low DHg concentrations found in the GF streams at Mt. Gongga.

Much more attention has been given to study Hg cycling in the Arctic and Antarctic compared to alpine environments. Glacial meltwater in Antarctic streams was reported to have THg concentrations of 0.54-0.90 ng/L (Vandal et al., 1998) and 0.27-1.80 ng/L (Lyons et al., 1999) in two baseline studies. These concentrations are similar to what was found in the fall 2012 sampling in this project (figure 4.2-1), but quite a lot lower than the high concentrations seen in the YZG valley in the spring 2013 sampling (figure 4.2-2). Several studies have also been focused on Hg concentrations in Arctic rivers, which receive varying degrees of glacier runoff, and some of these are summarized in table 5.1-1. The DHg concentrations found in these arctic rivers (0.34-1.6 ng/L) are somewhat higher than what was found in this study (<0.1 – 0.3 ng/L). It must be mentioned, however, that the Lena, Ob, Yeisei and Mackenzie rivers are major rivers of Siberia and the Northern Territories of Canada, which do receive meltwater from glaciers, but also large amounts of runoff from a plethora of mountain- and forest sub catchments (Coquery, Cossa, & Martin, 1995; Outridge et al., 2008). Furthermore, the Katun river lies in an area with geologic formations carrying Hg-containing minerals such

as Cinnabar (Sukhenko, Papina, & Pozdnjakov, 1992). The arctic Zackenberg river in Greenland had more similar concentrations of DHg to the Mt. Gongga streams and in Zackenberg and the Mt. Gongga streams alike, PHg was found to contribute to the most significant share of the total Hg load (Rigét et al., 2011).

Table 5.1-1: Mean concentrations of Hg_D (ng/L) and Hg_P (µg/g) in Arctic rivers from different studies. Table adopted from Riget. et al. (2011).

Arctic river	**Mean Hg concentrations**		**Reference**
	Hg_D (ng/L)	**Hg_P (µg/g)**	
Zackenberg, Greenland	0.34 ± 0.15	0.04 ± 0.03	(Rigét et al., 2011)
Lena, Siberia	5.0 ± 0.6	0.12 ± 0.12	(Coquery et al., 1995)
Ob, Siberia	2.8 ± 0.6	0.05 ± 0.003	(Coquery et al., 1995)
Yeisei, Siberia	1.5 ± 0.7	0.05 ± 0.007	(Coquery et al., 1995)
Katun, West Siberia	0.8	1.35	(Sukhenko et al., 1992)
Mackenzie, Canada	1.61	0.0013	(Outridge et al., 2008)

Hg_D – dissolved Hg (water filtered to <0.4 µm), Hg_P – particle bound Hg (in filtrates >0.4 µm)

THg concentrations in streams of other forested catchments, not affected by point-source pollution, in different parts of Southwestern China: Mt. Leigong, Mt. Tieshanping and Mt. Luchongguan, range from 1.9 to 36.3 ng/L with mean 4.3 ± 2.5 ng/L (Z. Wang, Zhang, Xiao, Zhijia, & Yu, 2009). As summarized by Lin et al. (2012), these concentrations are comparable to similar stream systems in Europe. The THg concentrations in the GF streams of Mt. Gongga are within, but in the lower part of this range. One would expect the concentrations to be even lower at Mt. Gongga, since this area is more remote than Mt. Leigong, Mt. Luchongguan and Mt. Tieshanping, which are located near the cities of Guiyang and Chongqing, in the largest Hg-producing districts in China (Z. Wang et al., 2009).

Compared to rivers affected by point-soruce Hg pollution, such as the Songhua and Wuli rivers, where THg concentrations of >700 ng/L and ~200 ng/L respectively have been recorded (Lin et al., 2012), it is obvious that the concentrations found at Mt. Gongga were low. Finally it should be noted that the THg concentrations in the streams in and around Mt. Gongga are well below the WHO upper limit value for THg in drinking water – 1000 ng/L (WHO, 2004).

5.2 THg in GF and NGF streams

The trends reported for the GF and NGF streams at Mt. Gongga are not unified in supporting the hypothesis of Hg release by melting glaciers. Hg in GF streams was significantly higher than in NGF streams in the fall 2012 sample set, but not for the YZG valley. Why the THg concentrations were lower in YZG than in HLG could be related to a lower particle load in the YZG streams, but unfortunately no TSS data is available for this sample set. In spring 2013 there are no statistical significant differences between Hg in GF and NGF streams, but THg concentrations are 28 and 19 times higher in the GF side rivers YZG05 and YZG09 respectively, than the mean NGF concentration of 0.7 ± 0.5 ng/L. It therefore seems highly plausible that the glaciers are important contributors of Hg to the catchments below.

If there is a continuous atmospherical deposition to the glacier snow and ice cover, one might expect the concentrations down through the snow pack to be uniform. However, this is not necessarily the case. As a snow pack core study by Zhang et al. (2012) from glaciers in Tibet showed, there are post-depositional processes which cause Hg to percolate down through the snow and accumulate in re-frozen ice layers. Furthermore, the atmospherical deposition is all but uniform, both temporally and spatially. It is affected by the amount precipitation, which is efficient in scavenging Hg from the atmosphere (Sakata & Asakura, 2007), and by other weather related phenomena, such as dust storms carrying PHg (J. Huang, Kang, Guo, et al., 2012) or re-volatilization of Hg due to strong solar irradiation (Poulain et al., 2004). The concentrations down through the snow layers could therefore be highly variable, as was shown in snow pack cores from several glaciers in Western China (Q. Zhang et al., 2012). Furthermore, Hg accumulated in deeper ice layers represent a temporal profile going back hundreds of years and will vary according to historical atmospherical deposition (Schuster et al., 2002). Thus one might receive pulses of high or low Hg to the meltwater depending on what part of the glacier is contributing to the meltwater at a specific point in time. Additionally the first days of spring melting have been shown to give pulses of ions, depleting Hg from the snowpack (Dommergue et al., 2003). The best way to properly show the differences between GF and NGF streams would therefore probably have been to sample during the start of spring melting, as was intended in this project or better to do continuous sampling over time, which was outside the scope of this project.

A few comments should be highlighted regarding the NGF tributary streams and the other sampling points included in the data sets (MHX and DDH). The relatively large variation (0.2-1.0 ng/L in fall 2012 and 0.1-1.6 ng/L in spring 2013) in the NGF streams are as expected, since these streams are all situated in different areas, being fed by water from separate parts of the local catchments. Additionally, the HLG14T stream runs by an area with geothermal hot springs (figure 4.1-2). Water from the hot springs and the pools of a hot spring resort mixes with the stream water and might add a source of Hg (Hg pollution from the resort and/or Hg from groundwater), which is not present in the other NGF streams, with YZG10T being the exception, as it is primarily fed by a groundwater source. The two NGF sampling points, HLG14T and YZG10T, show the highest concentrations of THg among the NGF streams in the spring 2013 set; 1.6 ng/L and 1.1 ng/L respectively.

The MXH sampling points were included to see if human activities around Moxizhen lead to elevated THg concentrations in the surrounding rivers. This is probably not the case, as these sampling points had concentrations similar to the NGF streams; 0.7 ± 0.2 ng/L and 0.7 ± 0.5 ng/L for fall 2012 and spring 2013 respectively. They were not reported as GF sampling points or included in statistical analysis, however, as they receive runoff from many different sources. The streams of Mt. Gongga all eventually drain into the Dadhing River (DDH). This river is much larger than any of the Gongga rivers and runs through populated areas and several small cities such as Danba and Luding. At Luding the river runs into a reservoir to be used for a hydroelectric power plant which was under construction at the time of the study. The DDH River therefore probably receives Hg from multiple sources, natural and anthropogenic, and as expected the THg concentrations are higher in this river than in the Gongga streams.

Due to the fact that the processes of Hg release to meltwater from alpine glaciers have not been studied to any large extent, there is little data available to make direct comparisons with this study. At the present time no other study has been focused solely on showing the release of Hg_{atm} in alpine glaciers to meltwater, but a few select studies have acknowledged the presence of Hg in glacial meltwater and used it in discussing related phenomena. These include a Hg budget of the Mt. Gongga area done by Fu et al. or a (2010) or a study by Nagorski et al. (2014) of the spatial distribution of Hg in Southeastern Alaskan streams as influenced by different landscape types (glaciers being one of these). The lack of material to

compare the results of this project with bears witness of the need to further document the processes in question.

5.3 Seasonal differences

As the intention was to capture two different type of melting profiles (section 3.1.3) it was important to identify whether or not the sampling campaigns were well timed. Arriving at Mt. Gongga in late September 2012, winter had not set in yet; there was no fresh snow in the lower parts of the mountain (500-4000 m.a.s.l), and the GF rivers were observed to have a moderate flow, probably resulting from firn- and ice-melt in addition to precipitation. It is reasonable to assume that the sampling was well timed and that the intended melting profile was captured.

The timing of the second sampling campaign was more critical, since the profile of spring melting onset was to be captured. In mid-March 2013 a contact at the mountain affirmed that the snow had been gone from the lower parts of the mountain for several weeks and that spring was about to set in. However, on the day after the arrival at Mt. Gongga (April 5th. 2013) it started snowing heavily. The heavy snowfall, which ended up blanketing the greater part of the study area (figure 4.3-1), probably meant that winter was still lingering, especially in the higher parts of the mountain. Also, the flows of the main GF streams in both valleys gave further indications that the glaciers had not yet been affected by spring melting, as they were observed to be significantly lower at that point compared to during the fall sampling campaign.

Figure 5.3-1: The Hailouguo valley covered in snow (05.04.2013), as seen from above the lower glacier (photo: Vemund S. Finstad).

The load of suspended solids in stream water usually increases with flow (Ongley, Bynoe, & Percival, 1981). TSS concentrations can therefore be used indirectly to compare the flow states during the two separate sampling campaigns. Unfortunately TSS data is only available for a few sample sites in the fall 2012 data set (due to logistical shallenges). At the highest altitude sampling point in HLG: HLG05 (3590 m.a.s.l.) (figure 4.1-1), the stream flow was observed to be strongly reduced, something which is also evident in the change of TSS concentration from 374.5 mg/L in fall 2012 to <1.0 mg/L in spring 2013. At HLG01, the lowest altitude sampling point in HLG (1818 m.a.s.l.) (figure 4.1-1), a reduction in TSS is also seen, from 198.3 mg/L in fall 2012 to 28.5 mg/L in spring 2013. These data support the observed change in flow between the two sampling campaigns, which suggests that spring had not yet set in at the time of the second sampling.

A reduction in THg concentrations from fall to spring for the majority of the sampling points was far from what was expected. Full scale spring melting was expected to cause high flows with subsequent high particle loads in the streams (Ongley et al., 1981) and thus probably higher THg concentrations, as seen from the THg-TSS correlation (section 4.4.2), in addition to possible ionic pulses from snow-melt (Dommergue et al., 2003). Therefore the lower THg concentrations in the GF streams in spring compared to fall also suggest that spring melting had not started.

However, it is probable that the profile of spring melting is captured in the two side-rivers, YZG05 and YZG09, which show THg concentrations at an order of magnitude higher in spring 2013 than in fall 2012. In addition, these two side rivers had THg concentrations at almost two orders of magnitude higher than the lowest concentrations found in the other GF streams (figure 4.3-2). The high THg concentrations seen in these two side-rivers are in the order of what had been expected for all the GF streams in the spring sampling. These two side rivers were also observed to have a higher flow in spring 2013 than during the previous sampling campaign and the water was clearly very turbid in both streams.

This notion is further strengthened by the TSS concentrations which were 4834 mg/L and 2923 mg/L in YZG05 and YZG09 respectively; a striking difference from the median TSS of 68.6 mg/L. The high particle load in these two side streams compared to the other GF streams might indicate that more dramatic hydrological processes were at work at their origin; the E-

Konka glacier. The E-Konka peak is at a lower altitude – 6618 m.a.s.l., than the Gongga peak which is at 7556 m.a.s.l.. The area of E-Konka peak is furthermore smaller, and so are its glaciers (Google Earth), making them more sensitive to temperature changes (Stern et al., 2012). It is therefore possible that the lower lying glacier at Mt. E-Konka was further ahead in the spring melting process than the glaciers at Mt. Gongga.

In addition to unfortunate timing of the 2013 sampling campaign, the fresh fallen snow created further complications. Snow samples taken at two points close to HLG05 had THg concentrations of 1.5 and 2.9 ng/L. This snow, which fell in varying amounts down through the valley, created an extra flux of Hg to GF and NGF streams alike, and might be one of the reasons why there is less difference between THg concentrations of these two systems in the spring 2013 sample set (figure 4.2-2) compared to the fall 2012 sample set (figure 4.2-1).

5.4 Fractionation

5.4.1 Dominant fractions and their significance

In order to support the fractionation analysis, showing that PHg is the dominant fraction, the relation of THg to TSS is helpful. The strong correlation between THg and TSS in the GF streams (figure 4.4.2-1) agrees with PHg being the dominant fraction in this system. Similar results have been found for GF rivers in Southeastern Alaska, where PHg was found to constitute 70% of THg (Nagorski et al., 2014). Glaciers grind up and crush the bedrock underneath and their release of meltwater will naturally wash out these materials into the GF streams (Bajewsky & Gardner, 1989). The PHg domination in the GF stream systems at Mt. Gongga thus suggests that the Hg might be primarily of a geogenic origin (Hg_{geo}) and not from atmospherically deposited Hg (Hg_{atm}) stored in the snow and ice of the glaciers.

The absence of correlation between THg and TSS in the NGF streams along with a strong THg-TOC correlation indicate that the Hg fractionation might be different in the NGF streams. These correlation relationships further supports a notion that DHg might be a more dominant fraction in this system than what could be detected since THg concentrations were close to LOD in the NGF streams and DHg was mostly below LOD (appendix G, table G-1). Thus, one cannot say anything about the relative amounts of DHg present in most of the samples, only the fact that it is <0.1 ng/L. Low TSS concentrations in the NGF streams mean

lower particle loads in these streams, probably due to less erosion, and thus less Hg_{geo}. It is likely that the Hg in these streams is of an atmospheric origin, delivered to the streams through precipitation and runoff from soil and vegetation. This hypothesis was tested through statistical analysis, and the presence of Hg_{atm} in the NGF streams was confirmed; more on this in section 5.5.

There are several aspects of the fractionation results which indicate that the two YZG side rivers, YG05 and YZG09, show different trends than the rest of the GF streams. Examples of this are that the THg-TSS correlation improves upon removing these points (appendix C, figures I.1-1 vs. I.1-2) and that the THg-TOC correlation worsens upon removing these points (appendix I, figures I.2-1 vs. I.2-2). There is, however, still very low amounts of DHg in these side rivers, both had concentrations <LOD (0.1 ng/L) (appendix G, table G-1), something which can possibly be explained by Hg_{atm} from the glacier sorbing to available sites on the surfaces of the plethora of particles present in the water.

5.4.2 Particle properties

Even though an intercomparison cannot be made between the BSE-SEM images it can be seen from the elemental contrast that there are small inherent variations in each sample. Furthermore, the EDS scans of representative particles in each sample show that they have similar elemental compositions. Thus it is reasonable to assume that the particles seen in both stream systems are generally the same and that the only major difference is the difference in the particle load, which is supported by the TSS data (appendix H, table H-1).

The dominance of oxygen, silicon along with aluminum suggests that the suspended particles in both river systems are mainly inorganic clay particles. Inorganic particles, such as clays, are well known to work as cation exchangers in natural waters by adsorbing metal cations to negatively charged surfaces (vanLoon & Duffy, 2011). The cation exchanger role of these particles is possibly exemplified in the fact that the scanned particles contained various amounts of alkaline- and alkaline earth metals and Fe. Of course these metals and the other heavy metals detected could also be a part of other minerals from the bedrock, but the recurring Al, O and Si combination indicates clay particles. This matter would be easier to settle if the relative amounts of each element could be quantified, but due to the high

uncertainty related to detecting lighter elements such as O and C the percentage distribution of the respective elements cannot be trusted.

The clay particle character of the suspended solids explains how Hg could be sorbed to the suspended solids in the water column and connects well with the PHg fractional dominance. Hg would also be present naturally within the particle fraction as part of mineral fragments from the bedrock. It is likely that any free Hg in the water column would readily be sorbed to the many clay surfaces available in the GF streams, something which could explain the low DHg concentrations (appendix G, G-1) despite there being Hg_{atm} present. The poorer Hg-TSS correlation seen in the NGF streams is probably due to the fact that there are fewer particles in these streams and higher TOC, which means less clay surfaces to adsorb Hg and more DNOM to keep Hg complexed in the dissolved fraction.

5.4.3 MMHg

Finding MMHg to be below or barely above 0.02 ng/L in all the sampled stream systems at Mt. Gongga agrees well with what is known about the potential for methylation in rivers. Methylation is favored in wetlands or lake sediments with anaerobic conditions, high THg and TOC concentrations, SRB and nutrients present (Ullrich et al., 2001). Although favored in the mentioned areas and situations, methylation does occur in other places, e.g. in the water column of lakes or rivers. Furthermore, the net production of MMHg is a result of continuous and competing methylation and de-methylation processes (Benoit et al., 2003).

As could be observed the GF rivers at Mt. Gongga were fast moving, well aerated streams. They have relatively low THg concentrations; 1.3 ± 0.8 and 2.5 ± 4.8 ng/L in fall 2012 and spring 2013 respectively, and TOC concentrations; 0.4 ± 0.2 and 0.7 ± 0.9 mgC/L in fall 2012 and spring 2013 respectively. The NGF streams were observed to be much narrower and not as fast moving as the GF streams, but they also have low THg concentrations; 0.5 ± 0.3 and 0.7 ± 0.5 ng/L in fall 2012 and spring 2013 respectively and low TOC; mean 0.56 ± and 0.53 ± mgC/L in fall 2012 and spring 2013 respectively. Both systems, GF and NGF, therefore do not provide conditions considered favorable for methylation.

Of the THg concentration, MMHg generally constitute less than 10% (Lin et al., 2012) and the potential for methylation is typically expressed as the fraction of MMHg present in a

sample (Eckley & Hintelmann, 2006; McClain et al., 2003). The potential for methylation in the streams of Mt. Gongga is assumed to be low as most of the sampling points had detectable THg concentrations (>0.1 ng/L), but not detectable MMHg concentrations (<0.02 ng/L). Among the sampling points with detectable MMHg concentrations, %MMHg ranged from 0.1-6.% (table 4.4.4-1), with the highest potentials being found at HLG03 (5%, spring 2013) and HLG04T (6%, fall 2012). The low methylation potential found in the GF streams of Mt. Gongga agrees well with what has been found for glacier runoff elsewhere (Nagorski et al., 2014; St. Louis et al., 2005). As expected the CHZ-bog had a much higher potential for methylation than any of the streams, but only in the fall 2012 data set where %MMHg was as high as 19% (table 4.4.4-1). This fraction is higher than the %MMHg found in soil in some Boreal wetlands that have been considered net sources of MMHg (Tjerngren, Karlsson, Bjoern, & Skyllberg, 2012; Tjerngren, Meili, Bjoern, & Skyllberg, 2012). In the spring 2013 data set the %MMHg fraction in the CHZ-bog has been reduced to a mere 5% (table 4.4.4-1).

5.5 The background archive – stream sediments and a peat bog core

5.5.1 Stream sediments

The surface sediment concentrations (figure 4.5.1-1) are quite low compared to the estimation of the average Hg content in the earth's crust (Wedepohl, 1995). Crustal Hg was about 40 times higher than the mean THg in the sediments of the GF streams and about 50 times higher than the mean NGF stream sediment THg (appendix J, table J-2). The crustal estimate however, is an estimate based of the average composition of a 3000 km stretch of the European continental crust, from north to south, and one would thus expect deviations from this estimate due to natural variations in the curst around the world. Few studies have documented sediment concentrations of Hg in rivers fed by glacier runoff, especially in the geographical region of this study. A study from a remote area in Alaska shows mean THg of 15.5 µg/kg in river bed sediments of GF rivers (Nagorski et al., 2014), which is also quite a lot higher than what was found in the Mt. Gongga stream sediments, where the highest concentration was 3.6 µg/kg (figure 4.5.1-1). Overall Hg concentrations in river sediments from around the world vary greatly and have been reported to range from 50 to 400 µg/kg in unpolluted sediments and up to 1000 mg/kg in polluted sediments, as summarized by Lin et

al. (2012). For the large Chinese rivers; Yangtze River, Pearl River and Yellow River, Hg concentrations have been reported to range from 0.1 to 1.0 mg/kg (Lin et al., 2012).

NOM, as represented by the analytical proxy – TOC, acts as an important complexing agent for heavy metals such as Hg in natural waters (Ravichandran, 2004; vanLoon & Duffy, 2011) and a positive correlation between Hg and TOC is also found in sediments (Ethier et al., 2010; Ravichandran, 2004; Sanei & Goodarzi, 2006). This means that sediments with high TOC generally have higher THg, as the NOM helps to bind and thus stabilize Hg in the sediment. The TOC-poor sediments of the Mt. Gongga streams are therefore naturally low in THg. Since Hg is mainly in the PHg fraction and TOC concentrations are low in both the GF water column and the river sediments, it is reasonable to assume that the main process driving the accumulation of Hg in the GF stream sediments is the settling of inorganic particles.

Sediment profiles have been used as historic records of deposited Hg (Lockhart et al., 2000; Yang et al., 2010). For such a record to be accurate however, previously deposited layers must remain undisturbed, so sediment records are therefore more commonly retrieved from deep lakes rather than rivers. The GF stream from which the HLG09 profile is retrieved is fast moving and has a turbulent flow, especially at flood events during spring melting or high precipitation, and therefore probably does not constitute a good historical record. However, assuming the profile could be used as a record, the uniform concentrations seen down through the layers in this profile (figure 4.5.2-1) could indicate that there has been little change in Hg deposition to the stream bank during the captured time frame.

In the HLG13T profile however, a slight increase in THg with depth is seen (figure 4.5.2-2). This profile is taken from a distinctly different stream; a small mountain stream tributary to the main GF river in the HLG valley. This stream might be subject to increased flow during snow melt and episodes of high precipitation, but nothing in the scale of the increase in water flow levels caused by glacial melting. The TOC concentration is also higher in the sediments from this stream, making Hg capture and storage more efficient and stable (Sanei & Goodarzi, 2006). It cannot be said that this sediment profile could constitute a fully reliable historic record, but more so than the other profile and a qualitative comparison with the peat bog core will be made.

5.5.2 Peat bog core

Ombrotrophic peat bogs such as the CHZ-bog have been widely used as historical records of Hg deposition from the atmosphere (Benoit, Fitzgerald, & Damman, 1998; Liu, Wang, Lu, Fang, & Wang, 2003; Madsen, 1981; Martínez-Cortizas, Pontevedra-Pombal, García-Rodeja, Nóvoa-Muñoz, & Shotyk, 1999) The chemical environment in the peat layers; complexation by NOM and favorable pH and pE conditions, contribute to immobilizing and storing Hg (Benoit et al., 1998). The positive correlation seen between THg and TOC (R^2=0.75, P<0.001) in the layers of the CHZ peat bog core, along with a relatively high TOC concentration of 4.1 mgC/L in the bog water (appendix H, table H-1) agree well with the storage conditions mentioned above.

What is generally seen in peat bog profiles is a pattern which reflects the history of Hg emissions to the atmosphere. Low concentrations in the lower part of the profile represent the background atmospheric Hg at pre-industrial times, then a dramatic increase upwards in the profile which reflect industrialization. In some parts of the world (e.g. Europe and North America), a decrease in concentration towards the very top of the profile, as a result of reduction in deposition due to local emission reduction (Benoit et al., 1998). A somewhat similar pattern can be seen for the peat bog core from the CHZ bog (figure 4.6-1). The peak concentrations occur around the middle of the profile (8-11 cm) with a not so sharp decrease towards the top (0-5 cm). The peak probably represents the height of industrialization, which came later in China than in the west. The slight decrease towards the top might be due to the top part of the profile not yet being as compacted as the lower layers, thus having less Hg per volume. A decrease of atmospheric deposition is not expected for this area, as atmospheric Hg emissions are still increasing in China (Pirrone et al., 2010). A sharp decrease towards the bottom of the profile, representing pre-industrial times, is not apparent, but it is likely that this trend could have been clearer if a deeper profile was sampled, as according to Madsen (1981), a 20 cm profile only dates back 125-175 years. This, however, is not an accurate dating estimate, but rather a general comparison, since peat accumulation time is site specific and could be distinctly different in the CHZ-bog. A deeper peat bog profile from Northeastern China shows the sharp decrease at the bottom in addition to an otherwise similar concentration pattern (Liu et al., 2003). THg concentrations in the top layer were almost identical in the CHZ bog and Liu et al.'s study (2003), 189 µg/kg and 185 µg/kg respectively, but the peak in the CHZ bog was approximately 15 µg/kg higher.

If one assumes that the integrity of the NGF stream profile (figure 4.5.2-1) is intact as a historic record, it is possible that it shows the same trend as the upper part of the peat bog profile (figure 4.6-1). The bottom layer of the stream profile thus probably represents the start of the peak at the middle of the peat bog profile, and it is reasonable to assume that a similar dip in concentration, as seen in the peat bog, could have been observed if the stream profile was deeper. Both profiles are similar in depth, but they do not represent the same time scales. Accumulation of peat layers in the bog is likely a lot slower than the sedimentation rate of particles on the bank of the stream.

5.6 Glacial or geogenic mercury?

Due to the PHg fractional dominance and the strong correlation between Hg and TSS it seemed plausible that the Hg in the Mt. Gongga GF streams was mainly of a geogenic origin. This does agree with the fact that glacier related processes are causing the mobilization of Hg, but rather from the bedrock underneath the glacier than from Hg_{atm} in the ice and snow layers.

In order to explore to what extent the Hg in the GF streams is of atmospheric origin different types mathematical analysis have been applied, both quantitative and qualitative: 1) empirical correlation of Hg with trace elements considered typically of geogenic or atmospheric origin (section 5.6.1), 2) principal component analysis (PCA) of Hg and 18 supporting parameters (section 5.6.2), 3) indirect mathematical correction based on the empirical relations Al-Hg and Ti-Hg (section 5.6.3) and 4) direct mathematical correction using the literature based crustal relations Al-Hg and Ti-Hg (section 5.6.4).

5.6.1 Empirical correlation analysis

Al and Ti can be considered conservative elements in the earth's crust (Boës, Rydberg, Martinez-Cortizas, Bindler, & Renberg, 2011) and therefore representatives of geogenic species. In addition, there are several elements that can be thought of as representatives for atmospheric pollution, such as: Be, Cd, Co, Mn, Mo, Ni, Pb, V and Zn. These elements are typically released to the atmosphere through combustion of coal, oil, wood, gasoline and refuse and from various industrial activities such as metal production. They have been used as tracers of atmospheric pollution because they were found to be enriched in aerosols compared to their natural background concentrations (Pacyna, Semb, & Hanssen, 1984). Since Asia

contributes to 34-42 % of the world total emission of these trace metals (table 5.6.1-1) one would expect these metals to be present in atmospheric pollution in Asia. The correlation between Hg and these geogenic and atmospheric tracers was thus explored in order to say something about the origin of the Hg. A good correlation with Al and Ti would indicate Hg_{geo}, whereas good correlations with Be, Cd, Co, Mn, Mo, Ni, Pb, V and Zn would indicate Hg_{atm}. The details and procedure of the correlation analysis are shown in appendix O, section O.1.

Table 5.6.1-1: Emission of trace metals from combustion of fuels in stationary sources in 1995 (in tonne) for Asia and the world total, adopted from J. Pacyna and E. Pacyna (2001).

Source	**Cd**	**Mn**	**Mo**	**Ni**	**Pb**	**V**	**Zn**
Asia (tonne)	237	3974	1115	36320	4845	101254	3974
World total (tonne)	691	9417	2642	86110	11690	240084	9417
Asia (%)	**34**	**42**	**42**	**42**	**41**	**42**	**42**

In the fall 2012 data set it seems that THg is equally well correlated with the geogenic Al and Ti as with several of the atmospheric tracers, such as Be, Co, Mn, Ni, V and Zn (figure 5.6.1-1). Be, Co, Mn, Ni, V and Zn can be used as atmospherical tracers, but only if they are enriched compared to their natural abundance (Pacyna et al., 1984). If there were significant amounts of Hg_{atm}, one would expect to see strong correlations with some of the atmospheric tracers in addition to weak correlations with the geogenic tracers. Therefore these results do not provide further conclusions, but rather show the trend seen already; the Hg in the GF streams is probably mostly geogenic, but might also contain a small atmospheric component.

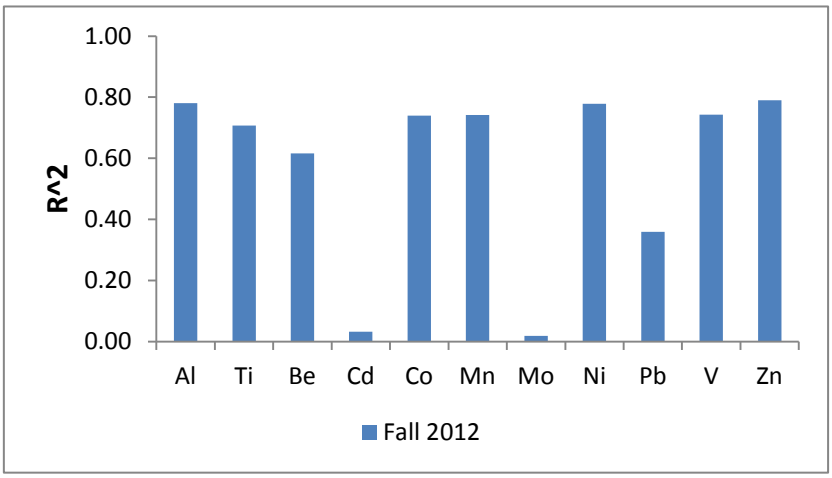

Figure 5.6.1-1: The R^2 values for the correlation of THg with 11 trace metals in water samples from GF streams, for the fall 2012 data set.

In the spring 2013 data set there are some obvious differences in correlations compared to the fall 2012 data set (figure 5.6.1-1) as can be seen in figure 5.6.1-2. The correlation with Al and Ti is much weaker at the same time as the correlation with Be, Cd and Zn is stronger. There are, however, three very influential data points which greatly affect linear regression line for both Al (appendix O, O.2-2) and Ti as well as Be, Ni and Zn (appendix O, figures O.3-1 – O.3-4) These three points are YZG05, YZG09 and YZG11; the two GF side rivers in the YZG valley and the first sampling point in the main river downstream of YZG09. It has already been pointed out that these two side rivers show a different trend than the rest of the GF streams. Removing these data points gives very strong correlations with both Al and Ti for the rest of the data set. Thus it is reasonable to assume that YZG05, YZG09 and YZG11 might have an Hg_{atm} component while the rest of the GF sampling points have primarily Hg_{geo}.

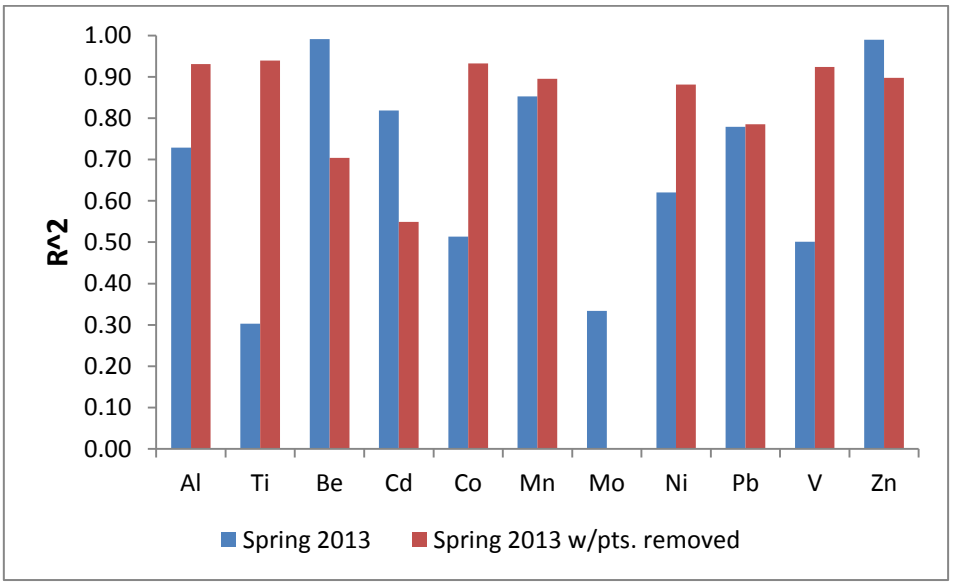

Figure 5.6.1-2: The R^2 values for the correlation of THg with 11 trace metals in water samples from GF streams, for the spring 2013 data set, with and without three influential data points.

Further evidence of YZG05 and YZG09 containing an atmospherically deposited trace metals is shown in figure 5.6.1-3, which show the enrichment factors (EFs) of the atmospheric tracers in the respective streams. Several of the atmospheric tracers, such as Cd, Pb and Zn, are heavily enriched in the stream water (EF>30). The EFs where calculated relative to Ti; the method is described in full detail in appendix O, section O.4.

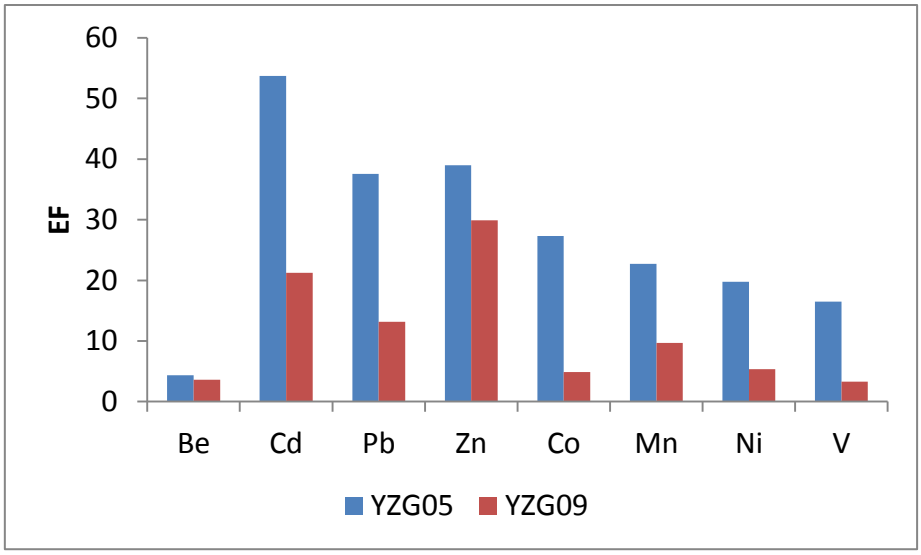

Figure 5.6.1-3: Enrichment factors (EF) for the atmospheric tracer elements; Be, Cd, Pb, Co, Mn, Ni and V, relative to Ti in the two YZG side rivers; YZG05 and YZG09.

5.6.2 Principal component analysis

A PCA has been used here to show the variability of each sampling point within a set of 19 analytical variables. Details and procedure of the PCA is shown in appendix O, section O.2.

Based on their respective loading values the main variables of the first principal component (PC1) are: Hg, TSS, Al, Ti, Be, Cd, Co, Cu, Fe, Mn, Pb, and Zn while the second principal component (PC2) is mainly: Mo, NO_3^-, SO_4^{2-}, TOC, DOC and possibly H^+ (pH) and Hg (table 5.6.2-1). It is evident that PC1 represents the particle load, as TSS and a range of trace metals constitute the variability in this component. Most of the tracers, both geogenic and atmospherical, used for the correlation analysis are combined within this component, something which indicates that they might all represent a contribution from the same geogenic source. However, the fact that Hg is represented in both PC1 and PC2, which otherwise are composed of distinctly different variables, agrees with there being two different Hg sources.

Table 5.6.2-1: The first five principal components (PCs) and the loading values for the 19 analytical variables for each PC. Also included: the eigenvalue, proportion of total variance and the cumulative proportion of the total variance of the respective PCs.

Variables	**PC1**	**PC2**	**PC3**	**PC4**	**PC5**
Hg	**0.25**	**0.19**	0.15	0.11	0.29
Al	**0.28**	-0.08	-0.15	0.05	-0.14
Be	**0.25**	0.12	-0.06	0.09	0.03
Cd	**0.27**	-0.01	0.04	-0.21	0.13
Co	**0.28**	-0.09	-0.05	0.10	-0.11
Cu	**0.28**	-0.01	0.07	-0.03	-0.01
Fe	**0.28**	-0.10	-0.11	0.10	-0.09
Mn	**0.28**	-0.06	-0.04	0.05	0.00
Mo	-0.01	**-0.41**	-0.33	0.42	0.04
Pb	**0.28**	-0.05	-0.10	-0.12	-0.16
Ti	**0.26**	-0.14	-0.14	0.18	-0.11
U	**0.20**	-0.15	0.20	-0.56	0.16
Zn	**0.28**	0.01	-0.14	-0.07	-0.09
H^+	-0.04	**0.22**	-0.75	-0.16	0.54
NO_3^-	-0.04	**0.47**	-0.16	0.17	-0.46
SO_4^{2-}	-0.04	**-0.45**	0.21	0.33	0.35
TOC	**0.21**	**0.31**	0.22	0.10	0.29
DOC	0.14	**0.38**	0.22	0.42	0.25
TSS	**0.28**	-0.06	-0.03	-0.06	-0.08
Eigenvalue	12.15	3.45	1.18	0.88	0.37
Proportion of total variance (%)	63.9	18.1	6.2	4.6	1.9
Cumulative proportion (%)	63.9	82.1	88.3	92.9	94.8

Figure 5.6.2-1 shows a score plot of the two first principal components (PCs). The bulk of the GF sampling points are grouped together in clusters 1 and 2, and vary as expected mostly along the PC1 due to their difference in particle load. Cluster 1 contain mainly sampling points which are found at the lower parts of the two valleys while cluster 2 contain sampling points close to the glacier front in HLG and sampling points downstream where the first side river in YZG merge with the main stream. Again the sampling points YZG05 and YZG09 show a different trend than the rest of the GF sampling points. They are found in cluster 3, which has large variations in both PCs, indicating a trend of different chemistry in the two YZG side rivers. YZG11 is found between clusters 2 and 3, as it is affected by both the main stream and the YZG09 side river. Cluster 4 features the three uppermost sampling points of

the YZG main stream while cluster 5 contains the sampling point above the lower HLG glacier, HLG05, as well as the GF steam joining the main stream at the top of the YZG valley, YZG02. The NGF sampling points vary both along PC1 and PC2 and show no unified profile, probably due to their relative differences in TSS, TOC and both sources of Hg.

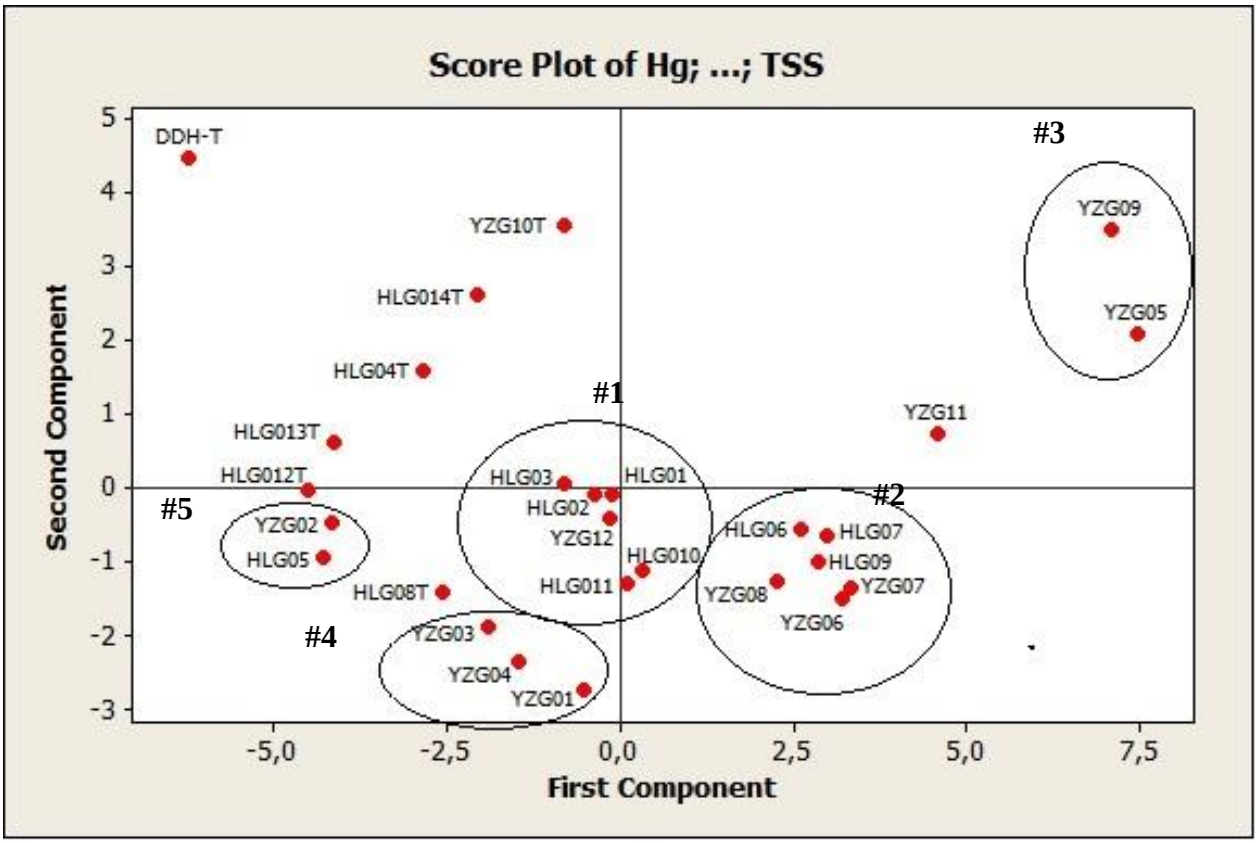

Figure 5.6.2-1: Score plot of the first two PCs for the PCA of GF (HLG# andYZG#) and NGF (HLG#T, YZG#T and DDH-T) sampling points in the spring 2013 data set. 5 clusters of sampling points are encircled and numbered (1-5).

5.6.3 Estimation of Hg_{atm} and Hg_{geo} based on linear regression models with Hg-Al and Hg-Ti.

As already stated, Al and Ti can be considered a conservative element in the earth's crust (Boës et al., 2011) and can therefore be thought of as a representative for the contribution of geogenic species in the water samples. Using this idea, a linear regression analysis of Al-Hg and Ti-Hg in samples considered to have mainly Hg_{geo} can provide models to predict the amount of Hg_{geo} in the other samples, based on their respective Al and Ti contents. The details and procedure of this estimation model are shown in appendix O, section O.3.

In the fall 2012 data set there is a strong correlation between both Hg- Al and Hg-Ti for all the GF sampling points; R^2=0.78, (p <0.001) and R^2=0.71 (p<0.0001) respectively. The linear regression equations for Hg-Al and Hg-Ti could have been used to correct for Hg_{geo} in the remaining sampling points, but not for any of the GF sampling points as they are all included in the model. Furthermore, better correlations would have been preferred for such a model to give good predictions, but there are unfortunately no scientific incentives to decide which data points to remove to create a better correlated model. Therefore, this approach does not yield the information required for the fall 2012 data set. It should be noted however, that for the linear regression lines the intercepts are 0.27 (p = 0.09) for THg-Al and 0.43 (p<0.05) for THg-Ti, which means that without a geogenic contribution, (Al or Ti) there is 0.3 ng/L or 0.4 ng/L of Hg present, based on Al and Ti respectively.

For the spring 2013 data set strongly correlated linear regression lines for Hg-Al and Hg-Ti, based on all the GF sampling points except YZG05, YZG09 and YZG11, provide the basis for two models to estimate the amount of Hg_{geo} in the remaining data points. The significant role of Ti and Al as representatives of a geogenic contribution is shown by a strong correlation between the two parameters for the sampling points included in the model (figure 5.6.3-1).

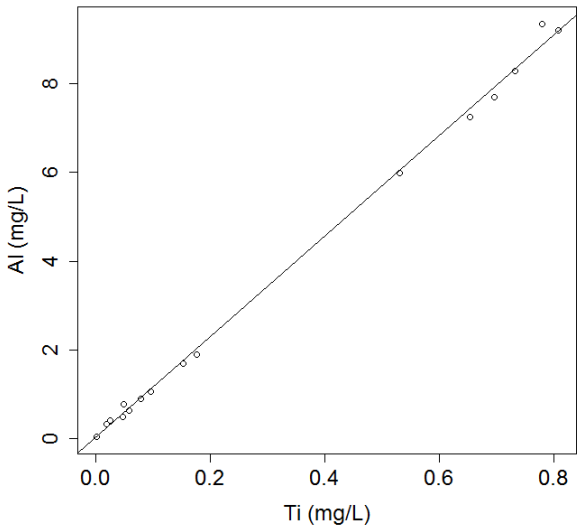

Figure 5.6.3-1: Linear regression plot of Al vs.s Ti for the GF sampling points included in the Al- and Ti-models for the estimation of Hg_{atm}. R^2 = 0.9980, p<0.0001.

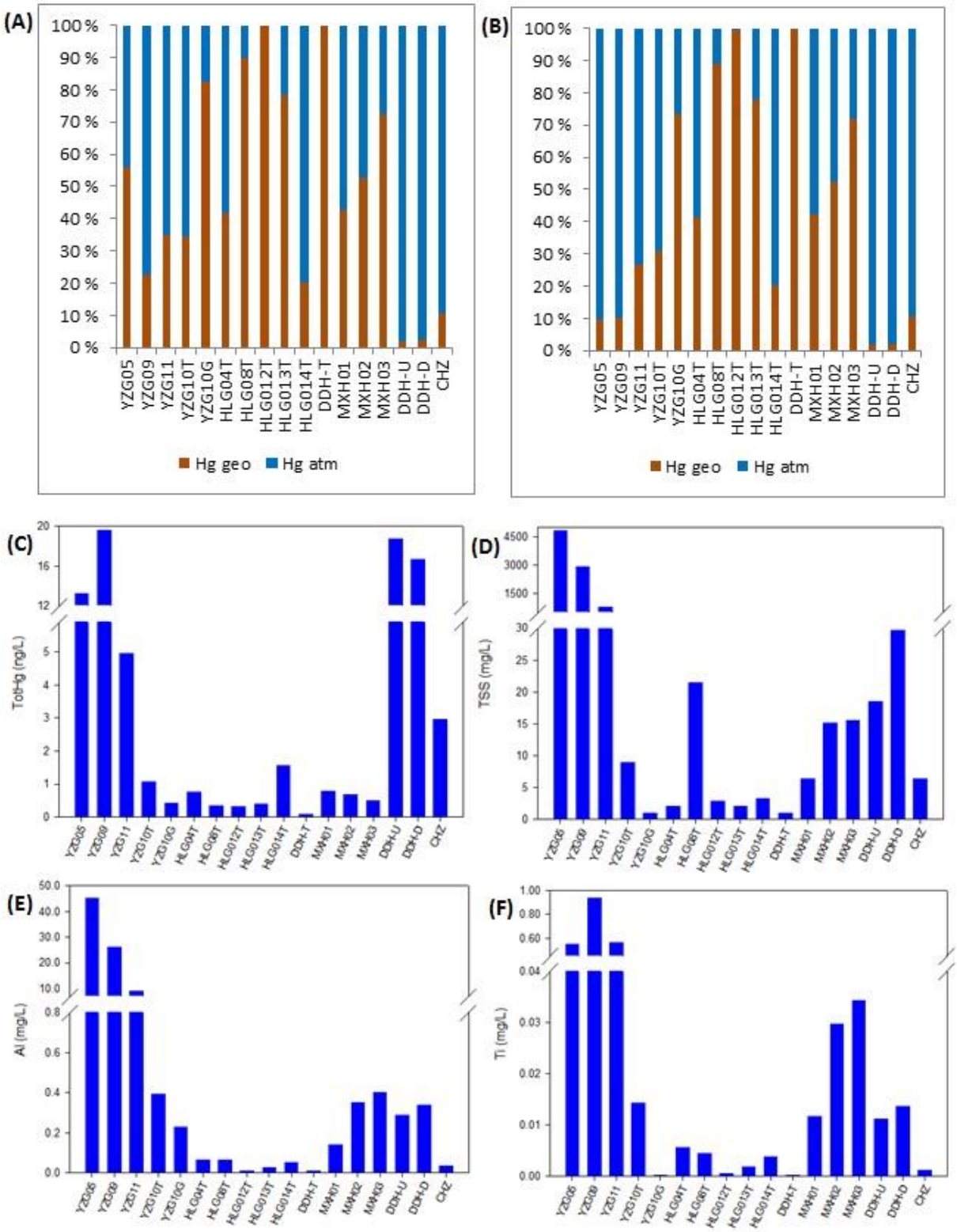

Figure 5.6.3-1: Fractions of geogenic (red) and atmospheric (blue) Hg (%) of THg at selected sampling points from the spring 2013 data set as determined by the Hg-Al (A) and Hg-Ti (B) linear regression models. Showing THg (ng/L) (C), TSS (mg/L) (D), Al (mg/L) (E) and Ti (mg/L) (F) for the respective sampling points.

Figure 5.6.3-2 (A) shows the fractions of Hg_{geo} and Hg_{atm} estimated by the Al-model. Here YZG05, YZG09 and YZG11 have relatively large fractions of Hg_{atm}: 44%, 78 % and 65% respectively while the NGF streams show varying amounts of Hg_{atm}: from 0% in HLG12T and DDH-T to 80% in HLG14T. Figure 5.5.3-2 (B) shows the fractions for the same sampling points, but estimated by the Ti-model. The estimated fractions of Hg_{atm} are almost identical in both models. The only noticeable difference is between the estimated Hg_{atm} for YZG05 which is 44% for the Al-model and 90% for the Ti-model.

The estimation of large fractions of Hg_{atm} in YZG05, YZG09 and YZG11supports the trends already discussed for these sampling points; that the side rivers contain significant amounts of Hg_{atm} released from the snow and ice of the E-Konka glacier.

Finding Hg_{atm} in the NGF streams agrees with the notion from the fractionation results discussed in section 5.4.1 which suggests that DHg could be a more dominating specie in this system. The models also shows that the DDH River is dominated by Hg_{atm}, but this Hg could stem from other sources than atmospheric deposition as well, since this large river is exposed to a variety of human activities upstream from the sampling points. The same goes for the MXH-sampling points, for which there is a possibility that the estimated non-Hg_{geo} fraction could be pollution from the town of Moxizhen.

The CHZ bog is found to be dominated by Hg_{atm} in the estimates from both models; 89% and 90% for the Al- and Ti-models respectively. This is in accordance with what is known about peat bogs, as discussed in section 5.5.2; they are fed primarily by atmospheric deposition.

It must be noted that some of the sampling points included in this model to contain Hg_{geo} exclusively (e.g. HLG01, HLG02 and HLG03), are found in the lower parts of the valley (figure 4.1-1) where the main GF river have received water from a number of NGF tributary streams further upstream. These NGF streams do contain Hg_{atm} (figure 5.6.3-1), which is drained into the main GF river. However, due to the small size of these streams relative to the main river and the low Hg concentrations, this contribution of Hg_{atm} to the main river is considered insignificant.

5.6.4 Direct mathematical estimation of H_{gatm} and Hg_{geo} based on the crustal relationships of Hg with Ti and Al.

Ti and Al are considered a conservative elements in the earth's crust (Boës et al., 2011), and thus the ratio between crustal Hg and Al or Ti is fixed. Using such a ratio to determine an enrichment factor (EF) and the amount of Hg not of a geogenic origin, is an established method which has been used for aerosols (Rahn, 1999), soils (H. Zhang et al., 2013) and precipitation (Kyllönen, Karlsson, & Ruoho-Airola, 2009). Here one assumes that if an element in a sample is of a geogenic origin the ratio of this element and a conservative element will be the same as the crustal ratio. If the ratio is higher, however, it means that there is a contribution from another source (Rahn, 1999). Estimates of crustal concentrations of Al, Hg and Ti were taken from Wedepohl (1995). The details and procedure for this correction method are shown in appendix O, section O.4. The results from this analysis will be shown as fractions of Hg_{atm} and Hg_{geo} of the total THg concentration in each sampling point.

For the fall 2012 sample set both models, Hg-Al and Hg-Ti, estimate that there is little or no Hg_{atm} in the GF water samples (figures 5.6.4-1 and 5.6.4-2). All the NGF sampling points however, are estimated to have significant amounts of Hg_{atm} (47.0 – 99.5 %). The estimates do not vary much between the two models, with the exception of HLG08T, where the Hg-Al model estimates 47% Hg_{atm} and the Hg-Ti model 0%.

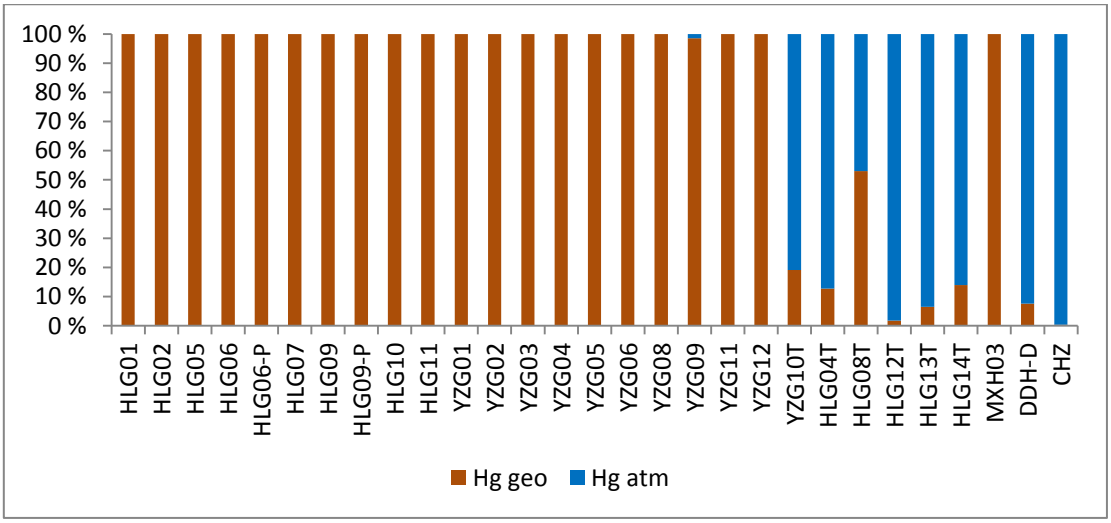

Figure 5.6.4-1: Fractions of Hg_{geo} and Hg_{atm} (%) in all water samples of the fall 2012 data set as estimated by Hg-Al crustal relation.

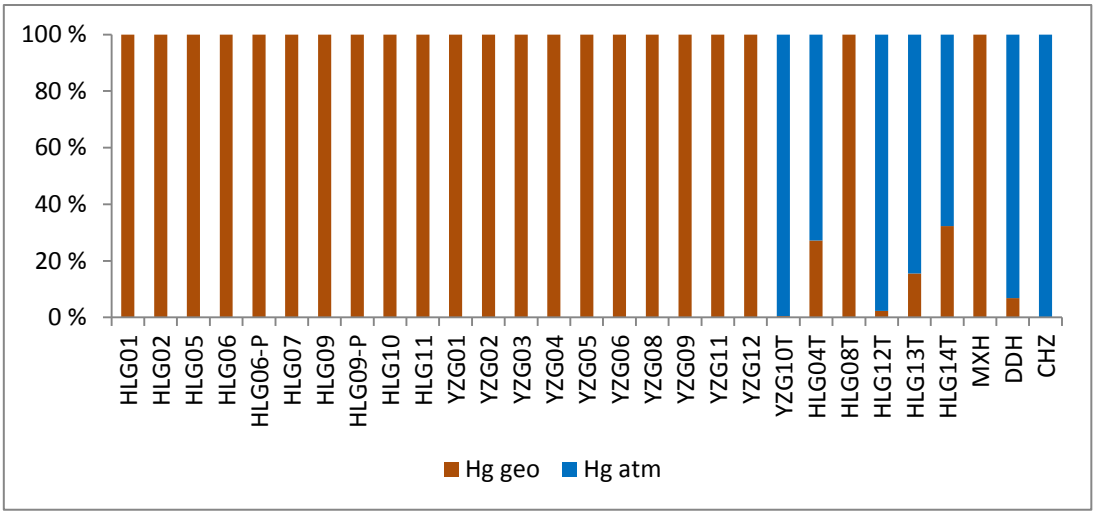

Figure 5.6.4-2: Fractions of Hg_{geo} and Hg_{atm} (%) in all water samples of the fall 2012 data set as estimated by Hg-Ti crustal relation.

In the spring 2013 sample set the situation is much the same for both models (figures 5.5.4-3 and 5.5.4-4); mostly no Hg_{atm} at the GF sampling points while significant amounts of Hg_{atm} at the NGF sampling points (76.2 – 99.4 %). There is, however, a difference since a few GF sampling points, HLG05 and YZG02, have Hg_{atm} of 86.5% and 80.9% or 89.4% and 82.7% according to the Hg-Al and Hg-Ti models respectively. HLG05 andYZG02 are both sampling points at high elevations, which have small particle loads (<2 mg/L and 3.2 mg/L respectively) and low THg concentrations (0.2 ng/L and 0.2 ng/L respectively) and strongly reduced flows were observed. The Hg_{atm} seen here could possibly be contributed to Hg from freshly fallen snow. The estimated fractions of Hg_{atm} in YZG05 and YZG09, however, vary quite a lot between the two models: 24.9% and 14.4 % in YZG05 and YZG09 respectively for the Hg-Ti model and only 0% and 3.8% respectively for the Hg-Al model. These fractions are much lower compared to the estimates by the linear regression models which range between 44% and 90% for YZG05 and 78% and 90% for YZG09 (section 5.5.3).

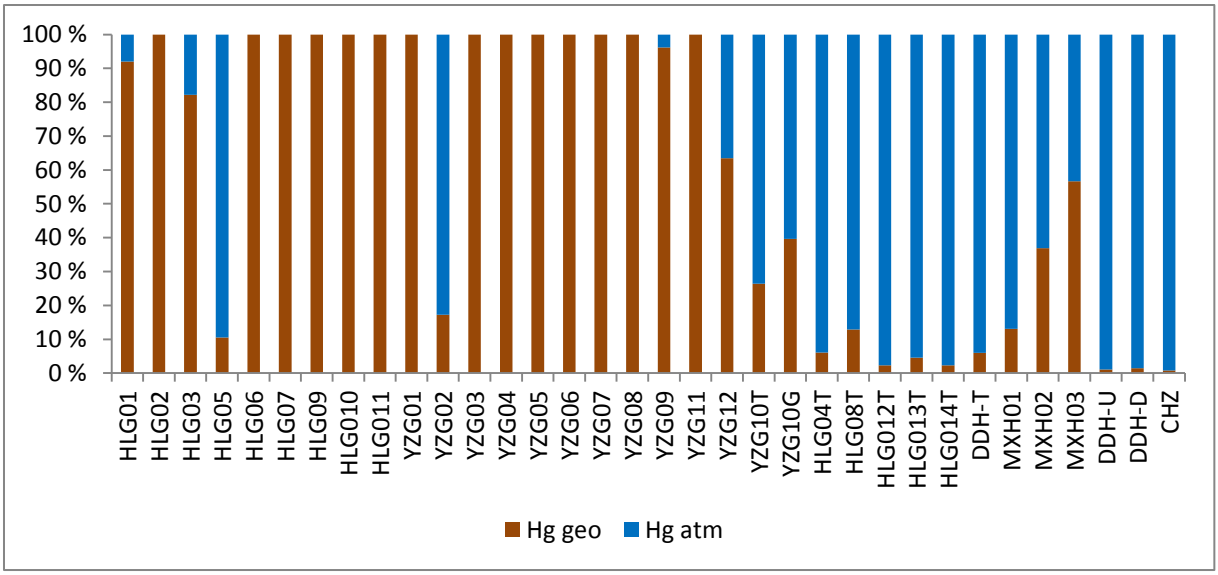

Figure 5.6.4-4: Fractions of Hg_{geo} and Hg_{atm} (%) in all water samples of the spring 2013 data set as determined by Hg-Al crustal relation.

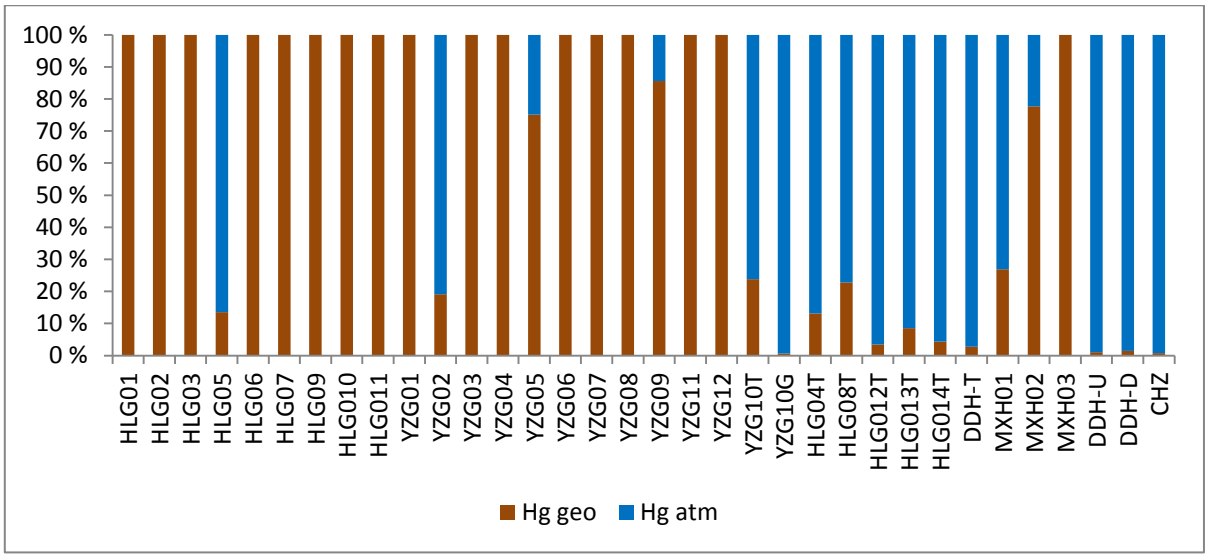

Figure 5.6.4-5: Fractions of Hg_{geo} and Hg_{atm} (%) in all water samples of the spring 2013 data set as determined by Hg-Ti crustal relation.

This model also shows that the DDH River is dominated by Hg_{atm} in both data sets, but this Hg could stem from other anthropogenic sources as discussed in section 5.6.3 The situation is the same for the CHZ bog which is mainly Hg_{atm} (>99%) in both data sets. Doing an intercomparison between the linear regression method (section 5.6.3) and the crustal relation method used here, one finds that DDH-U, DDH-D and CHZ have almost the exact same amounts of Hg_{atm} in the spring 2013 data set. Furthermore, the crustal method estimate the Hg_{atm} fractions to be somewhat larger in the NGF streams than the linear regression method.

It should be mentioned, however, that there is a problem with the estimates of this model. As was pointed out in section 5.5.1, the Hg sediment concentrations were well below the estimated average crustal Hg concentration of 56 µ/kg (Wedepohl, 1995). This might indicate that the natural background concentration of Hg in the bedrock of this area is lower than the average crustal concentration. If this is the case then the Hg/Ti and Hg/Al ratios based on estimated crustal concentrations by Wedepohl (1995), is too large and will cause an overestimation of Hg_{geo}. These general crustal estimates were used in lack of regional and/or local estimates.

5.6.5 Conclusive remarks on the models

The statistical models used to estimate the fractions of Hg_{atm} and Hg_{geo} did provide valuable insight, but the predictions made were not unambiguous. Both the empirical correlation analysis (section 5.6.1) and the PCA (section 5.6.2) exposed similar trends in the data set: the GF sampling points contain mostly Hg_{geo}, with the exception of YZG05 and YZG09, but at the same time the presence of Hg_{atm} could not be ruled out. Among the two quantitative models, the linear regression method (section 5.6.3) had the most solid fundament of the two, but this model had to assume (based on correlation) that all data points included in the model contain Hg_{geo}, thus strongly limiting its usefulness. The second quantitative model, estimation of the respective fractions based on crustal relations of Hg-Ti and Hg-Al (section 5.6.4), was applicable to all sampling points in the study, but suffered in accuracy since there was no data available on the local geogenic abundance of Hg, Al or Ti. The models agree on there being relatively large fractions of Hg_{atm} in the YZG side rivers (YZG05 and YZG09), the CHZ bog and the DDH River; varying amounts of Hg_{atm} in the NGF streams; and little or no Hg_{atm} in the remaining GF sampling points, although this could not be confirmed.

5.7 Implications of mercury mobilization by melting glaciers

In this study two mechanisms of Hg mobilization by melting glaciers have been seen: 1) the release of Hg_{atm} from glacier snow and ice through meltwater and 2) the mobilization of Hg_{geo} from the bedrock. Due to climatic warming an average retreat of 24 m/yr and subsequent increased glacier runoff flow has been estimated for the Mt. Gongga glacier since the 1930s (Li et al., 2010). Increased melting and runoff will eventually cause Hg stored in the glacier

snow and ice to be mobilized (Stern et al., 2012). As particle load increases with flow (Ongley et al., 1981) one can also expect the amount of Hg_{geo} released from glaciers to increase. So even though the stream Hg concentrations at Mt. Gongga and other remote and pristine alpine environments are low compared to contaminated sites, the dynamics of melting glaciers will mobilize vast reserves of Hg over time, little by little.

If transported into areas with higher potential for methylation, these relatively low concentrations of inorganic Hg can be transformed into the considerably more potent environmental contaminant, the neurotoxic and bioaccumulative MMHg. An example of this is the CHZ bog which has similar THg concentrations to the streams in the area (3.0 ng/L in fall 2102), while having about 50 times more MMHg.

6. Conclusions

The THg concentrations found in the streams of Mt. Gongga were low compared to sites known to be directly affected by Hg pollution, but higher in some of the streams than what have been observed in other remote, pristine alpine environments, far from point source pollution.

Data gathered at Mt. Gongga suggests that the glaciers contribute an extra source of Hg to the streams of the catchments below. The results are not unambiguous, but THg in the GF streams (1.3 ± 0.8 ng/L) were significantly higher ($p<0.01$) than THg in the NGF streams (0.5 ± 0.3 ng/L) in the fall 2012 sample set. In the spring 2013 sample set there is no such difference, most likely due to the poor timing of the sampling campaign, but two GF side rivers in YZG had THg concentrations which were about 200 and 10 times larger than the highest and lowest concentrations found in the NGF streams respectively. Hg is expectedly found in the NGF mountain streams as a result of the natural background in addition to a contribution from Hg_{atm}, which is deposited directly or added to the NGF streams through runoff from soil and vegetation. The fact that THg is higher in the streams which are fed by glaciers suggests that the glaciers provide an added component of Hg to the streams.

The analysis of Hg fractions indicated that PHg is the dominant fraction in most of the sampled streams, particularly in the GF streams; DHg was typically found below the LOD (0.1 ng/L). In samples with low THg concentrations, e.g. 0.2 ng/L, however, the DHg fraction could potentially account for up to 50% of THg. Strong correlations ($R^2>0.9$) between TSS and THg in GF streams further indicate that PHg, with Hg bound to inorganic particles, is the dominant fraction there, while a weak TSS-THg correlation in NGF streams ($R^2=0.01$) and a strong TOC-THg correlation ($R^2=0.93$) suggest that Hg in this system might be associated with organic matter. Considering the PHg dominance and high TSS loads in the GF streams, it is reasonable to conclude that the Hg seen in these streams is of a geogenic origin; particles from the bedrock, ground up beneath the glacier and flushed out with the meltwater. This means that Hg released to the GF streams is the result of a glacier related mechanism, either mobilization of geogenic Hg, or atmospherically deposited Hg stored in and mobilized from the glaciers.

The statistical analysis done in order to further separate the Hg in the GF streams into fractions of Hg_{geo} and Hg_{atm}, gave varying results, but some general trends could be established. For the fall 2012 sample set, the statistical analysis did not reveal any new trends; the results indicated that Hg in the GF streams is probably mainly Hg_{geo}, but the presence of Hg_{atm} is not ruled out. In the spring 2013 sample set two distinct trends were uncovered for the GF sampling points. In the majority of the GF stream sampling points Hg_{geo} was found to be dominant, whereas in the YZG GF side rivers there were significant components of Hg_{atm} as confirmed by the four different methods of statistical analysis. Furthermore, these two side rivers had strongly enriched concentrations of several other trace metals compared to their natural geogenic abundance. The evidence discussed in section 5.3, indicates that the timing of the spring 2013 sampling campaign was unfortunate and that the spring melting profile was only possibly captured in the two YZG side rivers. This all suggests that the high Hg concentrations seen in these two GF side rivers represent the release of Hg_{atm} from the glacier at Mt. E-Konka. Judging by these indications there is reason to believe that a better timing of the sampling campaign would have given similar results for the rest of the GF streams.

MMHg was found at concentrations below LOD (0.02 ng/L) or barely above in the stream systems of Mt. Gongga. In the samples with quantifiable amounts of MMHg, the %MMHg ranged from 0.1% to 6%; numbers which constitute a system with low potential for methylation. Finding MMHg at such low concentrations in the studied streams agrees well with what is known about different landscapes' potential for producing MMHg. The CHZ bog, however, had %MMHg of 19% and should thus be considered a system with high methylation potential and a net source of MMHg in the environment. These results show that the GF streams and NGF mountain streams are not liable to produce significant amounts of MMHg, but should the Hg from these streams end up in a system similar to the CHZ bog, there could be a significant conversion of inorganic and elemental Hg to the more toxic MMHg.

Sediments from the different stream systems at Mt. Gongga had low THg concentrations compared to estimates of the average crustal Hg content and unpolluted sediments found in other parts of the world. These sediments were also low in TOC and thus naturally low in Hg. It is believed that the accumulation of Hg in these sediments is mainly driven by the settling of particles.

The CHZ peat bog did provide a decent historic record of atmospheric deposition to the Mt. Gongga area. There was no dating for the profile, but comparisons with peat bogs from other studies give a rough dating estimate. The trend of atmospheric deposition rendered from the profile seems to follow global atmospheric emission patterns, but the profile should have been deeper in order to get a record dating back to pre-industrial times. The role of the bog as a recipient of atmospheric deposition was confirmed through statistical analysis which showed that 89-99% of the THg in the bog was Hg_{atm}.

This study has given insights in the Hg dynamics of a remote GF alpine catchment; how glaciers contribute Hg through meltwater to the stream systems below, both in the form of Hg_{geo} from the bedrock beneath the glacier and from Hg_{atm} stored in the ice and snow of the glaciers. The streams, GF and NGF alike, were found to have low potentials for Hg methylation, but the sampled peat bog was identified as a hot spot for MMHg production.

7. Future work

There is no further funding for this project, so it will not continue past the submission of this thesis. However, the results from this project were in no terms fully conclusive and there is still a general lack of data related to the release of Hg by alpine glaciers. Therefore a few short reflections and recommendations for future work on this topic will follow.

The processes of Hg release from glacier snow and ice at the onset of spring melting need be documented properly. The timing of the second sampling campaign was unfortunate and thus only peripheral data on the effects of spring melting on Hg release was documented in this project. A better timed sampling could possibly record an ionic pulse or at least properly show the meltwater contribution of Hg from the seasonal snow cover of a glacier. A time series of samplings during the first weeks of spring melting would be ideal to show the differences in the release of Hg before, during and after the onset of the melting.

To properly estimate and quantify the potential release of Hg from an alpine glacier to a catchment below, and thus properly assess the environmental impact, a record of the temporal variations throughout the course of a year could be necessary. This, however, is very labor intensive and thus expensive work; remote alpine glaciers can be hard to access and often include difficult and dangerous conditions for field work. Alternative sampling methods, either automated sampling or passive sampling could be possible means of overcoming these challenges.

Another study should also preferably include data on the local geogenic concentrations of Hg and Ti or Al, such that Hg_{geo} in the meltwater can be correctly estimated by the method used in section 5.6.4. Stable Hg isotope signatures could possibly also be used to track Hg_{atm} and Hg_{geo}, but this is an expensive and time consuming analytical method, and its application in source tracking is still in its infancy. A proper isotope signature of the geogenic background Hg from the local environment could possibly be rendered, but as for the atmospheric Hg it could have many different sources and thus probably not a uniform signature. With THg concentrations as low as what was recorded at Mt. Gongga, detecting the stable isotope distribution could also be a challenge.

8. References

ACAP. (2005). Arctic Mercury Releases Inventory. Copenhagen, Denmark: Arctic Council Action Plan to Eliminate Pollution of the Arctic (ACAP) & Danish Environmental Protection Agency.

Ariya, Parisa A., Dastoor, Ashu P., Amyot, Marc, Schroeder, William H., Barrie, Leonard, Anlauf, Kurt, . . . Steffen, Alexandra. (2004). The Arctic: a sink for mercury. *Tellus B, 56*(5), 397-403.

Bajewsky, Ingrid, & Gardner, James S. (1989). Discharge and sediment-load characteristics of the Hilda Rock-glacier stream, Canadian Rockey Mountains, Alberta. *Physical Geography, 10*(4), 295-306.

Benoit, J. M., Fitzgerald, W. F., & Damman, A. W. H. (1998). The biogeochemistry of an ombrotrophic bog: evaluation of use as an archive of atmospheric mercury deposition. *Environmental Research, 78*(2), 118-133.

Benoit, J. M., Gilmour, C. C., Heyes, A., Mason, R., & Miller, C. L. (2003). Geochemical and biological controls over methylmercury production and degradation in aquatic ecosystems *ASC Symposium Series* (Vol. 835, pp. 262-297). Washington DC, USA: American Chemical Society.

Berg, T., Bartnicki, J., Munthe, J., Lattila, H., Hrehoruk, J., & Mazur, A. (2001). Atmospheric mercury species in the European Arctic: measurements and modelling. *Atmospheric Environment, 35*(14), 2569-2582.

Black, Frank J., Poulin, Brett A., & Flegal, A. Russell. (2012). Factors controlling the abiotic photo-degradation of monomethylmercury in surface waters. *Geochimica et Cosmochimica Acta, 84*(0), 492-507.

Blais, J. M., Schindler, D. W., Muir, D. C., Sharp, M., Donald, D., Lafreniere, M., . . . Strachan, W. M. (2001). Melting glaciers: a major source of persistent organochlorines to subalpine Bow Lake in Banff National Park, Canada. *Ambio, 30*(7), 410-415.

Bloom, N. (1989). Determination of picogram levels of methylmercury by aqueous phase ethylation, followed by cryogenic gas chromatography with cold vapour atomic fluorescence detection. *Canadian Journal of Fisheries and Aquatic Sciences, 46*(7), 1131-1140.

Boës, X., Rydberg, J., Martinez-Cortizas, A., Bindler, R., & Renberg, I. (2011). Evaluation of conservative lithogenic elements (Ti, Zr, Al, and Rb) to study anthropogenic element enrichments in lake sediments. *Journal of Paleolimnology, 46*(1), 75-87.

Bogdal, C., Schmid, P., Zennegg, M., Anselmetti, F. S., Scheringer, M., & Hungerbühler, K. (2009). Blast from the past: melting glaciers as a relevant source for persistent organic pollutants. *Environmental Science & Technology, 43*(21), 8173-8177.

Braaten, H. F. V., de Wit, H. A., Harman, C., Hageström, U., & Larssen, T. (2013). Effects of sample preservation and storage on mercury speciation in natural stream water. *International Journal of Environmental Analytical Chemistry*, 1-4.

Braaten, H. F. V., Harman, C., Øverjordet, I. B., & Larssen, T. (2014). Effects of sample preparation on methylmercury concentrations in Arctic organisms. *International Journal of Environmental Analytical Chemistry*, 1-11.

Brooks-Rand-Labs. (2012a). MERX automated methylmercury analytical system: user's guide. Seattle WA, USA: Brooks Rand Labs.

Brooks-Rand-Labs. (2012b). MERX automated total mercury analytical system: user's guide. Seattle WA, USA: Brooks Rand Labs.

Compeau, G. C., & Bartha, R. (1985). Sulfate-reducing bacteria: principal methylators of mercury in anoxic estuarine sediment. *Applied and Environmental Microbiology, 50*(2), 498-502.

Coquery, M, Cossa, D, & Martin, J. M. (1995). The distribution of dissolved and particulate mercury in three Siberian estuaries and adjacent Arctic coastal waters. *Water Air & Soil Pollution, 80*(1-4), 653-664.

Creswell, J., Engel, V., Carter, A., & Davies, C. (2013). Interlaboratory comparison study for total mercury and methylmercury. Seattle WA, USA: Brooks Rand Instruments.

Dommergue, A., Ferrari, C. P., Gauchard, P. A., Boutron, C. F., Poissant, L., Pilote, M., . . . Adams, F. C. (2003). The fate of mercury species in a sub-arctic snowpack during snowmelt. *Geophysical Research Letters, 30*(12), 1621.

Ebinghaus, R., Kock, H. H., Temme, C., Einax, J. W., Löwe, A. G., Richter, A., . . . Schroeder, W. H. (2002). Antarctic springtime depletion of atmospheric mercury. *Environmental Science & Technology, 36*(6), 1238-1244.

Eckley, C S., & Hintelmann, H. (2006). Determination of mercury methylation potentials in the water column of lakes across Canada. *Science of The Total Environment, 368*(1), 111-125.

Esbensen, K. H., Guyot, D., Westad, F., & Houmoller, L. P. (2004). *Multivariate data analysis: In practice* (5th ed.). Oslo, Norge: CAMO Process AS.

Ethier, A. L. M., Scheuhammer, A. M., Blais, J. M., Paterson, A. M., Mierle, G., Ingram, R., & Lean, D. R. S. (2010). Mercury empirical relationships in sediments from three Ontario lakes. *Science of The Total Environment, 408*(9), 2087-2095.

Ferrari, C. P., Dommergue, A., Veysseyre, A., Planchon, F., & Boutron, C. F. (2002). Mercury speciation in the French seasonal snow cover. *Science of The Total Environment, 287*(1–2), 61-69.

Fu, X. W., Feng, X., Zhu, W., Rothenberg, S., Yao, H., & Zhang, H. (2010). Elevated atmospheric deposition and dynamics of mercury in a remote upland forest of Southwestern China. *Environmental Pollution, 158*(6), 2324-2333.

Gilmour, C. C., Podar, M., Bullock, A. L., Graham, A. M., Brown, S. D., Somenahally, A. C., . . . Elias, D. A. (2013). Mercury methylation by novel microorganisms from new environments. *Environmental Science & Technology, 47*(20), 11810-11820.

Hall, B. D., Aiken, G. R., Krabbenhoft, D. P., Marvin-Dipasquale, M., & Swarzenski, C. M. (2008). Wetlands as principal zones of methylmercury production in southern Louisiana and the Gulf of Mexico region. *Environmental Pollution, 154*(1), 124-134.

Harris, D. C. (2007). *Quantitative chemical analysis* (7th ed.). New York NY, USA: W. H. Freeman and Company.

Horvat, M., Liang, L., & Bloom, N. (1993). Comparison of distillation with other current isolation methods for the determination of methyl mercury compounds in low level environmental samples: part II, water. *Analytica Chimica Acta, 282*(1), 153-168.

Huang, J., Kang, S. C., Guo, J., Zhang, Q., Xu, J., Jenkins, M. G., . . . Wang, K. (2012). Seasonal variations, speciation and possible sources of mercury in the snowpack of Zhadang glacier, Mt. Nyainqêntanglha, southern Tibetan Plateau. *Science of The Total Environment, 429*(0), 223-230.

Huang, J., Kang, S. C., Zhang, Q., Jenkins, M. G., Guo, J., Zhang, G., & Wang, K. (2012). Spatial distribution and magnification processes of mercury in snow from high-elevation glaciers in the Tibetan Plateau. *Atmospheric Environment, 46*(0), 140-146.

Huang, X., Sillanpää, M., Duo, B., & Gjessing, E. T. (2008). Water quality in the Tibetan Plateau: metal contents of four selected rivers. *Environmental Pollution, 156*(2), 270-277.

ISO. (1997). Method 11923: Determination of suspended solids by filtration through glass-fibre filters: International Organization for Standardization.

Jens-Molecular-and-Nanoscale-Analysis-Laboratory.). Hg Analyzer: DMA-80. Retrieved 07.04.2014, 2014, from http://eecelabs.seas.wustl.edu/Hg.aspx

Johnson, R. A, & Bhattacharyya, G. K. (2001). *Statistics: Principles and methods* (4th ed.). New York NY, USA: John Wiley & Sons Inc.

Keith, L. H., Crummett, W., Deegan, J., Libby, R. A., Taylor, J. K., & Wentler, G. (1983). Principles of environmental analysis. *Analytical Chemistry, 55*(14), 2210-2218.

Kyllönen, K., Karlsson, V., & Ruoho-Airola, T. (2009). Trace element deposition and trends during a ten year period in Finland. *Science of The Total Environment, 407*(7), 2260-2269.

Lahoutifard, N., Sparling, M., & Lean, D. (2005). Total and methylmercury patterns in Arctic snow during springtime at Resolute, Nunavut, Canada. *Atmospheric Environment, 39*(39), 7597-7606.

Larssen, T., de Wit, H. A., Wiker, M., & Halse, K. (2008). Mercury budget of a small forested boreal catchment in southeast Norway. *Science of The Total Environment, 404*(2–3), 290-296.

Lehnherr, I., & St. Louis, V. L. (2009). Importance of ultraviolet radiation in the photodemethylation of methylmercury in freshwater ecosystems. *Environmental Science & Technology, 43*(15), 5692-5698.

Leng, Y. (2008). *Materials characterization: Introduction to microscopic and spectroscopic methods*: John Wiley and Sons (Asia) Pte. Ltd.

Li, Z., He, Y., Yang, X., Theakstone, W. H., Jia, W., Pu, T., . . . Du, J. (2010). Changes of the Hailuogou glacier, Mt. Gongga, China, against the background of climate change during the Holocene. *Quaternary International, 218*(1–2), 166-175.

Lin, Y., Vogt, R., & Larssen, T. (2012). Environmental mercury in China: a review. *Environmental Toxicology and Chemistry, 31*(11), 2431-2444.

Lindberg, S., Bullock, R., Ebinghaus, R., Engstrom, D., Feng, X., Fitzgerald, W., . . . Seigneur, C. (2007). A synthesis of progress and uncertainties in attributing the sources of mercury in deposition. *AMBIO: A Journal of the Human Environment, 36*(1), 19-33.

Lindqvist, O. (1985). Atmospheric mercury - a review. *Tellus B, 37B*(3), 136-159.

Liu, R., Wang, Q., Lu, X., Fang, F., & Wang, Y. (2003). Distribution and speciation of mercury in the peat bog of Xiaoxing'an Mountain, northeastern China. *Environmental Pollution, 124*(1), 39-46.

Lockhart, W. L., Macdonald, R. W., Outridge, P. M., Wilkinson, P., DeLaronde, J. B., & Rudd, J. W. M. (2000). Tests of the fidelity of lake sediment core records of mercury deposition to known histories of mercury contamination. *Science of The Total Environment, 260*(1–3), 171-180.

Loewen, M., Kang, S. C., Armstrong, D., Zhang, Q., Tomy, G., & Wang, F. (2007). Atmospheric transport of mercury to the tibetan plateau. *Environmental Science & Technology, 41*(22), 7632-7638.

Lu, J. Y., Schroeder, W. H., Barrie, L. A., Steffen, A., Welch, H. E., Martin, K., . . . Richter, A. (2001). Magnification of atmospheric mercury deposition to polar regions in springtime: the link to tropospheric ozone depletion chemistry. *Geophysical Research Letters, 28*(17), 3219-3222.

Lyons, W. B., Welch, K. A., & Bonzongo, J. C. (1999). Mercury in aquatic systems in Antarctica. *Geophysical Research Letters, 26*(15), 2235-2238.

Macalady, J. L., Mack, E. E., Nelson, D. C., & Scow, K. M. (2000). Sediment microbial community structure and mercury methylation in mercury-polluted Clear Lake, California. *Applied and Environmental Microbiology, 66*(4), 1479-1488.

Mackay, D., Wania, F., & Schroeder, W. H. (1995). Prospects for modeling the behavior and fate of mercury, globally and in aquatic systems. *Water, Air, and Soil Pollution, 80*(1-4), 941-950.

Madsen, P. P. (1981). Peat bog records of atmospheric mercury deposition. *Nature, 293*(5828), 127-130.

Manahan, S. E. (2005). *Environmental chemistry* (8th ed.). New York NY, USA: CRC Press LLC.

Martínez-Cortizas, A., Pontevedra-Pombal, X., García-Rodeja, E., Nóvoa-Muñoz, J. C., & Shotyk, W. (1999). Mercury in a Spanish peat bog: archive of climate change and atmospheric metal deposition. *Science, 284*(5416), 939-942.

McClain, M. E., Boyer, E. W., Dent, C. L., Gergel, S. E., Grimm, N. B., Groffman, P. M., . . . Pinay, G. (2003). Biogeochemical hot spots and hot moments at the interface of terrestrial and aquatic ecosystems. *Ecosystems, 6*(4), 301-312.

Milestone. (2002). DMA-80: direct mercury analyzer user manual (2nd ed.). Sorisole, Italy: Milestone Inc.

Nagorski, S. A., Engstrom, D. R., Hudson, J. P., Krabbenhoft, D. P., Hood, E., DeWild, J. F., & Aiken, G. R. (2014). Spatial distribution of mercury in southeastern Alaskan streams influenced by glaciers, wetlands, and salmon. *Environmental Pollution, 184*(0), 62-72.

NIVA. (2012). Valideringsrapport av metoden for analyse av THg i vann. Oslo, Norway: Norsk Institutt for Vannforskning - NIVA.

NIVA. (2013a). Internal protocol: control chart for Sartoris Basic Plus 1200 - Hg lab: Norsk Institutt for Vannforskning - NIVA.

NIVA. (2013b). Internal protocol: pipette calibration for Hg-lab: Norsk Institutt for Vannforskning - NIVA.

NS. (1979). NS 4720: Water analysis - determination of pH (2nd ed.). Oslo, Norway: Norsk Standard.

NS. (1991). NS 4745: Water analysis - determination of the sum of nitrite nitrogen and nitrate nitrogen. Oslo, Norway: Norsk Standard.

NS. (1997). NS-EN 1484: Water analysis: Guidelines for the determination of total organic carbon (TOC) and dissolved organic carbon (DOC) Oslo, Norway: Norsk Standard.

NS. (2007). NS-EN ISO 10304-1: Water quality - determination of dissolved anions by liquid chromatography of ions - part 1: determination of bromide, chloride, fluoride, nitrate, nitrite, phosphate and sulfate. Oslo, Norway: Norsk Standard.

O'Driscoll, N. J., Rencz, A., & Lean, D. R. S. (2005). The biogeochemistry and fate of mercury in the environment. *Metal ions in biological systems, 43*, 221-238.

Olmez, L., & Ames, M. R. (1997). Atmospheric mercury: how much do we really know? *Pure and Applied Chemistry, 69*(1), 35-40.

Ongley, E. D., Bynoe, M. C., & Percival, J. B. (1981). Physical and geochemical characteristics of suspended solids, Wilton Creek, Ontario. *Canadian Journal of Earth Science, 18*, 1365-1379.

Outridge, P. M., Macdonald, R. W., Wang, F., & Stern, G. A. (2008). A mass balance inventory of mercury in the Arctic Ocean. *Environmental Chemistry, 5*, 89-111.

Pacyna, J. M., & Pacyna, E. G. (2001). An assessment of global and regional emissions of trace metals to the atmosphere from anthropogenic sources worldwide. *Environmental Reviews, 9*(4), 269-298.

Pacyna, J. M., Semb, A., & Hanssen, J. E. (1984). Emission and long-range transport of trace elements in Europe. *Tellus B, 36B*(3), 163-178.

Parker, J. L., & Bloom, N. (2005). Preservation and storage techniques for low-level aqueous mercury speciation. *Science of The Total Environment, 337*(1–3), 253-263.

Pirrone, N., Cinnirella, S., Feng, X., Finkelman, R. B., Friedli, H. R., Leaner, J., . . . Telmer, K. (2010). Global mercury emissions to the atmosphere from anthropogenic and natural sources. *Atmospheric Chemistry and Physics, 10*, 5951–5964.

Popek, E. P. (2003). *Sampling and analysis of envrionmental chemical pollutants: A complete guide* (1st ed.): Elsevier Inc.

Poulain, A. J., Lalonde, J. D., Amyot, M., Shead, J. A., Raofie, F., & Ariya, P. A. (2004). Redox transformations of mercury in an Arctic snowpack at springtime. *Atmospheric Environment, 38*(39), 6763-6774.

Rahn, K. A. (1999). A graphical technique for determining major components in a mixed aerosol - I: descriptive aspects. *Atmospheric Environment, 33*(9), 1441-1455.

Ravichandran, M. (2004). Interactions between mercury and dissolved organic matter – a review. *Chemosphere, 55*(3), 319-331.

Rigét, F., Tamstorf, M. P., Larsen, M. M., Sondergaard, J., Asmund, G., Falk, J. M., & Sigsgaard, C. (2011). Mercury (Hg) transport in a high arctic river in Northeast Greenland. *Water Air & Soil Pollution, 222*(1-4), 233-242.

Rytuba, J. J. (2003). Mercury from mineral deposits and potential environmental impact. *Environmental Geology, 43*(3), 326-338.

Sakata, M., & Asakura, K. (2007). Estimating contribution of precipitation scavenging of atmospheric particulate mercury to mercury wet deposition in Japan. *Atmospheric Environment, 41*(8), 1669-1680.

Sanei, H., & Goodarzi, F. (2006). Relationship between organic matter and mercury in recent lake sediment: the physical–geochemical aspects. *Applied Geochemistry, 21*(11), 1900-1912.

Schmid, P., Bogdal, C., Blüthgen, N., Anselmetti, F. S., Zwyssig, A., & Hungerbühler, K. (2010). The missing piece: sediment records in remote mountain lakes confirm glaciers being secondary sources of persistent organic pollutants. *Environmental Science & Technology, 45*(1), 203-208.

Schroeder, W. H., & Munthe, J. (1998). Atmospheric mercury - an overview. *Atmospheric Environment, 32*(5), 809-822.

Schuster, P. F., Krabbenhoft, D. P., Naftz, D. L., Cecil, L. D., Olson, M. L., Dewild, J. F., . . . Abbott, M. L. (2002). Atmospheric mercury deposition during the last 270 Years: a glacial cce core record of natural and anthropogenic sources. *Environmental Science & Technology, 36*(11), 2303-2310.

Seller, P., Kelly, C. A., Rudd, J. W. M., & MacHutchon, A. R. (1996). Photodegradation of methylmercury in lakes. *Nature, 380*(6576), 694-697.

Skoog, D. A., Holler, F. J., & Crouch, S. R. (2007). *Principles of intrumental analysis* (6th ed.). Belmont CA, USA: Thomson Brooks/Cole.

Skoog, D. A., West, D. M., Holler, F. J., & Crouch, S. R. (2004). *Fundamentals of analytical chemisry* (8th ed.). Belmont, USA: Thomson-Brooks/Cole.

Slemr, F., Brunke, E. G., Ebinghaus, R., Temme, C., Munthe, J., Wängberg, I., . . . Berg, T. (2003). Worldwide trend of atmospheric mercury since 1977. *Geophysical Research Letters, 30*(10), 1516.

St. Louis, V. L., Sharp, M. J., Steffen, A., May, A., Barker, J., Kirk, J. L., . . . Smol, J. P. (2005). Some sources and sinks of monomethyl and inorganic mercury on Ellesmere Island in the Canadian high Arctic. *Environmental Science & Technology, 39*(8), 2686-2701.

Steffen, A., Douglas, T., Amyot, M., Ariya, P., Aspmo, K., Berg, T., . . . Temme, C. (2008). A synthesis of atmospheric mercury depletion event chemistry in the atmosphere and snow. *Atmospheric Chemistry and Physics, 8*(6), 1445-1482.

Stern, G. A., Macdonald, R. W., Outridge, P. M., Wilson, S., Chételat, J., Cole, A., . . . Zdanowicz, C. (2012). How does climate change influence arctic mercury? *Science of The Total Environment, 414*(0), 22-42.

Stumm, W., & Morgan, J. J. (1996). *Aquatic chemistry: Chemical equilibria and rates in natural waters* (3rd ed.). Hoboken NJ, USA: John Wiley & Sons Ltd.

Sukhenko, S. A., Papina, T. S., & Pozdnjakov, S. R. (1992). Transport of mercury by the Katun river, West Siberia. *Hydrobiologia, 228*(1), 23-28.

Temme, C., Ebinghaus, R., Einax, J. W., Steffen, A., & Schroeder, W. H. (2004). Time series analysis of long-term data sets of atmospheric mercury concentrations. *Analytical and Bioanalytical Chemistry, 380*(3), 493-501.

Thomas, A. (1999). Overview of the geoecology of the Gongga Shan range, Sichuan Province, China. *Mountain Research and Development, 19*(1), 17-30.

Thompson, M., Ellison, S. L. R., & Wood, R. (2002). Harmonized guidelines for single-laboratory validation of methods of analysis. *Pure and Applied Chemistry, 74*(5), 835-855.

Tjerngren, I., Karlsson, T., Bjoern, E., & Skyllberg, U. (2012). Potential Hg methylation and MeHg demethylation rates related to the nutrient status of different boreal wetlands. *Biogeochemistry, 108*(1-3), 335-350.

Tjerngren, I., Meili, M., Bjoern, E., & Skyllberg, U. (2012). Eight boreal wetlands as sources and sinks for methyl mercury in relation to soil acidity, C/N ratio, and small-scale flooding. *Environmental Science & Technology, 46*(15), 8052-8060.

Ullrich, S. M., Tanton, T. W., & Abdrashitova, S. A. (2001). Mercury in the aquatic environment: a review of factors affecting methylation. *Critical Reviews in Environmental Science and Technology, 31*(3), 241-293.

UNEP. (2002). Global mercury assessment. Geneva, Switzerland: UNEP Chemicals Branch.

UNEP. (2006). Improved estimates of anthropogenic mercury emissions in China. Geneva, Switzerland: UNEP Chemicals Branch.

UNEP. (2008). The global atmospheric mercury assessment 2008: sources, emissions and transport. Geneva, Switzerland: UNEP Chemicals Branch.

UNEP. (2013). The Minamata Convention on Mercury (U. United Nations Environment Programme, Trans.). Geneva, Switzerland: United Nations.

USEPA. (1996). Method 1669: Sampling ambient water for trace metals at EPA water quality criteria levels. Washington D.C.: USEPA: Office of Water.

USEPA. (1998). Method 1630: Methyl mercury in water by distillation, aqueous ethylation, purge and trap and cold vapor atomic fluorescence spectrometry. Washington D.C.: USEPA: Office of Water.

USEPA. (2002). Method 1631: Mercury in water by oxidation, purge and trap and cold vapor atomic fluorescence spectrometry, Revision E. Washingto D.C.: USEPA: Office of Water.

USEPA. (2007a). Method 6020A: Inductively coupled plasma-mass spectrometry. Washington D.C.: USEPA.

USEPA. (2007b). Method 7473: Mercury in solids and solutions by thermal decomposition, amalgamation and atomic absorption spectrometry. Washington D.C.: USEPA.

Vandal, G. M., Mason, R. P., & Fitzgerald, W. F. (1991). Cycling of volatile mercury in temperate lakes. *Water Air & Soil Pollution, 56*(1), 791-803.

Vandal, G. M., Mason, R. P., McKnight, D., & Fitzgerald, W. (1998). Mercury speciation and distribution in a polar desert lake (Lake Hoare, Antarctica) and two glacial meltwater streams. *Science of The Total Environment, 213*(1–3), 229-237.

vanLoon, G. W., & Duffy, S. J. (2011). *Environmental chemistry: A global perspective* (3rd ed.). New York, NY: Oxford University Press Inc.

Villa, S., Negrelli, C., Finizio, A., Flora, O., & Vighi, M. (2006). Organochlorine compounds in ice melt water from Italian alpine rivers. *Ecotoxicology and Environmental Safety, 63*(1), 84-90.

Vittinghoff, E., Shiboski, S. C., Glidden, D. V., & McCulloch, C. E. (2005). *Regression methods in biostatistics: Linear, logistic, survival, and repeated measures models*. New York NY, USA: Springer Science+Business Media Inc.

Wang, X. P., Yao, T. D., Wang, P. L., Wei, Y., & Tian, L. D. (2008). The recent deposition of persistent organic pollutants and mercury to the Dasuopu glacier, Mt. Xixiabangma, central Himalayas. *Science of The Total Environment, 394*(1), 134-143.

Wang, Z., Zhang, X., Xiao, J., Zhijia, C., & Yu, P. (2009). Mercury fluxes and pools in three subtropical forested catchments, southwest China. *Environmental Pollution, 157*(3), 801-808.

Warner, K. A. , Roden, E. E., & Bonzongo, J. C. (2003). Microbial mercury transformation in anoxic freshwater sediments under iron-reducing and other electron-accepting conditions. *Environmental Science & Technology, 37*(10), 2159-2165.

Wedepohl, K. H. (1995). The composition of the continental crust. *Geochimica et Cosmochimica Acta, 59*(7), 1217-1232.

WHO. (2004). Guidelines for drinking-water quality (3rd ed., Vol. Vol. 1: Recommendations). Geneva, Switzerland: World Health Organization.

Yang, H., Battarbee, R. W., Turner, S. D., Rose, N. L., Derwent, R. G., Wu, G., & Yang, R. (2010). Historical reconstruction of mercury pollution across the Tibetan Plateau using lake sediments. *Environmental Science & Technology, 44*(8), 2918-2924.

Yao, T. D., Wang, Y., Liu, S., Pu, J., Shen, Y., & Lu, A. (2004). Recent glacial retreat in high Asia in China and its impact on water resource in Northwest China. *Science in China Series D: Earth Sciences, 47*(12), 1065-1075.

Zahir, F., Rizwi, S. J., Haq, S. K., & Khan, R. H. (2005). Low dose mercury toxicity and human health. *Environmental Toxicology and Pharmacology, 20*(2), 351-360.

Zhang, H., Yin, R. S., Feng, X., Sommar, J., Anderson, C. W. N., Sapkota, A., . . . Larssen, T. (2013). Atmospheric mercury inputs in montane soils increase with elevation: evidence from mercury isotope signatures. *Scientiffic Reports, 3*.

Zhang, Q., Huang, J., Wang, F., Mark, L., Xu, J., Armstrong, D., . . . Kang, S. C. (2012). Mercury distribution and deposition in glacier snow over Western China. *Environmental Science & Technology, 46*(10), 5404-5413.

List of appendices

Appendix A – Sample logs

Table A-1: Sample log from September 2012. Samples marked: HLG = Hailuogou, YZG = Yanzigou, -T = NGF tributary, -D = downstream, -U = upstream, CHZ = peat bog, DDH = Dadhing river and MXH = Dadu river. Replicate samples marked with (P). GF = glacier-fed and NGF = non-glacier-fed.

#	Sample	Date	GPS location	Altitude (m.a.s.l.)	Sampling point description	Sample type	Analytical parameters determined	
							Water	Sediment
1	HLG01	22.09.2012	29°36'19.29"N 102° 5'30.09"E	1818	Main GF river	Water	THg, MeHg, TOC, TSS, trace metals, major ions, pH	-
2	HLG02	22.09.2012	29°36'7.96"N 102° 3'57.72"E	2070	Main GF river	Water	THg, MeHg, trace metals	-
3	HLG03	22.09.2012	29°35'35.13"N 102° 2'33.39"E	2324	Main GF river	Water	THg, MeHg, trace metals	-
4	HLG04T	22.09.2012	29°35'43.23"N 102° 2'39.47"E	2357	Tributary NGF stream	Water	THg, MeHg, TOC, TSS, trace metals, major ions, pH	-
5	HLG05	23.09.2012	29°32'59.69"N 101°58'14.65"E	3590	Main GF river	Water	THg, MeHg, TOC, TSS, trace metals, major ions, pH	-
6	HLG06	24.09.2012	29°34'3.57"N 101°59'36.74"E	2964	Main GF river	Water	THg (P), MeHg (P), trace metals	-
7	HLG07	24.09.2012	29°34'0.39"N 101°59'29.56"E	2981	Main GF river	Water, alluvial soil	THg (P), MeHg (P), trace metals	THg, TOC
8	HLG08T	24.09.2012	29°34'12.53"N 101°59'51.08"E	2938	Tributary NGF stream	Water, sediment	THg, MeHg, TOC, TSS, trace metals, major ions, pH	THg, TOC
9	HLG09	24.09.2012	29°34'12.97"N 101°59'54.43"E	2922	Main GF river	Water, sediment profile	THg (P), MeHg (P), TOC, TSS, trace metals, major ions, pH	THg, TOC
10	HLG10	25.09.2012	29°34'37.16"N 102° 0'41.88"E	2811	Main GF river	Water	THg, MeHg, TOC, trace metals, major ions, pH	-
11	HLG11	25.09.2012	29°34'38.22"N 102° 0'50.42"E	2769	Main GF river	Water, sediment	THg, MeHg, trace metals	THg, TOC
12	HLG12T	25.09.2012	29°34'37.15"N 102° 0'54.02"E	2768	Tributary NGF stream	Water, sediment	THg, MeHg, trace metals	THg, TOC
13	HLG13T	25.09.2012	29°34'38.85"N 102° 0'45.38"E	2794	Tributary NGF stream	Water, sediment profile	THg, MeHg, TOC, TSS, trace metals, major ions, pH	THg, TOC
14	HLG14T	25.09.2012	29°35'21.82"N 102° 1'39.46"E	2672	Tributary NGF stream	Water	THg, MeHg, trace metals	-
15	CHZ	25.09.2012	29°35'13.48"N 102° 1'34.64"E	2780	Peat bog	Water	THg, MeHg, TOC, trace metals, major ions, pH	-
16	MXH03	25.09.2012	29°36'17.28"N 102°10'30.88"E	1125	Dadu River	Water	THg, MeHg, TOC, trace metals, major ions, pH	-
17	DDH-D	25.09.2012	29°36'16.51"N 102°10'40.77"E	1118	Dadhing River	Water	THg, MeHg, TOC, trace metals, major ions, pH	-
18	YZG01	26.09.2012	29°40'44.01"N 101°54'3.35"E	3716	Main GF river	Water	THg, MeHg, trace metals	-
19	YZG02	26.09.2012	29°40'46.35"N 101°54'4.51"E	3699	Tributary GF river	Water	THg, MeHg, trace metals	-

20	YZG03	26.09.2012	29°40'55.49"N 101°54'46.77"E	3639	Main GF river	Water	THg, MeHg, trace metals	-
21	YZG04	26.09.2012	29°41'3.38"N 101°55'55.19"E	3370	Main GF river	Water	THg, MeHg, trace metals	-
22	YZG05	26.09.2012	29°41'11.50"N 101°56'21.64"E	3278	Tributary GF river	Water	THg, MeHg, trace metals	-
23	YZG06	26.09.2012	29°41'7.31"N 101°56'43.70"E	3148	Main GF river	Water	THg, MeHg, trace metals	-
24	YZG07	26.09.2012	29°41'3.52"N 101°57'6.15"E	3061	Main GF river	Water	THg, MeHg, trace metals	-
25	YZG08	26.09.2012	29°41'10.37"N 101°58'15.34"E	2817	Main GF river	Water	THg, MeHg, trace metals	-
26	YZG09	26.09.2012	29°41'29.44"N 101°59'3.17"E	2690	Tributary GF river	Water	THg, MeHg, trace metals	-
27	YZG10T	26.09.2012	29°42'14.65"N 102° 0'24.46"E	2554	Tributary NGF stream	Water	THg, MeHg, trace metals	-
28	YZG11	26.09.2012	29°42'9.09"N 102° 1'35.63"E	2282	Main GF river	Water	THg, MeHg, trace metals	-
29	YZG12	26.09.2012	29°39'18.94"N 102° 6'41.48"E	1571	Main GF river	Water	THg (P), MeHg, trace metals	-

Table A-2: Sample log from April 2013. Samples marked: HLG = Hailuogou, YZG = Yanzigou, -T = NGF tributary, -D = downstream, -U = upstream, CHZ = peat bog, DDH = Dadhing river and MXH = Dadu river. Replicate samples marked with (P). GF = glacier-fed and NGF = non-glacier-fed.

#	Sample	Date	GPS location	Altitude (m.a.s.l.)	Sampling point description	Sample type	Analytical parameters determined	
							Water	Sediment
1	HLG01	07.04.2013	29°36'19.29"N 102° 5'30.09"E	1818	Main GF river	Water, sediment	THg, MeHg, TOC, TSS, trace metals, major ions, pH	THg, TOC
2	HLG02	07.04.2013	29°36'7.96"N 102° 3'57.72"E	2070	Main GF river	Water, sediment	THg, MeHg, TOC, TSS, trace metals, major ions, pH	THg, TOC
3	HLG03	11.04.2013	29°35'35.13"N 102° 2'33.39"E	2324	Main GF river	Water, sediment	THg, MeHg, TOC, TSS, trace metals, major ions, pH	THg, TOC
4	HLG04T	07.04.2013	29°35'43.23"N 102° 2'39.47"E	2357	Tributary NGF stream	Water, sediment	THg, MeHg, TOC, TSS, trace metals, major ions, pH	THg, TOC
5	HLG05	06.04.2013	29°32'59.69"N 101°58'14.65"E	3590	Main GF river	Water, sediment	THg, MeHg, TOC, TSS, trace metals,major ions, pH	THg, TOC
6	HLG06	05.04.2013	29°34'3.57"N 101°59'36.74"E	2964	Main GF river	Water, sediment	THg, MeHg, TOC, TSS, trace metals, major ions, pH	THg, TOC
7	HLG07	05.04.2013	29°34'0.39"N 101°59'29.56"E	2981	Main GF river	Water, sediment	THg (P), MeHg (P), TOC, TSS, trace metals, major ions, pH	THg, TOC
8	HLG08T	05.04.2013	29°34'12.53"N 101°59'51.08"E	2938	Tributary NGF stream	Water	THg, MeHg, TOC, TSS, trace metals, major ions, pH	-
9	HLG09	05.04.2013	29°34'12.97"N 101°59'54.43"E	2922	Main GF river	Water	THg, MeHg, TOC, TSS, trace metals, major ions, pH	-
10	HLG10	07.04.2013	29°34'37.16"N 102° 0'41.88"E	2811	Main GF river	Water, sediment	THg, MeHg, TOC, TSS, trace metals, major ions, pH	THg, TOC

11	HLG11	07.04.2013	29°34'38.22"N 102° 0'50.42"E	2769	Main GF river	Water	THg, MeHg, TOC, TSS, trace metals, major ions, pH	-
12	HLG12T	07.04.2013	29°34'37.15"N 102° 0'54.02"E	2768	Tributary NGF stream	Water	THg, MeHg, TOC, TSS, trace metals, major ions, pH	-
13	HLG13T	07.04.2013	29°34'38.85"N 102° 0'45.38"E	2794	Tributary NGF stream	Water	THg, MeHg, TOC, TSS, trace metals, major ions, pH	-
14	HLG14T	07.04.2013	29°35'21.82"N 102° 1'39.46"E	2672	Tributary NGF stream	Water	THg, MeHg, TOC, TSS, trace metals, major ions, pH	-
15	CHZ	11.04.2013	29°35'13.48"N 102° 1'34.64"E	2780	Peat bog	Water, peat profile	THg, MeHg, TOC, TSS, trace metals, major ions, pH	THg, TOC
16	MXH01	07.04.2013	29°38'50.87"N 102° 6'54.87"E	1511	Main GF river, by Moxizhen	Water, sediment	THg, MeHg, TOC, TSS, trace metals, major ions, pH	THg, TOC
17	MXH02	07.04.2013	29°36'24.35"N 102° 8'57.31"E	1235	Dadu River	Water, sediment	THg, MeHg, TOC, TSS, trace metals, major ions, pH	THg, TOC
18	MXH03	07.04.2013	29°36'17.28"N 102°10'30.88"E	1125	Dadu River	Water, sediment	THg, MeHg, TOC, TSS, trace metals, major ions, pH	THg, TOC
19	DDH-D	07.04.2013	29°36'16.51"N 102°10'40.77"E	1118	DDH River	Water, sediment	THg, MeHg, TOC, TSS, trace metals, major ions, pH	THg, TOC
20	DDH-U	07.04.2013	29°36'22.33"N 102°10'34.48"E	1119	DDH River	Water, sediment	THg, MeHg, TOC, TSS, trace metals, major ions, pH	THg, TOC
21	DDH-T	07.04.2013	29°36'28.18"N 102° 8'55.02"E	1273	Tributary NGF stream	Water	THg, MeHg, TOC, TSS, trace metals, major ions, pH	-
22	YZG01	08.04.2013	29°40'44.01"N 101°54'3.35"E	3716	Main GF river	Water, sediment	THg, MeHg, TOC, TSS, trace metals, major ions, pH	THg, TOC
24	YZG02	08.04.2013	29°40'46.35"N 101°54'4.51"E	3699	Tributary GF river	Water, sediment	THg, MeHg, TOC, TSS, trace metals, major ions, pH	THg, TOC
25	YZG03	08.04.2013	29°40'55.49"N 101°54'46.77"E	3639	Main GF river	Water, sediment	THg, MeHg, TOC, TSS, trace metals, major ions, pH	THg, TOC
26	YZG04	08.04.2013	29°41'3.38"N 101°55'55.19"E	3370	Main GF river	Water, sediment	THg, MeHg, TOC, TSS, trace metals, major ions, pH	THg, TOC
27	YZG05	08.04.2013	29°41'11.50"N 101°56'21.64"E	3278	Tributary GF river	Water, sediment	THg, MeHg, TOC, TSS, trace metals, major ions, pH	THg, TOC
28	YZG06	08.04.2013	29°41'7.31"N 101°56'43.70"E	3148	Main GF river	Water, sediment	THg, MeHg, TOC, TSS, trace metals, major ions, pH	THg, TOC
29	YZG07	08.04.2013	29°41'3.52"N 101°57'6.15"E	3061	Main GF river	Water, sediment	THg, MeHg, TOC, TSS, trace metals, major ions, pH	THg, TOC
30	YZG08	08.04.2013	29°41'10.37"N 101°58'15.34"E	2817	Main GF river	Water, sediment	THg, MeHg, TOC, TSS, trace metals, major ions, pH	THg, TOC
31	YZG09	08.04.2013	29°41'29.44"N 101°59'3.17"E	2690	Tributary GF river	Water, sediment	THg, MeHg, TOC, TSS, trace metals, major ions, pH	THg, TOC
32	YZG10T	08.04.2013	29°42'14.65"N 102° 0'24.46"E	2554	Tributary NGF stream	Water, sediment	THg, MeHg, TOC, TSS, trace metals, major ions, pH	THg, TOC
33	YZG10G	08.04.2013	29°42'18.94"N 102° 0'22.45"E	2666	Ground water	Water	THg, MeHg, TOC, TSS, trace metals, major ions, pH	-
34	YZG11	08.04.2013	29°42'9.09"N 102° 1'35.63"E	2282	Main GF river	Water, sediment	THg, MeHg, TOC, TSS, trace metals, major ions, pH	THg, TOC
35	YZG12	08.04.2013	29°39'18.94"N 102° 6'41.48"E	1571	Main GF river	Water, sediment	THg, MeHg, TOC, TSS, trace metals, major ions, pH	THg, TOC

Table A-3: The distribution of sampling points within different systems for both sampling campaigns.

System	# of sampling pts. (n)	
	Fall 2012	**Spring 2013**
GF	20	20
NGF	6	8
HLG GF	9	9
HLG NGF	5	5
YZG GF	11	11
YZG NGF	1	2
Other NGF	n/a	1
MXH	1	3
DDH	1	2
CHZ	1	1
Total	**29**	**34**

Appendix B – Chemicals, reagents, gases, standards and reference materials

B.1 Chemicals, gasses and water

Table B.1-1: List of chemicals used for preservation- and analytical procedures.

Chemical/Reagent	**Supplier**
Acetic acid (CH_3COOH) glacial 100%	Merck KGaA, Darmstadt, Germany
Deconex® Cleaning Solution	Groesfjeld Diagnostics, Rudkøbing, Denmark
Hydrochloric acid (HCl) fuming, 37%, EMSURE®	Merck KGaA, Darmstadt, Germany
Hydroxylamine-HCl (NH_2OH-HCl)	Brooks Rand Labs, Seattle WA, USA
Potassium bromide (KBr), ≥99.0%	Sigma Aldrich Co. LLC, St. Louis Mo, USA
Potassium hydroxide (KOH), EMSURE®	Merck KGaA, Darmstadt, Germany
Pyrrolidine-1-dithiocarboxylic acid ammonium salt (APDC)	Merck KGaA, Darmstadt, Germany
Sodium acetate anhydrous (CH_3COONa), EMSURE®	Merck KGaA, Darmstadt, Germany
Sodium tetraethylborate ($C_8H_{20}BNa$) 98%	Alfa Aesar, Ward Hill MA, USA
Stannous chloride ($SnCl_2$)	Brooks Rand Labs, Seattle WA, USA

Table B.1-2: List of gasses and their respective purities.

Gas	**Purity**	**Supplier**
Nitrogen (N_2) 5.0	99.999%	AGA, Oslo, Norway
Argon (Ar) 5.0	99.999%	AGA, Oslo, Norway
Oxygen (O_2) 4.5	99.995%	Yara, Oslo, Norway

Table B.1-2: Quality parameters for water used for analytical- and cleaning procedures.

Purification method	**Resistance**	**Temperature**
De-ionization and reverse membrane osmosis	18 MΩ	25 °C

B.2 Standards and reference materials

Table B.2-1: List of standards and reference materials and their respective concentrations used for the analytical procedures.

Stock Solution/Reference material	**Concentration**	**Supplier**
Methylmercury(II)hydroxide Stock Solution	1 µg/mL	Brooks Rand Labs, Seattle WA, USA
Methylmercury(II)chloride Stock Solution	1 µg/mL	Brooks Rand Labs, Seattle WA, USA
Total Mercury Stock Solution,	1 µg/mL	Brooks Rand Labs, Seattle WA, USA
TCLP Mercury Standard	20 µg/mL	Ultra Scientific, Bologna, Italia
MESS-3 Marine Sediment CRM - THg	0.091 ± 0.009 µg/kg	NRC, Ottawa ON, Canada

Appendix C – Instrument specifications and experimental settings

Table C-1: Instrumental specifications for the MERX® Automated Total Mercury System from Brooks Rand (Brooks-Rand-Labs, 2012b).

Specification	**Setting/Type**
UV light source peak emission wavelength (nm)	253.7
Optical band pass filter (nm)	253.7
Detector	PMT
Traps	Gold-amalgamation
Working range (ng/L)	0.1 – 50.0
Detection limit (ng/L)	0.2
Purging gas	N_2
Drying gas	N_2
Carrier gas	Ar

Table C-2: Experimental settings for the MERX® Automated Total Mercury System from Brooks Rand (Brooks-Rand-Labs, 2012b).

Parameter	**Setting**
Needle injection depth (mm)	156
Run duration (min)	2.5
Heating time (min)	2.5
Cooling time (min)	1.0
Purge duration (min)	6

Table C-3: Instrumental specifications for the MERX® Automated Methylmercury System from Brooks Rand (Brooks-Rand-Labs, 2012a)

Specification	**Setting/Type**
UV light source peak emission wavelength (nm)	253.7
Optical band pass filter (nm)	253.7
Detector	PMT
GC column material	15% OV-3 on Chromosorb W-AW
Traps	Tenax®
Working range (ng/L)	0.02 – 10.00
Detection limit (ng/L)	0.01
Purging gas	N_2
Drying gas	N_2
Carrier gas	Ar

Table C-4: Experimental settings for the MERX® Automated Total Mercury System from Brooks Rand (Brooks-Rand-Labs, 2012a)

Parameter	**Setting**
Needle injection depth (mm)	155
Run duration (min)	5.0
Heating time (min)	9.2
Cooling time (min)	3.0
Purge duration (min)	5.0
Drying duration (min)	3.0
GC-column temp. (°C)	36
Pyrolytic column temp. (°C)	700

Table C-5: Instrumental specifications for the DMA-80 from Milestone (Milestone, 2002)

Specification	**Setting/Type**
Instrument optics	Single beam spectrophotometer with sequential flow through of measurement cells
Light source	Low pressure Hg-vapor lamp
Wavelength (nm)	253.65
Interference filter (nm) / bandwidth (mm)	254/9
Detector	Si-photodiode sensor
Working range (ng)	Low: 0.02-35 High: 35-600
Detection limit (ng)	0.02
Carrier gas	O_2
Input pressure	7 bar

Table C-6: Experimental settings for the DMA-80 from Milestone (Milestone, 2002).

Parameter	**Setting**
Decomposition temp. (°C)	750
Decomposition time (s)	60
Amalgamator temp. (°C)	200-900
Amalgamation time (s)	12
Cuvette temp. (°C)	120
Signal recording time (s)	24

Appendix D – Calibration

D.1 Calibration information for the analysis of THg in water

Table D.2-1:Hg concentrations (pg) of each of the seven calibration solutions along with the volume (mL) of working solution needed to prepare them.

Calibration solution ID	Volume (mL)	Working solution conc.
5 pg	0.050	0.1 ng/ml
10 pg	0.100	0.1 ng/ml
25 pg	0.025	1.0 ng/ml
100 pg	0.100	1.0 ng/ml
500 pg	0.050	10.0 ng/ml
2500 pg	0.250	10.0 ng/ml
10000 pg	1.00	10.0 ng/ml

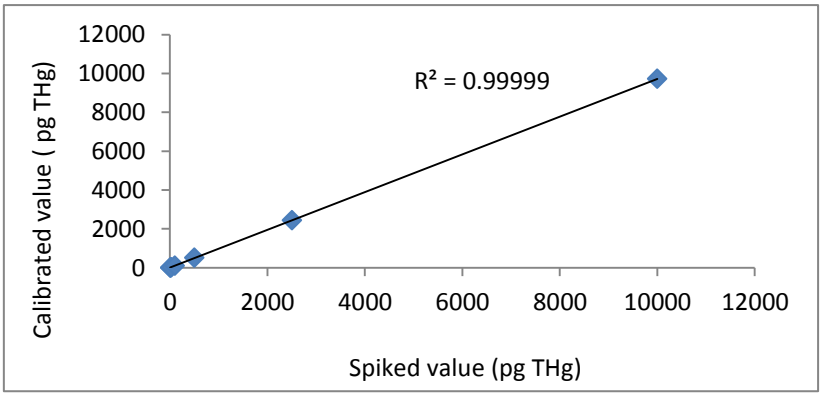

Figure D.1-1: Calibration curve for the analysis of THg in water samples from fall 2012.

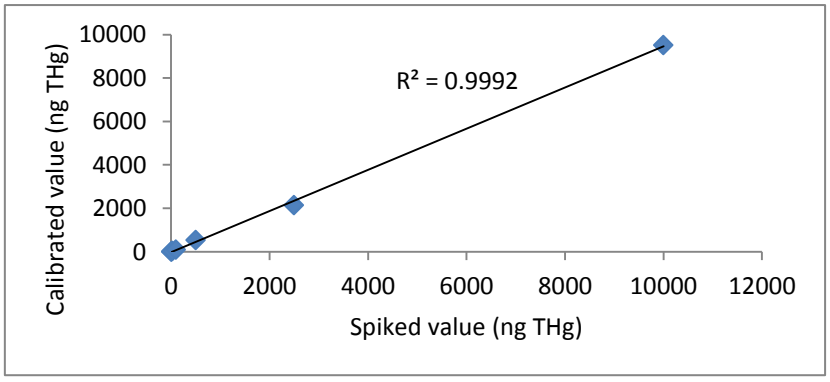

Figure D.1-2: Calibration curve for the analysis of THg in water samples from spring 2013.

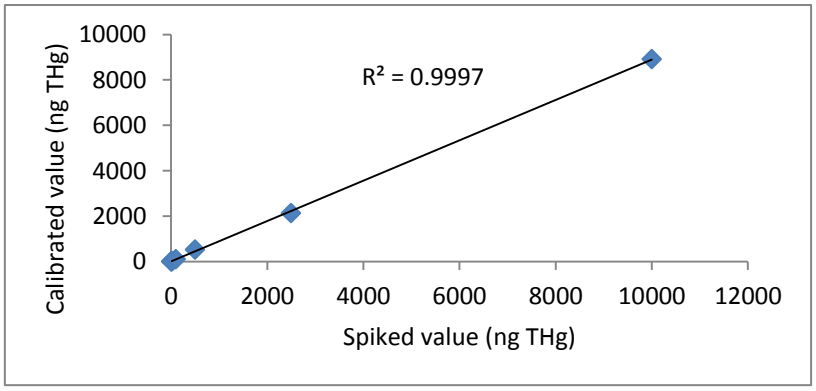

Figure D.1-3: Calibration curve for the analysis of DHg in water samples from spring 2013.

D.2 Calibration curves for the analysis of MMHg in water

Table D.2-1: MMHg concentrations (pg) of each of the seven calibration solutions along with the volume (mL) of working solution needed to prepare them.

Calibration solution ID	Volume (ml)	Working solution conc.
0.5 pg	0.050	0.01 ng/ml
1.0 pg	0.100	0.01 ng/ml
2.0 pg	0.200	0.01 ng/ml
10 pg	1.00	0.01 ng/ml
50 pg	0.050	1.0 ng/ml
250 pg	0.250	1.0 ng/ml
1000 pg	1.00	1.0 ng/ml

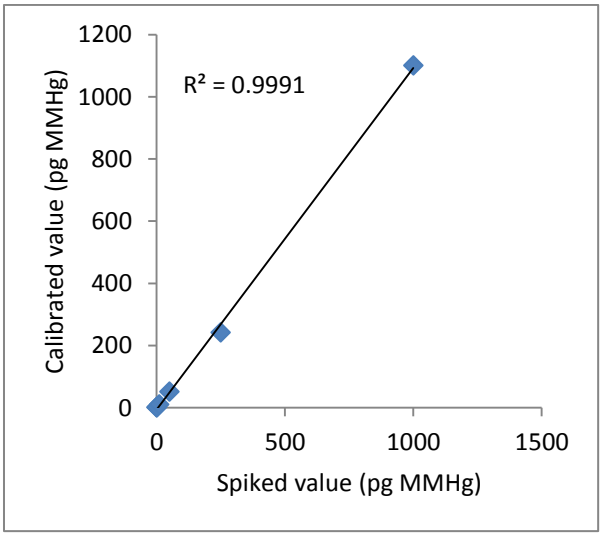

Table D.2-1: First calibration curve for the analysis of MMHg in water samples from fall 2012.

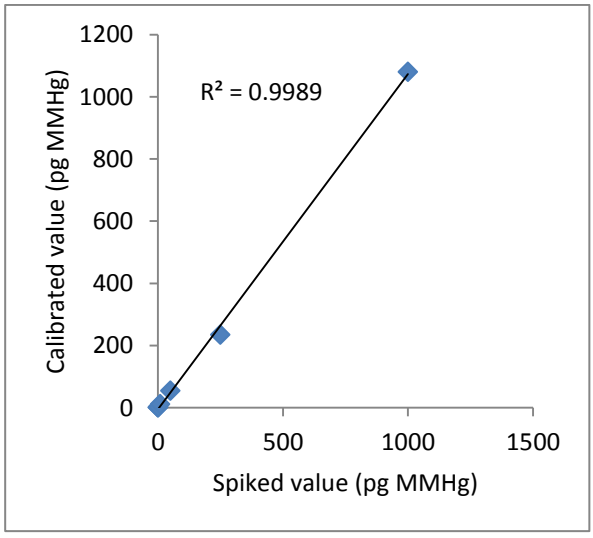

Table D.2-3: Third calibration curve for the analysis of MMHg in water samples from fall 2012.

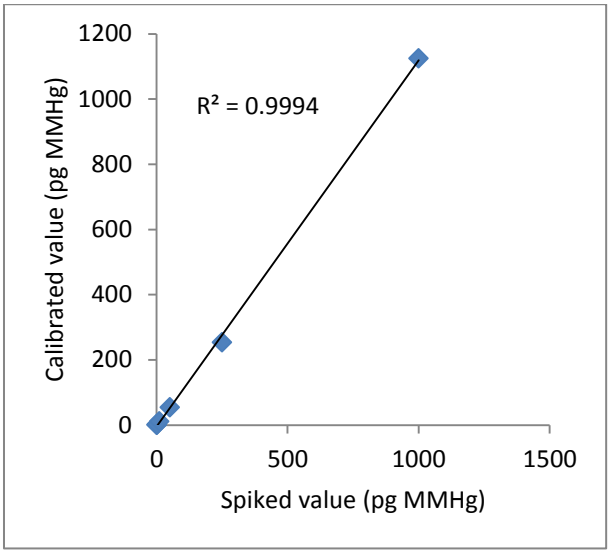

Table D.2-2: Second calibration curve for the analysis of MMHg in water samples from fall 2012.

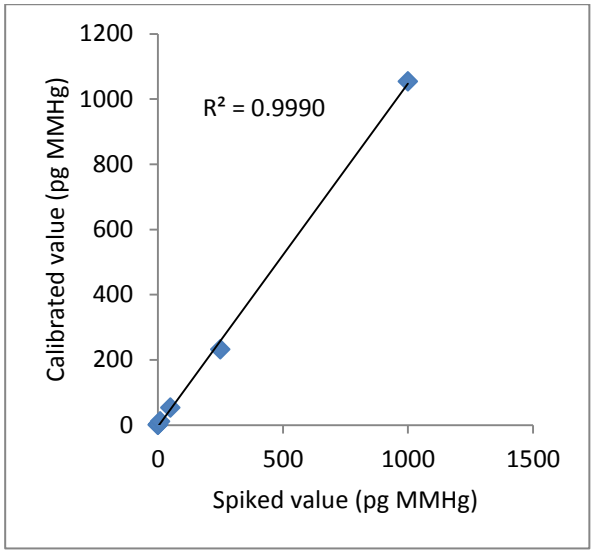

Table D.2-4: Fourth calibration curve for the analysis of MMHg in water samples from fall 2012.

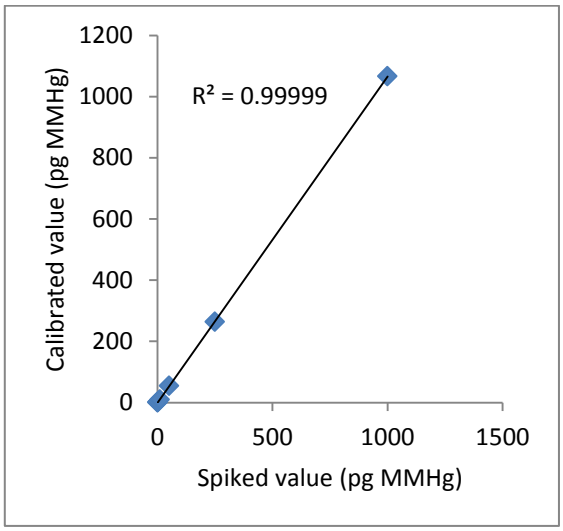

Table D.2-5: First calibration curve for the analysis of MMHg in water samples from spring 2013.

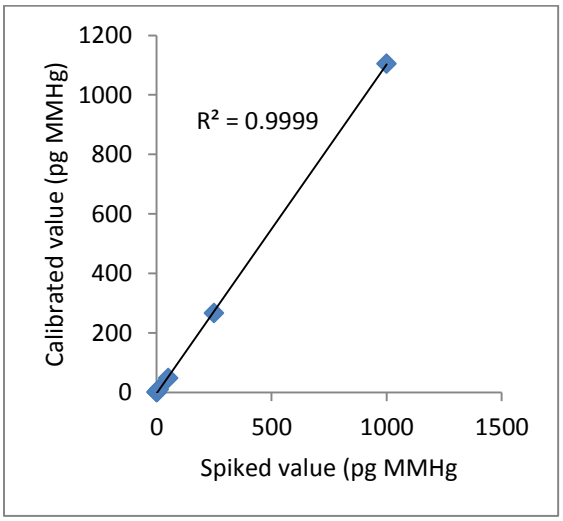

Table D.2-6: Second calibration curve for the analysis of MMHg in water samples from spring 2013.

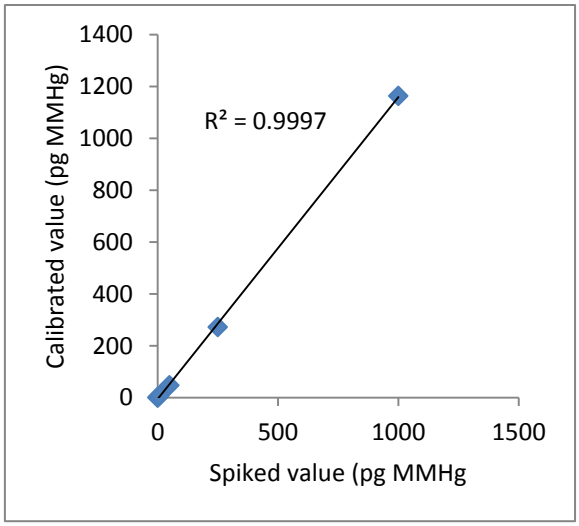

Table D.2-7: Third calibration curve for the analysis of MMHg in water samples from spring 2013.

D.3 Calibration curves for the analysis of THg in sediments and soil

Table D.3-1: Weight (g) of CRM used for the calibration for DMA-80 with estimated Hg-content (pg) and the recorded absorbance for the fall 2012 sample set analysis.

#	Weight (g)	Hg (pg)	Abs
1	0.0000	0	0.0045
2	0.0253	2	0.0771
3	0.0458	4	0.1441
4	0.1057	10	0.3167
5	0.1747	16	0.5009
6	0.2515	23	0.7016

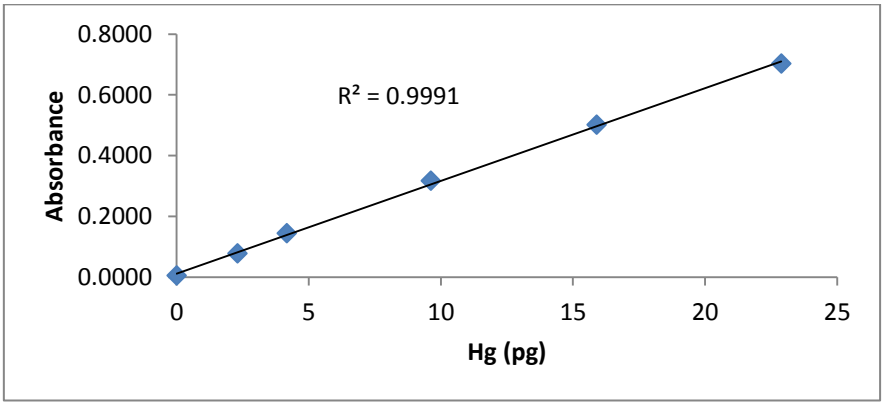

Table D.2-7: Calibration curve for the analysis of THg in sediment samples from fall 2012.

Table D.3-1: Weight (g) of CRM used for the calibration of the DMA-80 with estimated Hg-content (pg) and the recorded absorbance for the spring 2013 sample set analysis.

#	Weight (g)	Hg (pg)	Abs
1	0.0000	0	0.0007
2	0.0331	3	0.084
3	0.0679	6	0.159
4	0.0944	9	0.2154
5	0.1210	11	0.2677
6	0.1493	14	0.3212

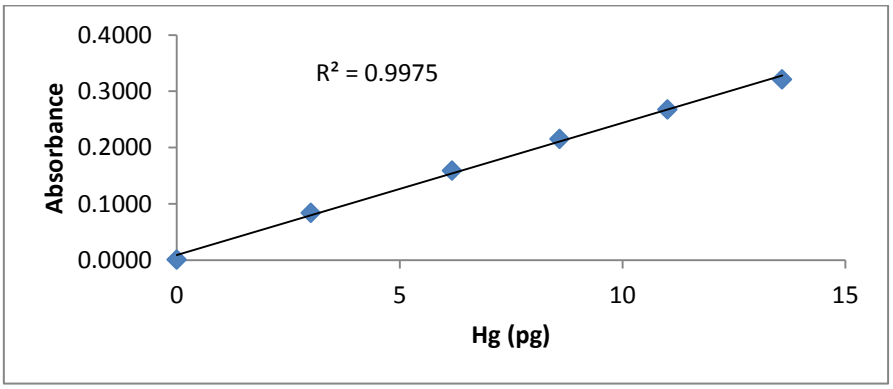

Table D.2-8: Calibration curve for the analysis of THg in sediment and soil samples from spring 2013.

Appendix E - Quality control and quality assurance

E.1 Blanks

THg in water

Method blank values for THg analysis runs are shown in the tables below. All samples analyzed were automatically corrected for the blank value by the system software.

Table E.1-1: Method blank values with mean and standard deviation for the THg analysis of the fall 2012 sample set.

	THg (ng/L)
BLK1	0.13
BLK2	0.16
BLK3	0.17
Mean	0.15
St. dev.	0.02

Table E.1-2: Method blank values with mean and standard deviation for the THg analysis of the spring 2013 sample set.

	THg (ng/L)
BLK1	0.13
BLK2	0.14
BLK3	0.12
Mean	0.13
St. dev.	0.01

Table E.1-3: Method blank values with mean and standard deviation for the DHg analysis of the spring 2013 sample set.

	DHg (ng/L)
BLK1	0.30
BLK2	0.18
BLK3	0.23
Mean	0.24
St. dev.	0.06

LOD and LOQ were calculated as per the blank method (equations 3.3.1-1 and 3.3.1-2 respectively) for the THg and DHg analysis based on the blanks in the separate runs (tables E.1-1 – E.1-3) and are shown in table E.1-4. As there were only a total of 6 and 3 blanks for

the THg and DHg analysis runs an extra blank test for each method was run with n=10 to estimate LOD and LOQ (tables E.1-5 and E.1-6). The THg blanks have an unusually low standard deviation (0.01) giving a LOD of 0.03 ng/L. LOD and LOQ for this method will be set to 0.1 ng/L and 0.3 ng/L respectively as this is has been shown to be a stable limit over time (NIVA, 2012).

Table E.1-4: Mean method blank values and standard deviation for THg (n=6) and DHg (n=3) runs and LOD and LOQ values based on these.

	THg (ng/L)	**DHg (ng/L)**
Mean	0.14	0.24
St. dev.	0.02	0.06
LOD	0.1	0.2
LOQ	0.2	0.6

Table E.1-5: Method blank samples for the LOD test for the THg in water method, with mean, standard deviation and calculated LOD and LOQ.

	THg (ng/L)
BLK-1	0.16
BLK-2	0.16
BLK-3	0.15
BLK-4	0.15
BLK-5	0.14
BLK-6	0.13
BLK-7	0.15
BLK-8	0.16
BLK-9	0.14
BLK-10	0.14
Mean	0.15
St. dev.	0.01
LOD	**0.03**
LOQ	**0.1**

Table E.1-6: Method blank samples for the LOD test for the DHg in water method, with mean, standard deviation and calculated LOD and LOQ.

	DHg (ng/L)
BLK-1	0.17
BLK-2	0.17
BLK-3	0.19
BLK-4	0.17
BLK-5	0.17

BLK-6	0.17
BLK-7	0.23
BLK-8	0.16
BLK-9	0.17
BLK-10	0.16
Mean	0.18
St. dev.	0.02
LOD	**0.1**
LOQ	**0.2**

MMHg in water

Method blank values for THg analysis runs are shown in the tables below. All samples analyzed were automatically corrected for the blank value by the system software.

Table E.1-7: Method blank values with mean and standard deviation for the MMHg analysis of the fall 2012 sample set.

	MMHg (ng/L)
BLK1	0.003
BLK2	0.004
BLK3	0.005
BLK4	0.015
BLK5	0.008
BLK6	0.007
BLK7	0.002
BLK8	0.002
BLK9	0.003
BLK10	0.004
BLK11	0.005
BLK12	0.007
Mean	0.005
St. dev.	0.004

Table E.1-8: Method blank values with mean and standard deviation for the DMMHg analysis of the fall 2012 sample set.

	DMMHg (ng/L)
BLK1	0.005
BLK2	0.003
BLK3	0.003
BLK4	0.003
BLK5	0.002

BLK6	0.004
Mean	0.0034
St. dev.	0.0008

Table E.1-9: Method blank values with mean and standard deviation for the MMHg analysis of the spring 2013 sample set.

	MMHg (ng/L)
BLK1	0.010
BLK2	0.012
BLK3	0.019
BLK4	0.010
BLK5	0.017
BLK6	0.007
BLK7	0.008
BLK8	0.016
BLK9	0.011
BLK10	0.008
BLK11	0.010
BLK12	0.014
Mean	0.012
St. dev.	0.004

LOD and LOQ were calculated as per the blank method (equations 3.3.1-1 and 3.3.1-2 respectively) based on all the blanks in the separate runs (tables E.1-7 – E.1-9) and are shown in table E.1-10

Table E.1-10: Mean method blank values and standard deviation for all MMHg analysis runs and LOD and LOQ values based on these.

	MMHg (ng/L)
Mean	0.008
St. dev.	0.005
LOD	0.02
LOQ	0.05

.

TSS in water

Method blank values for TSS analysis runs are shown in the tables below. All blanks have negative concentrations of TSS resulting from mass loss from the filter. All samples analyzed were corrected for this filter mass loss.

Table E.1-11: Method blank values with mean and standard deviation for the TSS analysis of samples from fall 2012.

	TSS (mg/L)
BLK1	-0.68
BLK2	-0.56
BLK3	-0.16
Mean	-0.5
St. dev.	0.3

Table E.1-12: Method blank values with mean and standard deviation for the TSS analysis of samples from spring 2013.

	TSS (mg/L)
BLK1	-0.30
BLK2	-0.06
BLK3	-0.74
BLK4	-0.57
Mean	-0.4
St. dev.	0.3

LOD and LOQ were calculated as per the blank method (equations 3.3.1-1 and 3.3.1-2 respectively) based on all the blanks in the separate runs (tables E.1-11 and E.1-12) and are shown in table E.1-13

Table E.1-13: Mean method blank values and standard deviation for all MMHg analysis runs and LOD and LOQ values based on these.

	TSS (mg/L)
Mean	-0.4
St. dev.	0.3
LOD	1
LOQ	3

THg in sediments

Method blank values for THg in sediment runs are shown in the tables below. All samples analyzed were corrected for the mean blank value by the author

Table E.1-14: Method blank values with mean and standard deviation for the THg in sediments analysis of samples from both sampling campaings.

	THg (ng)
BLK1	0.11
BLK2	0.08
BLK3	0.08
BLK4	0.08
BLK5	0.08
BLK6	0.09
BLK7	0.07
BLK8	0.07
BLK9	0.17
BLK10	0.14
Mean	0.10
St. dev.	0.03

LOD and LOQ were calculated as per the blank method (equations 3.3.1-1 and 3.3.1-2 respectively) based on all the blanks (tables E.1-14) and are shown in table E.1-15

.

Table E.1-15: LOD amd LOQ for the determination of THg in sediments based on the method blank.

LOD (ng)	0.1
LOQ (ng)	0.3
Mean sample weight (g)	0.5855
LOD (ng/g)	0.2
LOQ (ng/g)	0.6

E.2 Reproducibility

THg in water

Analysis parallels for samples in the fall 2012 and spring 2013 data sets are shown in the tables below. For the samples analyzed in parallels and adhering to the quality requirement of RPD<15% the mean value is reported in the findings.

Table E.2-1: THg (ng/L) analysis parallels of samples in the fall 2012 data set.

Sample	THg (ng/L)	RPD (%)	Mean (ng/L)
HLG01	1.17	6.9	1.1
HLG01 P	1.09		
HLG04T	0.47	7.7	0.5
HLG04T P	0.51		
HLG05	1.49	8.3	1.4
HLG05 P	1.38		
HGL09	2.77	6.6	2.7
HGL09 P	2.59		

Table E.2-2: THg (ng/L) analysis parallels of samples in the spring 2013 data set.

Sample	THg (ng/L)	RPD (%)	Mean (ng/L)
HLG01	0.74	10.9	0.7
HLG01 P	0.66		
HLG02	0.65	4.9	0.7
HLG02 P	0.68		
HLG03	0.55	0.1	0.6
HLG03 P	0.56		
HLG04T	0.72	11.1	0.8
HLG04T P	0.81		

Table E.2-3: DHg (ng/L) analysis parallels of samples in the spring 2013 data set. Mean values below LOQ shown as <0.3.

Sample	DHg (ng/L)	RPD (%)	Mean (ng/L)
D-HLG01	0.37	89.0	<0.3
D-HLG01 P	0.14		
D-HLG02	0.11	0.9	<0.3
D-HLG02 P	0.11		
D-HLG03	0.07	107.0	<0.3
D-HLG03 P	0.02		
D-HLG04T	0.12	45.8	<0.3
D-HLG04T P	0.20		

MMHg in water

Analysis parallels for samples in the fall 2012 and spring 2013 data sets are shown in the tables below. For the samples analyzed in parallels and adhering to the quality requirement of RPD<15% the mean value is reported in the findings.

Table E.2-4: MMHg (ng/L) analysis parallels of samples in the fall 2012 data set. Mean values below LOQ shown as <0.05.

Sample	MMHg (ng/L)	RPD (%)	Mean (ng/L)
HLG01	0.017	65.9	<0.05
HLG01 P	0.009		
HLG09	0.016	32.1	<0.05
HLG09 P	0.012		
YZG02	0.005	36.5	<0.05
YZG02 P	0.004		
YZG03	0.004	2.0	<0.05
YZG03 P	0.004		
YZG05	0.005	6.2	<0.05
YZG05 P	0.005		
YZG08	0.004	7.9	<0.05
YZG08 P	0.004		

Table E.2-5: MMHg (ng/L) analysis parallels of samples in the fall 2012 data set. Mean values below LOQ shown as <0.05.

Sample	MMHg (ng/L)	RPD (%)	Mean (ng/L)
HLG01	-0.003	n/a	<0.05
HLG01 P	-0.001		
HLG12T	-0.001	n/a	<0.05
HLG12T P	-0.001		
YZG01	-0.004	n/a	<0.05
YZG01 P	0.002		
YZG12	0.000	190.0	<0.05
YZG12 P	0.005		
MXH01	0.009	8.5	<0.05
MXH01 P	0.009		

TSS in water

Analysis parallels for samples in the fall 2012 and spring 2013 data sets are shown in the tables below. For the samples analyzed in parallels and adhering to the quality requirement of RPD<15% the mean value is reported in the findings.

Table E.2-6: TSS (mg/L) analysis parallels of samples in the fall 2012 data set

Sample	TSS(mg/L)	RPD (%)	Mean (mg/L)
HLG01	194.7	0.4	194.2
HLG01 P	193.8		

HLG05	373.7	1.0	375.5
HLG05 P	377.2		
HLG09	334.3	12.0	355.7
HLG09 P	377.1		

Table E.2-7: TSS (mg/L) analysis parallels of samples in the spring 2013 data set

Sample	TSS (mg/L)	RPD (%)	Mean (mg/L)
DDH-T	1.6	5.6	1.6
DDH-T P	1.5		
DDH-D	26.5	10.1	27.9
DDH-D P	29.4		
YZG05	5604.5	31.9	4833.9
YZG05 P	4063.3		
YZG10	9.2	5.0	9.0
YZG10 P	8.7		

THg in sediments and soil

Analysis parallels for samples in the fall 2012 and spring 2013 data sets are shown in the tables below. For the samples analyzed in parallels and adhering to the quality requirement of RPD<15% the mean value is reported in the findings.

Table E.2-8: THg (µg/kg) analysis parallels of samples in the fall 2012 data set

Sample	THg (µg/kg)	RPD (%)	Mean (µg/kg)
HLG13T 0-5	1.10	2.4	1.1
HLG13T 0-5 P	1.08		
HLG13T 5-10	1.54	6.3	1.5
HLG13T 5-10 P	1.45		
HLG13T 10-15	1.54	5.7	1.6
HLG13T 10-15 P	1.63		
HLG13T 15-20	2.14	1.3	2.1
HLG13T 15-20 P	2.16		
HLG13T 20-25	3.88	12.5	3.7
HLG13T 20-25 P	3.42		
HLG13T	1.16	1.8	1.1
HLG13T P	1.14		
HLG09 0-3	1.67	9.6	1.6
HLG09 0-3 P	1.52		
HLG09 6-9.5	1.08	11.4	1.0
HLG09 6-9.5 P	0.96		
HLG09 9.5-11	1.12	5.4	1.1

HLG09 9.5-11 P	1.06		
HLG09 11-15	1.15	1.3	1.1
HLG09 11-15 P	1.13		
HLG14T	2.42	14.9	2.6
HLG14T P	2.81		
HLG08T	0.61	8.2	0.6
HLG08T P	0.66		
HLG11	0.91	6.5	0.9
HLG11 P	0.97		
HLG12T	1.11	1.6	1.1
HLG12T P	1.09		

Table E.2-9: THg (µg/kg) analysis parallels of samples in the spring 2013 data set

Sample	**THg (µg/kg)**	**RSD (%)**	**Mean (µg/kg)**
YZG01	0.81	0.3	0.8
YZG01 P	0.81		
YZG02	1.62	2.5	1.6
YZG02 P	1.57		
YZG04	0.93	2.1	0.9
YZG04 P	0.96		
YZG05	1.13	4.6	1.2
YZG05 P	1.21		
YZG06	1.31	12.2	1.2
YZG06 P	1.10		
YZG07	3.08	14.3	2.8
YZG07 P	2.51		
YZG08	3.98	10.1	3.7
YZG08 P	3.45		
YZG09	0.57	14.8	0.5
YZG09 P	0.46		
YZG11	0.94	10.5	1.0
YZG11 P	1.09		
HLG02	1.79	12.9	1.6
HLG02 P	1.49		
MXH01	0.68	5.0	0.7
MXH01 P	0.64		
MXH02	1.82	8.9	1.7
MXH02 P	1.60		
MXH03	1.08	5.7	1.1
MXH03 P	1.17		
DDH-D	0.85	2.8	0.8
DDH-D P	0.82		
DDH-U	12.83	5.3	13.3
DDH-U P	13.83		

E.3 Replicate samples

THg in water

Determination of THg in sample replicates from the two sample sets are shown below.

Table E.3-1: Replicate samples for THg (ng/L) in the fall 2012 data set.

Sample	THg (ng/L)	RPD (%)
HLG06	1.59	3.7
HLG06-P	1.65	
HGL07	2.60	21.3
HGL07-P	2.10	
HGL09	2.77	3.0
HGL09-P	2.68	
YZG12	0.98	24.1
YZG12-P	0.77	

Table E.3-2: Replicate samples for THg (ng/L) in the spring 2013 data set.

Sample	THg (ng/L)	RPD (%)
HLG07	1.65	8.4
HLG07-P	1.52	

Table E.3-3: Replicate samples for DHg (ng/L) in the spring 2013 data set

Sample	DHg (ng/L)	RPD (%)
HLG07	0.1	n/a
HLG07-P	-0.1	

MMHg in water

Determination of MMHg in sample replicates from the two sample sets are shown below.

Table E.3-4: Replicate samples for MMHg (ng/L) in the fall 2012 data set.

Sample	MMHg (ng/L)	RPD (%)
HLG06	0.009	46.9
HLG06-P	0.006	
HGL07	0.007	134.5
HGL07-P	0.035	
HGL09	0.016	87.5
HGL09-P	0.006	

Table E.3-5: Replicate samples for MMHg (ng/L) in the spring 2013 data set.

Sample	MMHg (ng/L)	RPD (%)
HLG07	-0.011	n/a
HLG07-P	-0.003	

E.4 Internal standard

An internal standard as an initial calibration verification (ICV) was used for both THg and MMHg analysis. The results are summarized in the tables below.

THg in water

Table E.4-1: Initial calibration verification (ICV) results from the calibrations for THg analysis.

Sample set	ICV (pg)	Exp. (pg)	Recovery (%)	Rec. Criteria (%)
THg (2012)	2000	1959.1	98.0	75-125
THg (2013)	2000	1781.4	89.1	75-125
DHg (2013)	2000	1753.3	87.7	75-125

MMHg in water

Table E.4-2: Initial calibration verification (ICV) results from the calibrations for MMHg analysis.

Sample set	ICV (pg)	Exp. (pg)	Recovery (%)	Rec. Criteria (%)
MMHg (2012) #1	25	26.4	106	75-125
MMHg (2012) #2	25	28.2	113	75-125
MMHg (2012) #3	25	31.3	125	75-125
MMHg (2012) #4	25	26.6	106	75-125
MMHg (2013) #1	25	32.1	128	75-125
MMHg (2013) #2	25	30.5	122	75-125
MMHg (2013) #3	25	30.0	120	75-125

E.5 Calibration verification

THg in water

Table E.5-1: Continuing calibration verification (CCV) results from the THg analysis of the fall 2012 data set.

#	CCV (pg)	Exp. (pg)	Recovery (%)	Rec. Criteria (%)
1	500	534.53	106.9	80-120
2	500	533.48	106.7	80-120
3	500	528.34	105.7	80-120
4	500	512.93	102.6	80-120
5	500	523.89	104.8	80-120
6	500	525.53	105.1	80-120
7	500	520.72	104.2	80-120
8	500	522.76	104.6	80-120

Table E.5-2: Continuing calibration verification (CCV) results from the THg analysis of the spring 2013 data set.

#	CCV (pg)	Exp. (pg)	Recovery (%)	Rec. Criteria (%)
1	500	545.58	109.1	80-120
2	500	464.76	93.0	80-120
3	500	454.38	90.9	80-120
4	500	440.79	88.2	80-120
5	500	433.74	86.7	80-120
6	500	418.85	83.8	80-120

Table E.5-3: Continuing calibration verification (CCV) results from the DHg analysis of the spring 2013 data set.

#	CCV (pg)	Exp. (pg)	Recovery (%)	Rec. Criteria (%)
1	500	548.66	109.7	80-120
2	500	586.29	117.3	80-120
3	500	561.99	112.4	80-120
4	500	543.64	108.7	80-120
5	500	525.57	105.1	80-120
6	500	515.39	103.1	80-120
7	500	509.69	101.9	80-120

MMHg in water

Table E.5-4: Continuing calibration verification (CCV) results from the MMHg and DMMHg analysis of the fall 2012 data set.

#	CCV (pg)	Exp. (pg)	Recovery (%)	Rec. Criteria (%)
1	25	25.17	100.7	80-120
2	25	25.39	101.6	80-120
3	25	26.36	105.4	80-120
4	25	26.21	104.9	80-120
5	25	25.23	100.9	80-120
6	25	25.26	101.1	80-120
7	25	29.04	116.2	80-120
8	25	29.08	116.3	80-120
9	25	22.47	89.9	80-120
10	25	22.99	92.0	80-120
11	25	23.05	92.2	80-120
12	25	23.96	95.8	80-120
13	25	25.67	102.7	80-120

Table E.5-5: Continuing calibration verification (CCV) results from the MMHg analysis of the spring 2013 data set.

#	CCV (pg)	Exp. (pg)	Recovery (%)	Rec. Criteria (%)
1	25	28.96	115.9	80-120
2	25	23.09	92.4	80-120
3	25	25.37	101.5	80-120
4	25	25.40	101.6	80-120
5	25	28.82	115.3	80-120
6	25	26.97	107.9	80-120
7	25	24.47	97.9	80-120
8	25	25.90	103.6	80-120
9	25	24.02	96.1	80-120
10	25	23.92	95.7	80-120
11	25	24.84	99.4	80-120
12	25	24.46	97.8	80-120
13	25	22.78	91.1	80-120
14	25	23.17	92.7	80-120
15	25	20.96	83.8	80-120

E.6 Spike-and-recovery assessment

Spike-and-recovery assessments are shown for THg and MMHg analysis results in the form of blank spikes and sample spikes.

THg in water

Table E.6-1: Sample spike data from the THg analysis of the fall 2012 sample set.

Sample	Spike (ng/L)	THg (ng/L)	Sample THg (ng/L)	Spike Recovery (%)	Rec. Criteria (%)
HLG01	2	3.21	1.17	102.1	75-125
HLG04T	2	2.33	0.47	93.1	75-125
HLG05	2	3.49	1.49	99.8	75-125
HGL07	2	4.61	2.60	100.2	75-125
HGL08	2	2.11	0.17	96.9	75-125

Table E.6-2: Blank spike data from the THg analysis of the fall 2012 sample set.

Sample	Spike (ng/L)	THg (ng/L)	Spike Recovery (%)	Rec. Criteria (%)
BLK Spike 1	2	2.11	105.5	80-120
BLK Spike 2	2	2.06	103.1	80-120
BLK Spike 3	4	3.97	99.3	80-120

Table E.6-3: Sample spike data from the THg analysis of the spring 2013 sample set.

Sample	Spike (ng/L)	THg (ng/L)	Sample THg (ng/L)	Spike Recovery (%)	Rec. Criteria (%)
HLG01	2	2.92	0.74	108.9	75-125
HLG02	2	2.56	0.65	95.8	75-125
HLG03	2	2.71	0.55	108.0	75-125
HLG04T	2	2.64	0.72	95.8	75-125

Table E.6-4: Blank spike data from the THg analysis of the spring 2013 sample set.

Sample	Spike (ng/L)	THg (ng/L)	Spike Recovery (%)	Rec. Criteria (%)
BLK Spike 1	2	1.87	93.3	80-120
BLK Spike 2	2	2.02	101.0	80-120
BLK Spike 3	4	4.05	101.2	80-120
BLK Spike 4	4	4.11	102.7	80-120

Table E.6-5: Sample spike data from the DHg analysis of the spring 2013 sample set.

Sample	Spike (ng/L)	THg (ng/L)	Sample THg (ng/L)	Spike Recovery (%)	Rec. Criteria (%)
D-HLG01	2	2.48	-0.05	121.7	75-125
D-HLG02	2	1.96	-0.28	84.0	75-125
D-HLG03	2	2.33	-0.29	102.1	75-125
D-HLG04T	2	2.04	0.12	95.9	75-125

Table E.6-6: Blank spike data from the DHg analysis of the spring 2013 sample set.

Sample	Spike (ng/L)	THg (ng/L)	Spike Recovery (%)	Rec. Criteria (%)
BLK Spike 1	2	2.21	110.4	80-120
BLK Spike 2	2	2.43	121.4	80-120
BLK Spike 3	4	4.10	102.4	80-120

MMHg in water

Table E.6-7: Sample spike data from the MMHg and DMMHg analysis of the fall 2012 sample set.

Sample	Spike (ng/L)	MMHg (ng/L)	Spike Recovery (%)	Rec. Criteria (%)
HLG01	0.05	0.043	50.6	65-135
YZG08	0.05	0.072	135.5	65-135
YZG02	0.05	0.021	30.3	65-135
YZG05	0.05	0.045	78.8	65-135
YZG03	0.05	0.074	140.0	65-135
HLG09	0.05	0.055	77.1	65-135

Table E.6-8: Blank spike data from the MMHg and DMMHg analysis of the fall 2012 sample set.

Sample	Spike (ng/L)	MMHg (ng/L)	Spike Recovery (%)	Rec. Criteria (%)
BLK Spike 1	0.05	0.045	90.2	70-130
BLK Spike 2	0.05	0.040	79.0	70-130
BLK Spike 3	0.05	0.039	78.3	70-130
BLK Spike 4	0.05	0.058	115.1	70-130
BLK Spike 5	0.05	0.058	115.1	70-130
BLK Spike 6	0.05	0.049	98.9	70-130
BLK Spike 7	0.05	0.040	79.9	70-130
BLK Spike 8	0.05	0.049	98.0	70-130
BLK Spike 9	0.05	0.040	79.9	70-130
BLK Spike 10	0.05	0.043	85.9	70-130

BLK Spike 11	0.05	0.051	101.7	70-130
BLK Spike 12	0.05	0.044	88.8	70-130
BLK Spike 13	0.05	0.044	88.4	70-130
BLK Spike 14	0.05	0.040	79.9	70-130
BLK Spike 15	0.05	0.049	98.0	70-130
BLK Spike 16	0.05	0.040	79.9	70-130
BLK Spike 17	0.05	0.043	85.9	70-130
BLK Spike 18	0.05	0.051	101.7	70-130
BLK Spike 19	0.05	0.044	88.8	70-130
BLK Spike 20	0.05	0.044	88.4	70-130

Table E.6-9: Sample spike data from the MMHg analysis of the spring 2013 sample set.

Sample	Spike (ng/L)	MMHg (ng/L)	Spike Recovery (%)	Rec. Criteria (%)
HLG01	0.05	0.039	83.7	65-135
MXH01	0.05	0.081	144.7	65-135
YZG01	0.05	0.041	89.9	65-135
YZG12	0.05	0.057	114.6	65-135

Table E.6-10: Blank spike data from the MMHg analysis of the spring 2013 sample set.

Sample	Spike (ng/L)	MMHg (ng/L)	Spike Recovery (%)	Rec. Criteria (%)
BLK Spike 1	0.05	0.046	92.7	70-130
BLK Spike 2	0.05	0.038	75.4	70-130
BLK Spike 3	0.05	0.043	87.0	70-130
BLK Spike 4	0.05	0.038	76.6	70-130
BLK Spike 5	0.05	0.038	75.6	70-130
BLK Spike 6	0.05	0.040	80.2	70-130
BLK Spike 7	0.05	0.045	89.0	70-130
BLK Spike 8	0.05	0.040	79.1	70-130
BLK Spike 9	0.05	0.045	90.4	70-130

E.7 Reference material

Table E.7-1: CRM-CCV data for the analysis of the sediment samples from the fall 2012 sample set.

Sample	Weight (g)	THg (ng)	THg (µg/kg)	QC Criteria (µg/kg)
CRM1	0.1080	9.32	86.3	82-100
CRM2	0.0193	1.90	98.2	82-100
CRM3	0.0987	8.95	90.7	82-100
CRM4	0.1094	9.84	90.0	82-100

Table E.7-2: CRM-CCV data for the analysis of the sediment samples from the spring 2013 sample set.

Sample	Weight (g)	THg (ng)	THg (µg/kg)	QC Criteria (µg/kg)
CRM1	0.1271	10.76	84.7	82-100
CRM2	0.0844	7.29	86.4	82-100
CRM3	0.0855	7.68	89.7	82-100
CRM4	0.0402	3.88	96.4	82-100
CRM5	0.0411	3.37	82.0	82-100
CRM6	0.0852	7.87	92.4	82-100
CRM7	0.0670	5.69	84.9	82-100
CRM8	0.0567	4.56	80.5	82-100
CRM9	0.1063	9.13	86.0	82-100
CRM10	0.1003	8.26	82.3	82-100

The water content of the MESS-3 was determined by measuring out three parallels of the CRM with 0.1 mg precision into small aluminum cups and drying them at 105 °C for 3 hrs. The dry weight was determined and the water content calculated. Results are shown in table E.7-3. The CRM-CCVs were adjusted for the water content and are shown in table E.7-4.

Table E.7-3: Water content (%) of the MESS-3 CRM based on three parallels.

Sample ID	Before	After	Water content (%)
	Weight (g)	Weight (g)	
1	0.6460	0.6343	1.8
2	0.3312	0.3246	2.0
3	0.5868	0.5764	1.8
Mean			**1.9**

Table E.7-4: CRM-CCV data for the analysis of the sediment samples from the spring 2013 sample set with the weights adjusted for water content.

Sample	Adjusted weight (g)	THg (ng)	THg (µg/kg)	QC Criteria (µg/kg)
CRM1	0.1245	10.76	86.4	82-100
CRM2	0.0827	7.29	88.2	82-100
CRM3	0.0838	7.68	91.6	82-100
CRM4	0.0394	3.88	98.4	82-100
CRM5	0.0403	3.37	83.7	82-100
CRM6	0.0834	7.87	94.3	82-100
CRM7	0.0657	5.69	86.6	82-100
CRM8	0.0555	4.56	82.1	82-100
CRM9	0.1041	9.13	87.7	82-100
CRM10	0.0983	8.26	84.0	82-100

Appendix F – Mathematical concepts of statistical methods

Emperical means, standard deviations, relative standard deviations and relative percent differences were calculated using Microsoft Excel (2010), while t-tests, paired t-tests, wilcoxon-tests and linear regression analysis was done using R (2.15.2). Principal component analysis was done using Minitab (16). Here the basic mathematical concepts of these statistical methods are presented.

The empirical mean or sample mean, $\bar{x}$, of a set of data points is defined as the sum of all data points, $x_1 + x_2 + \ldots + x_n$, divided by the number of data points, n, as defined by equation F-1 (Johnson & Bhattacharyya, 2001).

$$\bar{x} = \frac{1}{n}\sum_{i=1}^{n} x_i \qquad \text{F-1}$$

There are several ways to describe the spread in a data set. The standard deviation, s, describes how much the data points, x_1, x_2, …., x_n, deviate from the mean, $\bar{x}$, and is defined by equation F-2. The relative standard deviation, RSD(%), is the standard deviation, s, defined as a fraction of the mean, $\bar{x}$, as shown in equation F-3. The relative percent difference, RPD(%), between two data points, x_1 and x_2, is defined as the absolute difference between the two points divided by their mean, as shown in equation F-4 (Johnson & Bhattacharyya, 2001).

$$s = \sqrt{\frac{1}{n-1}\sum_{i=1}^{n}(x_i - \bar{x})^2} \qquad \text{F-2}$$

$$RSD(\%) = \frac{s}{\bar{x}} \times 100 \qquad \text{F-3}$$

$$RPD(\%) = \frac{|x_1 - x_2|}{\frac{x_1 + x_2}{2}} \times 100 \qquad \text{F-4}$$

The linear relation between two parameters, x and y, is described by the Pearson correlation coefficient, r. For n observation pairs, (x_1,y_1), (x_2,y_2), … , (x_n,y_n), with standard deviations s(x) and s(y) and means $\bar{x}$ and $\bar{y}$, r is defined by equation F-5. The strength of the x-y correlation is thence described by the absolute value of r for which r=1 means a perfect correlation. The squared value of r, R^2, tells how much of the variation that can be explained by a linear relation. Hence a r value of 0.8 gives an R^2 value of 0.64 and signifies that 64% of

the variation can be explained by a linear relation (Vittinghoff, Shiboski, Glidden, & McCulloch, 2005).

$$r(x,y) = \frac{Cov(x,y)}{s(x)s(y)} = \frac{\sum_{i=1}^{n}(x_i - \bar{x})(y_i - \bar{y})/(n-1)}{\sqrt{\sum_{i=1}^{n}(x_i - \bar{x})^2/(n-1)}\sqrt{\sum_{i=1}^{n}(y_i - \bar{y})^2/(n-1)}} \quad \text{F-5}$$

To test if the correlation is significant and not just a coincidence a t-test is performed, based on the Student t-distribution and the calculation of the test statistic, t, in equation F-6. Here β is the slope of the linear regression line (equation F-7) and s(β) the standard error of the estimated slope, computed for the data set in question by the R-software. The test-statistic, t, is t-distributed with n-2 degrees of freedom and used here with a confidence level of $p<0.05$ (Vittinghoff et al., 2005).

$$t = \frac{\beta}{s(\beta)} \quad \text{F-6}$$

$$y = \alpha + \beta x \quad \text{F-7}$$

The test-statistic T (equation F-8), is employed to find whether or not the difference between the normally distributed populations x and y, with means $\bar{x}$ and $\bar{y}$ and standard deviation s_x and s_y is significant. A paired t-test is employed to test the significance of differences between two measurements, x and y, for i data points by computing the test-statistic T_p (equation F-9), where d_i is the difference $x_i - y_i$ and $\bar{d}$ the difference mean. To test for significant differences between two non-normally distributed populations, n_A and n_B, the Z test-statistic is computed (equation F.10), where W_A is the rank sum of n_A which is approximately normally distributed for large populations (Johnson & Bhattacharyya, 2001). All test statistics are computed by the R-software which uses a normal table to produce a p-value for the test. A confidence level of $p<0.05$ is used.

$$T = \frac{\bar{x} - \bar{y}}{\sqrt{\frac{s_x^2}{n_x} + \frac{s_y^2}{n_y}}} \quad \text{F-8}$$

$$T_p = \frac{\bar{d}}{\sqrt{(\sum_{i=1}^{n}(d_i - \bar{d})^2)\frac{1}{n}}/\sqrt{n}} \quad \text{F-9}$$

$$Z = \frac{W_A - n_A(n_A + n_B + 1)/2}{\sqrt{n_A n_B(n_A + n_B + 1)/12}} \quad \text{F.10}$$

To explore trends in a data set with multiple variables a principle component analysis (PCA) is used. The PCA approximates a set of new variables from a given n x p dimensional data matrix with n objects (sampling points) and p variables (analytical parameters). The approximated, new variables or principal components (PCs) are specifically independent of each other and explain each their part of the total variation in in the data set. The first PC explains the largest part of the variation, the second PC the second largest part of the variation and the following PCs successively smaller parts of the variation. Usually most of the variation is accounted for by the few first PCs and thus only these need be considered. Each PC has loading values for the p variables included in the analysis. A high loading value ($> \pm 0.20$) signifies that a variable contributes to the variation within a PC. The results from a PCA are typically presented in a score plot which shows the relation between objects and PCs in addition to the correlation among objects (Esbensen, Guyot, Westad, & Houmoller, 2004).

Appendix G – Mercury concentrations in water samples

Table G-1: THg and DHg (ng/L) in water samples for all sampling points, from the sampling campaigns in fall 2012 and spring 2013. Values below LOD are shown as <0.1.

Sample	THg (ng/L)		DHg (ng/L)	
	Fall 2012	Spring 2013	Fall 2012	Spring 2013
HLG01	1.1	0.7	n/a	0.3
HLG02	1.7	0.7	n/a	0.1
HLG03	2.0	0.6	n/a	<0.1
HLG05	1.4	0.2	n/a	<0.1
HLG06	1.6	1.4	n/a	<0.1
HLG06 P	1.6	n/a	n/a	n/a
HLG07	2.7	1.7	n/a	<0.1
HLG07 P	2.0	1.5	n/a	<0.1
HLG09	2.7	1.8	n/a	<0.1
HLG09 P	2.8	n/a	n/a	n/a
HLG010	1.1	0.6	n/a	<0.1
HLG011	1.1	0.6	n/a	<0.1
YZG01	0.6	0.2	n/a	<0.1
YZG02	0.3	0.2	n/a	<0.1
YZG03	0.4	0.2	n/a	<0.1
YZG04	0.6	0.2	n/a	<0.1
YZG05	1.3	13.2	n/a	0.1
YZG06	0.6	1.4	n/a	<0.1
YZG07	0.5	1.8	n/a	<0.1
YZG08	0.6	1.3	n/a	<0.1
YZG09	1.3	19.6	n/a	0.1
YZG11	0.5	5.0	n/a	<0.1
YZG12	1.0	0.5	n/a	<0.1
YZG12 P	0.8	n/a	n/a	n/a
HLG04T	0.5	0.8	n/a	0.2
HLG08T	0.2	0.4	n/a	<0.1
HLG012T	0.2	0.3	n/a	<0.1
HLG013T	1.0	0.4	n/a	<0.1
HLG014T	0.5	1.6	n/a	0.1
DDH-T	n/a	0.1	n/a	<0.1
YZG10T	0.5	1.1	n/a	0.2
YZG10G	n/a	0.4	n/a	<0.1
MXH01	n/a	0.8	n/a	<0.1
MXH02	n/a	0.7	n/a	<0.1
MXH03	0.9	0.5	n/a	<0.1
DDH-U	7.4	18.7	n/a	1.1
DDH-D	n/a	16.7	n/a	0.9
CHZ	2.9	3.0	n/a	1.2

Table G-2: Mean THg concentrations (ng/L) in water samples with one standard deviation for the different stream systems.

System	Mean THg (ng/L)	
	Fall 2012	**Spring 2013**
GF	1.3 ± 0.8	2.5 ± 4.8
NGF	0.5 ± 0.3	0.7 ± 0.5
HLG GF	1.8 ± 0.6	1.0 ± 0.6
YZG GF	0.7 ± 0.3	4.0 ± 6.5

Table G-3: Fractionation results; THg (ng/L), DHg (ng/L) and PHg (ng/L) for the samples in the spring 2013 sample set which had detectable concentrations of DHg.

Sample	THg (ng/L)	DHg (ng/L)	PHg (ng/L)
HLG01	0.7	0.3	0.4
HLG02	0.7	0.1	0.6
YZG05	13.2	0.1	13.1
YZG09	19.3	0.1	19.2
HLG04T	0.8	0.2	0.6
HLG14T	1.6	0.1	1.5
YZG10T	1.1	0.2	0.9
DDH-U	18.7	1.1	17.6
DDH-D	16.7	0.9	15.8
CHZ	3.0	1.2	1.8

Table G-2: MMHg concentrations (ng/L) for all sampling points in the study area, from the sampling campaigns in fall 2012 and spring 2013. Values below LOD are shown as <0.02 and "-" signifies parameter not determined in sample.

	Fall 2012		Spring 2013	
Sample	**MMHg (ng/L)**	**DMMHg (ng/L)**	**MMHg (ng/L)**	**DMMHg (ng/L)**
HLG01	<0.02	<0.02	<0.02	n/a
HLG02	<0.02	<0.02	<0.02	n/a
HLG03	n/a	n/a	0.03	n/a
HLG05	<0.02	<0.02	<0.02	n/a
HLG06	<0.02	<0.02	<0.02	n/a
HLG06 P	<0.02	<0.02	n/a	n/a
HGL07	<0.02	<0.02	<0.02	n/a
HGL07 P	0.03	n/a	<0.02	n/a
HGL09	<0.02	<0.02	<0.02	n/a
HGL09 P	<0.02	n/a	n/a	n/a
HGL10	<0.02	0.02	<0.02	n/a
HLG11	0.03	n/a	<0.02	n/a
YZG01	<0.02	<0.02	<0.02	n/a
YZG02	<0.02	<0.02	<0.02	n/a
YZG03	<0.02	<0.02	<0.02	n/a
YZG04	<0.02	0.02	<0.02	n/a
YZG05	<0.02	<0.02	0.02	n/a
YZG06	<0.02	<0.02	<0.02	n/a
YZG07	n/a	n/a	<0.02	n/a
YZG08	<0.02	<0.02	<0.02	n/a
YZG09	0.02	n/a	0.02	n/a
YZG11	<0.02	<0.02	0.02	n/a
YZG12	0.02	n/a	<0.02	n/a
HLG04T	0.03	n/a	<0.02	n/a
HLG08T	n/a	n/a	<0.02	n/a
HLG12T	<0.02	0.03	<0.02	n/a
HLG13T	n/a	n/a	<0.02	n/a
HLG14T	<0.02	<0.02	0.02	n/a
DDH-T	n/a	n/a	<0.02	n/a
YZG10T	<0.02	<0.02	0.04	n/a
YZG10G	n/a	n/a	<0.02	n/a
MXH01	n/a	n/a	<0.02	n/a
MXH02	n/a	n/a	<0.02	n/a
MXH03	0.02	n/a	0.02	n/a
DDH-U	n/a	n/a	0.04	n/a
DDH-D	0.03	0.03	0.04	n/a
CHZ	0.56	0.54	0.14	0.08

Appendix H – TOC and TSS concentrations in water samples

Table H-1: TOC (mgC/L), DOC (mgC/L) and TSS (mg/L) concentrations for all sampling points in the study area, from the sampling campaigns in fall 2012 and spring 2013, TSS values below LOD shown as <2.00. Samples analyzed for TSS in fall 2012 were stored more than 4 hrs.

	Fall 2012		Spring 2013		
Sample	**TOC (mgC/L)**	**TSS (mg/L)**	**TOC (mgC/L)**	**DOC (mgC/L)**	**TSS (mg/L)**
HLG01	0.23	198.3	0.45	0.33	28.5
HLG02	n/a	n/a	0.37	0.37	33.6
HLG03	n/a	n/a	0.40	0.35	11.7
HLG05	0.69	374.5	0.18	0.17	<2.0
HLG06	n/a	n/a	0.70	0.28	339.7
HLG07	n/a	n/a	0.44	0.29	448.2
HLG09	0.45	378.9	0.46	0.33	431.7
HLG010	0.29	n/a	0.28	0.26	71.5
HLG011	n/a	n/a	0.27	0.25	65.7
YZG01	n/a	n/a	0.18	0.16	32.9
YZG02	n/a	n/a	0.14	0.15	3.2
YZG03	n/a	n/a	0.18	0.16	20.4
YZG04	n/a	n/a	0.20	0.16	15.0
YZG05	n/a	n/a	2.60	0.70	4833.9
YZG06	n/a	n/a	0.51	0.28	308.2
YZG07	n/a	n/a	0.61	0.28	321.5
YZG08	n/a	n/a	0.53	0.28	205.3
YZG09	n/a	n/a	3.90	0.67	2921.0
YZG11	n/a	n/a	1.50	0.46	779.4
YZG12	n/a	n/a	0.40	0.35	31.0
HLG04T	0.31	5.5	0.56	0.54	2.1
HLG08T	0.10	8.3	0.48	0.30	21.5
HLG012T	n/a	n/a	0.27	0.26	2.9
HLG013T	0.14	n/a	0.29	0.26	2.0
HLG014T	n/a	n/a	0.99	0.63	3.3
DDH-T	n/a	n/a	0.27	0.25	<2.0
YZG10T	n/a	n/a	0.81	0.68	9.0
YZG10G	n/a	n/a	0.43	0.38	<2.0
MXH01	n/a	n/a	0.54	0.51	6.4
MXH02	n/a	n/a	0.38	0.36	15.1
MXH03	n/a	n/a	0.52	0.39	15.6
DDH-U	n/a	n/a	0.67	0.55	18.5
DDH-D	1.00	n/a	0.62	0.54	29.7
CHZ	7.60	n/a	4.30	4.10	6.3

Table H-2: Mean TOC (mgC/L), DOC (mgC/L) and TSS (mg/L) concentration with one standard deviation for the different systems. Values below LOD included as LOD/2.

System	Fall 2012		Spring 2013		
	TOC (mgC/L)	**TSS (mg/L)**	**TOC (mgC/L)**	**DOC (mgC/L)**	**TSS (mg/L)**
GF	0.4 ± 0.2	317 ± 103	0.7 ± 0.9	0.3 ± 0.2	545 ± 1199
NGF	0.2 ± 0.1	7 ± 2	0.5 ± 0.3	0.4 ± 0.2	5 ± 7
HLG GF	0.4 ± 0.2	317 ± 103	0.4 ± 0.1	0.3 ± 0.1	159 ± 189
YZG GF	n/a	n/a	1.0 ± 1.2	0.3 ± 0.2	861 ± 1568
All	1.2 ± 2.4	193 ± 185	0.7 ± 1.0	0.5 ±0.7	325 ± 949

Appendix I – Linear regression plots of THg-TSS and THg-TOC in water

I.1 THg-TSS linear regression plots for water samples

Linear regression plots of Hg vs. TSS are shown for the sampling points of all GF streams (figure I.1-1), YZG (figure I.1-3) and HLG (figure I.1-5) and NGF streams (figure I.1-6). Three influential data points; YZG05, YZG09 and YZG11 affect the regression lines strongly, so regression plots are shown for all GF sampling points and the YZG system without these three in figures I.1-2 and I.1-4 respectively.

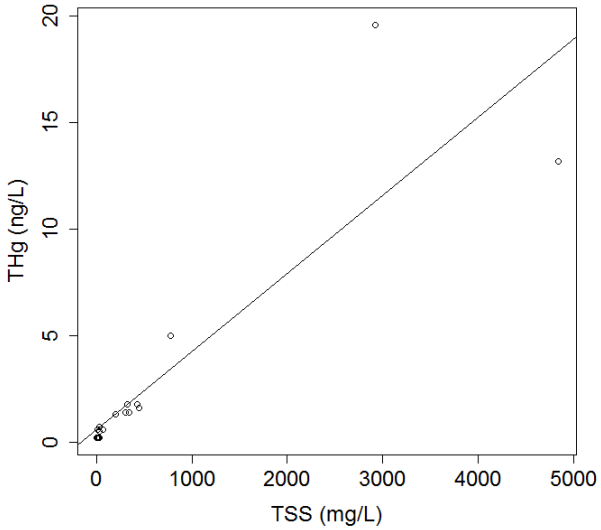

Figure I.1-1: Hg vs. TSS for GF streams (2013).
$R^2 = 0.7871$, $p<0.0001$

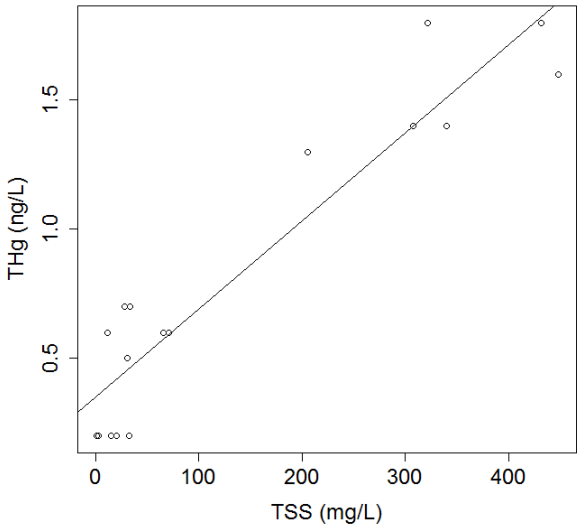

Figure I.1-2: Hg vs. TSS for GF streams (2013). Influential points removed.
$R^2 = 0.8845$, $p<0.0001$

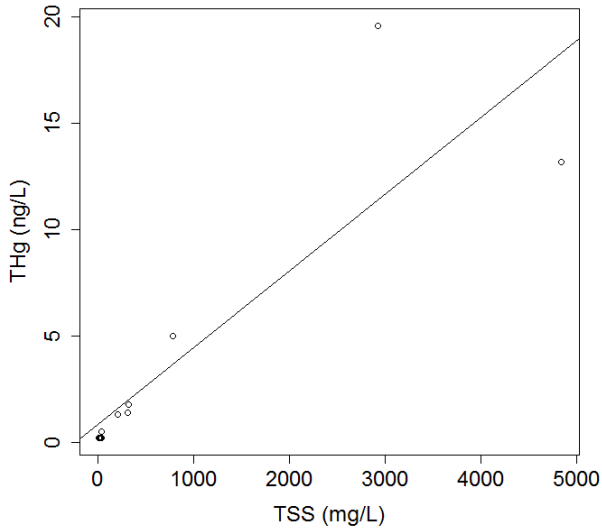

Figure I.1-3: THg vs. TSS for the GF streams in the YZG valley (2013).
R^2 = 0.7662, p<0.001

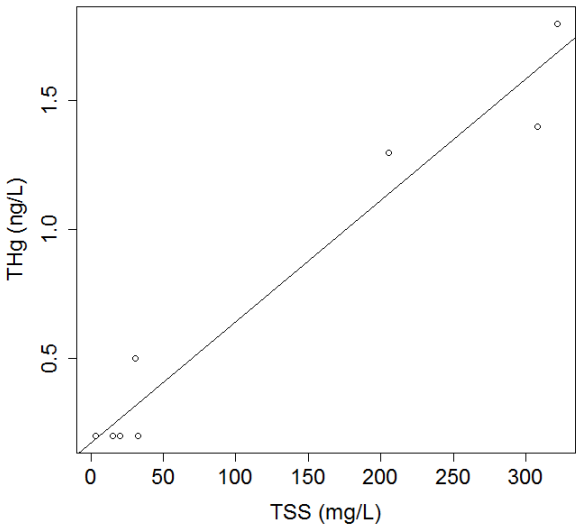

Figure I.1-4: THg vs. TSS for the GF streams in the YZG valley (2013). Influential points removed.
R^2 = 0.9533, p<0.0001

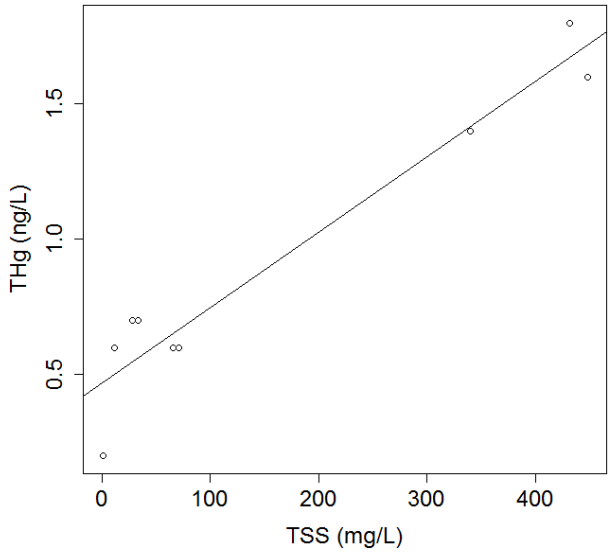

Figure I.1-5: THg vs. TSS for the GF streams in the HLG valley (2013).
R^2 = 0.9316, p<0.0001

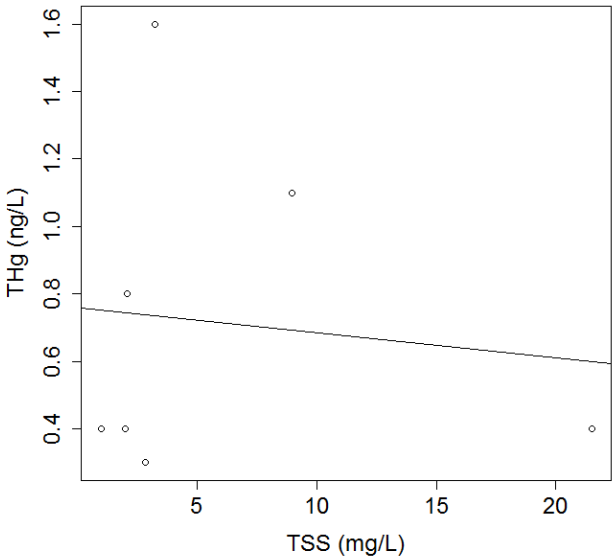

Figure I.1-6: THg vs. TSS for NGF tributary streams (2013).
R^2 = 0.0124, p=0.81

I.2 THg-TOC linear regression plots for water samples

Linear regression plots of Hg vs. TOC are shown for the sampling points of all GF streams (figure I.2-1), YZG (figure I.2-3) and HLG (figure I.2-5) and NGF streams (figure I.2-6). Three influential data points; YZG05, YZG09 and YZG11 affect the regression lines quite strongly, so regression plots are shown for all GF sampling points and the YZG system without these three in figures I.2-2 and I.2-4 respectively

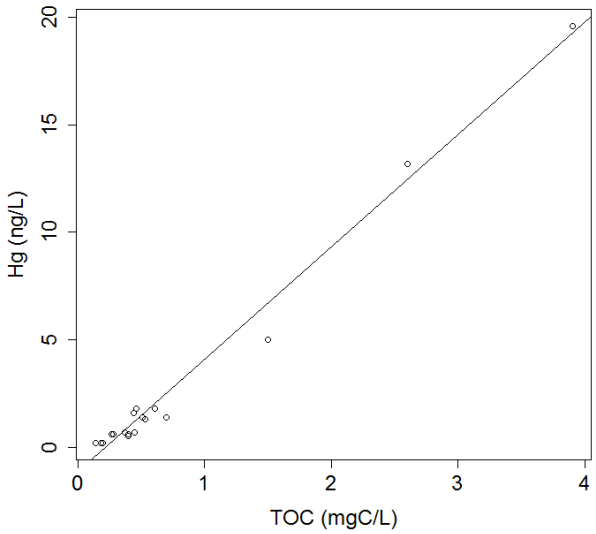

Figure I.2-1: THg vs. TOC for GF streams (2013)
$R^2 = 0.9845$, $p<0.0001$

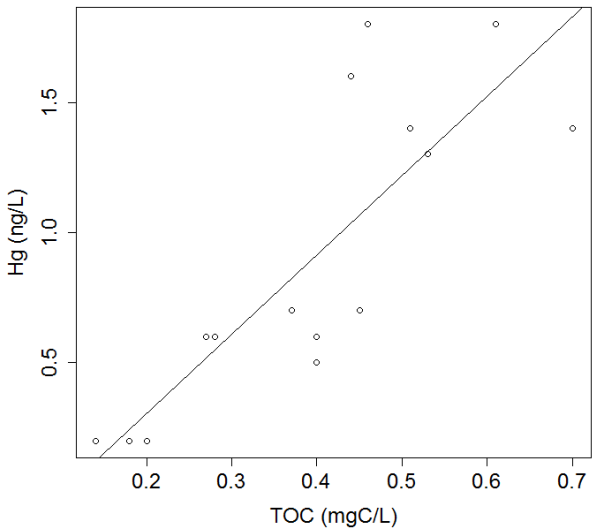

Figure I.2-2: THg vs. TOC for GF streams (2013). Influential points removed
$R^2 = 0.7281$, $p<0.0001$

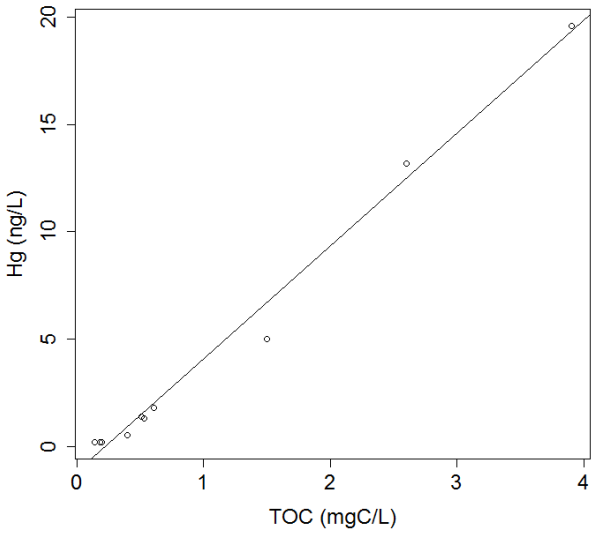

Figure I.2-3: THg vs. TOC for the glacier-fed streams in the YZG valley (2013).
R^2 = 0.9887, p<0.0001

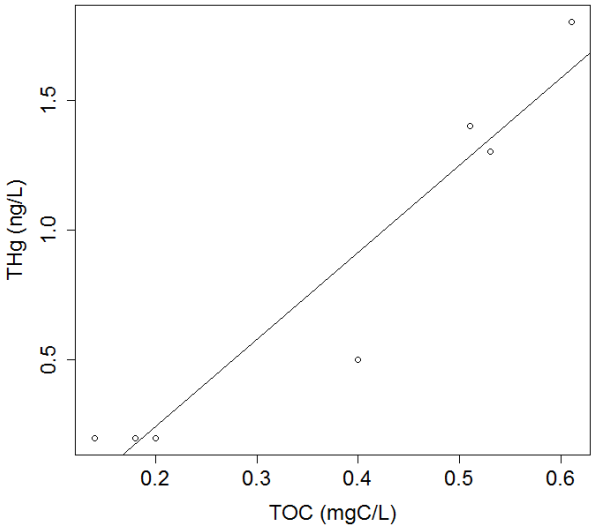

Figure I.2-4: THg vs. TOC for the glacier-fed streams in the YZG valley (2013). Influential points removed.
R^2 = 0.9197, p<0.001

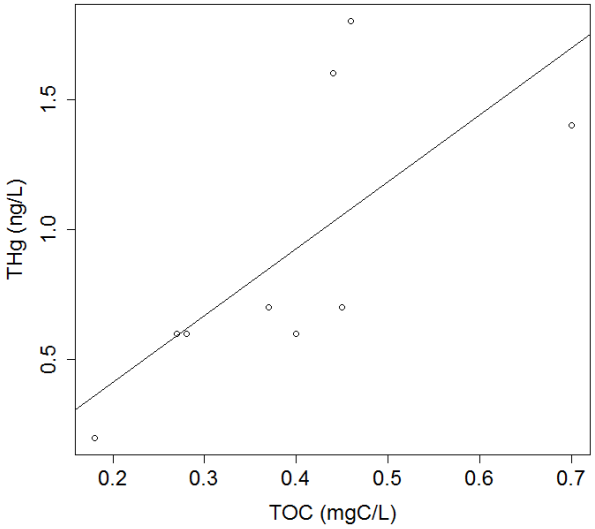

I.2-5: THg vs. TOC for the GF streams of the HLG valley (2013).
R^2= 0.4923, p<0.05

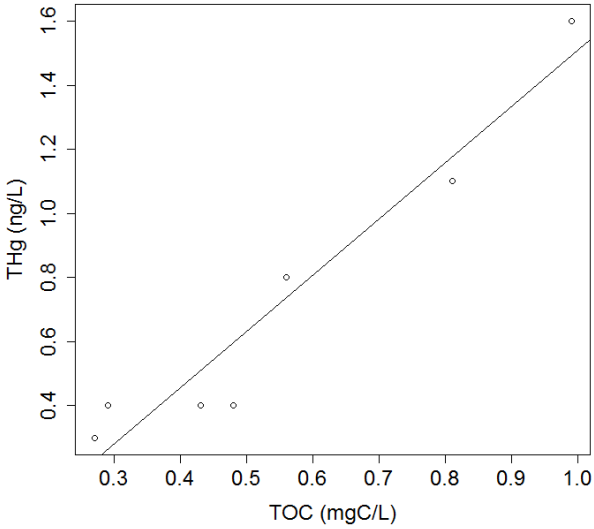

I.2-6: THg vs. TOC for the NGF tributary streams (2013).
R^2= 0.9320, p<0.001

Appendix J – THg and TOC concentrations in sediments and soil

Table J-1: Dry weight THg (µg/kg) and TOC (µg C/mg) concentrations in stream sediments and soil samples. TOC concentrations below LOD shown as <1.

Sample	THg (µg/kg)	TOC (µgC/mg)
HLG01	1.3	<1
HLG02	1.6	<1
HLG03	1.1	<1
HLG05	1.1	1.2
HLG06	1.2	<1
HLG07	1.4	<1
HLG09	1.6	<1
HLG10	0.9	<1
HLG11	0.9	<1
YZG01	0.8	1.7
YZG02	1.6	2.9
YZG03	1.6	2.7
YZG04	0.9	1.7
YZG05	1.2	<1
YZG06	1.2	1.2
YZG07	2.8	<1
YZG08	3.7	6.4
YZG09	0.5	<1
YZG11	1	<1
YZG12	0.9	<1
HLG04T	1.2	1.4
HLG08T	0.6	<1
HLG12T	1.7	1.7
HLG13T	1.1	1.1
HLG14T	0.6	<1
MXH01	0.7	<1
MXH02	1.7	<1
MXH03	1.1	<1
DDH-U	13.3	<1
DDH-D	0.8	<1
HLG07 Alluvial soil	3.6	3.3
HLG08T Soil	9.7	30.7

Table J-2: Mean concentrations of THg (µg/kg) and TOC (µgC/mg) in the surface sediments with one standard deviation for the different systems. Values below LOD included as LOD/2.

System	THg (µg/kg)	TOC (µgC/mg)
GF	1.4 ± 0.7	1.2 ± 1.4
NGF	1.0 ± 0.5	1.0 ± 0.5
HLG	1.2 ± 0.3	0.6 ± 0.2
YZG	1.5 ± 1.0	1.7 ± 1.8
All	1.7 ± 2.3	1.1 ± 1.2

Table J-3: Dry weight THg (µg/kg) and TOC (µg C/mg) concentrations in a 15 cm profile from the stream bank sediment at HLG09.

Depth (cm)	THg (µg/kg)	TOC (µgC/mg)
0-3	1.6	<1
3-6	1.3	<1
6-9.5	1.0	<1
9.5-11	1.1	<1
11-15	1.1	<1

Table J-4: Dry weight THg (µg/kg) and TOC (µg C/mg) concentrations in a 25 cm profile from the stream bank sediment at HLG13T.

Depth (cm)	THg (µg/kg)	TOC (µgC/mg)
0-5	1.1	1.1
5-10	1.5	<1
10-15	1.6	<1
15-20	2.1	1
20-25	3.7	1.8

Table J-5: Dry weight THg (µg/kg) and TOC (µg C/mg) in a 20 cm core profile from the CHZ peat bog. Mean THg and TOC included with one standard deviation.

Depth (cm)	**THg (µg/kg)**	**TOC (µg C/mg)**
0-1	188.7	361
1-2	186.7	381
2-3	193.7	370
3-4	203.8	354
4-5	202.3	380
5-6	176.9	351
6-7	177.1	339
7-8	216.1	360
8-9	231.8	382
9-10	228.4	358
10-11	215.2	339
11-12	178.2	310
12-13	175.5	316
13-14	177.8	327
14-15	145.9	274
15-16	123.5	256
16-17	142.2	241
17-18	132.2	227
18-19	158.4	245
19-20	133.0	189
Mean	**179 ± 32**	**318 ± 59**

Appendix K – Linear regression plots of THg-TOC in sediments and soil

K.1 THg-TOC linear regression plots for sediment- and sediment profile samples

Linear regression plots of Hg vs. TOC are shown for sediment samples from GF streams (figure K.1-1) and sediment samples from NGF streams (figure K.1-2) below.

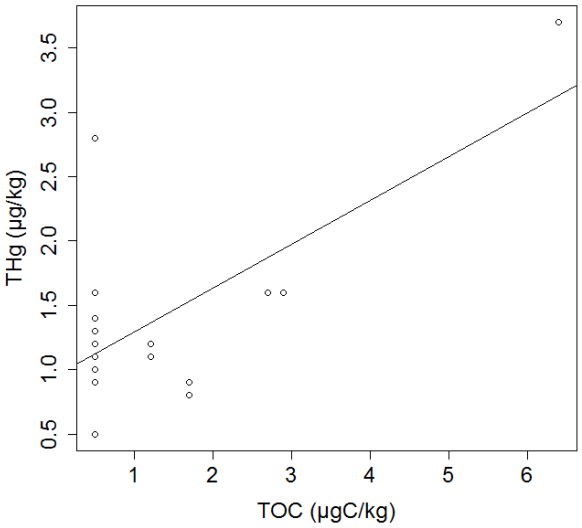

Figure K.1-1: THg vs. TOC for the GF sediment samples.

R^2 = 0.4533, p<0.01.

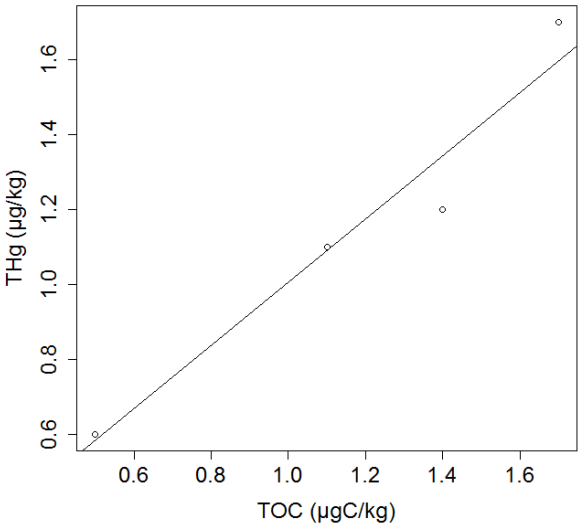

Figure K.1-2: THg vs. TOC for the NGF sediment samples.

R^2 = 0.9626, p<0.01.

Linear regression plot of Hg vs. TOC for the sediment profile at HLG13T is shown in figure K.1-4.,while such a plot was not created for the sediment profile from HLG09 since the TOC concentrations were all below detection limit (appendix J, table J-2).

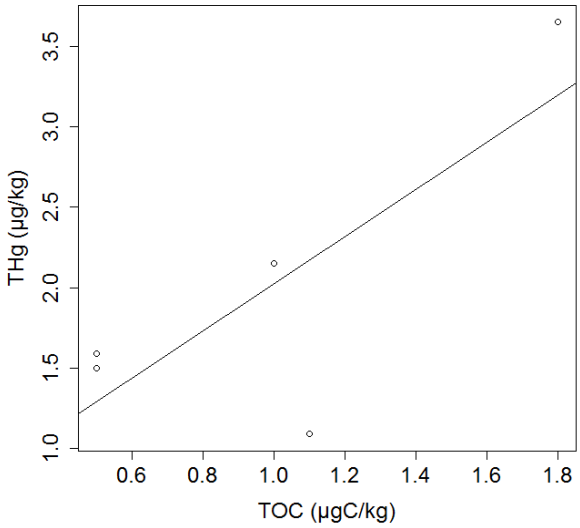

Figure K.1-3: THg vs. TOC for the NGF sediment profile at HLG13T.

R^2 = 0.6186, p = 0.12.

K.2 THg-TOC linear regression plots for the peat bog profile

Linear regression plots of Hg vs. TOC are shown for the peat bog profile in figure K.2-1

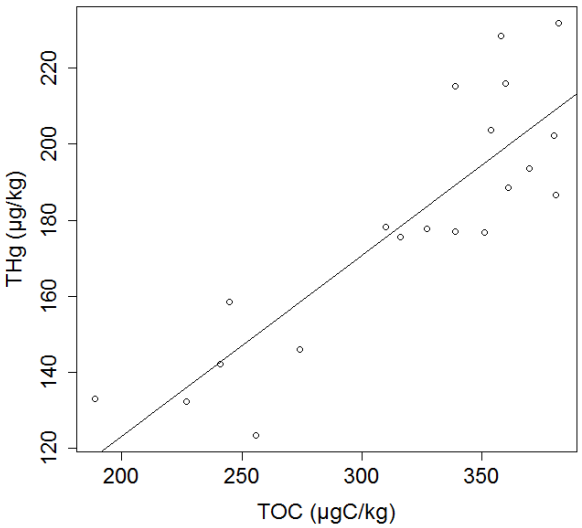

Figure K.2-1: THg vs. TOC for the peat bog profile.

R^2=0.7471, p<0.0001.

Appendix L – Test statistics for statistical hypothesis tests

Table L-1: Wilcoxon-tests of differences between water THg concentrations in different systems within the two data sets, showing the Z test-statistics and p values.

	Fall 2012		Spring 2013	
Systems tested	**Z**	**p**	**Z**	**p**
HLG-GF – NGF	72.0	0.0008	47.0	0.26
YZG-GF – NGF	53.5	0.11	48.0	0.41
HLG-GF – YZG-GF	138.0	0.0002	55.0	1.00
GF – NGF	125.5	0.006	95.0	0.26
YZG-US – YZG-DS	n/a	n/a	0.00	0.02

Table L-2: Paired t-tests of seaonal differences in water THg concentrations between different systems, showing the t-test statistics, p-values and degrees of freedom (df). "w/corr" refers to a correction of removing 6 influential data points.

System tested	**T_p**	**p**	**df**
GF2012 – GF2013	1.3	0.209	19
GF2012 – GF2013 w/corr.	5.6	<0.001	13
NGF2012 – NGF2013	1.23	0.273	5
All pts. 2012 – All pts. 2013	1.37	0.182	25

Table L-3: Paired t-tests of seasonal differences between MMHg concentrations in sampling points with concentrations above LOD in both data sets, showing the t-test statistics, p-values and degrees of freedom (df).

System tested	**T_p**	**p**	**df**
2012 - 2013	-1	0.423	2

Table L-4: Wilcoxxon tests of differences in water TSS concentrations between GF and NGF streams in the two sample sets, showing the Z test-statistics and p values.

System tested	**Z**	**p**
GF – NGF (2013)	147.0	0.0007
GF – NGF (2012)	6.0	0.20

Table L-5: Wilcoxon-tests of differences between sediment THg concentrations in different systems within the two data sets, showing the Z test-statistics and p values.

System tested	**Z**	**p**
GF - NGF	121.5	0.19
HLG YZG	51.5	0.91

Table L-6: Paired t-tests of sediment THg and TOC concentrations between a GF and a NGF sediment profile, showing the t-test statistics, p-values and degrees of freedom (df).

System tested	**T_p**	**p**	**df**
GF-THg – NGF-TOC	1.53	0.204	4
GF-TOC – NGF-TOC	2	0.116	4

Appendix M – Concentrations of supporting parameters

Table N-1: Supporting parameters for the fall 2012 data set.

Sample	Al (mg/l)	Be (µg/l)	Cd (µg/l)	Co (µg/l)	Mn (µg/l)	Mo (µg/l)	Ni (µg/l)	Pb (µg/l)	Ti (mg/l)	V (mg/l)	Zn (µg/l)
HLG01	3.6700	0.18	0.031	2.640	87.60	2.80	5.10	2.730	0.3710	0.016	21.2
HLG02	3.8000	0.15	0.036	2.880	95.10	2.70	5.45	3.200	0.3920	0.018	21.5
HLG05	7.6400	0.28	0.044	5.730	205.00	0.90	7.46	7.350	0.6400	0.039	36.7
HLG06	5.4000	0.18	0.045	4.460	153.00	0.48	7.44	5.180	0.3020	0.026	28
HLG06-P	6.7000	0.21	0.054	5.160	166.00	3.44	9.02	5.250	0.7440	0.034	37.2
HLG07	7.9900	0.27	0.068	5.720	196.00	3.75	10.80	5.960	0.8460	0.038	41.6
HLG09	9.5600	0.29	0.083	7.540	255.00	0.96	13.90	7.820	0.9560	0.051	54.6
HLG09-P	7.7600	0.20	0.062	6.190	220.00	0.63	11.00	6.520	0.5230	0.039	39.3
HLG10	4.3400	0.14	0.027	3.370	110.00	2.50	5.84	3.190	0.4080	0.020	21.7
HLG11	3.7500	0.14	0.037	2.910	99.30	1.50	5.14	3.260	0.2270	0.017	20.2
YZG01	2.1800	0.10	0.120	1.580	100.00	1.30	3.22	6.530	0.1600	0.008	21.4
YZG02	0.4910	0.03	0.072	0.225	19.60	0.85	0.52	1.930	0.0847	0.001	7.64
YZG03	1.5500	0.11	0.088	0.976	60.30	1.50	2.00	4.130	0.1010	0.004	11.9
YZG04	1.9000	0.12	0.088	1.030	64.10	2.10	2.09	4.240	0.1210	0.005	17
YZG05	1.9500	0.12	0.073	0.790	59.80	7.05	1.10	3.390	0.1420	0.004	19.1
YZG06	1.9800	0.12	0.081	1.190	65.50	3.73	2.10	3.720	0.1540	0.006	17.4
YZG08	2.0800	0.11	0.067	1.090	57.00	4.00	1.90	3.320	0.1380	0.006	16.1
YZG09	1.7100	0.15	0.031	0.524	50.90	6.04	0.67	1.400	0.1870	0.004	17.8
YZG11	1.1500	0.09	0.053	0.633	45.20	4.31	1.10	1.780	0.0954	0.003	11.4
YZG12	2.2600	0.21	0.052	0.925	68.50	4.48	1.80	2.770	0.1820	0.005	19.2
YZG10T	0.1330	1.88	0.007	1.280	427.00	1.50	0.98	0.086	<0.0003	<0.001	5.5
HLG04T	0.0858	<0.01	0.010	0.076	2.01	2.00	0.39	0.048	0.0074	<0.001	0.78
HLG08T	0.1320	0.02	0.020	0.170	21.80	4.24	0.86	0.120	0.0113	<0.001	1.2
HLG12T	0.0060	0.02	0.010	0.009	0.34	2.00	<0.05	0.010	0.0003	<0.001	0.43

HLG13T	0.0912	0.01	0.009	0.088	2.78	1.10	0.30	0.074	0.0088	<0.001	2.26
HLG14T	0.1010	0.05	0.007	0.130	3.75	1.10	0.88	0.043	0.0094	<0.001	1.4
MXH-03	2.4100	0.12	0.046	1.530	67.90	2.40	2.98	2.250	0.2010	0.009	15.5
DDH-D	0.7740	0.06	0.033	0.703	40.80	0.48	1.70	2.760	0.0278	0.002	8.99
CHZ	0.0133	<0.01	0.020	0.041	9.24	0.10	0.10	0.256	<0.0003	<0.001	1.4

Table N-2: Supporting parameters for the spring 2013 data set.

Sample	Al (mg/L)	Be (µg/L)	Cd (µg/L)	Co (µg/L)	Mn (µg/L)	Mo (µg/L)	Ni (µg/L)	Pb (µg/L)	Ti (mg/L)	U (µg/L)	V (mg/L)	Zn (µg/L)	NO_3^--N (µgN/L)	SO_4^{2-} (mg/L)	Cl^- (mg/L)	pH
HLG01	0.891	0.06	0.059	0.660	24.2	3.86	1.60	0.601	0.0797	3.66	0.0039	4.14	140	33.3	1.30	8.14
HLG02	1.050	0.05	0.010	0.803	27.9	4.35	2.01	0.707	0.0969	3.93	0.0046	4.39	140	32.7	1.39	8.09
HLG03	0.631	0.04	0.020	0.522	19.0	3.59	1.30	0.483	0.0580	3.40	0.003	3.32	150	32.8	1.31	8.18
HLG05	0.031	<0.01	0.023	0.027	0.7	11.80	0.08	0.028	0.0016	10.60	0.001	0.82	135	32.1	0.39	7.92
HLG06	7.250	0.31	0.049	5.280	167.0	5.73	10.40	5.470	0.6540	5.52	0.029	37.90	130	33.7	0.81	8.04
HLG07	9.360	0.35	0.099	7.430	220.0	5.58	15.30	7.520	0.7790	5.45	0.0378	53.00	135	33.2	0.84	8.00
HLG09	9.210	0.23	0.069	7.010	207.0	5.12	14.70	6.500	0.8070	5.75	0.0366	48.00	130	63.0	0.81	8.03
HLG010	1.890	0.08	0.020	1.400	47.4	6.40	2.84	1.170	0.1760	5.22	0.0078	10.60	105	34.8	0.82	8.02
HLG011	1.690	0.02	0.030	1.270	43.9	6.19	2.91	1.070	0.1530	5.09	0.007	10.20	105	36.2	0.80	8.05
YZG01	0.780	0.06	0.054	0.489	32.9	5.29	1.10	1.700	0.0488	12.40	0.002	6.84	85	89.4	0.19	8.11
YZG02	0.045	<0.01	0.008	0.021	1.7	1.20	0.08	0.100	0.0020	11.40	<0.001	0.66	98	29.0	0.08	7.94
YZG03	0.316	<0.01	0.022	0.190	13.2	2.90	0.57	0.729	0.0190	11.80	<0.001	2.83	100	51.8	0.12	8.13
YZG04	0.410	0.01	0.034	0.260	16.1	4.55	0.63	0.826	0.0253	12.90	0.001	3.52	84	60.3	0.14	8.13
YZG05	45.300	2.40	0.970	56.100	2120.0	<1	65.10	113.000	0.5520	40.80	0.155	359.00	155	12.3	0.08	8.38
YZG06	7.690	0.34	0.090	6.480	252.0	5.50	9.10	10.800	0.6960	17.10	0.029	55.00	100	49.1	0.14	8.11
YZG07	8.290	0.45	0.060	7.120	271.0	5.50	9.60	11.700	0.7320	17.10	0.03	59.10	100	47.8	0.14	8.10
YZG08	5.990	<0.01	0.060	4.950	189.0	5.30	7.10	8.410	0.5300	15.20	0.021	40.70	130	43.2	0.16	8.12
YZG09	26.100	3.37	0.650	17.000	1530.0	<1	30.00	67.200	0.9350	63.00	0.0527	466.00	175	7.5	0.44	7.79

YZG11	9.060	0.91	0.170	4.260	482.0	2.10	6.21	18.300	0.5630	26.80	0.019	136.00	150	26.1	2.51	8.18
YZG12	0.478	0.09	0.030	0.254	29.0	6.81	0.39	0.629	0.0474	18.80	0.001	5.60	180	28.4	2.39	8.41
YZG10	0.394	0.16	0.025	0.130	25.6	3.20	0.39	0.441	0.0143	1.79	<0.001	7.84	300	14.4	0.66	7.48
YZG10G	0.229	1.27	0.010	2.570	774.0	0.69	1.60	0.319	<0.0003	4.44	<0.001	8.96	0.5	3.4	35.50	6.67
HLG04T	0.064	<0.01	0.010	0.088	1.9	2.20	0.48	0.080	0.0056	2.99	<0.001	0.81	210	37.1	0.11	8.13
HLG08T	0.063	<0.01	0.010	0.099	12.2	4.96	0.51	0.081	0.0045	5.92	<0.001	0.73	63	55.4	1.06	8.23
HLG012T	0.010	<0.01	0.010	0.028	0.7	2.30	0.26	0.029	0.0006	2.36	0.001	0.44	98	38.6	1.87	8.16
HLG013T	0.025	<0.01	0.009	0.028	0.9	1.20	0.20	0.032	0.0019	3.40	<0.001	0.68	185	65.5	0.70	8.07
HLG014T	0.050	0.09	0.010	0.078	6.6	0.88	1.20	0.058	0.0038	2.13	<0.001	1.30	235	38.3	6.99	8.27
DDH-T	0.008	<0.01	<0.005	0.006	0.2	0.65	<0.05	0.033	<0.0003	0.89	<0.001	0.70	465	4.6	0.35	7.75
MXH01	0.140	<0.01	0.020	0.095	7.4	3.28	0.34	0.285	0.0116	5.92	<0.001	1.30	420	10.1	1.46	8.12
MXH02	0.350	0.04	0.020	0.222	14.8	5.35	0.61	0.378	0.0297	12.90	0.002	2.57	235	29.4	1.76	8.25
MXH03	0.401	0.02	0.023	0.271	16.6	5.11	0.90	0.499	0.0343	14.10	0.001	2.93	225	31.0	1.73	8.32
DDH-U	0.289	0.02	0.010	0.356	21.0	1.00	0.74	2.620	0.0112	1.88	<0.001	3.80	325	21.9	1.69	8.47
DDH-D	0.339	<0.01	0.010	0.385	22.6	1.00	0.77	2.200	0.0137	2.18	0.001	3.71	330	22.2	1.70	8.41
CHZ	0.034	<0.01	0.045	0.072	23.5	0.46	0.24	0.586	0.0012	0.05	<0.001	4.88	115	6.5	0.17	7.26

Appendix N – Determination of geogenic and atmospheric mercury

N.1 Empirical correlation analysis

Exploring how well THg in the water samples of the GF streams is correlated with elements that are typically atmospheric or geogenic tracers could say something about the origin of the Hg. The correlation of Hg with each the geogenic tracers; Al and Ti and the atmospheric tracers; Be, Cd, Mn, Mo, Ni, Pb, V and Zn are shown in tables N.1-1 and N.1-2 for the fall 2012 and spring 2013 data sets respectively.

Table N.1-1: Correlation parameters, R^2 and p-values, for the linear regression analysis of Hg with 11 trace metals in the GF stream water samples for the fall 2012 data set.

Hg vs.	**R^2**	**p**
Al	0.7803	<0.0001
Ti	0,7075	<0.0001
Be	0.6157	<0.0001
Cd	0.0322	0.45
Co	0.7399	<0.0001
Mn	0.7417	<0.0001
Mo	0.0189	0.56
Ni	0.7782	<0.0001
Pb	0.3593	<0.01
V	0.7431	<0.0001
Zn	0.7901	<0.0001

Table N.1-2: Correlation parameters, R^2 and p-values, for the linear regression analysis of Hg with 11 trace metals in the GF stream water samples for the fall 2013 data set.

Hg vs.	**R^2**	**p**
Al	0.7290	<0.0001
Ti	0.3032	<0.05
Be	0.9914	<0.0001
Cd	0.8185	<0.0001
Co	0.5138	<0.001
Mn	0.8528	<0.0001
Mo	0.334	<0.01
Ni	0.6204	<0.0001
Pb	0.7787	<0.0001
V	0.5011	<0.001
Zn	0.9898	<0.0001

As more variation in the correlations between Hg and the different tracers are seen in the spring 2013 data set the linear regression plots for Hg with some of the tracers are shown specifically below in figuresN.1-1-N.1.5. Studying these plots it is obvious that there are three points that greatly affect the linear regression lines and these are: YZG05, YZG09 and YZG11. By removing these three points from the data set the correlations between Hg and the tracers change drastically, as can be seen in table N.1-3. The correlation with Al and Ti strengthens while the correlation with several of the atmospheric tracers is weakened.

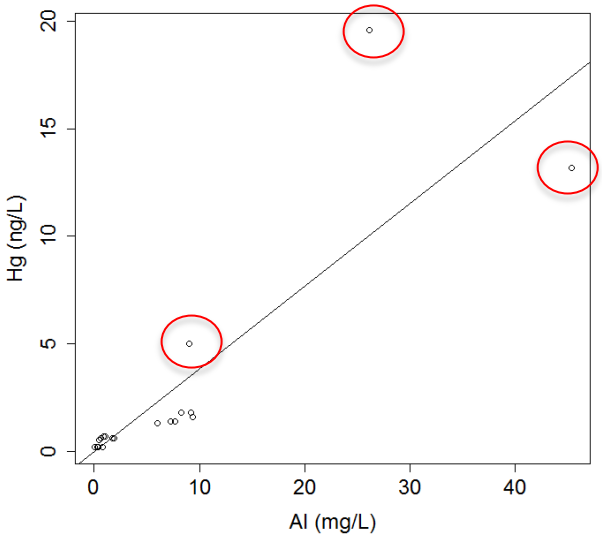

Figure N.1-1: Hg vs Al for the GF streams (2013). Influential data points encircled

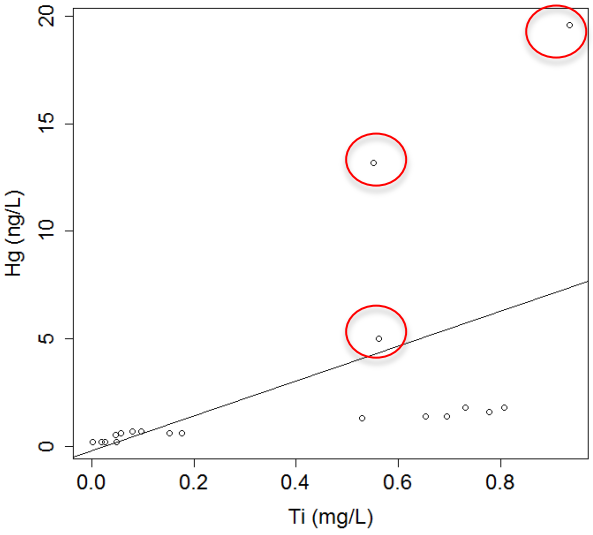

Figure N.1-2: THg vs. Ti for GF streams (2013). Influential data points encircled.

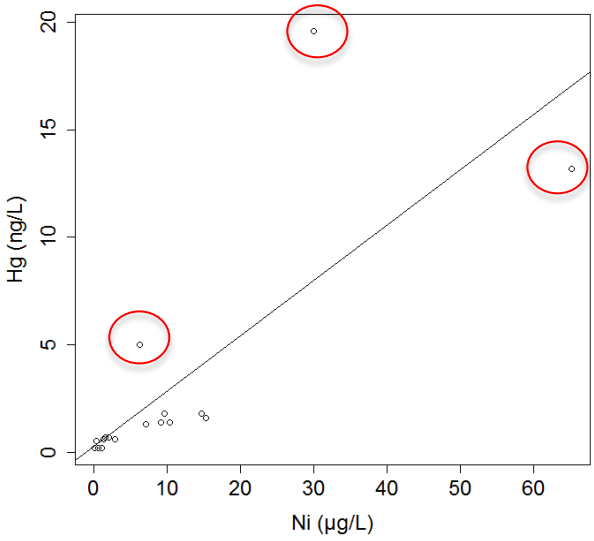

Figure N.1-4: THg vs. Ni for GF streams (2013). Influential data points encircled

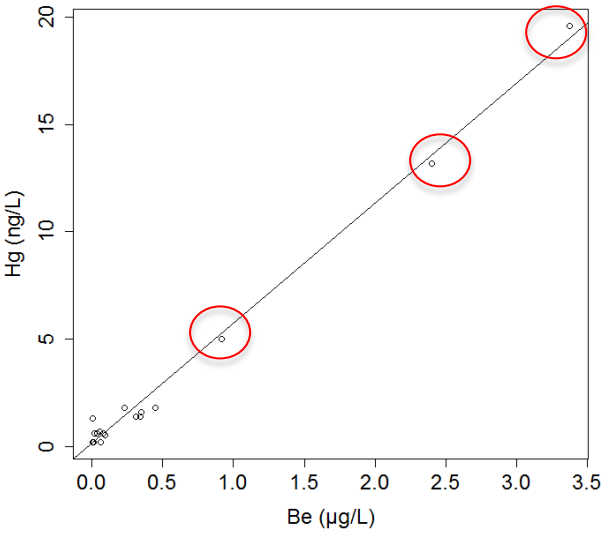

Figure N.1-3 THg vs. Be for GF streams (2013). Influential data points encircled

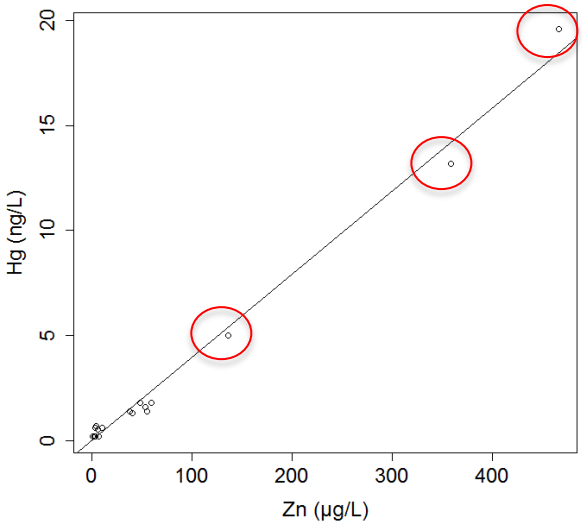

Figure N.1-5: THg vs. Zn for GF streams (2013). Influential data points encircled

Table N.1-3: Correlation parameters of Hg with 11 trace metals in the GF stream water samples for the fall 2013 data set with three influential observations removed.

Hg vs.	**R^2**	**p**
Al	0.9310	<0.0001
Ti	0.9393	<0.0001
Be	0.7039	<0.0001
Cd	0.5493	<0.001
Co	0.9325	<0.0001
Mn	0.8955	<0.0001
Mo	0.0016	0.88
Ni	0.8809	<0.0001
Pb	0.7851	<0.0001
V	0.9237	<0.0001
Zn	0.8971	<0.0001

To show whether or not the YZG side rivers possibly contain more atmospherically deposited heavy metals EF of the different atmospheric tracers were calculated using the method from section N.4 and equation N.4-1 as shown in table N.1-4. EF was not calculated for Mo since the concentration was below LOD for both sampling points (appendix M, table M-1).

Table N.1-4: Enrichment factors (EF) for atmospheric tracer elements in YZG05 and YZG09 based on each element's crustal relation with Ti.

Variable	Sample	Ti	Be	Cd	Pb	Zn	Co	Mn	Ni	V
	YZG05	552	2.40	0.97	113.0	359	56.1	2120	65.10	155.0
Water conc. (µg/L)	YZG09	935	3.37	0.65	67.2	466	17.0	1530	30.00	52.7
Crustal conc. (ppm)	-	3117	3.1	0.102	17	52	11.6	527	18.6	53
	YZG05	-	**4.4**	**53.7**	**37.5**	**39.0**	**27.3**	**22.7**	**19.8**	**16.5**
EF	YZG09	-	**3.6**	**21.2**	**13.2**	**29.9**	**4.9**	**9.7**	**5.4**	**3.3**

N.2 Principal Component Analysis

A principle component analysis (PCA) was performed on the spring 2013 data set. The fall 2012 data set was not considered for PCA since THg and trace metals were the only parameters available for the whole set.

The GF and NGF sampling points (excluding MXH01-03, DDH-U, DDH-D, YZG10G and CHZ) were chosen along with 19 analytical variables which can be seen in table N.2-1. Hg was chosen along with the geogenic and some of the atmospheric tracers used in the correlation analysis in addition to some other major variables such as TSS, DOC, TOC, pH, U, NO_3^- and SO_4^{2-}. pH is represented as the concentration of H^+ (mol/L) since the PCA can be sensitive to log scaled variables. The amount of variables which can be included is limited to be less than the amount of data points in the analysis. It must also be noted that the PCA is strongest and most effective in uncovering trends when dealing with a large sample set (Esbensen et al., 2004), which is not the case here. The full table of concentrations for all the analytical parameters used is shown in appendix M, table M-2.

The scree plot (figure N.2-1) shows the eigenvalues of all the PCs and from this it can be seen that that the first five principle components accounts for about 95% of the total variability. The first two, PC1 and PC2, explains as much as 82% of the variability, so the focus will be on these two components.

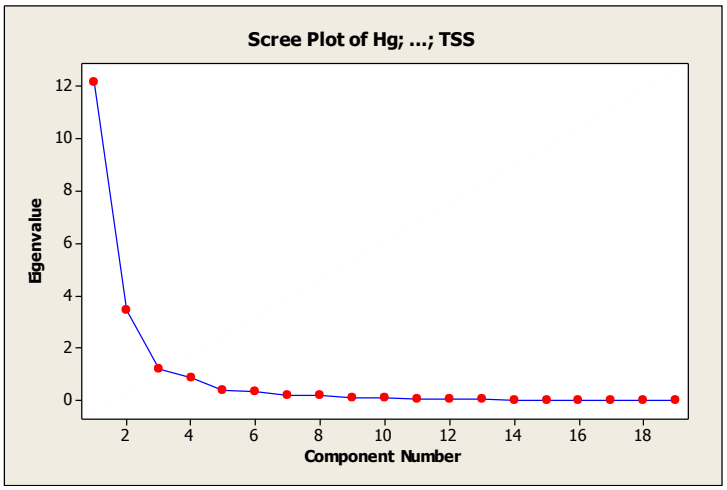

Figure N.2-1: Scree plot showing the eigenvalues of all the principle components.

N.3 Estimation of Hg_{atm} and Hg_{geo} based on linear regression models with Hg-Al and Hg-Ti.

Plotting THg vs. Al and THg vs. Ti for the GF sampling points in the fall 2012 data set and doing a simple linear regressions give fairly strong correlations; R^2=0.7803 ($p<0.0001$) and R^2=0.7075 ($p<0.0001$) respectively as shown in figures N.3-1 and N.3-2. However, according to this Al can only explain about 78% and Ti 71% of the variation in Hg. It is possible that better correlated models could have been found by removing some data points, but there is no scientific incentive for determining which points to remove.

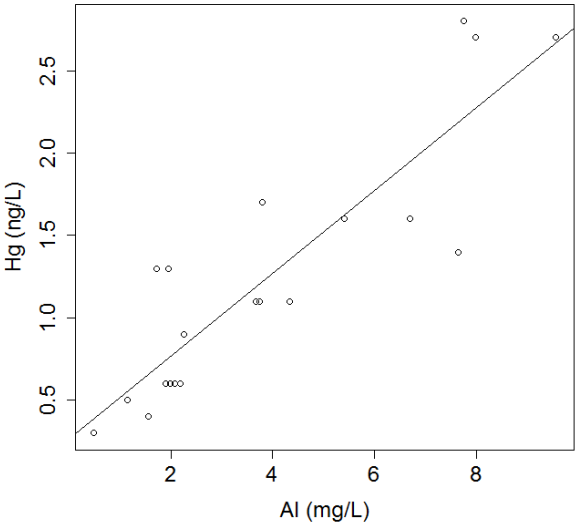

Figure N.3-1: Hg vs. Al (2012).

y = 0.25±0.03x + 0.3±0.2.

R^2 = 0.7803, $p<0.0001$

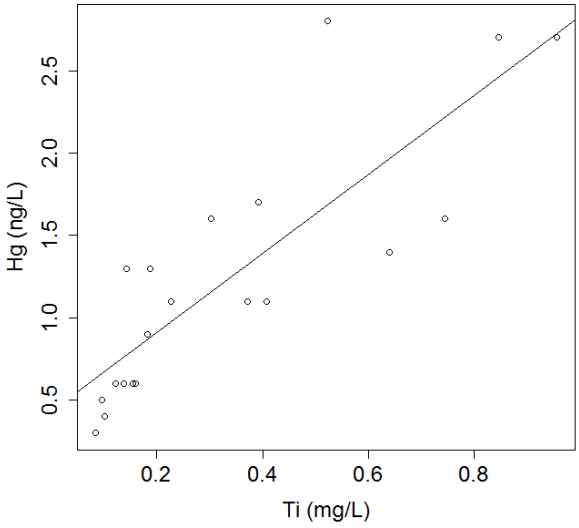

Figure N.3-2: Hg vs. Ti (2012).

y= 2.4±0.4x + 0.4±0.2

R^2 = 0.7075, $p<0.0001$

Plotting THg vs. Al and THg vs. Ti and doing a linear regression for the GF sampling points in the spring 2013 data set gives a fairly good correlation for THg-Al (R^2 = 0.7290, figure N.3-3) and a poor correlation for THg-Ti (R^2=0.3032, figure N.3-5). There are three data points with high Hg concentrations which obviously affect the regression line greatly (encircled in red in figures N.3.3 and N.3-5). These three points are YZG05, YZG09 and YZG11; the two GF side rivers in the YZG valley and the first sampling point in the main river below the second side river. If these three points are removed and a new linear regression is done, the correlation improves greatly for both THg-Al (R^2 = 0.9310) and THg-Ti (R^2=0.9393) as can be seen in figures N.3-4 and N.3-6 respectively.

With such strong correlations for both Al and Ti it can be assumed that the Hg in these samples are mainly Hg_{geo} and the regression line equations; Hg = 0.16Al + 0.31 and Hg = 1.79Ti + 0.31, can be used as models to predict Hg_{geo} in the remaining samples. Inserting values for Al and Ti for the remaining sampling points gives the Hg_{geo} values given in tables N.3-1 and N.3-2.

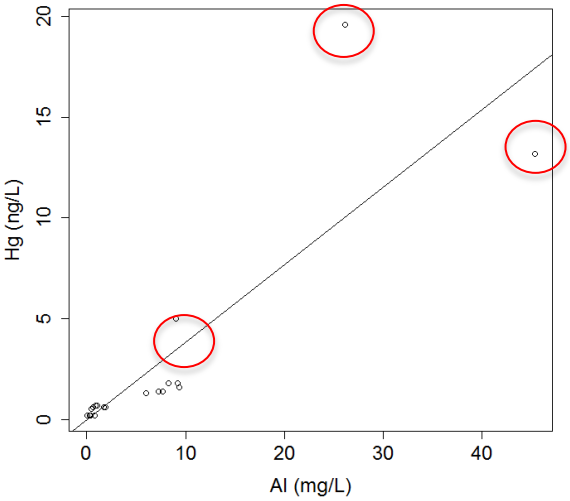

Figure N.3-3: Hg vs Al for the GF streams (2013). Influential data points encircled. y = 0.39±0.06x – 0.04±0.70, R^2 = 0.7290, p<0.0001

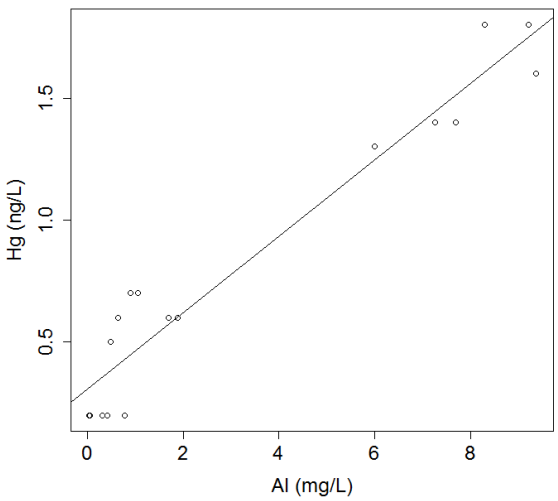

Figure N.3-4: Hg vs. Al for the GF streams (2013), with 3 data points removed. y = 0.16±0.01x + 0.31±0.05, R^2 = 0.9310, p<0.0001

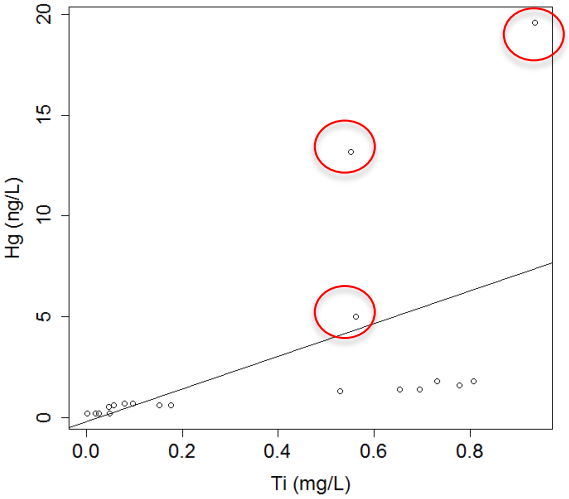

Figure N.3-5: Hg vs. Ti for GF streams (2013). Influential data points encircled. y = 8.1±2.9x – 0.2±1.4, R^2 = 0.3032, p<0.05

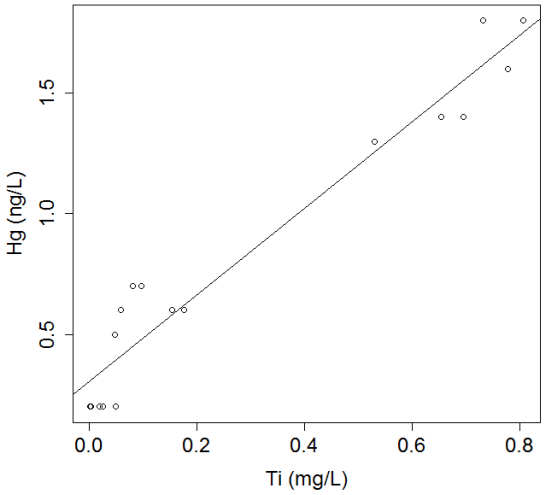

Figure N.3-6: Hg vs. Ti for GF streams (2013), with 3 data points removed. y =1.79±0.12x + 0.31±0.05, R^2 = 0.9393, p<0.0001

Table N.3.1: Estimated Hg_{geo} (ng/L) and Hg_{atm} (ng/L) in water samples from the spring 2013 data set, based on the Al-Hg linear regression model.

Sample	THg (ng/L)	Al (mg/L)	Hg geo (ng/L)	Hg atm (ng/L)	Hg atm (%)
YZG05	13.2	45.3	7.4	5.8	44.0
YZG09	19.6	26.1	4.4	15.2	77.6
YZG11	5.0	9.06	1.7	3.2	65.2
YZG10T	1.1	0.394	0.4	0.7	65.8
YZG10G	0.4	0.229	0.3	0.1	17.7
HLG04T	0.8	0.064	0.3	0.4	58.4
HLG08T	0.4	0.063	0.3	0.0	0.0
HLG012T	0.3	0.01	0.3	0.0	0.0
HLG013T	0.4	0.025	0.3	0.1	21.7
HLG014T	1.6	0.05	0.3	1.2	79.7
MXH01	0.8	0.14	0.3	0.4	57.4
MXH02	0.7	0.35	0.4	0.3	47.2
MXH03	0.5	0.401	0.4	0.1	27.6
DDH-U	18.7	0.289	0.4	18.4	98.1
DDH-D	16.7	0.339	0.4	16.3	97.8
CHZ	3.0	0.034	0.3	2.7	89.4

Table N.3.2: Estimated Hg_{geo} (ng/L) and Hg_{atm} (ng/L) in water samples from the spring 2013 data set, based on the Ti-Hg linear regression model. Samples with concentrations below LOD shown as LOD/2*.

Sample	THg (ng/L)	Ti (mg/L)	Hg geo (ng/L)	Hg atm (ng/L)	Hg atm (%)
YZG05	13.2	0.552	1.3	11.9	90.2
YZG09	19.6	0.935	2.0	17.6	89.9
YZG11	5.0	0.563	1.3	3.6	73.5
YZG10	1.1	0.0143	0.3	0.7	69.2
YZG10G	0.4	0.00015*	0.3	0.1	26.4
HLG04T	0.8	0.0056	0.3	0.4	58.5
HLG08T	0.4	0.0045	0.3	0.0	0.0
HLG012T	0.3	0.0006	0.3	0.0	0.0
HLG013T	0.4	0.0019	0.3	0.1	22.1
HLG014T	1.6	0.0038	0.3	1.2	79.9
DDH-T	0.1	0.00015*	0.3	0.0	0.0
MXH01	0.8	0.0116	0.3	0.4	57.7
MXH02	0.7	0.0297	0.4	0.3	47.5
MXH03	0.5	0.0343	0.4	0.1	28.0
DDH-U	18.7	0.0112	0.3	18.4	98.3
DDH-D	16.7	0.0137	0.3	16.4	98.0
CHZ	3.0	0.0012	0.3	2.7	89.6

N.4 Geogenic correction by Ti-Hg crustal relation

This method correcting for geogenic Hg in water samples has been adapted from Rahn (1999). The specific ratio between a trace metal, M, and a conservative geogenic element, G, in the earth's crust is used to calculate an enrichment factor (equation N.4-1) or to directly estimate the non-geogenic amount of the trace metal (equation N.4-2).

$$EF = \frac{M(water)/G(water)}{M(crust)/G(crust)} \quad \text{N.4-1}$$

$$M(atm/other) = M(water) - G(water) \times \frac{M(crust)}{G(crust)} \quad \text{N.4-2}$$

M = trace metal, G = conservative, geogenic element, (water) = concentration in water, (crust) = concentration in crust, (atm/other) = concentration of trace metal not of a geogenic origin

An enrichment-factor of less than one means that there is less geogenic Hg than the estimated natural background Hg and will yield a negative concentration for atmospheric Hg. This

should not happen if the crustal concentrations of Hg and Ti/Al are correct estimates for the area in question. Therefore EF<1 and negative Hg_{atm} concentrations will be considered as Hg_{atm} = 0. Estimated Hg_{atm} for all sampling points in both data sets (fall 2012 and spring 2013) according to the Al-Hg relation are shown in tables N.4-1 and N.4-3 while the estimates according to the Ti-Hg relation is shown in table N.4-2 and N.4-4.

Table N.4-1: Estimated Hg_{geo} (ng/L) and Hg_{atm} (ng/L) in water samples from the fall 2012 data set, based on the crustal relation between Al and Hg, showing the enrichment factor (EF) of Hg_{atm}.

Sample	**THg (ng/L)**	**Al (mg/l)**	**EF**	**Hg_{geo} (ng/L)**	**Hg_{atm} (ng/L)**	**Hg_{atm} (%)**
YZG01	0.55	2.18	0.4	0.55	0.00	0.0
YZG02	0.34	0.491	1.0	0.34	0.00	0.0
YZG03	0.41	1.55	0.4	0.41	0.00	0.0
YZG04	0.63	1.9	0.5	0.63	0.00	0.0
YZG05	1.28	1.95	0.9	1.28	0.00	0.0
YZG06	0.63	1.98	0.4	0.63	0.00	0.0
YZG08	0.61	2.08	0.4	0.61	0.00	0.0
YZG09	1.26	1.71	1.0	1.24	0.02	1.5
YZG11	0.50	1.15	0.6	0.50	0.00	0.0
YZG12	0.90	2.26	0.6	0.90	0.00	0.0
HLG01	1.13	3.67	0.4	1.13	0.00	0.0
HLG02	1.66	3.8	0.6	1.66	0.00	0.0
HLG05	1.43	7.64	0.3	1.43	0.00	0.0
HLG06	1.60	5.4	0.4	1.60	0.00	0.0
HLG06-P	1.60	6.7	0.3	1.60	0.00	0.0
HLG07	2.71	7.99	0.5	2.71	0.00	0.0
HLG09	2.68	9.56	0.4	2.68	0.00	0.0
HLG09-P	2.76	7.76	0.5	2.76	0.00	0.0
HLG10	1.14	4.34	0.4	1.14	0.00	0.0
HLG11	1.15	3.75	0.4	1.15	0.00	0.0
HLG04T	0.49	0.086	7.9	0.06	0.43	87.3
HLG08T	0.18	0.132	1.9	0.10	0.08	47.0
HLG12T	0.24	0.006	55.2	0.00	0.23	98.2
HLG13T	1.02	0.091	15.4	0.07	0.95	93.5
HLG14T	0.52	0.101	7.2	0.07	0.45	86.1
YZG10T	0.50	0.133	5.2	0.10	0.41	80.9
MXH03	0.95	2.41	0.5	0.95	0.00	0.0
DDH-D	7.35	0.774	13.1	0.56	6.79	92.4
CHZ	2.95	0.013	306.3	0.01	2.94	99.7

Table N.4-2: Estimated Hg_{geo} (ng/L) and Hg_{atm} (ng/L) in water samples from the fall 2012 data set, based on the crustal relation between Ti and Hg, showing the enrichment factor (EF) of Hg_{atm}. Samples with concentrations below LOD shown as LOD/2*.

Sample	**THg (ng/L)**	**Ti (mg/L)**	**EF**	**Hg_{atm} (ng/L)**	**Hg_{geo} (ng/L)**	**Hg_{atm} (%)**
YZG01	0.6	0.16	0.2	0.00	0.55	0.0
YZG02	0.3	0.0847	0.2	0.00	0.34	0.0
YZG03	0.4	0.101	0.2	0.00	0.41	0.0
YZG04	0.6	0.121	0.3	0.00	0.63	0.0
YZG05	1.3	0.142	0.5	0.00	1.28	0.0
YZG06	0.6	0.154	0.2	0.00	0.63	0.0
YZG08	0.6	0.138	0.2	0.00	0.61	0.0
YZG09	1.3	0.187	0.4	0.00	1.26	0.0
YZG11	0.5	0.0954	0.3	0.00	0.50	0.0
YZG12	0.9	0.182	0.3	0.00	0.90	0.0
HLG01	1.1	0.371	0.2	0.00	1.13	0.0
HLG02	1.7	0.392	0.2	0.00	1.66	0.0
HLG05	1.4	0.64	0.1	0.00	1.43	0.0
HLG06	1.6	0.302	0.3	0.00	1.60	0.0
HLG06-P	1.6	0.744	0.1	0.00	1.60	0.0
HLG07	2.7	0.846	0.2	0.00	2.71	0.0
HLG09	2.7	0.956	0.2	0.00	2.68	0.0
HLG09-P	2.8	0.523	0.3	0.00	2.76	0.0
HLG10	1.1	0.408	0.2	0.00	1.14	0.0
HLG11	1.1	0.227	0.3	0.00	1.15	0.0
HLG04T	0.5	0.0074	3.7	0.35	0.13	72.8
HLG08T	0.2	0.0113	0.9	0.00	0.18	0.0
HLG12T	0.2	0.0003	44.3	0.23	0.01	97.7
HLG13T	1.0	0.0088	6.4	0.86	0.16	84.5
HLG14T	0.5	0.0094	3.1	0.35	0.17	67.8
YZG10	0.5	0.00015*	187.1	0.50	0.00	99.5
MXH	0.9	0.201	0.3	0.00	0.95	0.0
DDH	7.4	0.0278	14.7	6.85	0.50	93.2
CHZ	2.9	0.00015*	1093.1	2.94	0.00	99.9

Table N.4-3: Estimated Hg_{geo} (nG/L) and Hg_{atm} (ng/L) in water samples from spring 2013 data set, based on the crustal relation between Al and Hg, showing the enrichment factor (EF) of Hg_{atm}.

Sample	**Hg (ng/l)**	**Al (mg/L)**	**EF**	**Hg_{geo} (ng/L)**	**Hg_{atm} (ng/L)**	**Hg_{atm} (%)**
HLG01	0.7	0.891	1.1	0.64	0.06	8.0
HLG02	0.7	1.05	0.9	0.66	0.00	0.0
HLG03	0.6	0.631	1.2	0.46	0.10	17.8
HLG05	0.2	0.031	9.5	0.02	0.19	89.4
HLG06	1.4	7.25	0.3	1.41	0.00	0.0
HLG07	1.6	9.36	0.2	1.59	0.00	0.0
HLG09	1.8	9.21	0.3	1.82	0.00	0.0
HLG010	0.6	1.89	0.4	0.61	0.00	0.0
HLG011	0.6	1.69	0.5	0.56	0.00	0.0
YZG01	0.2	0.78	0.3	0.19	0.00	0.0
YZG02	0.2	0.045	5.8	0.03	0.16	82.7
YZG03	0.2	0.316	0.7	0.23	0.00	0.0
YZG04	0.2	0.41	0.6	0.30	0.00	0.0
YZG05	13.2	45.3	0.4	13.21	0.00	0.0
YZG06	1.4	7.69	0.3	1.45	0.00	0.0
YZG07	1.8	8.29	0.3	1.77	0.00	0.0
YZG08	1.3	5.99	0.3	1.33	0.00	0.0
YZG09	19.6	26.1	1.0	18.87	0.75	3.8
YZG11	5.0	9.06	0.8	4.96	0.00	0.0
YZG12	0.5	0.478	1.6	0.35	0.20	36.6
YZG10	1.1	0.394	3.8	0.28	0.79	73.6
YZG10G	0.4	0.229	2.5	0.17	0.25	60.3
HLG04T	0.8	0.064	16.5	0.05	0.72	93.9
HLG08T	0.4	0.063	7.8	0.05	0.31	87.2
HLG012T	0.3	0.01	42.8	0.01	0.30	97.7
HLG013T	0.4	0.025	22.0	0.02	0.38	95.5
HLG014T	1.6	0.05	43.1	0.04	1.52	97.7
DDH-T	0.1	0.008	16.7	0.01	0.09	94.0
MXH01	0.8	0.14	7.7	0.10	0.67	86.9
MXH02	0.7	0.35	2.7	0.25	0.43	63.1
MXH03	0.5	0.401	1.8	0.29	0.22	43.4
DDH-U	18.7	0.289	89.6	0.21	18.52	98.9
DDH-D	16.7	0.339	68.1	0.25	16.45	98.5
CHZ	3.0	0.034	120.6	0.02	2.94	99.2

Table N.4-4: Estimated Hg_{geo} (nG/L) and Hg_{atm} (ng/L) in water samples from the spring 2013 data set, based on the crustal relation between Ti and Hg, showing the enrichment factor (EF) of Hg_{atm}.

Sample	**Hg (ng/l)**	**Ti (mg/l)**	**EF crust**	**Hg_{geo} (ng/L)**	**Hg_{atm} (ng/L)**	**Hg_{atm} (%)**
HLG01	0.70	0.0797	0.5	0.70	0.00	0.0
HLG02	0.66	0.0969	0.4	0.66	0.00	0.0
HLG03	0.56	0.058	0.5	0.56	0.00	0.0
HLG05	0.21	0.0016	7.4	0.03	0.18	86.5
HLG06	1.41	0.654	0.1	1.41	0.00	0.0
HLG07	1.59	0.779	0.1	1.59	0.00	0.0
HLG09	1.82	0.807	0.1	1.82	0.00	0.0
HLG010	0.61	0.176	0.2	0.61	0.00	0.0
HLG011	0.56	0.153	0.2	0.56	0.00	0.0
YZG01	0.19	0.0488	0.2	0.19	0.00	0.0
YZG02	0.19	0.002	5.2	0.04	0.15	80.9
YZG03	0.16	0.019	0.5	0.16	0.00	0.0
YZG04	0.19	0.0253	0.4	0.19	0.00	0.0
YZG05	13.21	0.552	1.3	9.92	3.29	24.9
YZG06	1.45	0.696	0.1	1.45	0.00	0.0
YZG07	1.77	0.732	0.1	1.77	0.00	0.0
YZG08	1.33	0.53	0.1	1.33	0.00	0.0
YZG09	19.62	0.935	1.2	16.80	2.82	14.4
YZG11	4.96	0.563	0.5	4.96	0.00	0.0
YZG12	0.54	0.0474	0.6	0.54	0.00	0.0
YZG10	1.08	0.0143	4.2	0.26	0.82	76.2
YZG10G	0.42	0.00015	155.0	0.00	0.41	99.4
HLG04T	0.76	0.0056	7.6	0.10	0.66	86.8
HLG08T	0.35	0.0045	4.4	0.08	0.27	77.2
HLG012T	0.31	0.0006	28.7	0.01	0.30	96.5
HLG013T	0.40	0.0019	11.7	0.03	0.36	91.4
HLG014T	1.56	0.0038	22.8	0.07	1.49	95.6
DDH-T	0.10	0.00015	35.8	0.00	0.09	97.2
MXH01	0.77	0.0116	3.7	0.21	0.57	73.1
MXH02	0.69	0.0297	1.3	0.53	0.15	22.3
MXH03	0.51	0.0343	0.8	0.51	0.00	0.0
DDH-U	18.73	0.0112	93.1	0.20	18.53	98.9
DDH-D	16.70	0.0137	67.8	0.25	16.45	98.5
CHZ	2.96	0.0012	137.5	0.02	2.94	99.3

Appenix O – Analysis reports from the NIVA laboratory

Table O-1: Analysis report of metals in samples from fall 2012, as determined by ICP-MS (MS) an ICP-OES (ICP) by the NIVA lab.

Analysevariabel						Ag/MS	Al/MS	As/MS	B/ICP	Ba/MS	Be/MS	Ca/ICP	Cd/MS	Ce/MS	Co/MS	Cr/ICP	Cs/MS	Cu/ICP	Fe/ICP	K/ICP
Enhet ==>						µg/l	µg/l	µg/l	mg/l	µg/l	µg/l	mg/l	µg/l	µg/l	µg/l	mg/l	µg/l	mg/l	mg/l	mg/l
Metode ==>					TESTNO	E 8-3	E 8-3	E 8-3	E 9-5	E 8-3	E 8-3*	E 9-5	E 8-3	E 8-3*	E 8-3	E 9-5	E 8-3*	E 9-5	E 9-5	E 9-5
PrNr		PrDato	Merking	Prøvetype																
1	!	20110927	DDH	fersk	2013-00039	<0.05	774	s1.7	<0.01	19.3	0.061	28.5	0.033	0.797	0.703	<0.002	0.359	0.003	1.16	1.3
2		20110927	CHZ	fersk	2013-00039	<0.05	13.3	s1.1	<0.01	4.81	<0.01	13.1	0.02	0.012	0.041	<0.002	0.132	<0.002	0.122	0.77
3		20110927	MXH	fersk	2013-00039	<0.05	2410	s0.67	<0.01	40.7	0.12	27.6	0.046	2.29	1.53	0.0095	1.78	0.003	3.72	5.0
4		20110927	YZG01	fersk	2013-00039	<0.05	2180	s0.92	<0.01	24.2	0.098	40.1	0.12	1.20	1.58	0.006	2.34	0.004	3.55	4.2
5		20110927	YZG02	fersk	2013-00039	<0.05	491	s0.72	<0.01	6.56	0.03	33.4	0.072	0.353	0.225	<0.002	0.631	<0.002	0.605	1.6
6		20110927	YZG03	fersk	2013-00039	<0.05	1550	s0.87	<0.01	17.5	0.11	36.8	0.088	0.656	0.976	0.004	1.57	<0.002	2.12	3.3
7		20110927	YZG04	fersk	2013-00039	<0.05	1900	s0.99	<0.01	18.4	0.12	37.0	0.088	0.828	1.03	0.005	1.80	<0.002	2.49	3.3
8		20110927	YZG05	fersk	2013-00039	<0.05	1950	s0.62	<0.01	18.3	0.12	14.1	0.073	3.30	0.790	0.005	1.79	0.002	2.55	2.2
9		20110927	YZG06	fersk	2013-00039	<0.05	1980	s0.62	<0.01	18.8	0.12	32.9	0.081	0.912	1.19	0.006	1.91	0.002	2.97	3.6
10		20110927	YZG08	fersk	2013-00039	<0.05	2080	s1.0	<0.01	20.5	0.11	31.6	0.067	0.900	1.09	0.006	1.81	0.002	2.65	3.6
11		20110927	YZG09	fersk	2013-00039	<0.05	1710	s0.47	<0.01	20.2	0.15	16.1	0.031	1.49	0.524	<0.002	1.40	<0.002	2.56	2.2
12		20110927	YZG10	fersk	2013-00039	<0.05	133	s0.87	1.41	42.5	1.88	40.2	0.007	0.367	1.28	<0.002	57.1	<0.002	4.16	15.2
13		20110927	YZG11	fersk	2013-00039	<0.05	1150	s0.81	0.03	14.7	0.093	29.7	0.053	0.620	0.633	0.003	1.55	<0.002	1.72	3.7
14		20110927	YZG12	fersk	2013-00039	<0.05	2260	s1.8	0.02	28.5	0.21	30.6	0.052	2.69	0.925	0.004	1.99	0.002	2.98	4.7
15		20110927	HLG01	fersk	2013-00039	<0.05	3670	s1.5	<0.01	69.6	0.18	27.3	0.031	2.00	2.64	0.022	2.43	0.004	6.45	6.87
16		20110927	HLG02	fersk	2013-00039	<0.05	3800	s1.1	<0.01	69.1	0.15	26.7	0.036	2.34	2.88	0.023	2.66	0.005	7.04	7.09
17		20110927	HLG04T	fersk	2013-00039	<0.05	85.8	s1.5	<0.01	26.9	<0.01	30.2	0.01	0.025	0.076	<0.002	0.158	<0.002	0.107	3.6
18		20110927	HLG05	fersk	2013-00039	<0.05	7640	s1.0	<0.01	104	0.28	20.6	0.044	3.41	5.73	0.060	5.22	0.0075	15.1	12.9
19		20110927	HLG06	fersk	2013-00039	<0.05	5400	s0.96	<0.01	89.5	0.18	21.4	0.045	3.82	4.46	0.030	3.67	0.006	10.6	9.20
20		20110927	HLG06-P	fersk	2013-00039	<0.05	6700	s1.6	<0.01	104	0.21	21.5	0.054	3.80	5.16	0.042	4.38	0.0071	13.3	10.4
21		20110927	HLG07	fersk	2013-00039	<0.05	7990	s2.02	<0.01	119	0.27	22.2	0.068	4.29	5.72	0.047	4.90	0.011	14.9	10.8
22		20110927	HLG08	fersk	2013-00039	<0.05	132	s1.8	<0.01	58.3	0.02	57.6	0.02	0.0724	0.17	<0.002	0.219	<0.002	0.228	11.6
23		20110927	HLG09	fersk	2013-00039	s<0.05	9560	s1.7	<0.01	152	0.29	23.0	0.083	8.48	7.54	0.064	6.42	0.013	19.8	13.1
24		20110927	HLG09-P	fersk	2013-00039	<0.05	7760	s1.5	<0.01	127	0.20	21.1	0.062	6.24	6.19	0.048	5.15	0.011	15.3	11.2
25		20110927	HLG10	fersk	2013-00039	<0.05	4340	s1.5	<0.01	70.9	0.14	21.8	0.027	2.35	3.37	0.026	2.66	0.004	7.83	7.59
26		20110927	HLG11	fersk	2013-00039	<0.05	3750	s1.1	<0.01	73.0	0.14	22.9	0.037	3.41	2.91	0.021	2.36	0.004	6.54	7.23
27		20110927	HLG12T	fersk	2013-00039	<0.05	5.98	s2.19	0.03	43.7	0.02	49.1	0.01	0.002	0.009	<0.002	1.50	<0.002	0.0094	5.3
28		20110927	HLG13T	fersk	2013-00039	s<0.05	91.2	s2.64	<0.01	21.6	0.01	33.3	0.009	0.0306	0.088	<0.002	0.482	<0.002	0.142	3.0
29		20110927	HLG14T	fersk	2013-00039	s<0.05	101	s2.82	<0.01	18.8	0.047	28.8	0.007	0.024	0.13	<0.002	0.703	<0.002	0.153	3.4

Table continues:

Analysevariabel					Li/MS	Mg/MS	Mn/MS	Mo/MS	Na/ICP	Ni/MS	P/ICP	Pb/MS	Sb/MS	Se/MS	Sn/MS	Ti/ICP	U/MS	V/ICP	Zn/MS
Enhet ==>					µg/l	µg/l	µg/l	µg/l	mg/l	µg/l	mg/l	µg/l	µg/l	µg/l	µg/l	mg/l	µg/l	mg/l	µg/l
Metode ==>					E 8-3	E 8-3*	E 8-3	E 8-3	E 9-5	E 8-3	E 9-5	E 8-3	E 8-3	E 8-3	E 8-3	E 9-5	E 8-3	E 9-5	E 8-3
PrNr		PrDato	Merking	Prøvetype															
1	!	20110927	DDH	fersk	6.4	7440	40.8	0.48	2.89	1.7	0.05	2.76	0.2	<1	<0.1	0.0278	1.05	0.002	8.99
2		20110927	CHZ	fersk	0.6	1660	9.24	0.1	0.32	s0.1	<0.04	0.256	<0.05	<1	<0.1	<0.0003	0.028	<0.001	1.4
3		20110927	MXH	fersk	21.5	4760	67.9	2.4	2.88	2.98	0.19	2.25	<0.05	<1	0.1	0.201	6.71	0.0092	15.5
4		20110927	YZG01	fersk	14	6390	100	1.3	1.3	3.22	0.1	6.53	<0.05	<1	<0.1	0.160	5.29	0.0079	21.4
5		20110927	YZG02	fersk	8.7	4910	19.6	0.85	0.97	s0.52	<0.04	1.93	<0.05	<1	0.2	0.0847	13.1	0.001	7.64
6		20110927	YZG03	fersk	13	5780	60.3	1.5	1.2	2.0	0.05	4.13	<0.05	<1	<0.1	0.101	9.11	0.0044	11.9
7		20110927	YZG04	fersk	15	5810	64.1	2.1	1.2	2.09	0.07	4.24	<0.05	<1	0.2	0.121	10.3	0.0050	17.0
8		20110927	YZG05	fersk	20.2	2010	59.8	7.05	1.0	1.1	0.1	3.39	0.1	<1	0.3	0.142	34.1	0.0042	19.1
9		20110927	YZG06	fersk	16	5360	65.5	3.73	1.2	2.10	0.09	3.72	<0.05	<1	<0.1	0.154	12.5	0.0063	17.4
10		20110927	YZG08	fersk	15	4910	57.0	4.00	1.3	1.9	0.06	3.32	0.07	<1	0.2	0.138	11.6	0.0057	16.1
11		20110927	YZG09	fersk	20.3	1720	50.9	6.04	1.4	s0.67	0.07	1.40	0.09	<1	0.3	0.187	12.4	0.0035	17.8
12		20110927	YZG10	fersk	492	1960	427	1.5	147	s0.98	<0.04	0.086	<0.05	<1	<0.1	<0.0003	2.65	<0.001	5.50
13		20110927	YZG11	fersk	26.6	3770	45.2	4.31	3.52	s1.1	0.05	1.78	0.05	<1	<0.1	0.0954	11.7	0.0033	11.4
14		20110927	YZG12	fersk	33.8	4180	68.5	4.48	3.80	1.8	0.08	2.77	0.06	<1	0.3	0.182	11.7	0.0051	19.2
15		20110927	HLG01	fersk	20.7	5860	87.6	2.8	1.89	5.10	0.27	2.73	<0.05	<1	0.1	0.371	3.15	0.016	21.2
16		20110927	HLG02	fersk	22.9	6140	95.1	2.7	1.77	5.45	0.36	3.20	<0.05	<1	<0.1	0.392	3.41	0.018	21.5
17		20110927	HLG04T	fersk	3.4	3100	2.01	2.0	0.75	s0.39	<0.04	0.048	<0.05	<1	<0.1	0.0074	2.02	<0.001	0.78
18		20110927	HLG05	fersk	28.4	8910	205	0.90	0.66	7.46	0.60	7.35	<0.05	<1	<0.1	0.640	10.4	0.0391	36.7
19		20110927	HLG06	fersk	26.8	6110	153	0.48	0.99	7.44	0.56	5.18	<0.05	<1	<0.1	0.302	4.36	0.026	28.0
20		20110927	HLG06-P	fersk	31.5	7690	166	3.44	1.1	9.02	0.56	5.25	<0.05	<1	<0.1	0.744	4.49	0.0336	37.2
21		20110927	HLG07	fersk	33.7	8150	196	3.75	1.2	10.8	0.61	5.96	s0.07	s<1	0.1	0.846	4.40	0.0378	41.6
22		20110927	HLG08	fersk	32.3	5090	21.8	4.24	2.57	s0.86	<0.04	0.12	<0.05	<1	<0.1	0.0113	5.33	<0.001	s1.2
23		20110927	HLG09	fersk	42.1	10400	255	0.96	0.96	13.9	1.3	7.82	<0.05	<1	<0.1	0.956	4.03	0.0510	54.6
24		20110927	HLG09-P	fersk	34.1	7930	220	0.63	0.91	11.0	0.89	6.52	<0.05	<1	<0.1	0.523	3.97	0.0386	39.3
25		20110927	HLG10	fersk	20.3	5400	110	2.5	0.94	5.84	0.35	3.19	<0.05	<1	<0.1	0.408	4.50	0.020	21.7
26		20110927	HLG11	fersk	19	5040	99.3	1.5	1.0	5.14	0.35	3.26	<0.05	<1	<0.1	0.227	4.28	0.017	20.2
27		20110927	HLG12T	fersk	37.2	6670	s0.34	2.0	8.82	<0.05	<0.04	0.01	<0.05	<1	<0.1	0.0003	1.89	<0.001	s0.43
28		20110927	HLG13T	fersk	7.5	3450	2.78	1.1	1.81	s0.30	<0.04	0.074	<0.05	<1	<0.1	0.0088	3.04	<0.001	s2.26
29		20110927	HLG14T	fersk	10	2690	3.75	1.1	1.7	s0.88	<0.04	0.043	<0.05	<1	<0.1	0.0094	2.90	<0.001	s1.4

Table O-2: Analysis report of metals in samples from spring 2013, as determined by ICP-MS (MS) an ICP-OES (ICP) by the NIVA lab.

Analysevariabel						Ag/MS	Al/ICP	As/MS	B/ICP	Ba/ICP	Be/MS	Ca/ICP	Cd/MS	Ce/MS	Co/MS	Cr/ICP	Cs/MS	Cu/MS	Fe/ICP	K/ICP
Enhet ==>						µg/l	mg/l	µg/l	mg/l	mg/l	µg/l	mg/l	µg/l	µg/l	µg/l	mg/l	µg/l	µg/l	mg/l	mg/l
Metode ==>					TESTNO	E 8-3	E 9-5	E 8-3	E 9-5	E 9-5	E 8-3*	E 9-5	E 8-3	E 8-3*	E 8-3	E 9-5	E 8-3*	E 8-3	E 9-5	E 9-5
PrNr		PrDato	Merking	Prøvetype																
1	!	201130407	HLG01	fersk	2013-01609	<0.05	0.891	<0.05	0.023	0.0408	0.056	36.5	0.059	0.416	0.660	0.005	1.47	1.63	1.37	5.8
2		201130407	HLG02	fersk	2013-01609	<0.05	1.05	<0.05	0.022	0.0437	0.053	35.3	0.01	0.505	0.803	0.006	1.70	1.76	1.63	5.9
3		201130407	HLG03	fersk	2013-01609	<0.05	0.631	<0.05	0.020	0.0383	0.036	37.1	0.02	0.364	0.522	0.003	1.49	1.53	0.991	5.5

4	201130407	HLG004T	fersk	2013-01609	<0.05	0.064	<0.05	<0.005	0.0352	<0.01	38.2	0.01	0.017	0.088	<0.002	0.165	1.19	0.0813	3.9
5	201130407	HLG05	fersk	2013-01609	<0.05	0.031	<0.05	0.007	0.014	s<0.01	24.7	0.023	0.014	0.027	<0.002	0.0984	0.384	0.0347	5.0
6	201130407	HLG06	fersk	2013-01609	<0.05	7.25	<0.05	0.01	0.113	0.311	28.8	0.049	4.46	5.28	0.039	4.67	10.7	11.7	10.9
7	201130407	HLG07	fersk	2013-01609	<0.05	9.36	<0.05	0.01	0.135	0.347	27.9	0.099	6.53	7.43	0.046	6.37	17.1	15.1	12.3
8	201130407	HLG07P	fersk	2013-01609	<0.05	9.23	<0.05	0.01	0.131	0.337	27.7	0.066	4.09	7.17	0.044	6.03	16.9	14.8	12.2
9	201130407	HLG08T	fersk	2013-01609	<0.05	0.063	<0.05	0.006	0.0534	<0.01	49.8	0.01	0.0375	0.099	<0.002	0.162	0.889	0.0916	10.3
10	201130407	HLG09	fersk	2013-01609	<0.05	9.21	<0.05	0.009	0.142	0.23	29.3	0.069	4.99	7.01	0.050	5.91	14.8	14.5	12.5
11	201130407	HLG010	fersk	2013-01609	<0.05	1.89	<0.05	0.008	0.0509	0.079	30.1	0.02	0.979	1.40	0.010	1.32	2.43	2.95	7.11
12	201130407	HLG011	fersk	2013-01609	<0.05	1.69	<0.05	0.007	0.0487	0.02	30.8	0.03	0.952	1.27	0.0089	1.24	2.34	2.60	6.79
13	201130407	HLG012T	fersk	2013-01609	<0.05	0.01	<0.05	0.025	0.0427	<0.01	45.8	0.01	0.0072	0.028	<0.002	1.26	0.603	0.025	5.2
14	201130407	HLG013T	fersk	2013-01609	<0.05	0.025	<0.05	<0.005	0.031	s<0.01	41.4	0.009	0.018	0.028	<0.002	0.563	0.765	0.032	3.5
15	201130407	HLG014T	fersk	2013-01609	<0.05	0.050	s<0.05	0.11	0.031	0.086	40.5	0.01	0.0310	0.078	<0.002	10.6	1.03	0.0829	6.4
16	201130407	CHZ	fersk	2013-01609	<0.05	0.034	<0.05	<0.005	0.013	<0.01	11.5	0.045	0.0369	0.072	<0.002	0.157	0.554	0.0834	1.7
17	201130407	MXH01	fersk	2013-01609	<0.05	0.14	<0.05	0.008	0.013	<0.01	22.4	0.02	0.104	0.095	<0.002	0.242	0.703	0.205	2.0
18	201130407	MXH02	fersk	2013-01609	<0.05	0.350	<0.05	0.021	0.023	0.04	35.7	0.02	0.252	0.222	<0.002	1.02	1.11	0.517	4.7
19	201130407	MXH03	fersk	2013-01609	<0.05	0.401	<0.05	0.019	0.023	0.02	36.1	0.023	0.335	0.271	<0.002	0.944	1.35	0.586	4.8
20	201130407	DDH-a	fersk	2013-01609	<0.05	0.289	<0.05	0.020	0.021	0.02	37.3	0.01	0.399	0.356	<0.002	0.478	3.87	0.424	1.8
21	201130407	DDH-D	fersk	2013-01609	<0.05	0.339	<0.05	0.019	0.022	<0.01	37.5	0.01	0.425	0.385	<0.002	0.507	3.66	0.495	1.9
22	201130407	DDH-T	fersk	2013-01609	<0.05	0.008	<0.05	<0.005	0.001	<0.01	9.30	<0.005	0.003	0.006	<0.002	0.0032	0.17	0.0041	0.67
23	201130407	YZG01	fersk	2013-01609	<0.05	0.780	<0.05	0.005	0.014	0.06	50.3	0.054	0.652	0.489	<0.002	1.03	1.96	1.02	4.1
24	201130407	YZG02	fersk	2013-01609	<0.05	0.045	<0.05	0.005	0.002	<0.01	21.1	0.008	0.0692	0.021	<0.002	0.360	0.371	0.0392	1.3
25	201130407	YZG01+02	fersk	2013-01609	<0.05	0.316	<0.05	<0.005	0.0066	s<0.01	32.4	0.022	0.235	0.19	<0.002	0.551	0.978	0.396	2.4
26	201130407	YZG04	fersk	2013-01609	<0.05	0.410	<0.05	<0.005	0.0091	0.01	36.8	0.034	0.301	0.260	<0.002	0.646	1.14	0.535	3.0
27	201130407	YZG05	fersk	2013-01609	<0.5	45.3	<0.5	0.008	0.371	2.4	67.4	0.97	59.6	56.1	0.119	46.5	163	77.9	40.0
28	201130407	YZG06	fersk	2013-01609	<0.5	7.69	<0.5	<0.005	0.0602	0.34	36.5	0.09	3.62	6.48	0.029	6.00	19.0	12.8	9.27
29	201130407	YZG07	fersk	2013-01609	<0.5	8.29	<0.5	<0.005	0.0648	0.45	36.0	0.06	4.32	7.12	0.031	6.64	20.2	13.5	9.45
30	201130407	YZG08	fersk	2013-01609	<0.5	5.99	<0.5	<0.005	0.0498	<0.1	33.4	0.06	2.74	4.95	0.023	4.78	15.4	9.62	7.98
31	201130407	YZG09	fersk	2013-01609	<0.5	26.1	<0.5	<0.005	0.317	3.37	25.2	0.65	74.4	17.0	0.034	32.1	79.9	34.9	14.7
32	201130407	YZG10	fersk	2013-01609	<0.05	0.394	<0.05	0.02	0.0051	0.16	11.1	0.025	2.61	0.13	<0.002	0.897	0.642	0.537	0.82
33	201130407	YZG10G	fersk	2013-01609	<0.05	0.229	<0.05	1.01	0.024	1.27	28.4	0.01	0.555	2.57	<0.002	43.2	0.23	4.30	11.4
34	201130407	YZG11	fersk	2013-01609	<0.05	9.06	<0.05	0.067	0.104	0.914	37.8	0.17	17.4	4.26	0.012	14.6	17.7	13.1	8.98
35	201130407	YZG12	fersk	2013-01609	<0.05	0.478	<0.05	0.053	0.017	0.094	39.6	0.03	0.677	0.254	<0.002	2.05	1.33	0.751	4.8

Table continues:.

Analysevariabel					Li/MS	Mg/ICP	Mn/MS	Mo/MS	Na/ICP	Ni/MS	P/ICP	Pb/MS	Sb/MS	Se/MS	Sn/MS	Ti/ICP	U/MS	V/ICP	Zn/MS
Enhet ==>					µg/l	mg/l	µg/l	µg/l	mg/l	µg/l	mg/l	µg/l	µg/l	µg/l	µg/l	mg/l	µg/l	mg/l	µg/l
Metode ==>					E 8-3	E 9-5	E 8-3	E 8-3	E 9-5	E 8-3	E 9-5	E 8-3	E 8-3	E 8-3	E 8-3	E 9-5	E 8-3	E 9-5	E 8-3
PrNr		PrDato	Merking	Prøvetype															
1	!	201130407	HLG01	fersk	21.9	5.12	24.2	3.86	4.55	1.6	0.05	0.601	0.06	<1	0.1	0.0797	3.66	0.0039	4.14
2		201130407	HLG02	fersk	24.3	5.26	27.9	4.35	4.57	2.01	0.07	0.707	0.07	<1	0.1	0.0969	3.93	0.0046	4.39
3		201130407	HLG03	fersk	21.7	5.04	19.0	3.59	4.67	s1.3	0.05	0.483	<0.05	<1	<0.1	0.0580	3.40	0.003	3.32
4		201130407	HLG004T	fersk	3.3	4.09	1.9	2.2	0.82	s0.48	<0.04	0.08	<0.05	<1	<0.1	0.0056	2.99	<0.001	s0.81
5		201130407	HLG05	fersk	2.8	1.32	0.74	11.8	1.0	s0.08	<0.04	0.028	<0.05	<1	<0.1	0.0016	10.6	0.001	s0.82
6		201130407	HLG06	fersk	32.2	7.48	167	5.73	1.83	10.4	0.60	5.47	s0.08	<1	s<0.1	0.654	5.52	0.029	37.9
7		201130407	HLG07	fersk	39.6	9.07	220	5.58	1.84	15.3	0.58	7.52	s0.08	s<1	s0.1	0.779	5.45	0.0378	53.0
8		201130407	HLG07P	fersk	37.0	8.96	210	4.95	1.85	14.2	0.50	7.16	s0.07	<1	s<0.1	0.775	5.43	0.0361	49.4
9		201130407	HLG08T	fersk	26.4	4.70	12.2	4.96	2.57	s0.51	<0.04	0.081	<0.05	<1	<0.1	0.0045	5.92	<0.001	s0.73
10		201130407	HLG09	fersk	37.2	9.35	207	5.12	1.87	14.7	0.66	6.50	s0.06	<1	s<0.1	0.807	5.75	0.0366	48.0

11	201130407	HLG010	fersk	16	4.53	47.4	6.40	1.83	2.84	0.1	1.17	0.06	<1	<0.1	0.176	5.22	0.0078	10.6
12	201130407	HLG011	fersk	15	4.54	43.9	6.19	1.87	2.91	0.1	1.07	0.06	<1	<0.1	0.153	5.09	0.0070	10.2
13	201130407	HLG012T	fersk	29.1	6.75	0.67	2.3	7.65	s0.26	<0.04	0.029	<0.05	<1	<0.1	0.0006	2.36	0.001	s0.44
14	201130407	HLG013T	fersk	9.9	5.42	0.93	1.2	2.78	s0.2	<0.04	0.032	<0.05	<1	<0.1	0.0019	3.40	<0.001	s0.68
15	201130407	HLG014T	fersk	118	4.25	6.56	0.88	24.6	s1.2	<0.04	0.058	<0.05	<1	<0.1	0.0038	2.13	<0.001	s1.3
16	201130407	CHZ	fersk	0.6	1.52	23.5	0.46	0.41	s0.24	<0.04	0.586	0.1	<1	0.2	0.0012	0.047	<0.001	4.88
17	201130407	MXH01	fersk	9.3	2.91	7.42	3.28	4.84	s0.34	<0.04	0.285	<0.05	<1	0.1	0.0116	5.92	<0.001	1.3
18	201130407	MXH02	fersk	23.8	5.04	14.8	5.35	6.29	s0.61	<0.04	0.378	<0.05	<1	0.1	0.0297	12.9	0.002	2.57
19	201130407	MXH03	fersk	22.3	5.14	16.6	5.11	6.24	s0.90	<0.04	0.499	0.05	<1	0.1	0.0343	14.1	0.001	2.93
20	201130407	DDH-a	fersk	12	10.3	21.0	1.0	6.53	s0.74	<0.04	2.62	0.2	<1	<0.1	0.0112	1.88	<0.001	3.80
21	201130407	DDH-D	fersk	13	10.2	22.6	1.0	6.47	s0.77	<0.04	2.20	0.2	<1	<0.1	0.0137	2.18	0.001	3.71
22	201130407	DDH-T	fersk	2.0	0.776	0.24	0.65	3.85	<0.05	<0.04	0.033	<0.05	<1	<0.1	<0.0003	0.887	<0.001	0.70
23	201130407	YZG01	fersk	14	9.12	32.9	5.29	2.22	s1.1	0.04	1.70	0.06	<1	0.2	0.0488	12.4	0.002	6.84
24	201130407	YZG02	fersk	5.2	3.46	1.7	1.2	1.2	s0.08	<0.04	0.10	<0.05	<1	<0.1	0.0020	11.4	<0.001	s0.66
25	201130407	YZG01+02	fersk	8.5	5.51	13.2	2.9	1.6	s0.57	<0.04	0.729	<0.05	<1	<0.1	0.0190	11.8	<0.001	2.83
26	201130407	YZG04	fersk	11	6.24	16.1	4.55	1.79	s0.63	<0.04	0.826	<0.05	<1	<0.1	0.0253	12.9	0.001	3.52
27	201130407	YZG05	fersk	269	34.1	2120	<1	1.94	65.1	8.05	113	<0.5	<10	<1	0.552	40.8	0.155	359
28	201130407	YZG06	fersk	45	10.5	252	5.5	1.92	9.1	0.39	10.8	<0.5	<10	<1	0.696	17.1	0.029	55.0
29	201130407	YZG07	fersk	48	10.8	271	5.5	1.87	9.6	0.40	11.7	<0.5	<10	<1	0.732	17.1	0.030	59.1
30	201130407	YZG08	fersk	37	8.31	189	5.3	1.77	7.1	0.22	8.41	<0.5	<10	<1	0.530	15.2	0.021	40.7
31	201130407	YZG09	fersk	337	9.93	1530	<1	2.79	30.00	0.73	67.2	<0.5	<10	<1	0.935	63.0	0.0527	466
32	201130407	YZG10	fersk	17	0.609	25.6	3.20	3.02	s0.39	<0.04	0.441	<0.05	<1	<0.1	0.0143	1.79	<0.001	7.84
33	201130407	YZG10G	fersk	388	3.19	774	0.69	110	1.6	<0.04	0.319	<0.05	<1	<0.1	<0.0003	4.44	<0.001	8.96
34	201130407	YZG11	fersk	146	6.36	482	2.1	9.85	6.21	0.23	18.3	s0.08	s<1	s0.35	0.563	26.8	0.019	136
35	201130407	YZG12	fersk	48.8	4.21	29.0	6.81	9.06	s0.39	<0.04	0.629	0.06	<1	0.1	0.0474	18.8	0.001	5.60

Table O-3: Analysis report of parameters included in the “sur pakke” in samples from fall 2012, as determined by the NIVA lab.

Analysevariabel					pH	KOND	ALK	Tot-N/L	NO3-N	TOC	Cl	SO4	Al/R	Al/Il	Ca	K	Mg	Na
Enhet ==>					pH	mS/m	mmol/l	µg N/l	µg N/l	mg C/l	mg/l	mg/l	µg/l	µg/l	mg/l	mg/l	mg/l	mg/l
Metode ==>				TESTNO	A 1-4	A 2-3	C 1	D 6-1	C 4-3	G 4-2	C 4-3	C 4-3	E 3-2	E 3-2	C 4-3	C 4-3	C 4-3	C 4-3
PrNr	PrDato	Merking	Prøvetype															
1	20120922	HLG 01	fersk	2012-02426	8.13	16.7	1.180	155	85	0.23	0.39	23.6	48	15	32.3	3.89	2.53	1.45
2	20120922	HLG 04T	fersk	2012-02426	8.09	18.0	1.414	195	125	0.31	0.07	20.2	12	<5	33.2	3.35	2.93	0.60
3	20120922	HLG 05	fersk	2012-02426	8.11	11.5	0.914	119	40	0.69	0.14	11.4	94	45	22.0	5.54	1.19	0.41
4	20120922	HLG 08T	fersk	2012-02426	8.26	34.6	2.636	88	31	<0.10	0.65	49.4	11	<5	68.0	10.8	4.81	2.30
5	20120922	HLG 09	fersk	2012-02426	8.11	13.0	0.812	130	43	0.45	0.26	23.0	106	49	23.8	5.39	1.56	0.73
6	20120922	HLG 10	fersk	2012-02426	8.00	13.6	0.861	133	60	0.29	0.26	22.5	79	41	23.1	4.84	1.88	0.75
7	20120922	HLG 13T	fersk	2012-02426	8.08	21.1	0.450	205	87	0.14	0.37	44.5	11	<5	41.8	2.87	3.19	1.62
8	20120922	CHZ	fersk	2012-02426	7.42	8.00	0.791	490	2	7.6	0.30	1.39	<5	<5	14.9	0.90	1.68	0.29
9	20120922	MXH	fersk	2012-02426	8.06	17.5	1.250	210	125	0.26	0.73	24.1	45	<5	28.8	3.18	2.96	2.46
10	20120922	DDH	fersk	2012-02426	8.11	20.3	1.854	365	170	1.0	1.12	13.2	21	<5	30.4	1.04	7.42	2.66

Table O-3: Analysis report of parameters included in the “sur pakke” in samples from spring 2013, as determined by the NIVA lab.

Analysevariabel						pH	KOND	ALK	Tot-N/L	NO3-N	TOC	Cl	SO4	DOC	Al/R	Al/Il	Ca	K	Mg	Na
Enhet ==>						pH	mS/m	mmol/l	µg N/l	µg N/l	mg C/l	mg/l	mg/l	mg C/l	µg/l	µg/l	mg/l	mg/l	mg/l	mg/l
Metode ==>					TESTNO	A 1-4	A 2-3	C 1	D 6-1	C 4-3	G 4-2	C 4-3	C 4-3	G 4-2	E 3-2	E 3-2	C 4-3	C 4-3	C 4-3	C 4-3
PrNr		PrDato	Merking	Prøvetype																
1	!	20130407	HLG01	fersk	2013-00831	8.14	24.8	1.712	220	140	0.45	1.30	33.3	0.33	34	8	35.8	5.03	4.67	4.31
2		20130407	HLG02	fersk	2013-00831	8.09	24.3	1.659	220	140	0.37	1.39	32.7	0.37	31	7	34.3	5.14	4.57	4.35
3		20130407	HLG03	fersk	2013-00831	8.18	25.3	1.768	240	150	0.40	1.31	32.8	0.35	20	<5	36.2	4.92	4.77	4.42
4		20130407	HLG04T	fersk	2013-00831	8.13	23.6	1.527	295	210	0.56	0.11	37.1	0.54	9	<5	37.0	3.83	4.14	0.79
5		20130407	HLG05	fersk	2013-00831	7.92	16.3	0.819	190	135	0.18	0.39	32.1	0.17	9	<5	24.6	4.86	1.31	0.98
6		20130407	HLG06	fersk	2013-00831	8.04	17.4	0.895	210	130	0.70	0.81	33.7	0.28	93	38	26.6	5.54	1.73	1.63
7		20130407	HLG07	fersk	2013-00831	8.00	17.0	0.859	230	135	0.44	0.84	33.2	0.29	56	21	26.1	5.53	1.69	1.61
8		20130407	HLG08T	fersk	2013-00831	8.23	32.3	1.995	119	63	0.48	1.06	55.4	0.30	8	<5	48.5	10.0	4.70	2.50
9		20130407	HLG09	fersk	2013-00831	8.03	17.7	0.944	220	130	0.46	0.81	63.0	0.33	139	63	27.1	5.95	1.94	1.63
10		20130407	HLG010	fersk	2013-00831	8.02	20.4	1.185	180	105	0.28	0.82	34.8	0.26	62	23	29.5	5.59	3.16	1.73
11		20130407	HLG011	fersk	2013-00831	8.05	20.8	1.196	170	105	0.27	0.80	36.2	0.25	48	16	30.2	5.49	3.30	1.78
12		20130407	HLG012T	fersk	2013-00831	8.16	31.9	2.371	170	98	0.27	1.87	38.6	0.26	13	6	46.1	5.08	7.05	7.28
13		20130407	HLG013T	fersk	2013-00831	8.07	28.0	1.227	280	185	0.29	0.70	65.5	0.26	9	<5	41.6	3.38	5.54	2.72
14		20130407	HLG014T	fersk	2013-00831	8.27	35.1	2.501	400	235	0.99	6.99	38.3	0.63	6	<5	39.7	6.37	4.27	23.7
15		20130407	CHZ	fersk	2013-00831	7.26	7.37	0.541	525	115	4.3	0.17	6.52	4.1	<5	<5	10.7	1.53	1.42	0.41
16		20130407	MXH01	fersk	2013-00831	8.12	16.1	1.305	530	420	0.54	1.46	10.1	0.51	14	<5	22.3	1.90	3.03	4.64
17		20130407	MXH02	fersk	2013-00831	8.25	25.3	1.822	350	235	0.38	1.76	29.4	0.36	11	<5	35.3	4.42	4.95	6.03
18		20130407	MXH03	fersk	2013-00831	8.32	25.6	1.824	340	225	0.52	1.73	31.0	0.39	9	<5	37.7	4.52	5.04	5.98
19		20130407	DDH-u	fersk	2013-00831	8.47	28.4	2.439	500	325	0.67	1.69	21.9	0.55	24	10	38.3	1.65	10.7	6.25
20		20130407	DDH-D	fersk	2013-00831	8.41	28.5	2.440	490	330	0.62	1.70	22.2	0.54	26	12	37.6	1.73	10.2	6.27
21		20130407	DDH-T	fersk	2013-00831	7.75	7.35	0.576	550	465	0.27	0.35	4.55	0.25	<5	<5	9.7	0.64	0.78	3.70
22		20130407	YZG01	fersk	2013-00831	8.11	33.5	1.420	137	85	0.18	0.19	89.4	0.16	9	5	48.3	3.54	8.73	2.03
23		20130407	YZG02	fersk	2013-00831	7.94	15.2	0.814	180	98	0.14	0.08	29.0	0.15	<5	<5	21.7	1.27	3.44	1.15
24		20130407	YZG01+02	fersk	2013-00831	8.13	22.7	1.064	155	100	0.18	0.12	51.8	0.16	7	<5	33.4	2.18	5.48	1.52
25		20130407	YZG04	fersk	2013-00831	8.13	25.6	1.194	126	84	0.20	0.14	60.3	0.16	6	<5	38.0	2.74	6.17	1.67
26		20130407	YZG05	fersk	2013-00831	8.38	11.5	0.924	425	155	2.6	0.08	12.3	0.70	242	115	40.6	5.12	0.96	1.13
27		20130407	YZG06	fersk	2013-00831	8.11	23.0	1.158	180	100	0.51	0.14	49.1	0.28	60	13	36.6	3.50	4.74	1.66
28		20130407	YZG07	fersk	2013-00831	8.10	22.8	1.148	190	100	0.61	0.14	47.8	0.28	57	16	37.1	3.57	4.65	1.64
29		20130407	YZG08	fersk	2013-00831	8.12	21.4	1.106	210	130	0.53	0.16	43.2	0.28	30	9	34.2	3.85	3.91	1.57
30		20130407	YZG09	fersk	2013-00831	7.79	10.8	0.878	765	175	3.9	0.44	7.47	0.67	91	47	25.3	1.34	1.22	1.54
31		20130407	YZG10	fersk	2013-00831	7.48	8.42	0.404	415	300	0.81	0.66	14.4	0.68	90	60	11.5	0.72	0.62	2.88
32		20130407	YZG10G	fersk	2013-00831	6.67	66.9	5.827	75	<1	0.43	35.5	3.43	0.38	143	13	28.5	11.6	3.4	105
33		20130407	YZG11	fersk	2013-00831	8.18	25.3	1.861	350	150	1.5	2.51	26.1	0.46	32	7	38.1	3.80	3.14	9.04
34		20130407	YZG12	fersk	2013-00831	8.41	27.7	2.090	265	180	0.40	2.39	28.4	0.35	11	<5	40.3	4.48	4.13	8.66